CAPROCK SYSTEMS FOR CO_2 GEOLOGICAL STORAGE

Report: 2011/01

May 2011

INTERNATIONAL ENERGY AGENCY

The International Energy Agency (IEA) was established in 1974 within the framework of the Organisation for Economic Co-operation and Development (OECD) to implement an international energy programme. The IEA fosters co-operation amongst its 28 member countries and the European Commission, and with the other countries, in order to increase energy security by improved efficiency of energy use, development of alternative energy sources and research, development and demonstration on matters of energy supply and use. This is achieved through a series of collaborative activities, organised under more than 40 Implementing Agreements. These agreements cover more than 200 individual items of research, development and demonstration. IEAGHG is one of these Implementing Agreements.

DISCLAIMER

COPYRIGHT

ACKNOWLEDGEMENTS AND CITATIONS

This report describes research sponsored by IEAGHG. This report was prepared by:

- CO2CRC

The principal researchers were:

- Kaldi, J
- Daniel, R
- Tenthorey, E
- Michael, K
- Schacht, U
- Nicol, A
- Underchultz, J
- Backe, G.

To ensure the quality and technical integrity of the research undertaken by IEAGHG each study is managed by an appointed IEAGHG manager. The report is also reviewed by a panel of independent technical experts before its release.

The IEAGHG manager for this report was:

- Neil Wildgust

The expert reviewers for this report were:

- Christian Hermanrud, Statoil
- Andrew Cavanagh, Permedia
- Andrew C Aplin, University of Newcastle
- Jean-Philippe Nicot, University of Texas
- Lingli Wei, Shell
- Andreas Busch, Shell
- Andy Chadwick, BGS
- Charlie Gorecki, EERC

The report should be cited in literature as follows:

'IEAGHG, "Caprock Systems for CO_2 Geological Storage", 2011/01, May, 2011.'

Further information or copies of the report can be obtained by contacting IEAGHG at:

IEAGHG, Orchard Business Centre,
Stoke Orchard, Cheltenham,
GLOS., GL52 7RZ, UK
Tel: +44 (0)1242 680753 Fax: +44 (0)1242 680758
E-mail: mail@ieaghg.org
Internet: www.ieaghg.org

CAPROCK SYSTEMS FOR CO_2 GEOLOGICAL STORAGE

Background to the Study

In terms of geological storage of CO_2, caprocks are layers of low permeability rock that overlay the storage formation, ensuring that buoyant dense or vapour-phase CO_2 does not leak into overlying strata and towards sensitive environmental receptors. Storage security, especially in early stages after the start of injection, is largely influenced by the caprock integrity.

Caprocks can be in the form of a laterally extensive thick single seal layers across the entire formation, or part of a multilayered system, where permeable layers are interbedded with low permeability layers. Multilayered systems are more risky because small faults, which might escape seismic detection, can create a connected leakage pathway through fault offset and inter-connected permeable intervals. Low permeability intervals may consist of shales, anhydrites, coals, salts or other mineralogy that normally prevents upward migration of CO_2 at pressures below either fracturing pressure or capillary entry pressures.

Although the caprock is a seal, the lower boundary of the caprock will be in contact with CO_2 saturated pore water or pore fluid consisting of pure CO_2. Chemical interaction between the pore fluid and the caprock may change the material properties of the caprock. Therefore knowledge of the composition of the seal rock as well as the formation waters is important to gauge the geochemical properties and the minerals formed after CO_2 injection. There may be coupling between CO_2 and geochemical reactions that could be self-enhancing (with permeability increases due to dissolution) or self-limiting (with permeability decreases due to precipitation).

The sealing integrity of the caprock formations may be affected by faults, fractures and microfractures, which may exist already, or be caused or enhanced by the pressure changes upon injection of CO_2. The magnitude of the pressure on the caprock can depend on the permeability, the location of the injector and whether the system is open or closed to displacement of brine. Understanding the geomechanical properties of the caprock, the change in stress state with CO_2 injection, and identification and understanding of changes in material properties as a result of interaction with CO_2 rich fluids are essential for the overall evaluation of its sealing capacity.

CO2CRC of Australia was commissioned by IEAGHG in March 2010 to provide a comprehensive review of caprock systems for CO_2 storage, in terms of required properties for storage integrity and predictive modelling of performance.

Scope of Work

The study involved a detailed literature review of recent and ongoing research in this topic, with engineering judgement drawn from the findings. The study focussed on caprocks in the context of CO_2 storage in deep saline formations, although depleted hydrocarbon fields were also considered, in the context of the associated wide body of available knowledge.

Particular issues considered by the study included:

- Caprock characteristics for site selection purposes;
- Geomechanical, geochemical and other relevant processes, and their coupling into predictive performance models;
- Potential leakage pathways and mechanisms, including faults, fractures and by diffusion;
- Discussion of the time frames and rates of leakage for the various mechanisms and caprock systems;
- Best practices for caprock assessment including data collection and modelling methodologies.

The study aimed to produce a 'high level' overview of caprock systems issues. The study also aimed to highlight the current state of knowledge and / or gaps and recommend further research priorities on these topics.

The contractor was referred to the following recent or ongoing IEAGHG studies relevant to caprocks, to avoid obvious duplication of effort and ensure that reports issued by the programme provide a coherent output:

- Development Issues for Saline Aquifer Storage, CO2CRC, Report 2008/12
- Injection Strategies for Storage Sites, CO2CRC, Report 2010/04
- Pressurisation and Brine Displacement, Permedia, Report 2010/15
- CO_2 Impurities, Natural Resources Canada, publication due May 2011

Findings of the Study

Seal Potential – Capacity, Geometry and Integrity

The seal potential of a caprock system may be defined as the capacity, geometry and integrity of the caprock. Seal capacity refers to the maximum CO_2 column height that can be retained in the underlying reservoir, before pressure exerted by buoyancy exceeds capillary entry pressure, thus allowing CO_2 to migrate through the caprock. Seal geometry refers to the thickness and lateral extent of the caprock. Seal integrity refers to caprock geomechanical properties, in the context of ambient stress fields that may be modified by CO_2 injection and any associated abstraction of reservoir fluids.

Seal Capacity

Assessment of seal capacity for depleted hydrocarbon fields can be made from consideration of measured hydrocarbon column heights, allowing for conversion to CO_2 properties. In the absence of measured oil or gas column heights, a viable alternative approach is to use known similar caprocks as analogues.

Factors that control capillary entry pressures are: size of caprock pore throats; CO_2-water interfacial tension (IFT); and wettability of CO_2 to rock in the presence of water (Figure 1). Whilst IFT and wettability parameters for hydrocarbons are well known from extensive research, there is much less data for CO_2 storage, particularly for wettability.

Most modelling studies have assumed that reservoirs and caprocks are water-wet; however, recent research in the oil industry has suggested that certain rocks can be oil-wet or CO_2-wet. A further area of uncertainty relates to possible miscibility of water and supercritical CO_2, which could result in full wetting with no IFT between the two phases – although this phenomenon has not been demonstrated yet in storage reservoir conditions. As most calculated CO_2 column heights have been based on non-wetting assumptions, changes to this behaviour could serve to reduce seal capacities from previous estimates. The reports presents case study calculations for caprocks in several Australian basins, showing how changes in wettability assumptions could reduce column heights by 50%.

Figure 1 Cartoon of Wettability in water-supercritical CO_2 system

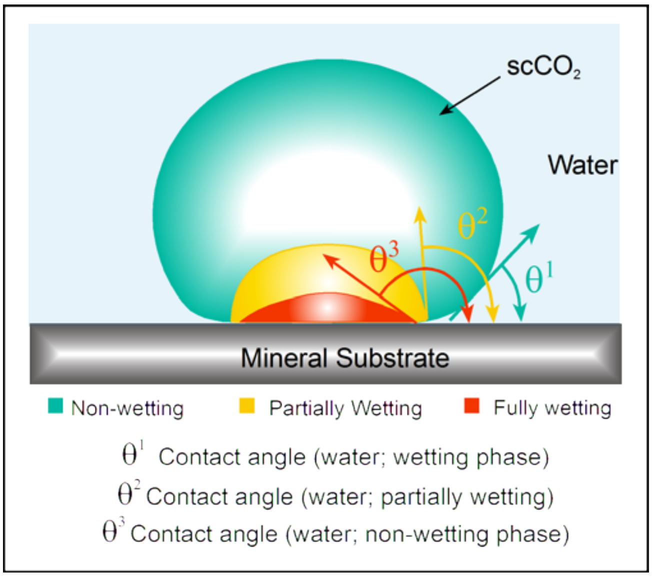

It is also worth noting that supercritical CO_2 is fully wetting in the presence of coal – this may also be true for carbonaceous shales – and hence such strata may not act as membrane or capillary seals to CO_2 migration.

Seal Geometry

Seal geometry refers to structural position, thickness and areal extent of caprocks. These are estimated using integrated studies of seismic surveys, core data, well correlations, regional geological relationships and depositional models. Note that in theory, thickness has no effect on capillary entry pressures – but thinner caprocks are more likely to be compromised by faults, sedimentary discontinuities etc.

Seal Integrity

Seal integrity is a function of lithology, pre-existing planes of weakness, regional stresses, and orientation/magnitude of induces stresses from injection and storage. Compressible (ductile) strata have relatively low strength, but are correspondingly least liable to develop structural permeability (i.e fluid migration pathways through fracturing). Increasing carbonate or siliciclastic content of caprocks will cause a higher tendency for development of structural permeability.

The ductile nature of caprocks can be estimated from the unconfined compressive strength of core samples; test data can be used to compile a brittleness index for caprocks.

Practical Application of Seal Potential Assessment

The report considers how the concept of seal potential – with components of capacity, geometry and integrity – can be used in practical assessments of storage prospects. An essentially qualitative approach is described, where seal potential of various formations can be ranked at a basin scale to assist with site selection studies. Confidence limits are used to constrain the quantity and quality of characterisation data available.

Note that the methodology described does not evaluate the probability of caprocks forming an effective seal at any given site, and hence is not a substitute for detailed, site-specific characterisation and risk assessment.

Geomechanics

The bulk permeability of many caprocks may be controlled by fractures and faults, which can enhance or retard fluid flow. Characteristics that may control the potential for fractures to form fluid flow conduits include the absolute and relative permeability of host and fault rocks, pressure and temperature conditions, inter-connection of fractures and apertures (i.e. openness to fluid flow). The characteristics of fractures and faults can change between different rock types, e.g. a given fault may have different effects on fluid flow properties in a caprock compared to the corresponding reservoir.

The report notes that the details of how, where and why faults and fractures can affect caprock integrity are still largely unresolved, and describes the mechanisms which lead to faulting/fracturing, and some typical distributions of such discontinuities in the subsurface. Fractures of potential significance to caprock integrity include those present in and around fault zones, and those present at the crest of anticlinal structures which are typically identified as likely traps for buoyant fluids. The aperture of such fractures is typically a function of the contemporary stress regime.

Although a range of techniques can be used to assess fracture patterns, seismic surveys remain the primary source of data for interpretation of the deep subsurface. Whilst faults with displacements less than 10m typically cannot be resolved, properties of seismic waveforms can be utilised to infer the presence and orientation of smaller fracture sets. Data from well logs and cores effectively provide detailed but isolated and 1-D information, except where multiple wells cross prevailing fracture sets at high angles.

Statistical distributions of fault and fracture set frequency versus size can be used to predict fault and fracture sets below the resolution of seismics. Well and seismic data (where available), can then be used to test the validity of these predictions.

Following construction of an adequate geological model, fluid flow modelling for storage requires assignment of permeability properties to faults and fractures. Due to smearing of clay minerals along faults, lateral fluid flow across fault boundaries is often impeded and this phenomenon has been extensively studied in petroleum geology; in contrast, upwards flow of buoyant fluids along faults and fractures is less well constrained, yet this is a critical topic for storage security. The report identifies that more work is needed to upscale fault/fracture flow properties to grid blocks for predictive modelling, and that the architecture and permeability of faults/fractures in mudstone caprocks should be the target of further studies.

Injection of CO_2 has the potential to increase pore pressures within reservoirs and this can lead to reduction of effective stress acting on faults – in turn leading to increased probability of fault reactivation. Fault reactivation analysis is subject to considerable uncertainty in defining key parameters such as in-situ stresses and geomechanical properties.

Increased reservoir pore pressures could affect caprocks in a number of ways:

- Geomechanical failures in the reservoir could propagate into the caprock;
- Expansion of the reservoir could lead to deformation of the caprock;
- Stress arching could lead to an increase in vertical stresses above the reservoir, possibly leading to reactivation of normal faults;
- Complex stress transfer patterns between reservoir and caprock, associated with the poroelastic properties of the lithologies involved and the reservoir stress path resulting from injection, could result in tensile or shear failures and enhanced fluid flow.

Development of highly detailed 3D geomechanical models for storage has advanced in recent years as recognition of the importance of geomechanics has grown. Detailed characterisation of poromechanical properties is required for reservoirs, caprocks and surrounding strata. An important aim of geomechanical models is to provide an opportunity for coupling with flow models.

Thermo-mechanical effects of CO_2 injection are also discussed. The temperature of the injected supercritical CO_2 is likely to be lower than that of the reservoir, leading to possible cooling of the reservoir and caprock, which could potentially lead to the creation or reopening of fractures perpendicular to the well. In extreme cases with a high temperature drop gas hydrate formation by the wellbore could occur, however modelling studies indicate that temperature drops are likely to be $< 4^{\circ}C$ and the effect on the reservoir and caprock are unlikely to be significant. This is however, still a knowledge gap and needs further investigation.

Hydrodynamics

Previous sections of the report considered 'membrane seals', where CO_2 is the non-wetting phase and can only migrate into the caprock if it overcomes capillary entry pressures, by buoyancy effects through build up of sufficient column height. In considering the effects of hydrodynamics, the authors introduce the term 'hydrodynamic seal', for situations where caprocks rely on permitting very slow rates of leakage. This broadly corresponds to the distinction used by hydrogeologists between aquicludes (formations that possess negligible permeability, such as anhydrite) and aquitards (formations with very low permeability that permit low rates of fluid migration).

Differential excess pressures above and below caprocks (Figure 2) can affect sealing capacity; sustained pressure gradients across caprocks depend on seal thickness and permeability. The report describes a scenario whereby over-pressured aquifers above caprocks effectively control the CO_2 column height that can be supported by the seal. The scenario described is somewhat idealised – heterogeneity will further complicate assessment of seal capacity in relation to any hydrodynamic effects.

Vertical or steep-angled fault seals are also considered, with similar principles of hydrodynamic effects. However, because fault zones have limited thickness, over-pressure on either side of the fault will always control seal capacity.

The report also acknowledges the increasing application of invasion percolation models, which simulate multiphase fluid flow in situations where capillary forces are more significant than viscous forces.

Figure 2 Effects of Hydrodynamics on Seal Capacity

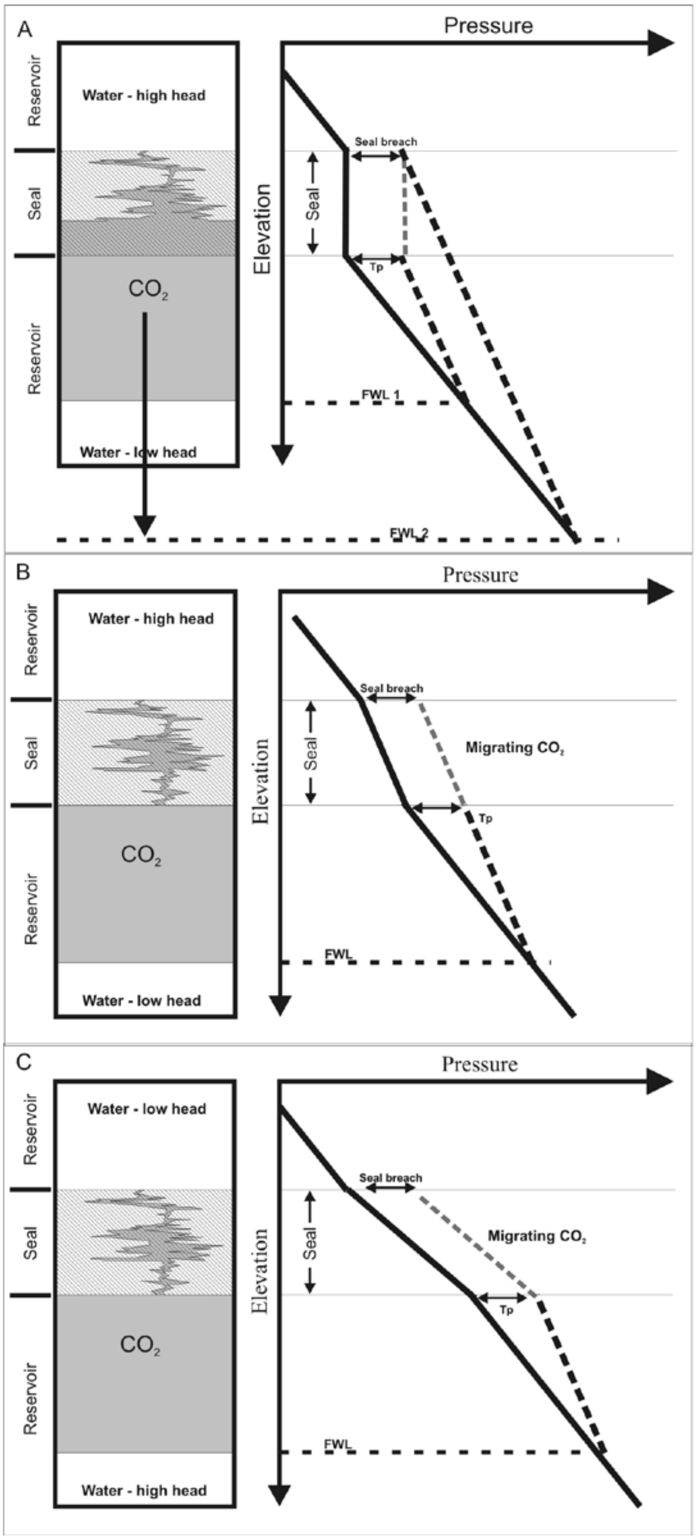

A. Excess pressure above the seal. The threshold pressure of the lowermost pores of the seal (T_P) underestimates the total seal capacity due to the water pressure profile through the seal (thick solid line). The total seal capacity is determined by the uppermost pores of the seal which is balanced by the buoyancy pressure of the CO_2 column defined by FWL 2.

B. Excess pressure above the seal matching the critical head contrast Δh. Here the water pressure gradient through the seal (thick solid line) exactly matches the CO_2 hydrostatic pressure gradient (dashed line).

C. Excess pressure below the seal. The threshold pressure of the lowermost pores of the seal defines the total seal capacity and is balanced by the buoyancy pressure of the CO_2 column.

Geochemistry

Geochemical effects on caprocks can serve to either increase or decrease permeability and hence storage security. As a general case, although the dissolution of CO_2 in formation fluids will lower pH with possible dissolution of mineral species and enhancement of permeability, the buffering capacity of most shale caprocks could be of greater significance and actually promote the precipitation of minerals, with the effect of reducing permeability and potential leakage. Modelling geoechemical processes over long timescales remains problematic, and meaningful predictions for site-specific models require precise characterisation of mineralogy and fluid chemistry, which can be difficult given the natural heterogeneity of the subsurface.

The report illustrates the principles above by summarising 4 case studies on geochemical modelling of storage, with an emphasis on possible caprock effects.

Leakage Pathways and Mechanisms

The report provides data on leakage from natural and industrial analogues as a guide to potential leakage rates. The report acknowledges that leakage rates from CO_2 storage sites are likely to be lower, and any significant leakage that does occur would probably relate to flow through faults and fractures, especially in situations where faults were reactivated as a result of injection.

Expert Review Comments

Expert comments were received from 7 reviewers, representing industry (corporate sponsors of IEAGHG) and academia. There was an overall positive response from the majority of the reviewers and there was agreement that this is a valuable piece of work, which provides a good summary of this area of study.

Reviewers considered that the equations dealing with the seal potential could be improved and this can be seen in the final report.

Reviewers suggested inclusion of a section on thermo-mechanical effects, more thorough discussion on contact angles and interfacial tension, discussion on the limitations of MICP analysis and the inclusion of a section on monitoring of caprocks. These points were all addressed in the final report.

Conclusions

Assessment of caprock systems will be highly site-specific and rely on a multi-disciplinary approach, utilising a combination of seismic surveys, exploration wells, wireline log data, stratigraphic and sedimentological analyses, well tests and laboratory scale testing of caprock samples.

The study has presented a qualitative methodology for assessment of seal potential at the basin scale. The seal potential of a caprock system may be defined as the capacity, geometry and integrity of the caprock. Seal capacity refers to the maximum CO_2 column height that can be retained in the underlying reservoir, before pressure exerted by buoyancy exceeds capillary entry pressure, thus allowing CO_2 to migrate through the caprock. Seal geometry refers to the thickness and lateral extent of the caprock. Seal integrity refers to caprock geomechanical properties, in the context of ambient stress fields that may be modified by CO_2 injection and any associated abstraction of reservoir fluids.

Key knowledge gaps identified for further research include: wettability and interfacial tension effects on supercritical CO_2-water-rock systems; hydrodynamic effects of large scale injection in DSF; effects of faults on caprock performance; and coupling of flow, geochemical and geomechanical effects on caprocks in predictive modelling. There is also a case for the compilation of a comprehensive database on caprock systems, including mineralogical and petrophysical properties, to provide analogue data in storage site assessment. A compendium of caprock properties at existing CO_2 storage sites would also prove useful.

Recommendations

IEAGHG should consider a follow up study on caprock systems, with the modelling network providing a suitable forum for the discussion of knowledge gaps identified. The modelling network can also be used to discuss the possible compilation of a caprocks database, one of the knowledge gaps identified.

A future review of the topic would be particularly useful as data is generated by future large scale demonstration projects.

Caprock Systems for Geological Storage of CO_2

Reference IEA/CON/10/179

Kaldi, J, Daniel, R, Tenthorey, E, Michael, K,
Schacht, U, Nicol, A, Underschultz, J
and Backe, G.

CONFIDENTIAL

CO2CRC PARTICIPANTS

Core Research Participants

CSIRO
Curtin University
Geoscience Australia
GNS Science
Monash University
Simon Fraser University
University of Adelaide
University of Melbourne
University of New South Wales
University of Western Australia

Industry & Government Participants

Anglo American
ANLEC R&D
BG Group
BHP Billiton
BP Developments Australia
Brown Coal Innovation Australia
Chevron
Dept. of Primary Industries - Victoria
Foundation of Research Science & Technology
INPEX
KIGAM
NSW Government Dept. Industry & Investment
Queensland Energy Resources Ltd
Queensland Government
Rio Tinto
SASOL
Shell
Solid Energy
Stanwell Corporation
Schlumberger
Total
Western Australia Dept. of Mines and Petroleum
Xstrata Coal

Supporting Participants

CANSYD Australia
Charles Darwin University
Government of South Australia
Lawrence Berkeley National Laboratory
Process Group
The Global CCS Institute
University of Queensland

CRC AUSTRALIA
Established and supported under the Australian Government's Cooperative Research Centres Program

Caprock Systems for Geological Storage of CO_2

Reference IEA/CON/10/179

Kaldi, J, Daniel, R, Tenthorey, E, Michael, K, Schacht, U, Nicol, A, Underschultz, J and Backe, G.

April 2011
CO2CRC Report: RPT10-2774

Cooperative Research Centre for Greenhouse Gas Technologies (CO2CRC)

Ground Floor NFF House, 14-16 Brisbane Avenue, Barton ACT 2601
GPO Box 463
CANBERRA ACT 2601
Phone: +61 2 6120 1600
Fax: +61 2 6273 7181
Email: pjcook@co2crc.com.au
Web: www.co2crc.com.au

Kaldi, J, Daniel, R, Tenthorey, E, Michael, K, Schacht, U, Nicol, A, Underschultz, J and Backe, G, 2010. Caprock Systems for Geological Storage of CO_2. Cooperative Research Centre for Greenhouse Gas Technologies, Canberra, Australia, CO2CRC Publication Number RPT10-2774: 133 pp.

Table of Contents

Figures and Captions

Tables

Executive Summary

This report provides a comprehensive review of caprock systems for CO_2 storage, with focus on the geological properties required for storage integrity and predictive modelling of performance. It aims to produce a 'high level' overview of caprock issues and to highlight the current state of knowledge and gaps so as to identify further research priorities around these topics.

The successful commercial scale deployment of carbon capture and storage (CCS) requires assurance of the confinement of the injected CO_2 at each potential storage site. The most critical element of the confinement of CO_2 is the caprock system overlying the storage formation. Caprock system refers to the petrophysical, geometric, geomechanical and geochemical properties of the caprock, the faults or fractures which pass through it and the hydrodynamics regime in which it occurs.

Several potential leakage pathways exist for stored CO_2 to migrate out of the reservoir into which it has been injected. These are intrinsically related to the specifics of the geology and in-situ conditions at each storage site. The range of possibilities for potential leakage, with respect to timeframes (flux rates) and volumes, conceptually spans everything from major amounts in a very short time to virtually no leakage over geological time. However, it is noted that loss of containment from the intended storage reservoir does not necessarily equate to leakage to the atmosphere, nor necessarily have any impact on other resources such as potable aquifers, hydrocarbons, coal or other minerals.

In order to assess the risk of leakage to the biosphere, atmosphere or into overlying formations, which may contain potential economic resources such as potable water, oil, gas, coal or other minerals, it is imperative to understand the entire confining system at each potential storage site. The caprock overlying the storage reservoir is the fundamental element of any such confining system. Therefore, it is necessary to evaluate the key properties of the caprock, including its mineralogy and capillary properties, its geomechanical properties, any potential geochemical reactions that might occur in the presence of CO_2, as well as the effects of hydrodynamics.

A significant component of the caprock is its seal potential, which is defined as the capacity, geometry and integrity of the caprock. The sealing capacity refers to the CO_2 column height that the caprock can retain before capillary forces allow the migration of the CO_2 through the caprock. Determination of capacity is achieved primarily through petrophysical analyses such as mercury injection capillary pressure (MICP) tests which can be utilised for analysing caprocks. In depleted field storage systems, assessments of seal capacity can be made from empirical observations of actual hydrocarbon column heights and converting these to CO_2 physical properties (density, temperature, pressure). Where these data sources are unavailable, the use of analogs (from known similar caprocks) can be a viable alternative. The measured seal capacity from MICP data must, however, be tempered by the hydrodynamic environment above and below the seal which modifies the total seal capacity.

Seal geometry refers to the thickness and lateral extent of the caprock. The caprock must have sufficient lateral extent to cover whatever structural, stratigraphic or hydrodynamic storage reservoir is used for trapping the CO_2. In addition, it must be thick enough to maintain an effective seal across faults that displace it. Seal geometry is evaluated through detailed stratigraphic and sedimentological analyses, wireline log data and seismic techniques, which are also required for baseline surveys prior to CO_2 injection.

Seal integrity refers to the geomechanical properties of the caprock. These properties are controlled by caprock mineralogy, regional and local stress fields as well as any stress changes induced by injection or withdrawal of water or CO_2. The modification of the stress field within a storage formation during and after injection of CO_2 can lead to reservoir and caprock mechanical failure. This failure can produce compaction or expansion of the rocks in the reservoir or seal and may result from a number of processes including generation of new faults and fractures, reactivation of existing faults and/or bedding parallel slip. The greatest likelihood of fluid migration up faults is during or immediately after reactivation. The presence of faults and their extent within caprock formations can be determined by seismic reflection techniques and analysis of well core or well bore imaging. Stresses within the caprock can be estimated from literature or through site specific well analyses (borehole breakout, leak-off or extended leak-off tests). The effects of induced stress changes are determined via geomechanical / rock physics analyses. However, the mere existence of faults should not automatically prohibit geological storage of carbon dioxide. On the contrary, sealing faults commonly trap hydrocarbons and compartmentalize oil and gas reservoirs. Such sealing faults could also form suitable confining barriers at CO_2 storage sites.

The impact of hydrodynamics on the sealing capacity of caprocks and faults can be significant. Hydrodynamics have been discussed in the literature primarily with respect to hydrocarbon migration. However, those findings are directly applicable to CO_2 geological storage as CO_2 in its supercritical state is a buoyant fluid and the same principle of migration applies. The hydrodynamic effects increase as the subsurface pressure regimes diverge from hydrostatic conditions. Pressure build-up due to injection in both saline aquifers and depleted hydrocarbon reservoirs has been identified as being one of the most limiting factors for large-scale geological storage. Commonly, existing analytical models and numerical simulations model CO_2 storage reservoirs as either open or closed systems, thereby largely ignoring the hydraulic properties of the sealing units. Capacity and injectivity estimates using an open- or closed system approach can vary significantly. Therefore, fluid pressures in the specific system (open vs closed) of a potential storage reservoir need to be considered when assessing the sealing capacity.

The geochemical interactions between the caprock and CO_2 consider the rock fluid interaction potential between the CO_2 and contacted minerals. The resulting reaction of acidic CO_2-rich fluids on the caprock can be either advantageous or disadvantageous for containment. The leaching of minerals within the caprock may increase the shale's permeability leading to potential CO_2 movement through the caprock. In contrast, a decrease in permeability could further seal off the caprock and contribute to improved sealing capacity. In most instances, because of their low permeability and capillary properties, CO_2 is unlikely to enter seals. Therefore, any potential reactions are likely to be limited to the base of the caprock. In addition, because the pH buffering capabilities of the seal lithology are generally greater than the dissolution capabilities of carbonic acid, reactions are likely to be mineral precipitation rather than dissolution, thus leading to seal capacity enhancement instead of degradation.

Assessing the risk of injected CO_2 leaking through the caprock and contaminating valuable resources above (e.g., water, coal, gas and oil) and/or to leak into the atmosphere is an important consideration as these outcomes could result in health and safety, economic, social and technical outcomes which impact on the ability of some CCS projects to be completed successfully. An important aspect of determining such risks is establishing how long the CO_2 should remain in the sub-surface and what rates of migration from the primary container are acceptable. Acceptable levels of leakage will vary between sites depending on where the CO_2 is predicted to migrate and what, if any, the resulting levels of exposure of people, ecosystems and resources to CO_2 might be.

Should migration of CO_2 through the caprock or along faults or fractures occur, it can be monitored by seismic imagery, fluid, atmospheric and soil gas measurements. These techniques are commonly used to confirm *containment* of injected CO_2 in the reservoir, and to provide *assurance* that groundwater, soil and air are unaffected. In addition, these techniques are useful to validate dynamic and geochemical models at storage sites. The assurance measurements compare pre- and post-injection properties, and thus need to begin well before CO_2 injection commences, continue throughout the injection period, and continue for some years post-injection. Seismic measurements investigate an overlying aquifer, while groundwater, soil gas and atmospheric monitoring provide assurance at increasing distances from the injection location.

Several areas where knowledge gaps exist in the understanding of caprocks are highlighted. These relate to both site-specific information that will always need to be collected before reservoir/caprock systems can be utilized for CO_2 storage, and more generic issues applicable to caprock characterisation. Development of a database of caprock properties from existing sites (mainly EOR and demonstration sites) could include caprock properties (such as seal capacity, mineralogy, well-log signatures, geochemical and petrophysical characteristics) of regional, local and intraformational seals. This type of data could be used as analogs when assessing containment potential for a specific area where such data are lacking. Generic issues include the uncertainty with up-scaling MICP measurements and the role of IFT and wettability in the CO_2-water-rock systems (or how supercritical CO_2 affects these two properties). Though the impact of hydrodynamics and pressure changes on the sealing capacity of top seals and faults has been demonstrated theoretically and numerically, the magnitude and significance of this process needs to be confirmed by studies utilizing empirical field examples. Further research is required to establish the response of different caprock types to both natural and induced stresses to determine which are most likely to be faulted and fractured, and what the possible flow rates of CO_2 along these might be). Also, very few studies exist that couple the chemical and mechanical processes occurring within the caprock as a result of CO_2 injection.

1. Introduction

The geological storage of carbon dioxide (CO_2) requires a porous reservoir rock (such as a sandstone or limestone) overlain by an impermeable confining layer, commonly known as a caprock or seal. The importance of the caprock is that it provides containment of buoyant CO_2, displaced brine and other mobilised substances ensuring that these do not leak into overlying strata and/or towards sensitive environmental receptors. Any successful commercial scale deployment of geological storage of CO_2 will require demonstrably viable assurance of confinement of the injected CO_2. The most critical component controlling confinement of CO_2 is the caprock system overlying the storage formation. Caprock systems refer to the petrophysical, geometric, geomechanical and geochemical properties of the caprock, the faults or fractures which pass through it and the hydrodynamics regime in which it occurs.

This study aims to provide a comprehensive review of caprock systems for CO_2 storage, with specific focus on the geological properties required for storage integrity and predictive modelling of performance. It is intended as a 'high level' overview of caprock systems to highlight the current state of knowledge and to identify further research required.

1.1 Technical Background

Caprocks are layers of low permeability rock that overlie the storage formation, ensuring that buoyant dense or vapor phase CO_2, displaced brine and other mobilised substances do not leak into overlying strata and towards sensitive environmental receptors. The storage security, especially in the early stages after the start of the injection, is largely influenced by the caprock integrity.

In order to assess the caprock system it is important to also understand the various leakage mechanisms that might result in CO_2 escaping from the zone of injection (the reservoir) to the biosphere, atmosphere or into overlying formations. Such overlying formations may be benign (as secondary storage reservoirs) or may contain potential economic resources such as potable water, oil, gas, coal or other minerals. Benson and Cook (2005) have identified several different mechanisms for such potential escape (Figure 1.1).

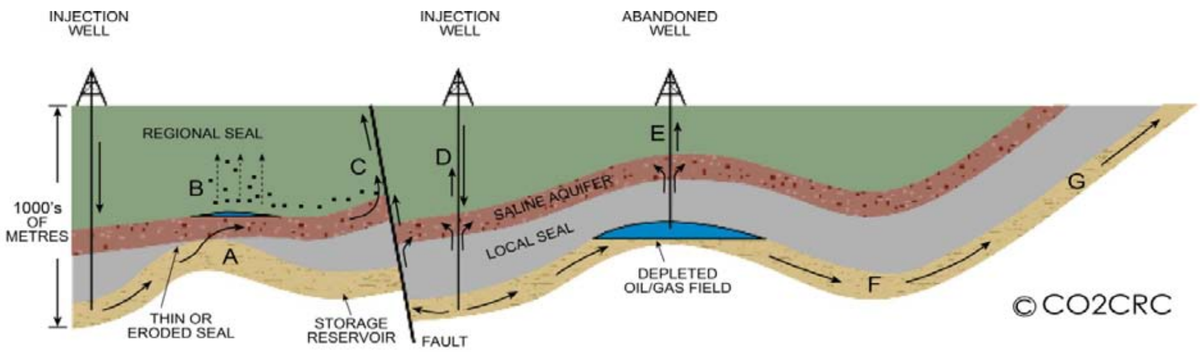

Figure 1.1 Potential Escape Mechanisms. A; CO_2 escapes the thin or eroded gap in the seal, B; CO_2 gas pressure exceeds capillary pressure and passes through the seal, C; CO_2 migrates from reservoir and up fault, D; CO_2 escapes up wellbore via poorly completed injection well and into shallower formation, E; CO_2 escapes up wellbore and into shallower formation via poorly plugged old abandoned well, F; Hydrodynamic flow transports dissolved CO_2 out of closure, G; In rare circumstances CO_2 migrates beyond regional seal (diagram modified after Benson and Cook, 2005).

Any lithology can theoretically act as a caprock; however, shales, evaporates (halite and anhydrite) are the most common seals and are responsible for the majority of all trapping of oil and gas in hydrocarbon reservoirs as well as other gasses such as CO_2, N_2 and He. Factors such as lithology, thickness, ductility and fracture density influence the seal properties, and are determined by microscopic and macroscopic analyses of the caprock. Determining which seals have the potential to trap economically viable hydrocarbon accumulations, versus those that hold sub-economic volumes, is an important aspect of evaluating both basin-wide hydrocarbon systems and field scale prospects in the petroleum industry. Similarly, determining the viability of caprocks for the safe, long-term retention of economic volumes of CO_2 is a critical element in the selection of sites for CO_2 injection and secure storage.

In order to determine the probability of containment (or risk of leakage), it is necessary to understand the various lithological properties of the caprock to determine its seal capacity (the volume of CO_2 it might be able to retain through capillary forces). The lower boundary of the caprock will be in contact with CO_2 saturated pore water or pore fluid consisting of pure or impurities-rich CO_2. Chemical interaction between the pore fluid and the caprock may change the material properties of the caprock. Therefore knowledge of the mineralogical composition of the seal rock as well as the chemistry of the formation waters and CO_2 properties (temperature, pressure, impurities, if any) is important to gauge the geochemical properties and the minerals formed after CO_2 injection. Data on these properties must be collected in order to anticipate potential geochemical reactions that might affect the caprock and thus containment

It is critical to analyse the caprock's geomechanical properties to determine its integrity and potential mechanical response to stresses introduced during injection and subsequent relaxation. Understanding the geomechanical properties of the caprock, the change in stress state with CO_2 injection, and identification and understanding of changes in material properties as a result of interaction with CO_2 rich fluids are essential for the overall evaluation of its CO_2 containment. Similarly, the sealing integrity of the caprock formations may be affected by existing faults, fractures and microfractures, which may be enhanced by the pressure changes upon injection of CO_2. The magnitude of the pressure on the caprock can depend on the permeability, the location of the injector and whether the system is open or closed to displacement of brine. Thus it is important to characterize the faults or fractures which occur within both the caprock and reservoir in order to determine the potential of these being seals or the risk of being leakage pathways.

There may be coupling between geomechanical and geochemical reactions that result in permeability increases due to dissolution and/or fracture enhancement or self-limiting (with permeability decreases due to mineral precipitation or fault/fracture filling). Which process has the greater effect will determine sealing properties of the caprock.

The hydrodynamic system affecting the caprock and the effects of pressure changes from both CO_2 injection and water movement must be modeled to quantify connectivity between the systems and continuity of both regional caprocks and intraformational seals or barriers (e.g., Underschultz, 2007) and to predict migration directions and rates.

Caprocks can be in the form of a laterally extensive thick single seal layers overlying the entire storage reservoir, or part of a multilayered system, where permeable layers are interbedded with low permeability layers. Each type presents different analytical challenges based on its unique set of stratigraphic, geophysical, geomechanical, and hydrodynamic characteristics (Gibson-Poole et al., 2004). Increased volumes of CO_2 can potentially be stored in multilayered sand/shale caprock systems compared to a single caprock/reservoir couplet (Gibson-Poole et al., 2006). The inherent uncertainty with this mode of storage is that the caprocks, or intraformational seals, may be too thin for seismic resolution, and it may not be possible to identify subseismic faulting or fracturing which can create a connected leakage pathway through fault offset and inter-connected permeable intervals. Low permeability intervals may consist of shales, anhydrites, coals, salts or other mineralogy that normally prevents upward migration of CO_2 at pressures below either fracturing pressure or capillary entry pressures.

The effect of $CO_{2,}$ across a range of pressures, on caprocks is clearly important for risk assessment on leakage and determination of possible leakage pathways. For stacked seal systems, the cumulative impact of multiple caprocks interspersed with reservoirs that have storage capacity should result in a cumulative mitigation of risk for leakage to sensitive environmental receptors. Also, an understanding of the relative pressure regimes between the multiple layers is a key determinant of the interplay between buoyant forces and hydrodynamic flow gradients.

2. Seal Potential

The ability of a caprock to hold back CO_2 is controlled by the size of the interconnected pore throats making up the seal, the relative densities of the CO_2 and water, and petrophysical properties such as the wettability and interfacial tension of the rock / CO_2 / water system. For a seal to be effective, however, it also needs to be laterally continuous (over the extent of the potential storage reservoir), relatively thick, stratigraphically homogenous, and lack open fracture or faults (Vavra et al., 1992). Murris (1980, Sluijk and Nederlof (1984) and Sluijk and Parker (1986) documented the empirical interdependence of these factors for seals to hydrocarbon accumulations from more than 160 oil and gas fields from around the world.

Much of the work on caprocks has been focused on their role as seals in hydrocarbon systems (Schowalter, 1979, Downey, 1984, Watts, 1987, Vavra eta al, 1992, Kaldi and Atkinson, 1997, Sneider et al., 1997. Only recently have studies on the role of seals in CO_2 containment started to appear. Notable amongst these are the recent works of Chiquet and Broseta (2005), Daniel and Kaldi (2009), CO_2 Capture Project (2009) and Meckel (2010). Most of these authors consider primarily the hydrocarbon (or CO_2) column height retention of caprocks, however there are other considerations important for understanding the role of caprocks in both hydrocarbon and CO_2 storage systems. In their work on seals to hydrocarbon accumulations in the Arjuna Basin, offshore northwest Java, Indonesia, Kaldi and Atkinson (1997) introduced the term" seal potential", which they defined as the capacity, geometry and integrity of the caprock.. Similar principles are applicable to evaluating caprocks for CO_2 storage. Seal potential (SP), as defined by (Kaldi and Atkinson, 1997) comprise 1) Seal Capacity; 2) Seal Geometry; and 3) Seal Integrity. Seal Capacity is the calculated column height of CO_2 that can be supported by the capillary properties of the caprock (see Daniel and Kaldi, 2009). Seal Geometry combines the areal extent of the seal (lateral continuity) and its thickness (as determined from seismic interpretation, wireline correlation and analogues). Seal Integrity refers to the propensity of the caprock to either brittle failure or ductile behaviour (as determined through geomechanical interpretations of the relationship between composition, compressibility and ductility of the seal lithology.

Seal Potential is commonly defined on a structure by structure (or storage site by storage site) basis (Kaldi and Atkinson 1997, Dragomirescu et al., 2001, Kivior et al., 2002 and Root et al., 2004). The relationship used to evaluate and compare seal potential (SP) in different caprock seals occurring in the same structure or potential storage site (Kivior et al., 2002) is suggested as:

Seal Potential (SP) = (SC / VSC).(AES / AEC).(ST / FT).(1-SI) (Equation 2.1)
where:

SC = seal capacity; VSC = the vertical structural closure; AES = areal extent of the seal; AEC = areal extent of structural or stratigraphic closure; ST = seal thickness and FT = the fault throw in top seal; SI = seal integrity component.

These variables can be assigned semi-quantitative values in order to compare seal potential of caprocks at different potential storage sites. This value, in turn, can be incorporated with assessments of reservoir storage capacity, injectivity, and trapping to provide overall storage strategies. Kaldi and Atkinson (1997) describe a work flow for seal potential assessment for hydrocarbon seals. A similar workflow is described herein for evaluating seal potential of caprocks for CO_2 containment. The methodologies proposed by Kaldi and Atkinson (1997) for oil and gas seal potential assessment and in this paper for CO_2 are effective only where significant data are available for the various analyses described. The methods are generally semi quantitative and provide a useful template for comparative assessment of one caprock to another, where all other parameters are equal. While not fully covering every aspect of caprock assessment, the Seal Potential (SP) method is the only such comprehensive technique known to the authors.

Details of each of the components of Seal Potential are detailed below:

2.1 Seal Capacity

Seal capacity refers to the CO_2 column height that the caprock can retain before capillary forces allow the migration of the CO_2 into, and possibly through, the pore system of the caprock. Determination of seal capacity is achieved primarily through petrophysical analyses such as mercury injection capillary pressure (MICP) tests which can be utilised for analysing caprocks (Daniel & Kaldi, 2008). In depleted field storage systems, assessments of seal capacity can be made from empirical observations of actual hydrocarbon column heights and converting these to CO_2 physical properties (density, temperature, pressure). Where these data sources are unavailable, the use of analogs (from known similar caprocks) has been demonstrated to be a viable alternative (Daniel & Kaldi, 2010 and Appendix A2). The measured seal capacity from MICP data must, however, be tempered by the hydrodynamic environment above and below the seal which modifies the total seal capacity (Underschultz, 2007).

When CO_2 is injected into a reservoir, the pore space of that reservoir is generally filled with water (known as formation water). As CO_2 has a lower density than the formation water occupying the pore space, the CO_2 will rise upwards through the reservoir via buoyancy (the density difference between CO_2 and water). The greater the density difference between the two phases, the greater the buoyant force wanting to move the less dense, more buoyant CO_2-phase upward. The upward movement of the CO_2 through the pore system is resisted by capillary pressure. Capillary pressure is defined as the pressure (of the injected CO_2) required to displace the formation water from the pores and pore throats of the seal (Vavra et al, 1992); (Figure 2.1).

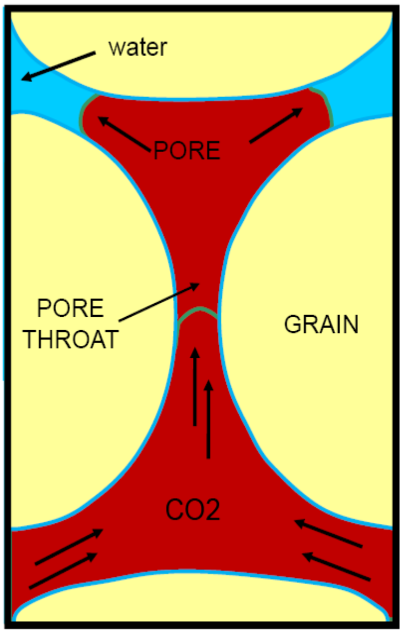

Figure 2.1 **Upward migration of CO_2 driven by buoyancy (density difference between water and CO_2). Buoyancy pressure is opposed by capillary pressure (capillary forces at each pore throat). In order to migrate, CO_2 needs sufficient buoyancy pressure to exceed capillary pressure and displace water from the pores.**

The factors that control capillary pressure, and thus determine the magnitude of this resistance to buoyancy are 1) the size of the pore throats connecting the pores space of the rock 2) the CO_2-water interfacial tension (σ) and 3) the wettability of the CO_2 to the rock surface in the presence of water (expressed as the contact angle, θ). Should the buoyancy pressure exceed the capillary displacement pressure, the CO_2 enters the pore system of the caprock resulting in 'capillary failure' of the seal. The seal capacity of a rock is therefore a function of pore-throat size, wettability (θ) and interfacial tension (σ). The column height of CO_2 capable to be held in a reservoir therefore increases as (a) pore throat size in the seal decreases; (b) the contact angle θ (between CO_2 -water –rock) decreases and (c) the interfacial tension (σ) between CO_2 and water increases. This relates directly to the pressure exerted on the caprock from the buoyancy of injected CO_2 and the added pressure from injection. When this pressure exceeds the capillary threshold pressure of the caprock, CO_2 will begin to migrate upwards through the caprock, although containment is not lost until the CO_2 has migrated through the seal. A more thorough discussion of capillary pressure is provided by Berg (1975), Schowalter (1979) and Vavra et al, (1992). Seals controlled primarily by these capillary pressure relationships are commonly known as "membrane" seals (Watts, 1987). For a membrane seal, capillary pressure is simply the difference between the pressure in the wetting phase (normally formation water) and that in the non-wetting phase (hydrocarbons or CO_2). At the reservoir-caprock interface where there is a change of permeability from reservoir rock to seal rock, the non-wetting phase is trapped below the seal until the capillary entry pressure is exceeded (referred to as 'threshold pressure'). If a trap is filled to its seal capacity, the threshold pressure of the seal is balanced by the upwards buoyancy pressure of the hydrocarbon, leading to:

$T_P = \Delta\rho\, gH$ (Equation 2.2)

where:

$\Delta\rho$ = the density contrast between the formation water and the CO_2; g = the gravitational constant; H = the height of the CO_2 column above the free water level (FWL) at the point the seal is breached.

Seal capacity is the calculated vertical column height of CO_2 that a particular seal can support before capillary failure allows the CO_2 to leak into the seal. This is a function of the relationship between the buoyancy pressure of the CO_2 column and the capillary properties of the caprock. The properties of caprocks are analysed on the macro-scale (seismic and drilling) and micro-scale (petrophysical analyses) to determine the suitability for containment and the volume of super critical CO_2 ($scCO_2$) that can be contained. Therefore, seal capacity depends on capillary displacement pressure, interfacial tension, contact angle (wettability), formation water density and carbon dioxide density.

Mercury injection capillary pressure (MICP) analysis is the most common method for determining threshold pressure. Seal capacity or column height determination using mercury injection capillary pressure (MICP) analysis has been utilised in the petroleum industry since the technique was developed by Purcell (1949) and refined by Picknell et al. (1966) and Wardlaw and Taylor (1976). With the burgeoning interest in geological storage of CO_2, this technology is being applied to establish the suitability of a top seal for containment of CO_2. The background theory to MICP analysis is presented below and demonstrates the importance of the wettability, as determined by the contact angle (θ), and interfacial tension (IFT) parameters in determining column height in the analytical procedure.

2.1.1 Mercury Injection Capillary Pressure Background

MICP analysis uses the physical principle that a non-reactive, non-wetting liquid will only penetrate a porous medium once sufficient pressure is applied to force its entrance into the pore system. The relationship between the applied pressure and the pore throat radius into which mercury will intrude is given by the modified Washburn (1921) equation, as suggested by Purcell (1949) and Schowalter (1979):

$P_c\, r = 2\,\sigma \cos\theta$ (Equation 2.3)

where:

P_c = the applied capillary pressure; r = the pore throat radius, σ is the interfacial tension between mercury and air; θ = the contact angle between mercury and the pore wall.

These equations assume that all pores are right circular cylinders. As pressure increases during analysis, the MICP instrument senses the intrusion volume of mercury by the change in capacitance between the mercury column and a metal sheath surrounding the stem of the penetrometer (Vavra et al. 1992a and b). The pressure and volume data are continuously acquired by an attached computer as the mercury column shortens in the stem and intrudes the sample.

The following values for the air-mercury system are suggested to convert capillary pressure data to effective pore throat size (Vavra et al. 1992a & b):

Air/mercury contact angle ($\theta_{a/m}$) = 140º;

Interfacial tension ($\sigma_{a/m}$) = 481 mN/m;

$(\sigma_{a/m})_*\cos(\theta_{a/m}) \approx 368$

These result in the following approximate relationship of air/mercury capillary pressure to pore throat radius:

1 psi ≈ 100µm; 10 psi ≈ 10 µm; 100 psi ≈ 1 µm; 1000 psi ≈ 0.1 µm

Limitations of MICP analysis,

Several assumptions are made when using data derived from MICP analysis. The determination of pore throat size (Washburn Equation) is based on the assumption that the pore throats are cylindrical, this holds for caprocks and clay-rich lithologies in particular. Scanning electron photomicrographs showing the pore geometries of many shale caprocks suggest that these pores are generally slot-like and highly irregular in shape (see Figure A4 in the Appendix of this report and Daniel and Kaldi, 2009). If the primary purpose of the MICP analysis is to determine threshold pressure of a caprock to estimate the containment potential, then the above assumption is not critical. A further limitation is that the MICP technique can only measure pore throats and not the actual size of the pore, making pore characterisation difficult (Webb, 2001, Giesche, 2006). MICP analysis also will not be able to detect blind or "dead-end" pores as the mercury stream will not have access to these pore spaces. A good example of this type of pore is the micro-moldic porosity commonly found in carbonate rocks.

The pore throats typically analysed using MICP fall between 100 micrometres and 0.003 micrometres due the fluid properties of mercury and limitations on experimental injection pressure (413.7 MPa or 60000 psi). Gas sorption techniques can extend the lower pore throat size limit down to 0.00035 micrometres if needed for containment calculations (Webb, 2001). Gas sorption comparisons can also be used to examine and verify any compressional effects that may occur in the finer range of pore throats as determined by mercury injection (Webb, 2001)

The general anisotropy of clastic caprocks may produce 'arbitrary' results as noted by Hildenbrand et al. (2002. Basically, this refers to the possibility of the mercury entering the sample not via individual pores and pore throats, but by utilizing inter-laminar heterogeneities. Fortunately, this effect can be corrected by coating the sides of the sample with a thin layer of resin (epoxy) so that only the capillary pressure in the cross-laminar direction is analysed, (which is the most likely vector for CO_2 migration).

Shrinkage through drying during sample preparation is also a risk as samples must be heated to 105°C (Hildenbrand et al. (2002). The authors' experience in preparing samples for MICP analysis over 10 years has shown that a drying temperature of 55°C over 48 hour period produces repeatable results and does not have the potential to distort the layered structure of the clays present. This is similar to the findings and recommendations of Folk, (1968) and Hardy and Tucker, (1988).

There are potential measurement variations which can arise in conjunction within the instrument itself (Giesche, 2006). The first is the detection and measurement of the injection pressure and the effects of the switch-over point between low and high pressure phases in the new generation of mercury porosimeters. These variations can be minimised by regular servicing and calibrating of the porosimeter. Another potential measurement error can occur when measuring the intrusion volume (Giesche, 2006). When measuring the volume of mercury, it is important to consider the volume filling a metal sheath on the outside of the penetrometer as well as the length of injected mercury inside. Again, regular calibration and inspections of the penetrometers can correct for this effect.

Finally, analysis repeatability is not possible as the MICP procedure is destructive (sample is filled with Mercury). Though it would be possible to analyse two adjacent samples the costs associated with MICP analysis generally preclude such multiple analyses being carried out.

2.1.2 Determination of Seal Capacity or Column Height

MICP analytical data is used to determine the maximum column height and the water saturation of the sedimentary rock as a function of height above the free water level (FWL). These data must be converted to a subsurface CO_2/water system before the mercury injection data can be used to determine seal capacity (column height). The following equation can be used (after Schowalter 1979):

$Pc_{bCO2} = Pc_{am} (\sigma_{bCO2}.\cos\theta_{bCO2}) / (\sigma_{am}.\cos\theta_{am})$ (Equation 2.4)
where:
Pc_{bCO2} = the capillary pressure in the water/CO2 system; Pc_{am} = the capillary pressure in the air/mercury system; σ_{bCO2} and σ_{am} = the interfacial tensions of the water/CO_2 and the air mercury systems respectively; θ_{bCO2} and θ_{am} = the contact angles of the water/CO_2/substrate and air/mercury/substrate systems respectively.

As highlighted in Equation 2.4, the role of wettability (contact angle) and interfacial tension (IFT) in determining column height is significant. In the petroleum industry these parameters are known experimentally through extensive research using both real and proxy (synthetic) hydrocarbons, as demonstrated by Smith (1966); Schowalter (1979); Anderson (1986); Morrow (1990); Zhang et al. (1997); Bi et al. (1999) and Al-Siyabi et al. (1999). In the geological storage of carbon dioxide, the role of wettability is not well known and only limited published research is available (Yang and Gu 2004; Hildenbrand et al. 2004; Chalbaud et al. 2006; Bennion and Bachu 2006 a&b; Chiquet et al. 2007; Bachu & Bennion, 2008).

Buoyancy pressure drives CO_2 (the non-wetting phase) movement in the subsurface and forces it into the pore throats of a rock, subsequently displacing water (wetting phase). Buoyancy is the density difference (in g/cc) between CO_2 and water, multiplied by the column height and the pressure gradient of pure water (0.433 psi/ft). This gradient is commonly used as a default and variations in site specific conditions (e.g. local salinity, temperature and pressure) may modify the actual gradient used in specific localities. Nevertheless, the greater the column thickness of CO_2, the greater will be the buoyancy pressure forcing CO_2 into the pore network. Threshold pressure (P_{th}) is the pressure at which the non-wetting phase (mercury or CO_2) begins to flow through the rock as a continuous phase (Figure 2.2). This pressure is determined graphically by, (a) combining the injection and incremental pore-throat size curves, (b) determining the point at which the pore-throat size distribution curve approaches the critical pore-throat size (modal pore-throat size), and (c) the point at which the injection curve has its maximum inflection upwards, as described by Kivior et al. (2002) and refined by Dewhurst et al. (2002) (Figure 2.2).

A reservoir being considered for CO_2 storage is certain to be made up of rocks of different pore throat sizes. These pore throats will therefore have different displacement (entry) and threshold pressures, and varying CO_2 saturations as a function of height (h) above the free water level (FWL). In any given CO_2 storage reservoir, the lowest indication (or maximum height) of CO_2 in a particular rock type approximates the threshold pressure (P_{th}) for that rock. The P_{th} (equivalent column height) can thus be considered as the CO_2/water contact for that particular rock type. It should be noted that a reservoir with multiple rock types may have several corresponding CO_2/water contacts, but will have only one FWL. It is therefore of significance to determine the FWL, which is required to ascertain the maximum column height (h_{max}) of CO_2 (or any non-wetting fluid) in the reservoir (Schowalter 1979).

In order to determine H_{max}, capillary pressure data must therefore first be converted to height above free water level by using the equation:

$Pc_{b/co2} = h\ (\rho b\text{-}\rho co_2)\ 0.433$ (Equation 2.5)

Seal capacity as determined by mercury injection capillary pressure (MICP) analyses, is calculated using the equation:

$H_{max} = (P_{ths} – P_{thr}) / (\rho_b\text{-}\rho_{CO2}).0.433$ (Equation 2.6)

where:

H_{max} = the seal capacity (i.e. maximum CO_2 column able to be retained by the seal); P_{ths} = the capillary threshold (displacement) pressure of the seal; P_{thr} = the capillary threshold (displacement) pressure of the reservoir; ρ_b and ρ_{CO2} = the brine and CO_2 densities, respectively; 0.433 = a gravitational constant based on the density of pure water at ambient conditions and will be a site specific value.

Typical subsurface properties for supercritical CO_2 are variable, with density ranging from 0.42 to 0.74 g/cc and water densities ranging from 0.97 to 1.05 g/cc for brines ~5000 to ~65000 ppm, although much higher salinities (with commensurate densities) are known from many potential storage areas e.g. Gulf Coast, USA; North Sea, UK; Northwest Shelf, Australia (from converted field data using Rowe and Chou (1970) and Span and Wagner (1996)).

Interfacial tension, CO_2 and water densities are determined using calculations after Span and Wagner (1996) and Rowe and Chou (1970). Generally the interfacial tension for water/CO_2 varies from 21 to 27 mN/m and the contact angle is usually assumed to be 0º (wetting phase). Once the capillary pressure values have been converted to h (height, ft or converted metres), height versus mercury (non-wetting phase) saturations can be plotted. Conversion of mercury (non-wetting phase) to CO_2 (non-wetting phase) yields a height versus CO_2 saturation plot. The non-wetting phase saturation can be converted to the water (wetting-phase) saturation (Schowalter 1979), using the conversion:

$S_w = 1 – S_{nw}$ (Equation 2.7)

where:

S_w = wetting phase (water) saturation; S_{nw} = non-wetting phase ($scCO_2$) saturation.

By plotting mercury injection pressure versus mercury saturation, a typical MICP plot can be constructed. Using mercury as the proxy for the non-wetting phase (CO_2) and 1-mercury saturation as the proxy for Sw, the column height (above FWL) versus water saturation can be graphed to estimate potential CO_2 storage volume at various water saturations (Figure 2.2). In addition, and more importantly to caprock analyses, the inflection points of the injection curve can be converted to threshold pressures and using equations (2.2) - (2.5), to actually calculate CO_2 seal capacity (column height retention).

2.1.3 CO_2 Contact Angle / Wettability

The pore systems in caprock and reservoir rocks are generally assumed to be water wet, however research investigating oil reservoirs suggests that reservoir and seal rocks can range between water-wet to oil/CO_2-wet (Robin, 2001; Benson & Cook, 2005) (Figure 2.3). Wettability can be evaluated by several methods. The most common method is the "pendant drop" technique which is based on contact angle measurements of the immiscible phase (oil or CO_2) placed on a mineral surface in the presence of the miscible phase (water). In order to determine CO_2 column height using MICP analysis, it is necessary to know the contact angle and interfacial tension of the CO_2-water-rock system, so that the mercury/air pressure system can be converted. The contact angle and IFT can be measured at subsurface pressure/temperature (P/T) conditions by viewing through windows in high pressure cells constructed for this purpose.

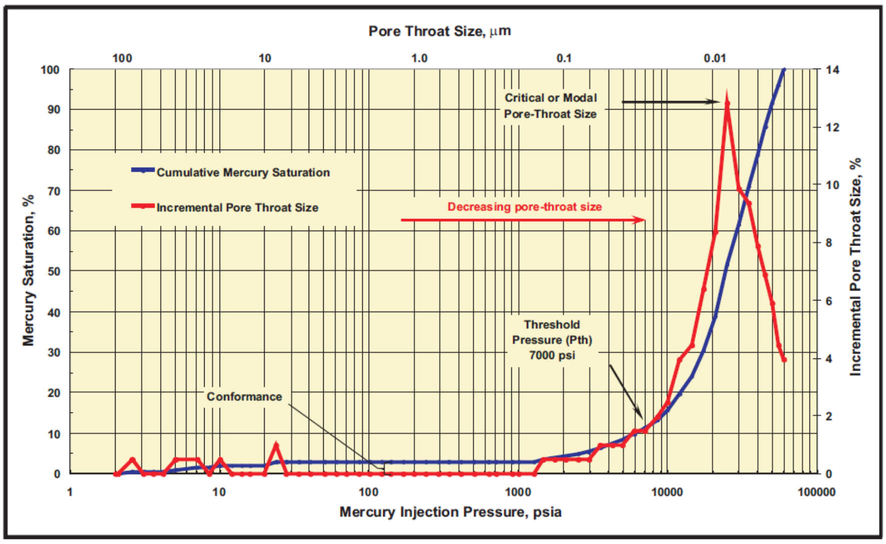

Figure 2.2 **Mercury injection capillary pressure analysis nomenclature: conformance = pressure-volume increment caused by rugosity of the sample surface; threshold pressure (P_{th}): pressure at which a continuous mercury filament forms and is able to migrate through the rock. Determination of difference in P_{th} between reservoir and seal determines seal capacity.**

Two other analytical methods commonly used by oil industry and service companies are the United States Bureau of Mines (USBM; Donaldson et al., 1969) and Amott-IFP (Cuiec, 1987) methods. These methods give a numerical indication or index of wettability, rather than a contact angle (see Anderson, 1986; Robin, 2001). It is not possible to use the USBM or Amott-IFP methods on very fine grained rocks typically found in seals because of the rapid dispersal of clay minerals and the difficulty of integrating these results into the mercury/air to CO_2/water conversion calculations.

Important considerations are the phase properties of CO_2 and formation water, once the water acidifies from CO_2 dissolution. These factors tend to alter the wettability up to and into the supercritical P/T range. Once the supercritical P/T has been reached, the CO_2 and water may become fully miscible and therefore fully wetting without interfacial tension between the two fluids (Yang et al., 2005). This area of research contains very little experimental evidence on a) the state of the CO_2 saturated water and b) its effect on seal rock mineralogy with respect to capillary pressure. These are pertinent to the associated controls in determining CO_2 column height of the sealing lithology (Yang & Gu, 2004; Yang et al., 2005). Supercritical CO_2 contact angle sensitivities are provided in Table 2.1, as the determination of CO_2-water-substrate contact angle is still subject to experimental research and discussion

Selected examples of top and intraformational seals from the Bowen, Otway, Gippsland and Cooper Basins in Australia are discussed in light of new experimental evidence on wettability and IFT variations in the CO_2-water-rock system by Daniel and Kaldi (in press). These variations may be more significant than in hydrocarbon-water-rock systems and based on non-wetting assumptions, the calculated CO_2 capillary column heights may be significantly lower than previously predicted. Supercritical CO_2 conditions are assumed (ie. where the subsurface pressure > 7.2 MPa and temperature > 31°C.

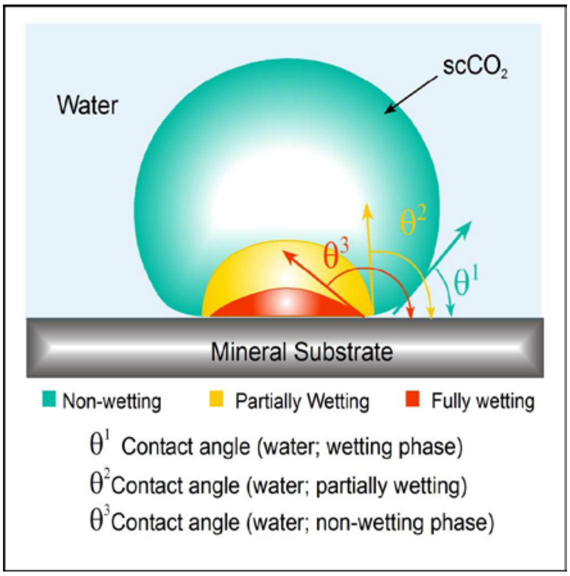

Figure 2.3 **Cartoon of a droplet of supercritical CO_2 confined by water on a mineral substrate, showing different wetting stages with respect to supercritical CO_2.**

CO_2 leakage can take place through three main processes; 1) diffusion through the wetting phase, 2) capillary movement through the pore structure, and 3) migration through possible fracture network (Zweigel et al. 2004, Gaus 2005). Zweigel et al. (2004) illustrated that capillary leakage starts at break-through pressure (threshold pressure) and stops when the pressure is reduced to around 20 -50% of the threshold pressure. However, the underlying assumption on these processes is that CO_2 is the non-wetting phase at sub-surface conditions. The following discussion examines this assumption in the light of recent experimental evidence.

Until recently gas in the sub-surface, either hydrocarbon gas or CO_2/water/rock was assumed to have a contact angle (θ) of 0º, as water was thought to be the wetting phase (Schowalter, 1979). Experimental work by Morrow et al. (1973) to determine wettability factor used the general assumption that most rocks are preferentially water wet, which can be expressed as:

$$Wettability = \sigma_{b/CO_2} . \cos\theta_{b/CO_2} \qquad \text{(Equation 2.8)}$$

where:
σ = the interfacial tension; θ = the contact angle of $scCO_2$/water/rock..

Summary of CO_2 – brine – rock contact angle experimental data

Pore-level injection modeling, incorporating a distribution of varying pore-throat radii and formation wettability (including contact angle, IFT and fluid viscosities) developed by Ferer et al. (2002), assumed that the injected CO_2 was immiscible in a water wet porous medium (CA = 0º). However, Span and Wagner (1996) have found that brine can contain up 58kg of $scCO_2$ per 1000kg of formation brine at optimum conditions, which has the affect of modifying the $scCO_2$/water/rock contact angle (see discussion below).

CO_2 column heights have been calculated for the Muderong Shale (a major top seal in the Carnarvon Basin, NW Shelf, Australia) by Dewhurst et al. (2002), who used the following data; interfacial tension of

25 mN/m, CO_2 density of 0.65 g/cm^3 and water density of 1.05 g/cm^3. A contact angle sensitivity analysis of between 0º and 45º was used, as there were little data available on $scCO_2$/water/rock contact angles at subsurface conditions. The maximum sensitivity resulted in a calculated reduction of CO_2 column height from 789m to 558m.

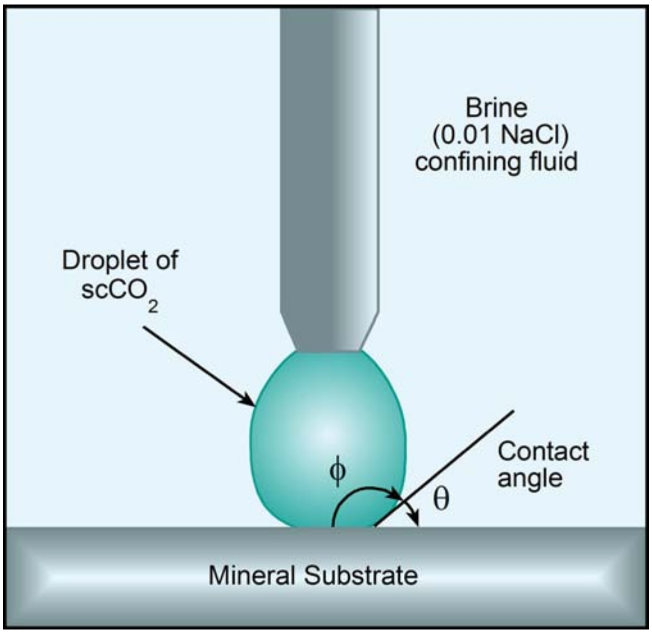

Figure 2.4 **Cartoon of a droplet of $scCO_2$ being introduced onto a mineral substrate, at subsurface conditions, to determine the contact angle (modified from Chiquet and Broseta, 2005). Yang and Gu (2004) used a similar method but introduced a water droplet via the needle into various CO_2 states to determine the IFT at subsurface conditions.**

Recent experimental data by Chiquet and Broseta (2005) and Chiquet et al. (2007a), using $scCO_2$ droplets immersed in brine (Figure 2.4), showed that quartz and mica substrates (as proxy minerals for fine grained rocks) under low pressures (<1.0 MPa or 14.7 psi) become less water-wet in the presence of $scCO_2$, i.e. contact angles (θ) vary from 0º to 20º for mica (a clay proxy, having a similar structure to clay) and 20º to 30º for quartz. Under higher pressures (10 MPa or 1450 psi: (ie, supercritical conditions), the contact angle (θ) increases to 60º - 80º for mica and 40º - 55º for quartz (Table 2.1). The contact angles were measured through the CO_2 droplet (φ, see Figure 2.4) and subtracted from 180º to give the wetting phase contact angle (θ). These experiments were carried out above the substrate in a pressure cell (Figure 2.4). In a second part of the experiment, the CO_2 droplet was introduced beneath the mineral substrates in the pressure cell and the experiment repeated. The results were determined to be 10-15º less at low pressure with negligible differences at high pressures (Table 2.1). The purpose of the experiment below the substrate was to test the contact angle results against a buoyancy effect (Chiquet and Broseta 2005). Chiquet et al. (2007a) also demonstrated that the difference in storage capacity between CO_2 as a non-wetting and as a partially wetting phase (CA - 74º) would be approximately 69% less at 1200m as a result of the commensurate lowering of the capillary membrane seal pressure (i.e. a reduced column height) due the changes in wettability.

The contact angle (CO_2-water- mica or quartz) is also affected by brine concentrations. For instance, θ decreased by ~20º from 0.01M NaCl to 0.1M NaCl then increased by ~20º from 0.1M NaCl to 1M NaCl brine solutions (Table 2.1). A decrease in CO_2 solubility also occurred with increasing salinity (Chiquet and Broseta 2005; Chiquet et al. 2007a).

These experiments were carried out on single mineral plates rather than a shale rock surface. Experimental $scCO_2$/water/rock contact angle studies on shale surfaces have not been reported in the literature, where difficulties occur due to rapid dispersion of clay platelets in aqueous solutions.

Subsequent research by Shah et al. (2008b) also determined that dense acid gases (CO_2 and H_2S) lowered the IFT when compared with water /hydrocarbon systems and are responsible for a loss in capillary sealing potential. The results obtained by the methodologies which Chiquet et al. (2007a) used on $scCO_2$/water/rock contact angle were repeated and found to be lower than originally reported (Table 2.2). Although the some of the pressures used in these experiments were not high enough for the CO_2 to be a saturated supercritical state.

Table 2.1 Carbon dioxide-water-substrate contact angle (θ) variation with increasing salinity and pressure (from Chiquet and Broseta, 2005)

Substrate / Salinity	Contact Angle (θ)	Contact Angle (θ)
	Low Pressure <0.5 MPa	High Pressure 10 MPa
Clay – 0.01M (584ppm)	0º - 20º	60º - 80º
Clay – 0.1 (5840ppm)	0º	40º - 60º
Clay – 1M (56000ppm)	0º - 20º	60º - 80º
Quartz – 0.01M (584ppm)	20º - 30º	40º – 55º
Quartz – 0.1 (5840ppm)	0º – 10º	20º – 45º
Quartz – 1M (56000ppm)	20º - 30º	40º - 55º

Wettability (contact angle) determinations by Yang et al. (2008) have also shown that the contact angle advances under the influence of high pressure. Experimental research, using the Vuggy Limestone (reservoir) rock at the Weyburn CO_2 storage site in Canada, illustrated that the contact angle advanced from 91.23º at 27ºC and 0.1 MPa (14.5 psi) to 116º at 27ºC and 12.01 MPa (1742 psi) and 130º at 27ºC and 25 MPa (3626 psi) (Table 2.3). This changed the $scCO_2$/water/rock system to a hydrophobic system; i.e. the water became the non-wetting phase. At a higher temperature (58ºC) the angle only advanced to 100º, which was attributed to each phase (CO_2 and water) permeating the other (Yang et al. 2008). This research demonstrates that the CO_2 wettability in $scCO_2$/brine/ calcareous or dolomitic caprocks rock is significantly higher than in quartz/ clay caprocks, showing contact angles above 90º, which is in the partial to fully wetting phase (Table 2.3)

Table 2.2 Results of contact angles obtained under the following sub-supercritical CO_2 conditions. Data from Shah et al., 2008b

Pressure (MPa)	Contact Angle CO_2/Brine/Mica	
	Advancing angle º (θ)	Receding angle (º)
1	28	62
2.2	28	68
3.1	32	70
5.7	38	80
Salinity 4gm/l NaCl – Temperature 35ºC, NB; supercritical conditions not reached.		

Shah et al. (2008b) also experimentally determined the advancing and receding contact angles for a CO_2/brine/ rock system on a muddy limestone reservoir rock from the south of France (Table 2.4). These results generally showed lower contact angles than Yang et al. (2008) determined for the Midale Vuggy Limestone in Canada. However, it is important to note that both the above experimental results do demonstrate that $scCO_2$ is a partially wetting phase when injected into the subsurface at super critical conditions.

Table 2.3 Contact angle variation with increasing pressure (sub to supercritical CO_2) on a calcareous substrate, Midale Vuggy Limestone, Canada (Data from Yang et al. 2008)

Pressure (MPa)	Temperature (ºC)	Contact Angle (º)
0.1	27	91.23
12.01	27	116
25	27 / 58	130 / 100
Midale Vuggy Limestone reservoir, Weyburn Canada. The reservoir is overlain by the Midale Marly Dolostone, overlying which is a regional anhydrite-rich caprock - Midale Evaporite		

Table 2.4 Results of contact angle determination using a muddy limestone substrate, (Data from Shah et al. 2008b).

Pressure (MPa)	Contact Angle CO_2/Brine/Mica	
	Advancing angle (º)	Receding angle (º)
1.1	32º	33º
15.5	27º	33º
Sample from depleted reservoir in southern France: 70% calcite; 10% chlorite; 13% quartz; and 4.5% illite/mica (% by weight). Temperature - 70ºC		

Yang et al. (2008) concluded that when incorporating the above properties of $scCO_2$ into an injection modeling routine, it would be easier to inject CO_2 and displace the brine, as the reservoir rock-brine changes from wetting to partially non-wetting as the pressure increases. This change in wettability can increase storage capacity by increasing CO_2 saturation in the pore space as $scCO_2$ becomes a partially wetting phase. However, when applying these conclusions comparatively to caprocks, it can also be determined that the CO_2 column height will be reduced using the contract angle parameters as suggested above. The outcome of these data presented above demonstrates that contact angle sensitivities need to be applied, when determining retention heights for the geological storage of CO_2.

Contact angle alteration by acid gas (other than CO_2)

Experimental work performed by Shah et al. (2008b) and Tonnet et al. (2008) have found that H_2S in conjunction with CO_2 and by itself significantly affects wettability on a mica substrate, but only exhibits minor affects on a quartz substrate. As mica has been used as the proxy for clay based clastic caprocks, this significant alteration of wettability (contact angle) needs to be taken into account when determining the containment potential of a caprock. This is important as a number of depleted gas fields containing H_2S in Western Canada and the Kashagan Oil Field –Caspian Sea are being explored for potential CO_2 storage (Shah et al., 2008b). The contact angles (mica-brine-H_2S) derived from the experiments of Shah et al. (2008b) ranged from ~ 118° at 1.5 MPa to ~ 92° at 20MPa and ~23° at 14MPa, the temperature was 50°C with a salinity of 4 g/l. Their observations described a wettability reversal with the mica plate being completely wetted by the H_2S phase, whereas when a quartz plate was used under similar conditions, the contact angles were similar to that of quartz-brine-CO_2. The main conclusion reached by Shah et al. (2008b) was that the presence of H_2S would be detrimental to the CO_2 geological storage process because of the affect on maximum gas column height and the resultant storage capacity.

As a result of the wide variation of contact angles as tabulated above, it is recommended that contact angle sensitivities are applied when determining the column height of $scCO_2$. A non-wetting contact of 0° as a baseline is recommended ~~and~~ increasing in 20° increments to 60°, as the available experimental data show that the highest predictable contact angle for mica – brine – $scCO_2$ is around this figure, provided that the scCO2 is relatively uncontaminated with acid gas (i.e. H_2S) (see Daniel and Kaldi, 2008, 2009).

2.1.4 CO_2 Interfacial Tension

Interfacial tension results when "…two immiscible fluids are in contact, and molecular attractions between like molecules within each fluid are greater than the attractions between different molecules of the two fluids" (Berg, 1975, p. 940). The free energy existing between two fluids controls the degree of miscibility between two fluids, such as CO_2 and brine. This is summarised by Meckel (2010) based on the work of previous researcher starting with the original research by Laplace, (first published in the fourth volume of Mécanique Céleste (1885), as summarised in Fox (1974).

The calculation of CO_2-water interfacial tension is a function of pressure, temperature and CO_2 density, and is based on research by Span and Wagner (1996) and Rowe and Chou (1970). The experimental data range from 0-140ºC with pressures up to 70 MPa (10152 psi) (Span and Wagner 1996; Rowe and Chou 1970). As CO_2 dissolution into the formation water occurs, the IFT increases slightly with increasing temperature but decreases with increasing pressure under experimental conditions to a point where both fluids may become miscible (Yang and Gu, 2004). However, this has not been thoroughly demonstrated in a CO_2-brine system at reservoir conditions (J. Ennis-King pers com).

The recent research into interfacial interactions by Yang and Gu (2004) and Yang et al. (2005), between water droplets immersed in $scCO_2$ using the pendant droplet method under reservoir conditions, have found several changes in the physical relationship (a variation of Figure 2.4, except the pendant droplets are water in a CO_2 atmosphere). The primary change that occurs is a significant increase in the water droplet size (swelling due to CO_2 saturation) with increasing pressure in the presence of CO_2, to a point where the droplet detaches from the needle. This is thought to be due to the solubility of CO_2 in the water to a point where the density difference is only 0.25 g/cm^3 and detaches due to gravity. A second change occurs with increasing pressure, which follows on from a density convergence where the water and CO_2 become completely miscible at elevated pressures (T= 58ºC (136.4ºF) and 12.238 MPa (1775 psi)). They noted that the IFT between CO_2 and water becomes zero as there is no interface between them at these pressure-temperature conditions, although it is briefly mentioned that the phases were not fully saturated and that this P/T regime was the point of maximum saturation of both liquids, which destabilized the experiment.

These data were questioned by Chalbaud et al. (2006) where they experimentally determined water/CO_2 IFT's up to 25.5 MPa with varying salinities (5k, 50k, 100k and 150k ppm) and temperatures (27ºC, 71ºC and 100ºC). It is also useful to note that if an IFT of 0 mN/m is used the capillary pressure equation (Equation 2.3) of Schowalter (1979) the resulting CO_2 column height is zero, which then assumes that the size of pore-throats is the principle flow inhibitor through the seal.

Subsequently Chiquet et al. (2007b) also performed pendant drop (water droplet in CO_2) experiments with temperatures from 34 to 109ºC (93 – 228ºF) and pressures from 5 to 45 MPa (725 – 6526 psi). The results generally showed that IFT was lowered with increasing pressure from 45.8 - 43.7 mN/m at 5 MPa with a temperature variation from 34 to 109ºC respectively, to 28.5 - 22.8 mN/m at 45 MPa with the same respective temperature variation. Both phases were saturated with respect to each other at the commencement of the experiments. Li et al. (2005) also found that for nitrogen (IFT - 57 mN/m). This demonstrated that the presence of CO_2 significantly changed the wettability of the Weyburn Midale Evaporite seal rock, indicating a requirement to re-evaluate potential seals once a site is selected for CO_2 storage (Li et al. 2005). Hildenbrand (2004) graphed previous data plotted against pressure with IFT where experimental temperatures are author(s) are also noted (Figure 2.5)

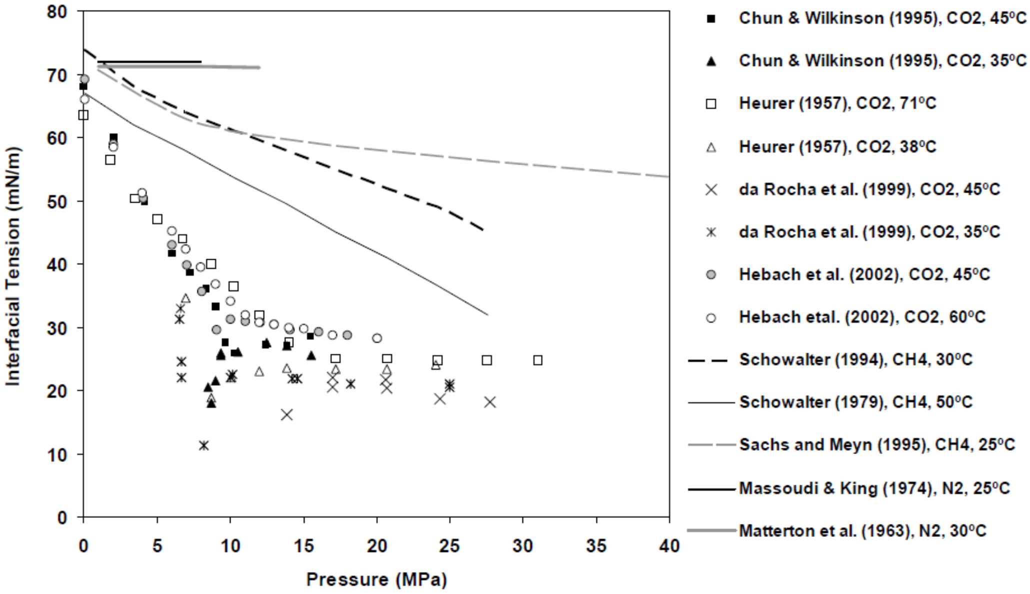

Figure 2.5 **IFT data based on studies by Heurer (1957), Masterton et al. (1963), Massoudi and King (1974), Schowalter (1979), Chun and Wilkinson (1995), daRocha etal. (1999) and Hebach et al. 2002. from Hildenbrand et al. 2004.**

Extensive results from IFT measurements (168) between CO_2 and water/brine over a range of pressures (2-27 MPa), temperatures (20-125°C) and salinities (0-334000 mg/L) were derived from an intensive laboratory program conducted by Bachu and Bennion (2009). Bachu and Bennion (2008) also developed an IFT relationship between pressure, temperature and salinity (Figure 2.6) ie;

$\sigma = 71.69243P^{-0.432629} + 0.210558T^{0.900261} + 0.075859^{1.457937}$ (regression co-efficient 0.94)
where σ – IFT (mN/m), P – pressure (MPa), T – temperature (°C), S – salinity (ppm)

Bachu and Bennion (2008) also confirmed that IFT decreases with increasing pressure, decreasing salinity and temperature.

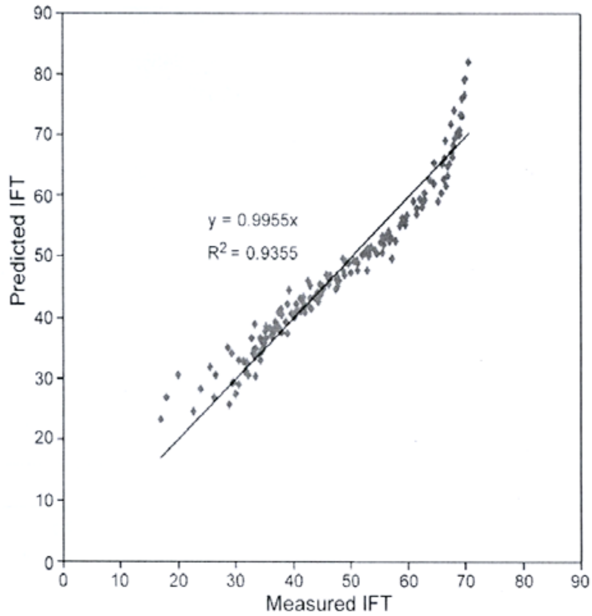

Figure 2.6 **Diagram of comparison of predicted and 168 laboratory derived results for CO_2 – Brine IFT of a range of pressure, temperature and water salinity data. (Bachu and Bennion, 2008).**

Meckel (2010) also graphically summarised some of the above CO_2-brine interfacial tension data from recent laboratory studies which highlights the change in IFT from ~70mN//m, (surface conditions) to 20 - 40 mN/m, at recommended CO_2 storage conditions, as shown in Figure 2.7.

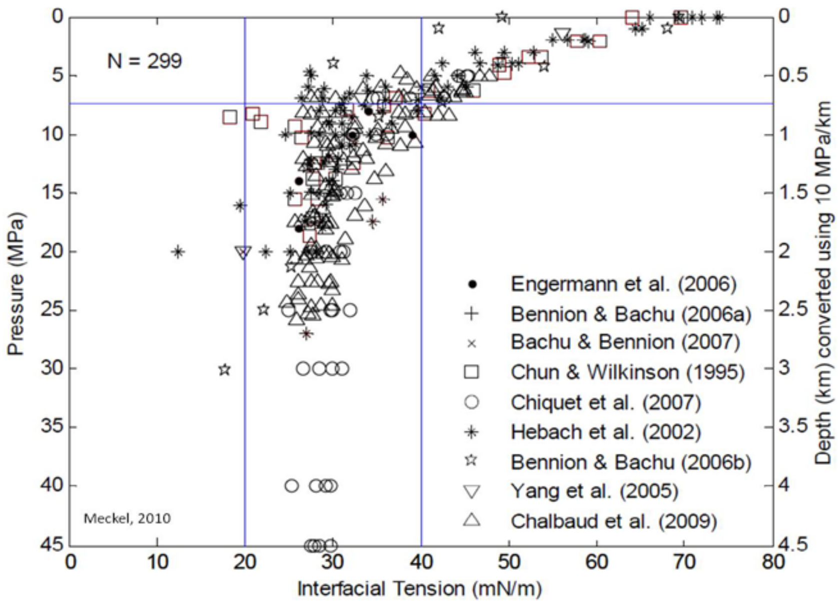

Figure 2.7 **Summary of interfacial tension data from laboratory studies (indicated on the graph) for CO_2 brine systems showing that IFT ranges from 20 to 40 mN/m at recommended storage pressure, temperature and salinity ranges (Meckel, 2010).**

Interfacial tension alteration by acid gas (other than CO_2)

The modification of IFT between CO_2 and brine has been analysed thoroughly on a regional basis, but IFT modifications between acid gas/liquid (H_2S) and brine appears to have received little attention to date. Shah et al. (2008a) performed a series of measurements over a range of pressures and temperatures that resulted in a significantly lower range of IFT's than found with CO_2-brine at the same parameters.

Table 2.5 highlights the significant modifications of IFT in a water/H_2S system. It should also be noted that a 70 mol%CO_2 + 30 mol%H_2S mixture does not result in the same low values of IFT and in most cases the IFT is modified downwards only ~16% of the CO_2-water IFTs (Shah et al., 2008a). Again the implications on caprock sealing capacity for geological storage of CO_2 (+H_2S) are similar to their above conclusions concerning the alteration of contact angle in acid (H_2S) conditions and the lowering of the gas column height with the effect of lowering storage capacity.

Table 2.5 Comparison between water/CH_4; water/CO_2; and water/H_2S IFTs at elevated pressure and temperature conditions (Shah et al., 2008a)

Gas	Temperature °C	P (MPa)	IFT (mN/m)
CH_4	40	12.5	59.8
CH_4	70	15.0	54.8
CH_4	120	15.0	50.5
CO_2	40	12.5	31.5
CO_2	70	15.0	32.5
CO_2	120	15.0	30.5
H_2S	40	12.5	15.9
H_2S	70	15.0	7.4
H_2S	120	15.0	10.5
Water/CH_4, water/CO_2 and water/H_2S IFT values are interpolated or extrapolated using the data of Ren et al. (2000), Chiquet et al. (2007a) and Shah et al.(2008a)			

2.1.5 Wettability and Carbonaceous Rocks

Research on the wettability effect of scCO_2 on coaly substrates suggests that the contact angle of CO_2-water-coal is considerably above 90º at subsurface conditions (>0.26 MPa). In other words, scCO_2 is fully wetting in the presence of coal (from brown to black) and that anthracite is fully wetting at all pressures (Siemons et al. 2006). The implications of this are that coals cannot be expected to act as a capillary or membrane seal to CO_2. Similar conditions may apply to carbonaceous shales, accentuating the diffusion aspect of CO_2 transport (Siemons et al. 2006).

Experiments were conducted on ground coal (40µm) particles to test the CO_2 adsorption qualities of water saturated coal under the influence of CO_2 injected at low pressure (37.5 kPa) in a confined test cell (Mazumder et al. 2003). At low pressures, water remained the wetting phase whilst the adsorption of CO_2 and desorption of CH_4 occurred at relatively slow rates. Subsequently a high pressure cell was built. Results indicate that under higher injection pressures (~10 MPa) this exchange takes place at a faster rate, due to a change in wettability occurring as the CO_2 enters the wetting phase (Mazumder et al. 2003). This increases the movement and subsequent adsorption of CO_2 into the less water-wet coal with commensurate desorption of methane.

2.1.6 Seal Capacity Sensitivity Examples

The majority of the seals analysed by MICP analysis, using a contact angle of 0º, produced CO_2 column retention heights well above the thickness of the reservoir formations. However, as the sensitivity of increasing contact angle is applied (up to 60º), a reduction of the column height of up to 50% occurs (Figure 2.8). Thus, seal potential of some rocks might be significantly lower than if assessed assuming a fully water-wet state (i.e. θ = 0º). These rocks wou ld no longer act as a membrane seal but might still act as a permeability baffle or an inhibitor to migration. Such baffling would increase residence time and thus increase the potential of dissolution and mineral trapping.

The CO2CRC (Australia) has identified several potential geological storage sites for CO_2, with the selection criteria based on sites having adequate reservoirs with significant confining top seals and have been analysed as part of a data base of caprock properties from sites within basins from Australian and New Zealand (see analytical methods in Appendix A2). These sites are located in the Gippsland, Otway (Victoria) and Bowen (Queensland) Basins. The Cooper Eromanga Basin (South Australia) is included to increase the variety of depositional environments. Selected examples of sealing formations from these basins are presented to demonstrate the effect of increasing CO_2/water/rock contact angles on calculated column heights (Table 2.6). The available maximum and minimum column height variation with the number of analyses from the formations are also shown to demonstrate that if the capacities of the seals are high enough, then they will still act as membrane seals at the highest contact angle sensitivity (i.e. CA - 60º). It is only when the thickness of the reservoir formation or intended injection height is larger than the height of maximum sensitivity that leakage may become an issue. Table 2.1 also highlights the importance of careful sampling to ensure that an accurate estimate of the seal capacity is calculated, as cap rocks can have significant variations of lithology with commensurate variations of CO_2 column height retention.

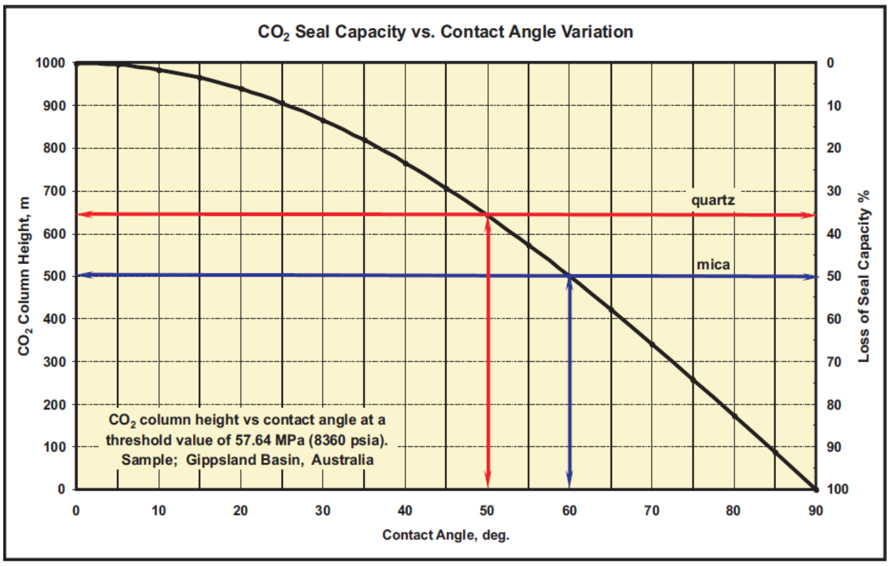

Figure 2.8 **Graphic sensitivity to increasing wettability (contact angle) versus calculated column height of $scCO_2$ based on equations 3 and 5 (from Daniel and Kaldi, 2009).**

Table 2.6 **Examples of seal capacities from potential geological storage sites (Australia) and the effect of wettability on column height (from Daniel and Kaldi, 2009). Max/Min values represent multiple MICP analyses on the particular formation, highlighting variation in lithology.**

Formation / No. of Samples	Depositional Environment	CO_2 Column Height (m) @CA 0º	CO_2 Column Height (m) @CA 20º	CO_2 Column Height (m) @CA 40º	CO_2 Column Height (m) @CA 60º
Bowen Basin		Max / Min	Max / Min	Max / Min	Max / Min
Snake Creek Mudstone /4	Marginal Marine	910 / 488	856 / 458	697 / 373	455 / 244
Note in all column height calculations P, T, Salinity, densities, and IFT all constant for each sample					
Formation / No. of Samples	**Depositional Environment**	**CO_2 Column Height (m) @CA 0º**	**CO_2 Column Height (m) @CA 20º**	**CO_2 Column Height (m) @CA 40º**	**CO_2 Column Height (m) @CA 60º**
Otway Basin		Max / Min	Max / Min	Max / Min	Max / Min
Belfast Mudstone /5	Prodelta	850 / 607	799 / 571	651 / 465	419 / 356
Flaxmans Formation /7	Upper Deltaic Plain	987 / 713	928 / 670	756 / 546	494 / 356
Waarre Formation /7	Fluvial Overbank	1631 / 15	1533 / 14	1250 / 12	816 / 8
Note in all column height calculations P, T, Salinity, densities, and IFT all constant for each sample					
Formation / No. of Samples	**Depositional Environment**	**CO_2 Column Height (m) @CA 0º**	**CO_2 Column Height (m) @CA 20º**	**CO_2 Column Height (m) @CA 40º**	**CO_2 Column Height (m) @CA 60º**
Cooper and Eromanga Basin		Max / Min	Max / Min	Max / Min	Max / Min
Murta Formation /4	Lacustrine	530 / 81	498 / 76	406 / 62	265 / 41
Birkhead Formation /3	Fluvio-Lacustrine	43 / 11	40 / 10	33 / 8	22 / 5
Cuddapan Formation /2	Flood Plain	834 / 90	784 / 84	639 / 69	417 / 45
Note in all column height calculations P, T, Salinity, densities, and IFT all constant for each sample					
Formation / No. of Samples	**Depositional Environment**	**CO_2 Column Height (m) @CA 0º**	**CO_2 Column Height (m) @CA 20º**	**CO_2 Column Height (m) @CA 40º**	**CO_2 Column Height (m) @CA 60º**
Gippsland Basin		Max / Min	Max / Min	Max / Min	Max / Min
Lakes Entrance Formation 4	Shelf	1070 / 17	1006 / 16	820 / 13	535 / 9
Gurnard Formation /2	Inner Shelf	723 / 41	680 / 38	554 / 31	362 / 20
Burong Formation /4	Back Barrier Lagoon	1191 / 63	1119 / 59	912 / 48	596 / 31
Kingfish Formation /3	Coastal Lake	764 / 53	718 / 50	585 / 41	382 / 26
Mackerel Formation /4	Shallow Marine	962 / 394	904 / 370	737 / 301	481 / 197
Note in all column height calculations P, T, Salinity, densities, and IFT all constant for each sample					

2.1.7 Effect of Solubility of CO_2 on Seal Capacity

The solubility of CO_2 in water increases with increasing pressure, decreasing temperature and decreasing salinity. As a result, a significant amount of the trapped CO_2 dissolves in the formation water over time and a significant portion of the CO_2 dissolves into the formation water over 10000s and 100000s of years depending on the reservoir and fluid properties. Maximum solubility (~58 kg/1000 litres) occurs within a window around 20 MPa at 40ºC with <10,000 ppm salinity (after Ennis-King and Patterson 2003; Span and Wagner 1996; Rowe and Chou 1970).

Reservoir simulations have shown that saturated CO_2 water becomes dense and sinks, countering the buoyancy effects of CO_2. An example of this phenomenon is discussed by Daniel and Kaldi (2009), who show that the calculated differences in column heights using fresh water and CO_2 saturated water indicate an increase in CO_2 retention with an increase in water density due to CO_2 saturation.

A study of the Miller Field (North Sea) found that natural CO_2 is dissolved in the reservoir fluids. Most of the CO_2 is present in the water phase (60-70 mol %) and the remainder in the oil phase (15-25%), which effectively increases the densities of both these phases (Baines and Worden, 2000). In general, however, where depleted oil reservoirs or deep saline reservoirs are used for storage, the main form of trapping initially will be the dissolution of CO_2 into the formation water. The remainder will rise and be trapped beneath the cap rock seal and then migrate outwards to fill the trap. As more CO_2 dissolves into the water it will become increasingly denser and may set up a downward trending convection current, depending on the homogeneity of the reservoir. As this occurs, it also results in lowering the buoyancy pressure at the reservoir / seal interface. Over time, as CO_2 dissolution increases, the buoyancy force will decrease and the CO_2 column height retention of the original caprock/reservoir system will increase.

Seal capacity calculations are commonly dependent on poorly defined subsurface fluid properties. Therefore, sensitivities for variability in contact angle, interfacial tension, formation water density and CO_2 density must be used to calculate seal capacity.

2.2 Seal Geometry

Seal geometry relates the structural position, thickness, and areal extent of the caprock to that of the reservoir and/or structure. Where the caprock's areal extent is equal to or greater than the areal extent of the reservoir or structure, (ie the caprock overlies the entire reservoir / structure), the membrane properties of the caprock seal are in effect throughout. Similarly, as caprock thickness increases, the likelihood of sub-seismic through-going faults or fractures decreases. Seal geometry is estimated by integrating seismic and core data, detailed well correlations, regional sedimentological/stratigraphic relationships and making comparisons to known depositional analogs. Seal integrity refers to geomechanical properties such as ductility, compressibility, and propensity for fracturing. Rocks with high seal integrity, such as salts and anhydrites are generally better seals than brittle rocks such as dolomite or quartzite. Seal integrity can be measured in a laboratory or evaluated qualitatively by core examination, borehole imaging and petrographic studies.

The areal extent component is estimated by comparing areal extent of the seal to the estimated areal extent of trap closure for structural and stratigraphic traps or aquifer area for saline aquifer storage. Where the sealing lithology covers the closure and the seal capacity does not significantly vary laterally, a low risk is assigned to the areal extent component. Kaldi and Atkinson (1997) described the geometries of several potential sealing lithologies in a deltaic depositional setting in the Miocene Talang Akar Formation (Figure 2.9).

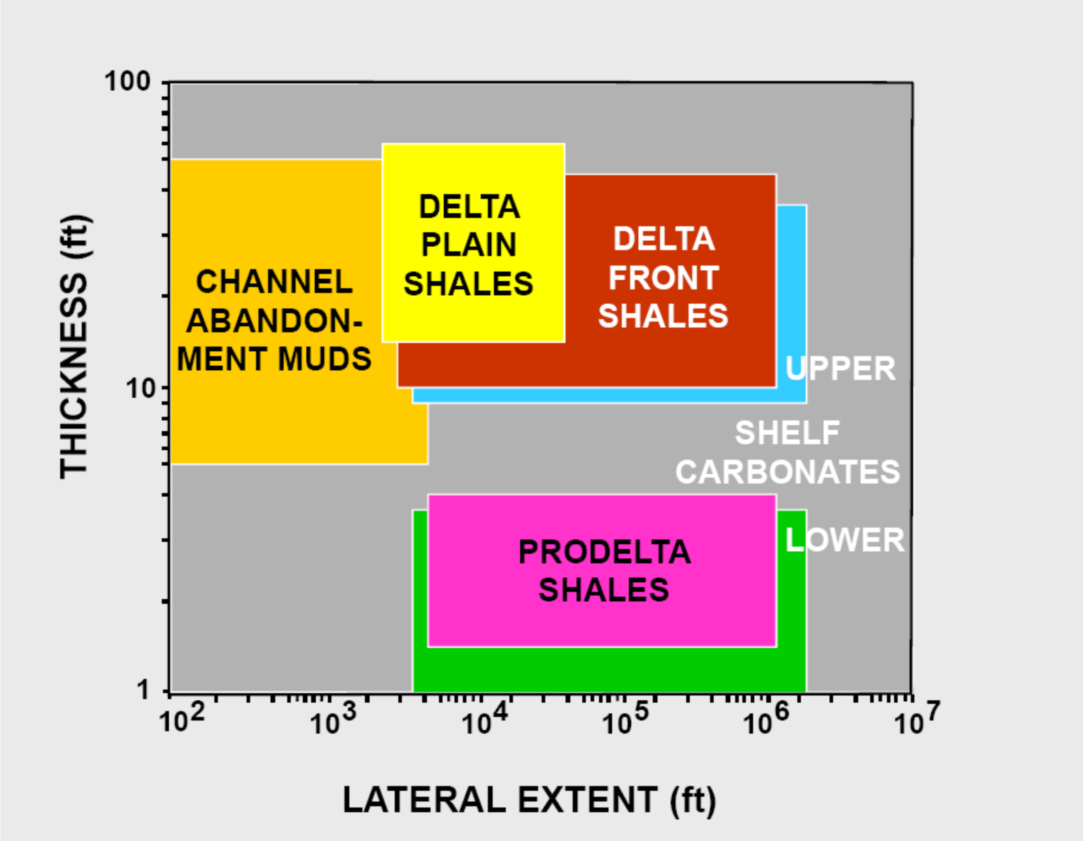

Figure 2.9 **Example of geometry of caprock lithologies in deltaic depositional settings, Miocene, Talang Akar Formation, Indonesia (after Kaldi and Atkinson, 1997).**

Seal thickness is included in the assessment of seal geometry. In theory the properties of a membrane seal should control the seal capacity of the caprock even where that caprock is only a few millimetres thick. However, the chances of such a thin seal extending over significant distances, without a fracture or offset or sedimentary discontinuity, is very small. Kaldi and Atkinson (1997) suggest that the minimum thickness of a caprock to minimise the risk of structural (fault) offset or erosional pinch-out is that thickness required for the seal to be resolved seismically. In other words, if the caprock is visible on seismic, any fault offset or erosional discontinuity can be assessed at the particular storage site. Thus, where the structure is dependent on fault seal, having the thickness of the caprock greater than the fault throw increases the confidence of seal integrity. Fault seal risk methods are presented in the section on geomechanics.

2.2.1 Geometry of Stratigraphic Traps

Subsurface containment and storage of CO_2 does not always have to be confined to one single reservoir overlain by a single caprock / seal as discussed above. Indeed when CO_2 is injected into a single thick reservoir, the tendency is for the CO_2 plume to migrate upwards to the seal in a more or less direct vertical pathway (Ennis King and Paterson, 2002). Many basins comprise large scale cyclic sedimentary sequences with depositional environments that contain multiple sedimentary packages of reservoir/seal couplets. Examples of such depositional environments range from braided fluvial systems through tidal flats to the lower shore face and braided fluvial environments, which are likely to form intraformational seals and baffles. Regional caprocks tend to be more areally extensive as exemplified by marine systems ranging from the near-shoreface to the outer shelf and beyond. The stratigraphic architecture and reservoir heterogeneity of such potential storage formation are such that the sandstone packages within the reservoir are commonly separated by thinner muddier siltstone or shale units (intraformational seals) creating varying permeabilities and porosity distributions i.e. stratigraphic heterogeneity. These units or intraformational seals provide a baffling or barrier to vertical migration and increases the possibility of sub-horizontal migration / dispersion away from the injection site, and access to a higher proportion of the storage reservoir pore space depending on the horizontal and vertical extent of the seal. This reduction in vertical permeability creates a more tortuous migration pathway for the CO_2 enhancing residual gas trapping, dissolution and more effective use of the potential storage volume (Gibson-Poole et al., 2009).

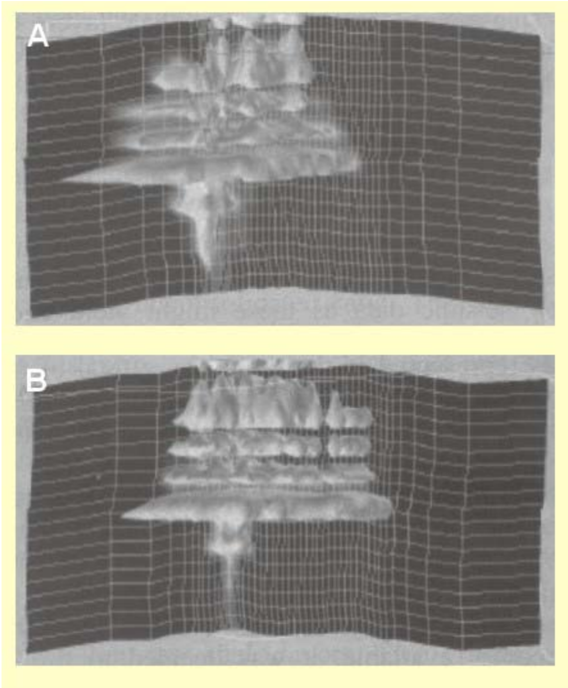

Figure 2.10 **Numerical flow simulation of CO_2 injection at Sleipner Vest Field, which has been history matched with time lapse 3D seismic reflection data. Two perpendicular cross-sections of a simulation result are shown (A & B). Intra-reservoir shale units (intraformational seals) act as barriers to vertical $scCO_2$ migration (Figure from Van der Meer et al., 2000).**

The architecture of such deposits generally consists of a series of smaller reservoirs (depending on the cyclicity) separated by sealing lithologies, which act as baffles to slow down the migration of CO_2 by increasing the tortuosity of the migration pathway of CO_2 to increase the effectiveness of each reservoir and maximise residual and geochemical trapping (Van der Meer et al. 2000; Flett et al., 2004; Benson and Cook, 2005; Gaus et al., 2005; Hovorka et al., 2004; Root, 2007; Ambrose et al., 2008; Gibson-Poole et al. 2009; Varma et al. 2009). Figure 2.10 shows numerical flow simulation results from the Sleipner Vest Field, in which intra-reservoir shale units (intraformational seals) act as barriers to vertical $scCO_2$ migration (Van der Meer, 2000).

Ambrose et al. (2007) noted that there are a variety stratigraphic and structural factors that can control heterogeneity in the subsurface to help or hinder the storage of carbon dioxide. Using examples of geological heterogeneity from oil and gas reservoirs, they have reviewed a series of depositional environments to evaluate the potential for CO_2 storage from both the reservoir and caprock capacity and integrity. There are numerous oil and gas reservoir characterisation studies highlighting the relationships between stratigraphic heterogeneity, internal reservoir architecture and fluid recovery (Galloway and Chen, 1985; Tyler and Ambrose, 1985; and Ambrose et al., 1995). These studies describe the relationships between depositional environments and recovery efficiencies, focusing on intraformational seals and seal pinch-outs, and the resulting increase in tortuosity for fluid migration. For CO_2 storage, this would contribute to greater CO_2-rock contact. Galloway and Chen (1985) and Tyler and Ambrose (1985) describe the Frio Formation stratigraphy in great detail, leading to selection of the Frio Formation as a pilot CO_2 storage project.

Ambrose et al. (2007) describes in detail the beach and near shore facies of the Frio Formation with respect to porosity and permeability, especially the areas of low poro/perm in the heterogeneous tidal inlet and back-barrier facies. These fine grained sediments of the tidal and back-barrier facies are highlighted as contributing to compartmentalisation of the reservoirs, as they act as either intraformational caprocks or as facies for enhancing tortuosity for the migration of injected CO_2. Increased heterogeneity is also described from mixed load fluvial systems, resulting from the juxtaposition of complex sand bodies and intraformational mud drapes which serve as baffles and barriers to migrating fluids.

An example investigated by Root, (2007) and expanded by Gibson-Poole et al (2009) highlights sequences of interbedded sandstones and shale/siltstones from the Paleocene to Eocene Latrobe Group in the Kingfish, Snapper, Barracouta Fields regional area of the Gippsland Basin in South Eastern Australia (Figure 2.11) which are regionally sealed by the overlying Lakes Entrance and the Gurnard Formations (Figure 2.12). The Latrobe Group is further subdivided into four subgroups of repetitious non-marine to marine depositional sequences, the upper section, the Cobia and Halibut Subgroups comprising the Burong, Gurnard and Turrum, Barracouta, Kingfish, Flounder and Mackerel Formations were the focus of the study (Figure 2.12).

These formations consist of alluvial and coastal plain facies; adjacent shallow marine wave dominated deltaic systems with back-barrier lagoons, barrier shorelines, and protected embayments (Root, 2007). The Burong and Kingfish Formations are comprised of reservoir facies interspersed with intraformational seals. Whereas the Flounder and Turrum Formation are local to seals with the Gurnard acting as a seal, thief zone or low grade reservoir depending on the local depositional environment (Gibson–Poole, 2009). The intraformational seals of the Burong Kingfish, Mackerel and Flounder Formations from the Latrobe Group are found in the fluvial, coastal plain and near shore marine facies of the reservoir intervals (Figure 2.12).

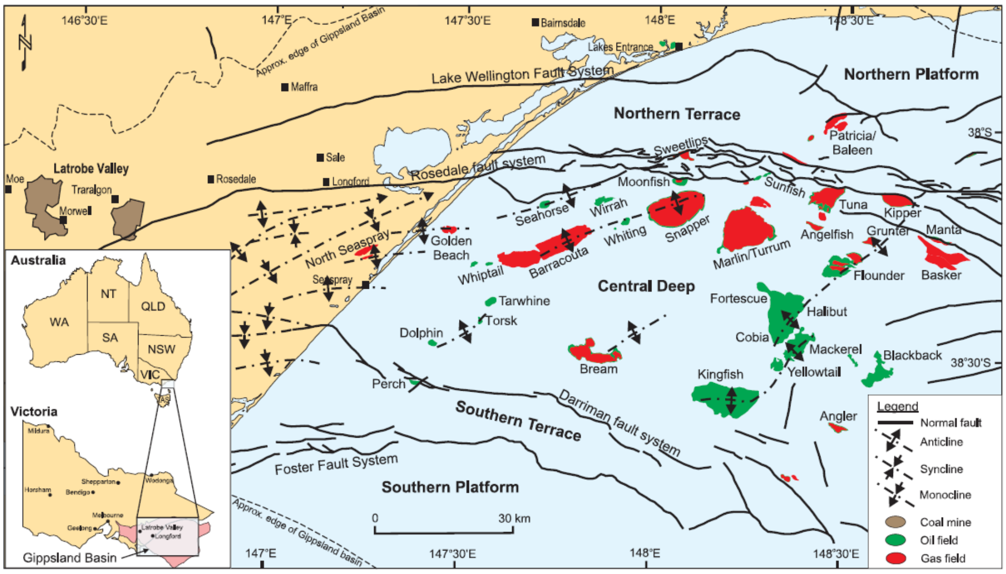

Figure 2.11 Map of the Gippsland Basin showing major structural features and the locations of oil and gas fields. (Figure courtesy of the Victoria Department of Natural Resources and Environment).

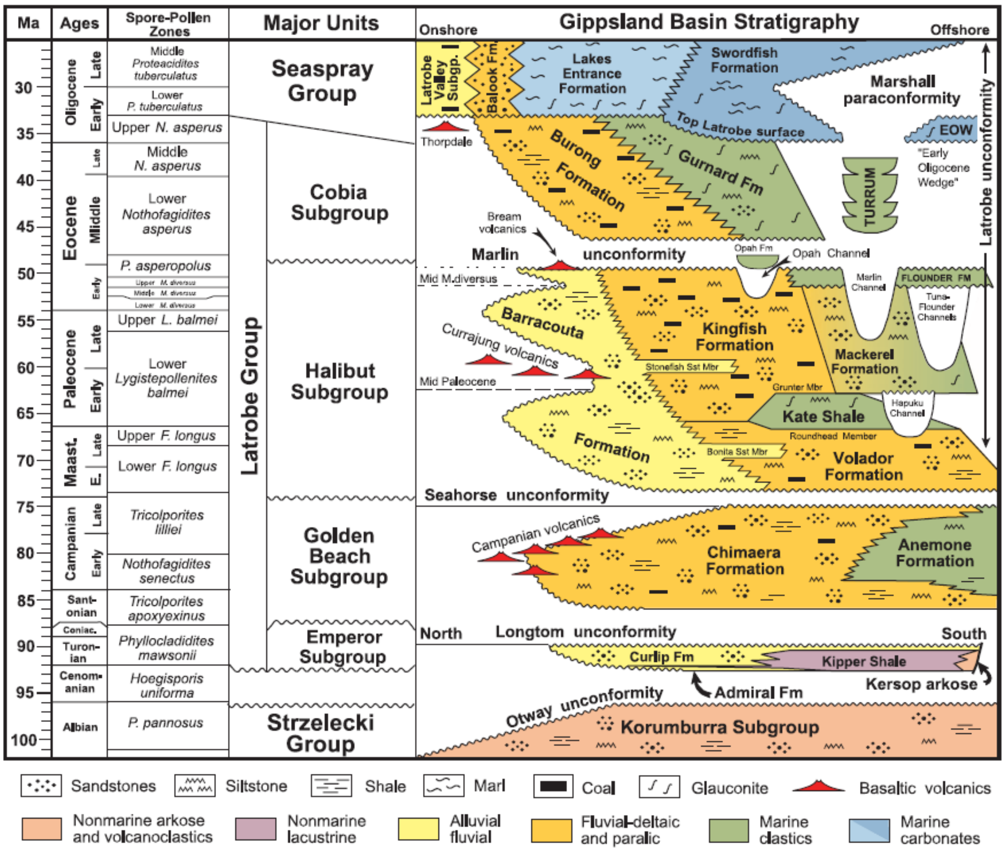

Figure 2.12 Stratigraphic column of the Gippsland Basin (after Bernecker and Partridge, 2001).

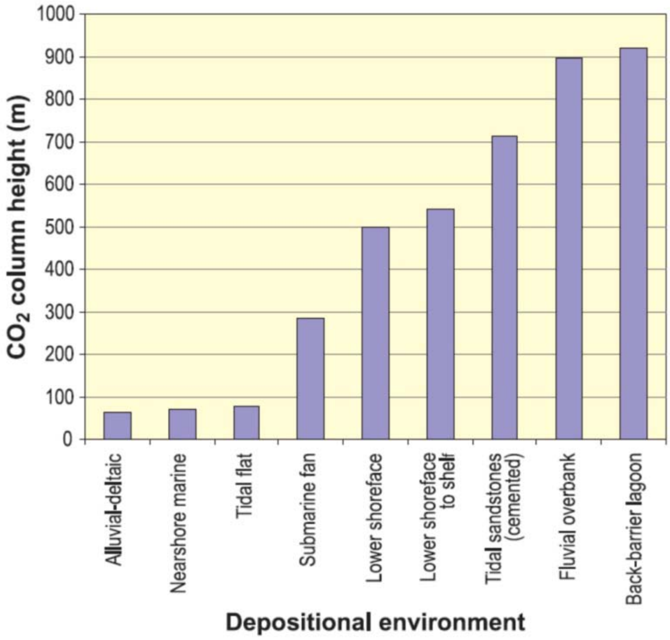

Figure 2.13 Histogram of average retention heights for CO_2 in caprocks from ifferent depositional environments (from Gibson-Poole et al., 2009).

MICP analyses indicate that that these intraformational seals have the ability to contain CO_2 column heights from 53 to 1191m, highlighting the possibility that these seals will provide barriers and baffling to vertically migrating CO_2, encouraging tortuous lateral flow within each of the multiple reservoirs. The potential retention heights of the various intraformational sealing depositional environments indicate that the mudstones from fluvial overbank and back-barrier lagoonal facies provide the most significant barrier to CO_2 migration with alluvial deltaic, near-shore marine and tidal environments showing weak baffling capabilities (Figure 2.13) (Root, 2007 and Gibson-Poole et al., 2009).

The lateral distance that injected CO_2 can migrate is dependent on the areal extent of the intraformational barriers and baffles. Graphed analog data sets are an ideal method to demonstrate the possible extent of sub-horizontal CO_2 migration under a seal of limited areal extent. Root (2007) compiled an extensive set of data on modern and ancient depositional environments from around the world to demonstrate the areal extent of potential seals and baffles (Figure 2.14). These data show very clearly the extents of various sealing/ baffling facies along with their thicknesses, which can help to determine, at a first pass, the sealing/baffling potential of these facies and the tortuosity of the migration route (Figure 2.15).

An important factor associated with most heterogeneous reservoirs/seal couplets is the occurrence of labile or reactive permeable sediments, which are usually found in the transition between ideal reservoir and seal couplets. These labile sediments contain minerals such as pyrite, goethite, chlorite, berthierine glauconite and dolomite, which act as a source of potential permanent mineral trapping of CO_2 through the precipitation of ferroan carbonate minerals (Gibson-Poole et al., 2009).

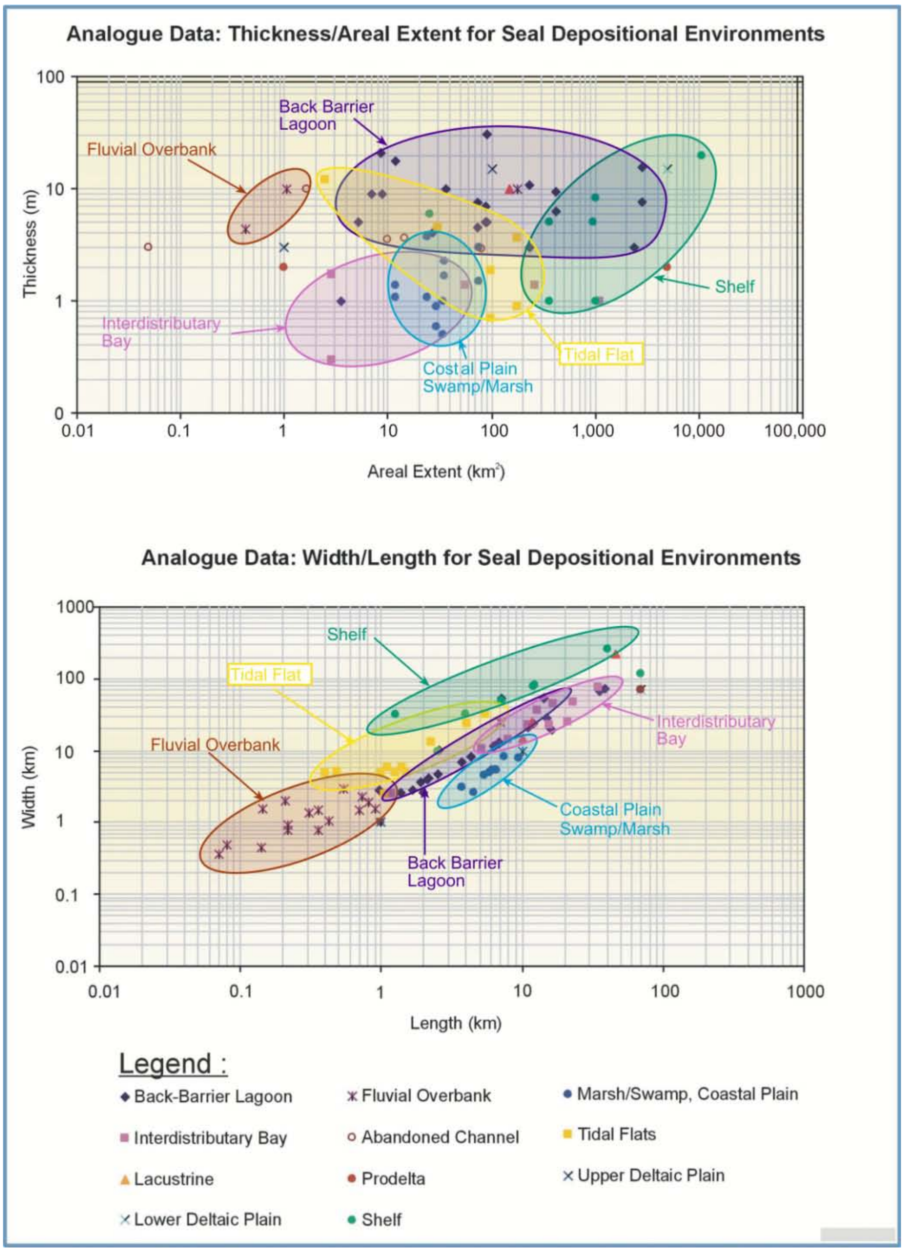

Figure 2.14 **Scatter plots of thickness versus areal extent and width versus length of fine-grained facies for various depositional environments derived from modern and ancient analog data (Gibson-Poole et al., 2009 modified after Root, 2007).**

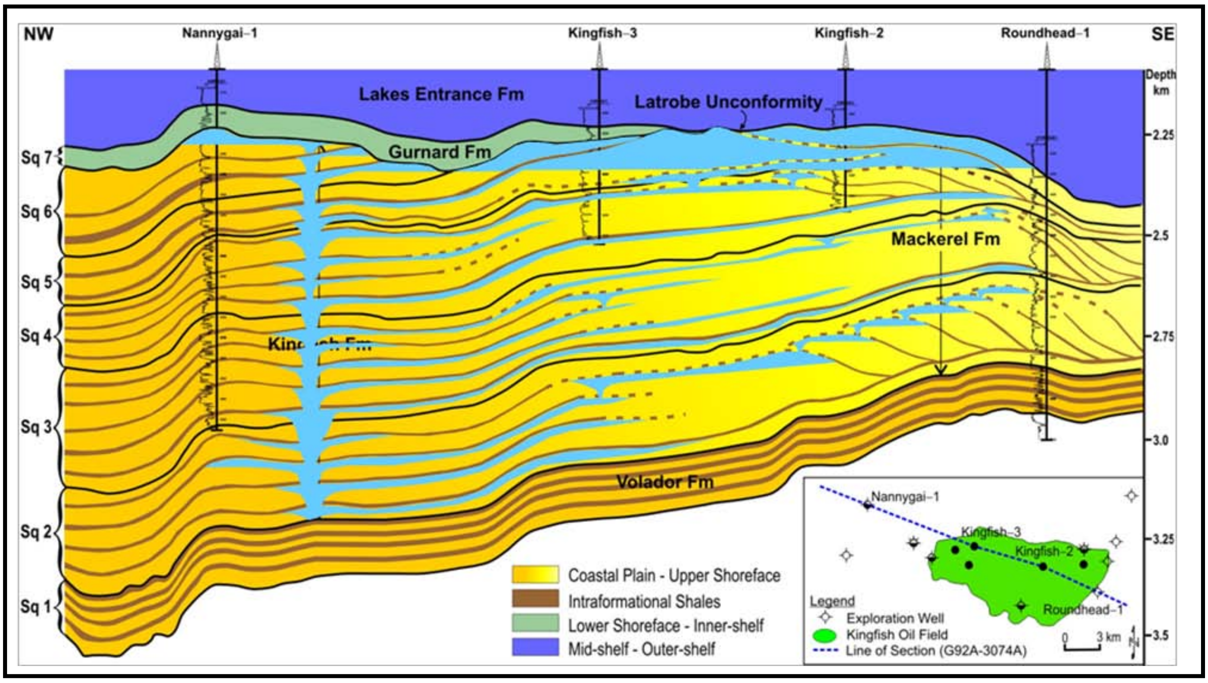

Figure 2.15 **Migration pathways concept of intraformational seals or baffles – increasing the length of CO_2 migration pathway (tortuosity); increasing the volume of pore space moved through, and a greater possibility for residual gas trapping and dissolution. Notional injected $scCO_2$ pathways - light blue; regional caprocks – Lakes Entrance Fm (dark blue) and Gurnard Fm. (green). From Gibson-Poole et al., 2009.**

2.3 Seal Integrity

Seal integrity refers to geomechanical properties of the caprock and is considered as the caprock propensity to develop structural permeability (Sibson, 1996) and is related to the presence or absence of fluid conducting fractures, and particularly in the case of caprock systems for CO_2 containment, the risk of creating new fractures or reactivating previously existing faults.

Seal integrity is a function of lithology, pre-existing planes of weakness, regional stresses, and orientation and magnitude of induced stress from fluid injection or withdrawal activities. Ductility/compressibility are inversely related to the sonic velocity/strength of a lithology (Stearns and Friedman, 1972). Figure 2.16 shows the relative ductility/compressibility and strength/velocity properties of various lithologies. These properties are calibrated using Integrity Factor (1.0 – 0) from upper left to lower right on the figure. Rocks such as halite and organic shales are the most ductile and compressible and have the lowest rock strength and slowest sonic velocities and have Integrity Factors approaching 1.0. These caprocks are thus the least likely to develop structural permeability, based on the assumption that conductive fractures are less likely to form in ductile lithologies. As the carbonate content or the siliciclastic composition of the caprock increases, the Integrity Factor decreases and the propensity to develop structural permeability also increases.

These properties are controlled by caprock mineralogy, regional and local stress fields as well as any stress changes induced by injection or withdrawal of water or CO_2. The modification of the stress field within a storage formation during and after injection of CO_2 can lead to reservoir and caprock mechanical failure. This failure can produce compaction or expansion of the rocks in the reservoir or seal and may result from a number of processes including generation of new faults and fractures, reactivation of faults and bedding parallel slip. The presence of faults and their extent within caprock formations can be determined by seismic reflection techniques and analysis of well core or well bore imaging. Stresses within the caprock can be estimated from literature (e.g., Hillis & Reynolds, 2000) or through site specific well analyses (borehole breakout, leak-off or extended leak-off tests). The effects of induced stress changes are determined via geomechanical / rock physics analyses (Mildren et al., 2005). Geomechanics of caprocks are addressed in detail in Section 3.

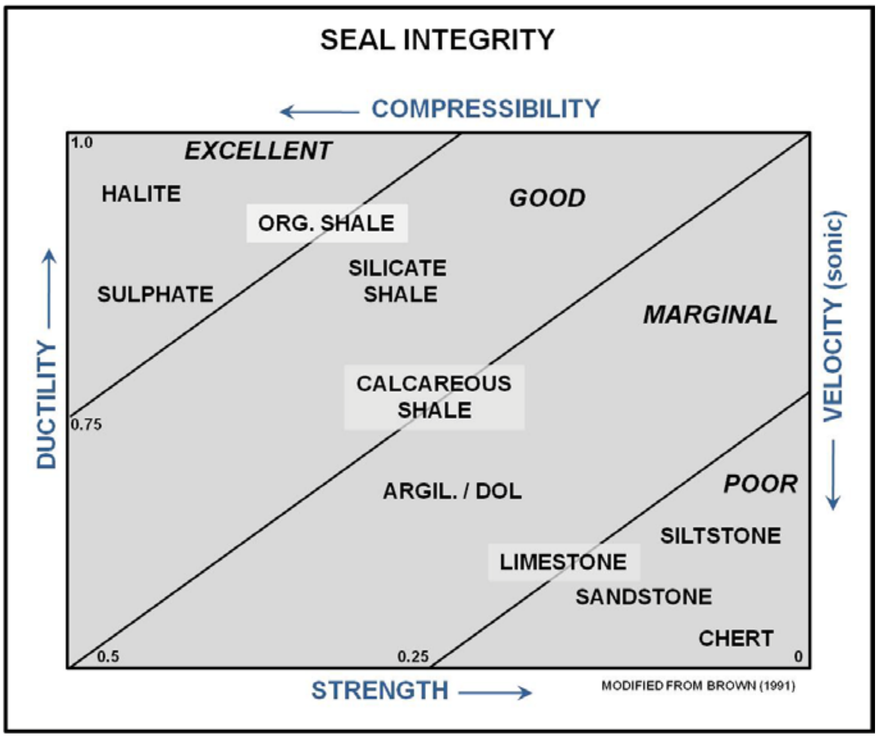

Figure 2.16 **Schematic showing the relative ductility and compressibility vs strength/sonic velocity of various lithologies. A relative Integrity Factor (IF) can be assigned (1.0 to 0 from upper left to lower right on the figure).**

The presence of conducting fractures is a qualitative assessment that should incorporate data such as core analysis, sidewall core petrographic analysis, across seal pressure differential, well bore image data (FMS/FMI/CBIL) and ultimately a combined stress field and rock strength evaluation.

2.4 Practical Applications of Seal Potential Assessment

This section outlines the methods employed to determine seal potential for caprocks for a regional to prospect scale storage evaluation. Seal potential has been defined and applied to provide a basin scale seal ranking. Thus, values for seal properties are assigned and can be compared between individual basins, structures or sites. The seal potential value represents a relative ranking and does not necessarily represent the probability of an effective seal. Top seal and lateral seal risk should be assessed on a prospect by prospect (site by site) basis using the factors in seal potential as a guide to seal properties (Kivior et al., 2002).

Nakanishi and Lang (2001, 2002) presented an approach to prospect risk analysis using the risk assessment matrix shown in Table 2.7, which is applicable to regional to prospect scale seal potential evaluation.

A confidence value for each component is allocated when estimating seal potential. This confidence value is assessed by the expression of the presence of each factor based on a geological interpretation and the quantity and quality of the data supporting the interpretation (Nakanishi and Lang 2001, Rose 2001). For each component used to determine seal potential, a qualitative assessment is made (e.g. ‘good’ or ‘bad’) and data quality and quantity is assigned (e.g. ‘moderate’ or ‘enough’) thus providing an interpretive value for each component using Table 2.7. Thus, the SP is represented as a product of all components as shown in the above relationship.

2.4.1 Practical Seal Capacity

The definitions for the seal capacity geological criteria and the data quality and quantity criteria are presented in Table 2.7, 2.8 and 2.9. Seal capacity is measured for numerous samples in the caprock. Based on measurements, sidewall core descriptions, cuttings descriptions and well log character the seal capacities are also estimated from other wells in each caprock. Vertical closure estimates are used from well completion reports and seismic structure maps. Where no valid trap is found, (i.e. migration trap in a saline aquifer) an estimated vertical structural closure height can be used. This value would be based on averaging the known vertical structural or stratigraphic closures in the proposed storage area.

Table 2.7 Risk matrix for expression of the existence of seal potential components and quality and quantity of information, 'X' represents 'more than even' or 'less than even' (after Nakanishi and Lang, 2002).

		Expression of the existence of seal potential components				
		Very bad	Bad	Even	Good	Very good
Quality and quantity of information	Plentiful	0.000	0.250	x	0.750	1.000
	Enough	0,125	0.313	x	0.638	0.875
	Moderate	0.250	0.375	0.500	0.625	0.750
	Poor	0.375	0.438	0.500	0.563	0.625
	Very poor	x	x	0.500	x	x

Table 2.8 Qualitative definitions for seal capacity (Kivior et al., 2002)

Very Good	Seal capacity = 100% (or more) of structural closure.
Good	Seal capacity between 50 and 100% of structural closure.
Bad	Seal holds back less than 50% of structural closure.
Very Bad	Not a sealing lithology (i.e. sandstone)

Table 2.9 Qualitative assessment for seal capacity data quality and quantity (Nakanishi and Lang, 2001)

Plentiful	Measured MICP value for seal capacity
Enough	Side wall core, cuttings descriptions and well log motifs suggest the type of seal present is the same as a directly measured seal from the same formation in a different well (analogue, rock catalogues).
Moderate	Existing well data are not enough to confidently estimate seal capacity.
Poor	There are no well data and seal capacities are estimated from a general geological concept of the area
Very Poor	No data & no geological concept – pure guess

Table 2.10 Qualitative definitions for Seal Geometry: areal extent (Kivior et al., 2002).

Very Good	Seal covers entire structural closure and seal lithology is uniform and homogeneous over structure
Good	Seal covers top of closure and most of structure and minimal lateral change in seal lithology
Bad	Seal does not cover structure and/or significant lateral variation in lithology
Very Bad	No seal lithology is present on top of structure

2.4.2 Practical Seal Geometry

Areal Extent **-** The definitions of the geological criteria applied to the areal extent of a seal are listed in Table 2.10. The areal extent of the top seal can be estimated from well log correlations, seismic interpretation, outcrops as well as depositional models made from modern analogues. The criteria used to evaluate the data quality and quantity of the areal extent component is listed in Table 2.11.

Seal Thickness - The definitions of the geological criteria applied to seal thickness are listed in Table 2.11. Seal thickness can be determined from well logs, biostratigraphy and cuttings descriptions. Minor fault throws are estimated from seismic data, well completion reports and published structure maps. The criteria used to evaluate the data quality and quantity of the seal thickness component is listed in Table 2.12.

Table 2.11 Qualitative definitions for Seal Geometry: thickness (Kivior et al., 2002)

Very Good	Seal thickness significantly greater than any fault throws observed in top seal.
Good	Faults in top seal offset the top seal (fault throw ~ 25 and 75% of top seal thickness)
Bad	Fault throws significantly offset top seal (fault throw >75% of seal thickness)
Very Bad	Fault throw is greater than seal thickness.

Table 2.12 Qualitative assessment for seal geometry data quality and quantity (Nakanishi and Lang, 2001)

Plentiful	Well and seismic data prove the existence of the geological factor.
Enough	Well and seismic data suggest existence of geological factor.
Moderate	Existing well and seismic data are not enough to provide confidence of existence of geological factor.
Poor	No well or seismic data, the expression of the geological factor comes from a general geological concept of the region.
Very Poor	No data & no geological concept – pure guess

2.4.3 Practical Seal Integrity

Ingram and Urai (1999) presented a method for determining a Brittleness Index (BRI) which is based on the assumption that a brittle mudrock is anomalously strong compared to normally consolidated rocks at the same depth. They defined a ductile mudrock as one that can deform without dilatancy and associated creation of fracture permeability, whereas a brittle mudrock was defined as one that dilates during deformation and allows fracture permeability to develop. Thus, a brittle mudrock was assumed anomalously strong compared to normally consolidated rocks at the same depth. Based on this assumption the brittle or ductile nature of a rock can be estimated from a rock's unconfined compressive strength. This method can be applied to estimate the brittleness of seal rocks in the storage area.

The BRI is calculated as a ratio (Equation 2.9) of the estimated in-situ unconfined compressive rock strength of the seal lithology (UCS) and the unconfined compressive strength of a normally consolidated rock at the same depth UCS_{NC}.

$$BRI = \frac{UCS}{UCS_{NC}} \qquad \text{(Equation 2.9)}$$

Brittleness index compares unconfined compressive strength of a rock to the unconfined compressive strength of a normally consolidated rock at the same depth.

Ingram and Urai (1999) presented empirical data that correlate unconfined compressive strength to p-wave velocity data for mud-rocks. The resulting correlation is shown in (Equation 2.10) where UCS is the unconfined compressive strength of a rock and v_p is the p-wave velocity.

$$\log UCS = -6.36 + 2.45\log(.86v_p - 1172)$$ (Equation 2.10)

The effective pressure corresponding to normal consolidation at depth estimates UCS_{NC} (Ingram and Urai (1999). The effective vertical stress, which is the vertical stress minus the pore pressure, was used to calculate UCS_{NC}. The relationship of vertical stress (σ_v) to depth (Equation 2.11) needs to be determined. This can be derived from graphing in situ pore pressures to calculate the hydrostatic pressure gradient, and hence the pressure gradient in the storage area.

$$\sigma_v = 10 \wedge \left(\frac{\log\left(\frac{depth}{62.759}\right)}{0.9197} \right)$$ (Equation 2.11)

In order to calculate BRI for seal rocks the empirically derived equation relating unconfined compressive strength to p-wave velocity can be assumed to hold for seal rocks in most regional storage areas.

Table 2.13 Qualitative definitions for Seal Integrity using brittle index (BRI) to estimate rock strength and likelihood of adequate seal integrity (Kivior et al., 2002)

Very Good	1<BRI<2
Good	2<BRI<4
Bad	4<BRI<6
Very Bad	6<BRI<8

Seal integrity can be estimated for a regional area by taking the mean BRI for each seal interval where well logs are available. BRI values above 4 are considered to be brittle (Ingram and Urai 1999). The definitions for seal integrity component geological and data quality and quantity criteria are presented in Table 2.13 and 2.14 respectively. Based upon these criteria a seal integrity component value is obtained and can be included in the assessment in Table 2.7.

Table 2.14 Qualitative assessment for seal integrity data quality and quantity (Nakanishi and Lang, 2002)

Plentiful	Data prove that fluid conducting fractures either exist or do not exist.
Enough	Data suggest that fluid conducting fractures either exist or do not exist.
Moderate	Data provide information on the rock properties, such as propensity of the seal to fracture, but no information on the actual existence of fractures.
Poor	The propensity of the seal to either contain or not contain fluid conducting fractures comes from a general geological concept of the region.
Very Poor	No data & no geological concept – pure guess

A BRI value does not necessarily indicate the presence of open fluid conducting fractures and thus a brittle rock may retain a hydrocarbon column Ingram and Urai (1999). The data quality and quantity level based on BRI values can thus be estimated for determining seal integrity (Table 2.14). Whereas the BRI index is one method for comparing seal integrity from site to site or prospect to prospect, it is by no means the only one or even the recommended methodology. Many other approaches to evaluating risk of loss of integrity are discussed in the Geomechanics section (Section 3) of this study.

3. Geomechanics

Successful prediction of the migration of CO_2 injected into the subsurface requires information about the rock units within, and surrounding, the injection target. Potential storage sites commonly comprise a reservoir and an overlying low permeability mudstone-dominated seal or caprock, which provides a barrier to the upward flow of fluids (Kaldi & Atkinson, 1997), (Chapter 2, this report). Core samples from these mudstone units can provide information about their sealing capacity, however, where the caprock is fractured, faulted or penetrated by disused wells its bulk permeability may be modified. It is important, therefore, to determine under what circumstances, and to what extent, faults and fractures in a caprock would increase its bulk permeability and reduce the ability of underlying reservoirs to store CO_2 for 1000 years or more.

Faults and fractures are widely acknowledged to locally modify rock permeability and may enhance or retard the flow of fluids (e.g., Odling et al., 1999; Manzocchi et al., 1999, 2008, 2010; Aydin, 2000; Wibberley et al., 2008; Faulkner et al., 2010). These studies generally focus on rock types that form hydrocarbon reservoirs (e.g., sandstones) and suggest that the same faults/fractures may represent barriers and conduits to flow. Precisely how faults and fractures will impact on fluid flow is dependent on many factors, including the permeabilities and relative permeabilities of fault rock and host rock, the pressure and temperature conditions of the reservoir and fluids, and the fracture geometries (e.g., dimensions, interconnectedness and apertures). Given the rheological differences between sandstones (reservoir) and mudstones (caprock), the permeabilities and geometries of fracture networks may change from one rock type to another.

The impact of conductive fracture systems on the bulk flow properties of otherwise low permeability caprocks is dependent on a variety of issues such as the aperture distributions and connectivity characteristics of the fracture system. These factors determine under what circumstances, and how, faults (and fractures) in mudstone caprocks are likely to impact on bulk permeability. In this section we will undertake a literature review of the key fault and fracture parameters that could impact on the ability of caprocks to prevent CO_2 from migrating out of the primary storage container. Here we address four main topics;

1. Basics of Geomechanics and Rock Failure,
2. Faults and Fracture Distributions,
3. Modelling Individual Faults,
4. Geomechanical Response of Seals during Injection.

3.1 Basics of Geomechanics

One of the big challenges facing the CO_2 storage community is to determine to what extent and under what conditions faults and fractures could result in the migration of CO_2 through caprocks. Faults and fractures have long been known to strongly influence rock permeability and the sub-surface movement of fluids and gas (e.g., Wade, 1913; Illing, 1942; Neglia, 1979; Sibson, 1990, 2000; Downey, 1984; Aydin, 2000; Bolas and Hermanrud, 2003; Crossey et al., 2009; Dockrill and Shipton, 2010). Therefore, they could also affect the flow of CO_2 at geological storage sites. Over the past 20 years many studies have focused on understanding the potential of faults to impede the lateral flow of fluid and gas (e.g. Yielding et al., 1997; Manzocchi et al., 1999, 2010; Eichhubl et al., 2009). These studies indicate that faults, which are typically barriers to lateral fluid flow, have the potential to trap migrating CO_2 and to compartmentalise CO_2 storage reservoirs, impacting on CO_2 injection and containment. Faults and fractures can also act as conduits to fluid migration enhancing their up-sequence flow and influencing the ability of caprocks to contain CO_2. In many of the world's petroleum provinces, for example, these structures are inferred to enhance the up-sequence flow of hydrocarbons through thick (e.g., >200 m) mudstone-dominated seal rocks (e.g., Cartwright et al. 2007). It is clear, however, that not all faults (and fractures) and certainly not all parts of faults, promote the up-sequence flow of fluids. It is widely accepted in the hydrocarbons and minerals industries that fluid flow is generally channelised (e.g., Carruthers and Ringrose, 1998). Understanding why parts of faults and fractures focus flow and others do not is essential for successfully determining CO_2 migration pathways and containment risk. The details of how, where and why faults and fractures compromise caprock integrity are still largely unresolved (e.g., Cartwright et al. 2007). Providing answers to these questions will help us to understand better the circumstances under which faults and fractures leak up-dip and the locations where they are likely to result in the migration of CO_2 through caprocks.

Faults and fractures may result from ancient tectonic processes, future natural earthquakes or induced earthquakes resulting from overpressurisation of the reservoir during injection (e.g., Shapiro and Dinske, 2009; Faulkner et al., 2010, and references therein). Here we discuss the stresses that result in faulting and fracturing, the geometries of fault and fracture networks, and how these may impact on the migration of CO_2, particularly into or through the caprock. The section first outlines rock deformation concepts and processes, the identification and description of natural fault and fracture systems, and the impact of stress changes due to CO_2 injection on fracture development and caprock geomechanics. Consideration of these processes may have implications for CO_2 containment risk at storage sites.

3.1.1 Rock Failure

Subjected to stress, geological formations deform in a way determined by their mechanical properties, the stress rate, temperature and pressure condition. Strain is a measure of the change in shape of a material in response to stress. Normal strains (strains perpendicular to a plane) result in lengthening or shortening of the rocks, while shear strains result in changes in the angles between pairs of lines in the material. In general, stressed rocks will follow a similar stress-strain curve. For example, relatively well-cemented sandstones exhibit nearly ideal elastic behaviour over a considerable range of applied stresses. At first, closure of micro-cracks triggers a small curvature in the stress-strain curve, before the rock exhibits a linear elastic behaviour. As pressure increases, the stress applied is non-recoverable, and the rock is permanently damaged. Permanent deformation initially takes the form of plastic deformation which occurs until rock failure by formation of faults and fractures (e.g., Byerlee, 1978; Zoback, 2007). Faults and fractures form when the intensity of stress overcomes the strength of the rock. Rock failure in compression and tension are very different. As tensile strength is generally quite low in sedimentary rocks, most rock strength tests are compressive in nature. Most predictions of compressive failure in rock structures are made on the basis of the failure of cylinders of rock under compression in laboratory tests. Zoback (2007) provides a clear and complete list of definitions and procedures for rock testing. Commonly, failure criteria for rocks are based on peak stress of triaxial test curve, derived from triaxial tests. The failure stress for a solid cylinder under ambient pressure is often described as either:

- Unconfined compressive strength ($\sigma1>\sigma2$, $\sigma2=\sigma3=0$), is the most common measurement of strength for rocks, where the sample is simply compressed axially (Zoback, 2007). Failure is generally violent and easy to define.
- Uniaxial compressive strength ($\sigma1>\sigma2=\sigma3$): most common test to measure rock strength in conditions that are simulating conditions prevailing at depth. The strength of the sample at a given confining pressure is the differential stress at which it fails.

Many factors influence failure in rocks, including:

- stress and pore pressure
- sample size and shape
- moisture content of sample
- defects in sample, stiffness of loading system, strain rate, friction on sample surfaces

3.1.2 Determination of the Stress Tensor at Depth

The stress field within the Earth can be represented as a tensor, which describes the density of forces acting on all surfaces passing through a given point (Jaeger et al., 2007). In three dimensions, the stress tensor has 9 components, each of them representing a force acting in a specific direction on a unit area of given orientation. Conveniently, the stress tensor is compatible with a stress field where three components of stress are acting normal to the surface (the normal stresses), and six components of stress are acting along the surface, or shear stresses. In equilibrium, the shear stresses acting on opposite faces are equal, and the tensor can be describe using only six stress magnitudes. Furthermore, the stress tensor can be expressed in any coordinate system via a tensor transformation. This transformation is important for evaluating the stability of a fault plane, or its propensity to slip under a given stress field. The stress field is generally described by the principal stresses, which are the stresses acting in the principal coordinate system. In this system, the shear stresses vanish. For ease of use, one of the principal stresses is chosen to be normal to the Earth's surface, with the two principal stresses being in the horizontal plane (Zoback and Zoback, 1980; 1989; Zoback, 1992). It is therefore possible to express the local stress field using the magnitudes of the vertical stress, and two horizontal stresses (maximum and minimum horizontal stresses). Knowledge of the magnitude of the three principal stresses and the direction of the maximal horizontal stress is sufficient to fully describe the in-situ stress field at depth (e.g., Zoback, 2007).

The relative magnitude of the greatest, intermediate and least principal stress at depth, namely σ_1, σ_2 and σ_3 in terms of the vertical stress ($\sigma_{v)}$, the maximum horizontal stress (σ_{Hmax}) and the minimum horizontal stress (σ_{hmin}) define three different stress regimes, following the scheme originally proposed by E.M. Anderson (1951)(Table 3.1).

Table 3.1 Relative magnitudes of σ_v, σ_{Hmax} and σ_{hmin} define the faulting regime of a reservoir/cap rock system (Anderson, 1951)

Regime	Stress		
	σ_1	σ_2	σ_3
Normal	σ_v	σ_{Hmax}	σ_{Hmin}
Strike-slip	σ_{Hmax}	σ_v	σ_{Hmin}
Reverse	σ_{Hmax}	σ_{Hmin}	σ_v

The stress field is generally determined by measuring the magnitudes of the three principal stresses, while the orientations of the principal horizontal stresses can be determined by analysing borehole breakouts and drilling induced tensile fractures in image logs. In vertical wells, borehole breakouts form at 90° to σ_{Hmax} and tensile fractures form parallel to σ_{Hmax}. The general assumption is that the overburden corresponds to one of the principal stresses (which is generally true), with σ_v being determined from the integration of density logs from well. σ_3 is obtained from mini-frac tests and leak-off tests during drilling (e.g., Brudy et al., 1997). Note that generally, σ_3 corresponds to σ_{hmin} (apart in case of a reverse stress regime). The magnitude of S_{Hmax} is typically the hardest stress magnitude to measure and must be derived from borehole failure features in conjunction with mini-frac tests and theoretical relationships involving the tensile strength properties of the rock.. However, observation of indirect geological indicators or focal mechanisms of earthquake can also provide important clues to the orientation and nature of the stress regime. In interpreting these data we must however be mindful of the fact that pre-existing faults can locally perturb the orientation and magnitude of the in-situ stress field. The orientations of the different principal stresses are, for example, often rotated around pre-existing faults (Morley, 2010). Knowledge of the mechanical characteristics of the rocks, the pore pressure at depth as well as the in-situ stress field of the regions where these rocks are hosted is crucial for evaluating the geomechanical risks associated to geological storage of CO_2. Following a strict and rigorous methodology, it is possible to determine these key parameters for further investigation.

3.1.3 The Effective Stress Concept

Injection of CO_2 invariably results in some degree of fluid overpressurization with respect to the hydrostatic gradient. If the system is pressurized sufficiently, then a number of deleterious effects may be observed such as fracturing of the reservoir or caprock or reactivation of previously existing faults. These physical weaknesses in the system arise due to the pore fluid pressure counteracting the forces from the in situ stress field and are a manifestation of a reduction in the system's effective stress state. The effective stress concept was first developed by Terzaghi (1943) for soil systems, where an increase in pore fluid pressure results in an equally reduced effective stress on the rock mass (e.g., Engelder, 1992), In such cases, reduction of the three principal stresses due to such pore fluid pressures results in elevated shear/normal stress ratios on virtually all planes within the rock mass (assuming a non-isotropic stress field), thereby shifting the system closer to shear failure. Similarly, elevated fluid pressures also shift the system closer to the tensile failure condition. This can be understood graphically by use of a Mohr diagram (Figure 3.1, figure 3.11a). Although the effects of elevated fluid pressures mainly have implications for localized failure within the reservoir formation, any shear or tensile fractures generated within the reservoir would have the potential of propagating into the overlying cap rock. As pointed out by Rutqvist and Tsang (2005) shear or tensile failure in a stress regime where the minimum stress is in the horizontal plane will lead to failure along a plane that is oriented near-vertically, a condition that is not favourable when preventing vertical migration of CO_2 is the main goal.

Changes in pore pressure and confining stress tend to modify the physical properties of rocks, namely strength, porosity, permeability, and seismic impedance (e.g., Sayers, 2010). The effective stress is therefore defined in relation to the stress tensor and pore pressure P_p by:

$$\boldsymbol{\sigma'_{ij} = \sigma_{ij} - \alpha P_p \delta_{ij}} \qquad \text{(Equation 3.1)}$$

Where α is an effective stress coefficient referred to as the Biot coefficient, δ_{ij} is the Kronecker delta ($\delta_{ij} = 1$ if i=j, 0 otherwise). For soft sediments, α is close to 1, and the effective stress can be defined by (Terzaghi, 1943):

$$\boldsymbol{\sigma'_{ij} = \sigma_{ij} - P_p \delta_{ij}} \qquad \text{(Equation 3.2)}$$

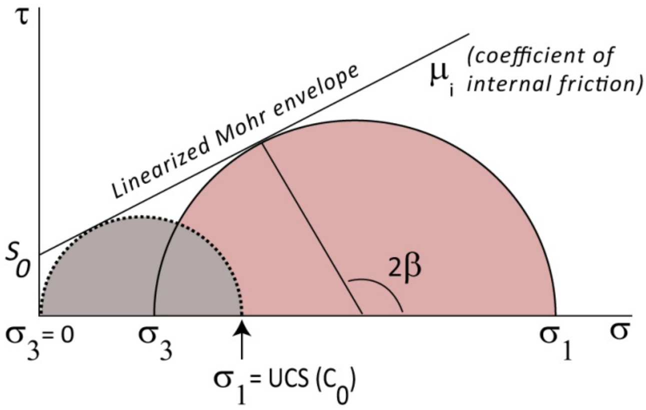

Figure 3.1 **Mohr diagram and Mohr envelope for two rock samples: the brown sample is unconfined and the pink sample under some confining pressure at depth. UCS: Unconfined Compressive Strength. Modified from Zoback (2007)**

3.2 Faults and Fractures

Faults and fractures typically form arrays which have the potential to displace both CO_2 reservoirs and caprocks. These structures may form due to a range of processes including; far-field plate motions, folding, gravitational sliding, volcanic intrusion, crustal unloading associated with uplift and anthropogenic activities, such as fluid injection or extraction. In this section we focus on faults and fractures that predate CO_2 injection which may enhance and/or retard the rates of fluid migration. In many cases these structures are of tectonic origin. In order to determine the impact faults and fractures have on CO_2 migration two key questions must be addressed. These are; 1) what are the locations, geometries, displacements and permeabilities of faults and fractures in the proposed reservoir and caprock units and, 2) to what extent will these faults and fractures impact (either positively or negatively) on the flow of CO_2 during and after injection. These questions have been examined mainly from a petroleum industry perspective in a number of review papers (e.g., Aydin, 2000; Jolley et al., 2007; Walsh et al., 2009; Faulkner et al., 2010; Manzocchi et al., 2010), while Dewhurst et al. (1999) present some discussion of faults and fractures in mudrocks. Here we focus on the detection, prediction and flow properties of faults and fractures as described in the literature. Attention is given to open fractures which may strongly influence fluid flow and are of particular importance for the migration of CO_2 through caprocks. The following discussion examines fractures that locally develop in association with larger faults and fractures formed by more regional processes. For the purposes of this report the term fracture refers to faults with displacements below the resolution of the available data and to joints, which are considered to be fractures that exhibit no appreciable shear displacement at outcrop scale.

3.2.1 Fractures in Fault Zones

Numerous studies in petroleum and mineral exploration indicate that fault displacement can locally increase fracture densities within fault zones (or fault damage zones) that have the potential to increase fluid flow. These increases in fracture densities can, for example, arise due to changes in the mechanical properties of the host rock, to interactions between faults and to changes in fault geometry (e.g., Sibson, 1990, 2000; Downey, 1984; Bolas and Hermanrud, 2003; Gartrell et al., 2004; Leckenby et al., 2005; Crossey et al., 2009; Eichhubl et al., 2009; Kim and Sanderson, 2010). Fault-related open fractures capable of influencing fluid flow and clay-rich fault rock associated with the primary fault slip surface(s) are considered to be parts of fault zones, which are also widely referred to in the literature as fault damage zones (e.g., Caine et al., 1996; Kim et al., 2004; Childs et al. 2009)(Figure 3.2).

Faults and fractures in fault zones typically form anastomosing networks of interconnected surfaces which are often sub-parallel to the primary slip surface (e.g., Walsh et al., 2009). One or more of these slip surfaces may be associated with clay-rich fault rock (also referred to as fault core, e.g., Caine et al., 1996). The thickness of fault rock can vary locally over the fault surface and generally increases with fault displacement (e.g., Hull, 1988; Childs et al., 2009). This variability could produce changes in horizontal permeability across the fault. In general, however, fault rock tends to have low horizontal permeabilities (e.g., <0.01 mD) which, in sandstone lithologies, are typically less than those of the host rock and provide lateral barriers to fluid flow, particularly on hydrocarbon production timescales (e.g., Yielding et al., 1997; Walsh et al., 2009; Faulkner et al., 2010). These barriers have the potential to elevate pressures adjacent to faults which could induce across and along fault fluid flow. Dynamic fluid-flow modelling is required to examine the interplay between reservoir pressures and fracture dilation.

The spatial distribution of open fractures is also variable in fault zones with the highest densities of fractures focused where the fault changes geometry, such as at bends and steps (e.g., at relays), at fault intersections and near to fault tips (e.g., Gartrell et al., 2004; Leckenby et al., 2005; Childs et al., 2009; Eichhubl et al., 2009)(Figure 3.2). In cross section bends or steps in the fault surface often occur at lithological boundaries. Changes in the surface geometry of faults are typically characterised by locally high displacement gradients and/or by displacement lows (e.g., Childs et al., 1995). High gradients and displacement lows could signify the presence of bed rotations and/or volumetric strains adjacent to the fault, both of which may be associated with fracturing. Therefore, analysis of variations in displacement coupled with mapping of fault-surface geometry could provide a means of predicting the locations of dense arrays of open fractures.

Spatial changes in fault zone permeability could arise in part due to changes in the densities and connectivity of small-scale open fractures (e.g., Eichhubl et al., 2009). Regions of high fracture densities are most likely to contain interconnected fracture networks which produce elevated permeability and provide important conduits for the up-sequence migration of CO_2 (e.g., Neglia, 1979; Crossey et al., 2009; Dockrill and Shipton, 2010). More research is required to test this model; however, if it proves correct then vertical migration of CO_2 from the storage reservoir would be most likely at fault tips, steps, bends or intersections (Figure 3.3). This model is consistent with analysis of veins which tend to be thicker, and suggest greater dilation at, fault steps, bends or intersections (e.g., Kim et al., 2004; Kim and Sanderson, 2010).

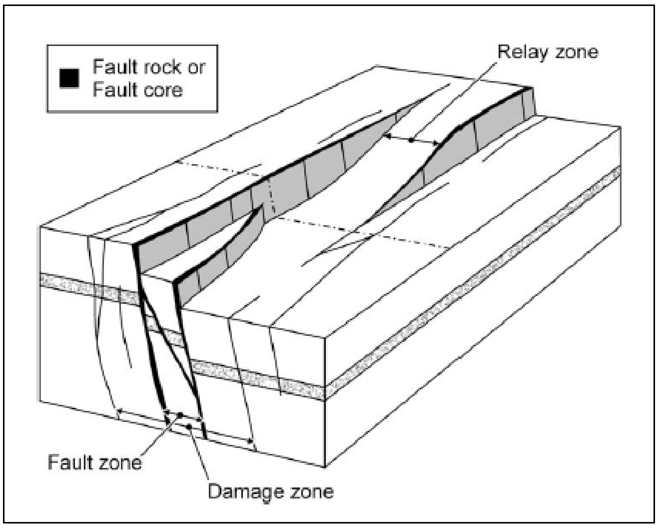

Figure 3.2 **Schematic diagram illustrating fault structure together with the meaning of the terms fault rock, fault core, fault zone, damage zone and relay zone (Childs et al., 2009). Relatively high densities of open fractures could be expected in the fault-bound lense at the front of the block diagram and in the relay zone.**

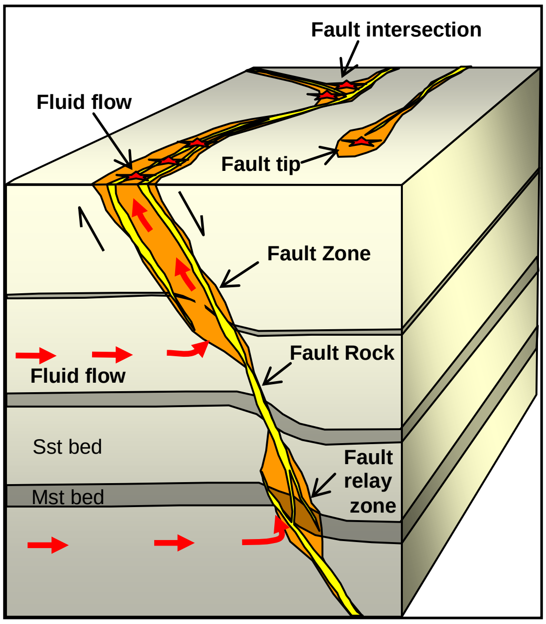

Figure 3.3 **Schematic block diagram showing fault zone architecture and potential fluid flow paths along sandstone beds and open fractures within fault zones. Densities of conductive fractures are highest at a number of sites within fault zones including, fault relay zones, fault intersections and fault tips.**

3.2.2 Regional Fractures

Many fractures do not form in association with larger faults and are of regional extent (e.g., Price, 1966; Engelder and Geiser, 1980; Hancock, 1985). These fractures, which in many cases are considered to be joints, can be curved or planar and generally comprise parallel or sub-parallel sets (e.g., Figure 3.4). Multiple cross-cutting fracture sets are often observed in a single outcrop. These fractures can range in spacing from millimetres to metres and lengths from metres to kilometres. In many cases, fracture spacings for individual sets are approximately uniform, however, line samples across multiple fracture sets with different orientations and containing the shortest fractures generally have negative exponential or random spacing distributions (e.g., Gillespie et al., 1993). Both the approximately uniform spacing of larger fractures (e.g., >5 m length) and the random spacing distribution of all fractures are highlighted by visual inspection of Figure 3.4. Fracture apertures are typically difficult to measure in outcrop because of gravitational and weathering processes. Rough measures of fracture apertures can be gained from core or image logs, drilling mud losses, wireline logs or combining porosity with fracture density (see Makel 2007 and references therein). Fracture apertures are likely to increase with injection of CO_2 and associated rises in reservoir/caprock pressures.

In addition to fracture aperture, the dimensions and connectivity of fractures are also important for fluid flow. There are many examples where the majority of fractures are contained within individual beds (i.e. stratabound fractures) and have spacings proportional to bed thickness (e.g., Ramsay and Huber, 1987; Bai and Pollard, 2000). While these fractures may locally increase porosity and permeability, they need not significantly increase the bulk permeability of caprocks beyond an individual bed. Of greatest importance for fluid flow are those open fractures that have large surface areas (e.g., km^2), pass from the reservoir through the caprocks and intersect many other smaller fractures. These larger fractures, which have been referred to as master joints or master fractures (e.g., Ramsay and Huber, 1987), may focus or channelise CO_2 migration and have the potential to accommodate Darcy flow (see flow rates section for further discussion). The expected numbers of master fractures in a given CO_2 storage site may be dependent on a range of parameters including, the relative and absolute rheology of individual beds in multilayer sequences together with the tectonic setting and stress conditions under which the fractures formed.

Understanding whether master fractures are present at CO_2 storage sites and, if they are, in what densities may be of importance for assessing caprock integrity.

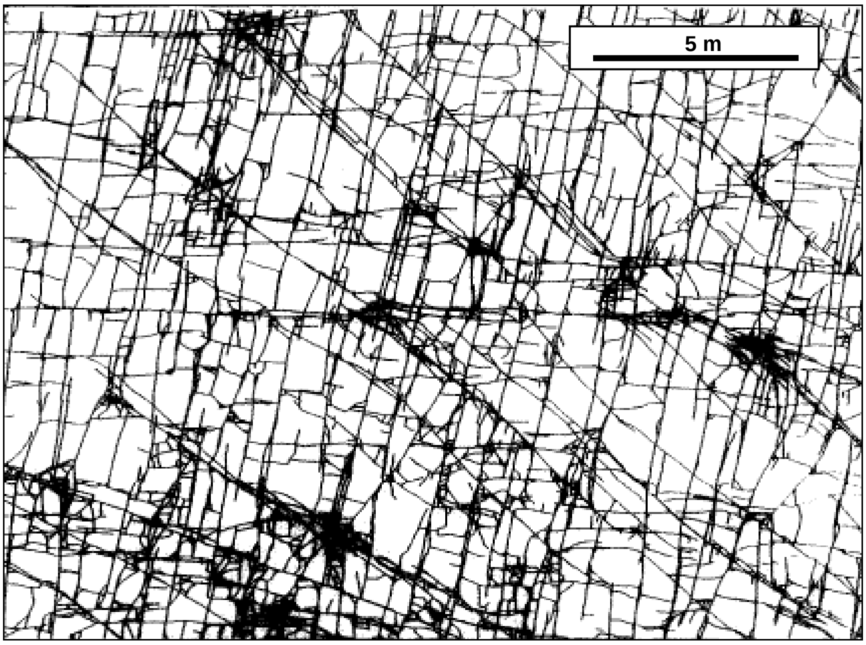

Figure 3.4 Map of joints exposed on a sandstone bedding plane from Whinney Hill Quarry, Lancashire, United Kingdom (Gillespie et al., 1993).

3.2.3 Folds and Fractures

Many potential CO_2 storage containers are located in the crests of anticline culminations and could contain fold-related fractures that pose a risk to caprock integrity. Fold–fracture relationships have been extensively studied over the last 50 years (e.g., Price, 1966; Ramsay and Huber, 1987; Price and Cosgrove, 1990) and a conceptual model for these relationships is presented in Figure 3.5. Key elements of these models are that the fractures generally dip at a high angle to bedding, the dominant fracture sets are parallel and orthogonal to the fold hinge (although conjugate faults at a high angle to the fold hinge are also common), and the highest density of fractures occurs in the region of greatest fold curvature (typically along the fold hinge). This last observation underpins the use of fold curvature analysis as a means of predicting fracture densities associated with folding (e.g., Lisle 1994) (see Detection and Prediction sections for further discussion). The patterns of fractures depicted in Figure 3.5 may be further complicated by the presence of fractures which pre or post date folding and by fractures clustered around faults which may, or may not, be related to folding. Which of these fold-related fracture sets are open may, in part, be related to the present-day tectonics and stress regime. Active folding promotes extension and open fractures along anticline hinges (Ramsay and Huber, 1987; Price and Cosgrove, 1990; Lisle, 1994). In addition, it is often the case that conductive or open fractures, whether they are formed in association with folds, regional stress fields or locally near to faults, strike perpendicular to the *in-situ* minimum compressive stress direction (Jolly et al., 2000).

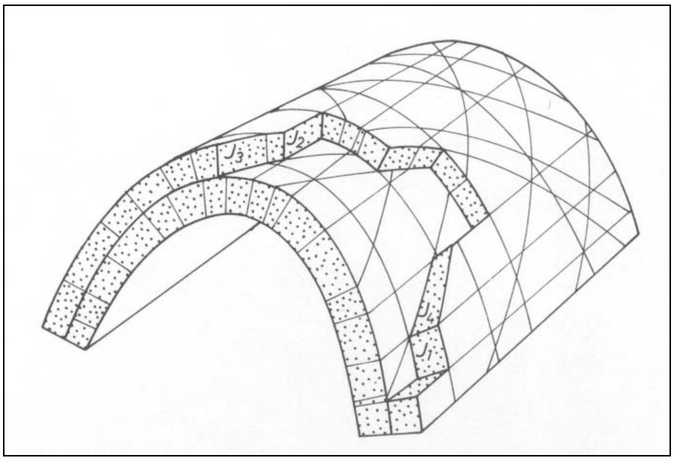

Figure 3.5 **Schematic diagram illustrating the relationships between folding and joints (Ramsay and Huber, 1987). Joint surfaces are stippled and bedding surfaces unstippled.**

3.2.4 Detection of Faults and Fractures

Being able to locate faults and fractures is a key component of establishing their potential impact on the containment and migration of CO_2. The locations and geometries of faults and fractures in hydrocarbon reservoirs and at CO_2 storage sites have been examined using a range of techniques, including; seismic-reflection lines, image-log interpretation (e.g., FMI or acoustic logs), well-core analysis and seismic-wave anisotropy (e.g., Jolley et al., 2007; Makel, 2007). In addition to these techniques horizon-curvature analysis and fault-population analysis may be used to predict the approximate locations, strains and numbers of faults/fractures below the resolution of the available seismic-reflection data.

Interpretation of conventional seismic reflection lines, time slices and coherence cubes are the standard petroleum industry technique used to image hydrocarbon reservoirs. Three-dimensional (3D) seismic-reflection data with a line spacing of 12.5 m is likely to be a requirement of most CO_2 storage sites and typically permits faults with vertical displacements as small as 5-10 m to be unambiguously resolved. For seismic-reflection datasets that image faults it can be expected that many more faults will have vertical displacements below the resolution of the data (e.g., Yielding et al., 1992). In addition, the tip regions of seismically-imaged faults, which are often elliptical in shape with a sub-horizontal long axis (e.g., Nicol et al., 1996), will be below the resolution of the data. The length of seismically-imaged faults that is sub-resolution is typically of the order of 400-500 m or 200-250 m at each tip (e.g., Meyer et al., 2002). Thus, the proportion of the fault below the seismic resolution increases with decreasing maximum vertical displacement. It should also be noted that the seismic resolution of faults can decrease in mudstone-dominated sequences with low seismic reflectivity. Despite this issue 3D seismic-reflection data represent the best available technique to determining the locations, geometries and displacement of faults in caprock at CO_2 storage sites. Seismic-reflection interpretation may also assist in the identification of fault bends, steps (or relays) and intersections which could be sites of relatively dense fracturing of the caprock and may locally increase its permeability (e.g., Kim et al., 2004; Childs et al., 2009; Eichhubl et al., 2009; Kim and Sanderson, 2010)(Figure 3.3).

Four dimensional (time lapse) seismic-reflection surveys have been used to follow depletion of hydrocarbon reservoirs and to track the location and dimensions of injected CO_2 plumes (e.g., Chadwick et al., 2009), including their relations to caprocks and mapped faults. Experience from Sleipner suggests that CO_2 can illuminate heterogeneities, so that even very small faults (e.g.$\lesssim$5 m vertical displacement) which were previously undetectable may be visible after CO_2 injection. The results from Sleipner are consistent with data from petroleum basins where gas has been imaged. Recent developments in the analysis and interpretation of high quality 2D and 3D seismic-reflection data provide a means of mapping gas chimneys and drawing conclusions about the migration of gas in both faulted and unfaulted strata (e.g., Heggland, 1997, 2004; Ligtenberg, 2005). These studies indicate that faults often provide migration pathways up through mudstone-rich caprocks. These conduits typically have pipe (rather than sheet) geometries, however, agreement has not been reached about which processes control the locations of these conduits on individual fault surfaces.

In addition to the explicit imaging the largest faults, indications of the presence and orientation of small sub-seismic faulting or fracturing can be obtained from the properties of seismic waveforms. The key requirement of these techniques is to have multi-azimuthal data, which can be obtained from high-fold conventional land 3D seismic, from purpose-acquired 2D seismic (e.g., a star configuration around boreholes) and from multi-azimuth Vertical Seismic Profiles (VSP). Multi-azimuthal seismic data provide an 'integrated' measure of rock-mass properties (rather than resolving individual faults), with the fast direction of seismic waves inferred to be parallel to the strike of open fractures. More sophisticated methods employing seismic shear-wave 'splitting' or 'birefringence' could also provide important information on the strike, density and apertures of fractures which are too small to be resolved individually in seismic-reflection lines (e.g., Maultzsch et al., 2003). As with conventional seismic-reflection data time-lapse datasets enable changes in the seismic properties to be tracked, providing insights into changing-rock mass parameters and fluid flow, both within the reservoir and through the caprock.

In the petroleum industry analysis of small sub-seismic fractures is typically conducted using image logs (micro-resistivity and ultrasonic tools are primarily used to generate electrical and acoustic images, respectively) and core from wells (e.g., Chueng, 1999; Makel, 2007). Analysis of faults and fractures observed in core and images of borehole walls represent one-dimensional samples of the fracture population which is strongly dependent on the angle between the well inclination and the dips of the fracture sets. They are of greatest value when data are available from multiple wells, the wells are oriented at a high angle to the main fracture sets and the data completeness is high. These data could contribute to an improved understanding of: 1) fault and fracture geometries and locations (both absolute and relative to the stratigraphy), 2) fault and fracture scaling properties from seismic to borehole scales, 3) fault permeabilities and, 4) fracture aperture widths.

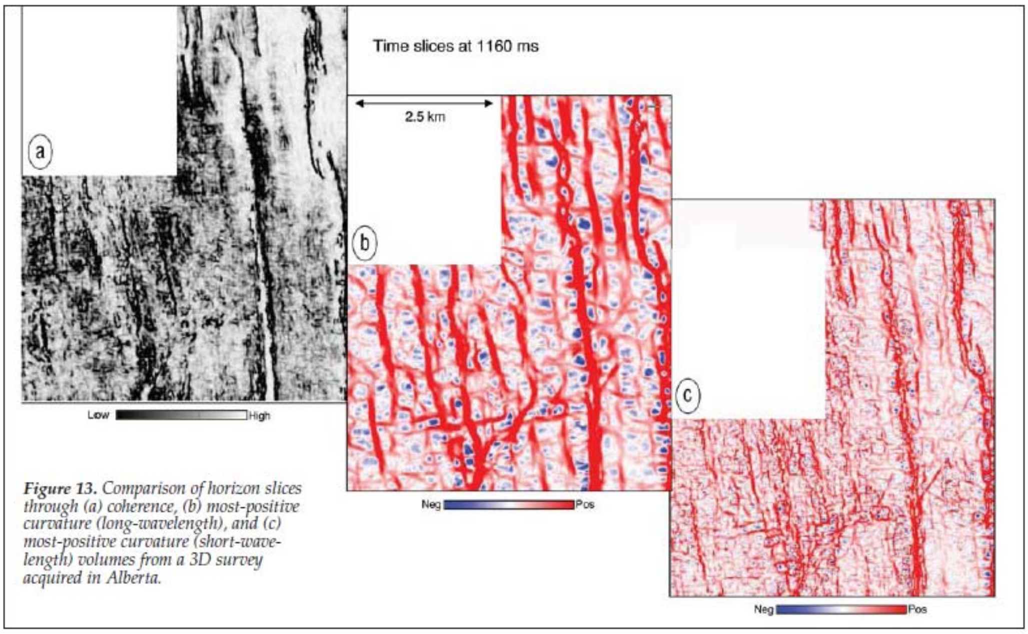

Figure 3.6 **Comparison of horizon time slices for (a) coherence, (b) long wavelength most-positive curvature, and (c) short wavelength most-positive curvature volumes from a 3D seismic reflection survey in Alberta (Chopra and Marfurt, 2007).**

In recent years, curvature analysis has been applied to processing of seismic-reflection volumes for the purpose of imaging fractures that would otherwise be unresolved (e.g., Al-Dossary and Marfurt, 2006; Chopra and Marfurt, 2007). Curvature attribute values extracted from seismic volumes enable identification of lineaments on time slices, in some cases in areas where seismic horizons cannot be tracked with confidence, and little information on fault/fractures would otherwise be available. Figure 3.6 compares the results from coherence with the most-positive long-wavelength and short-wavelength curvature analyses. Visual inspection of time slices supports the view that curvature analysis is capable of imaging both the larger faults identified in the coherency time slice and smaller fractures that are below the resolution of conventional seismic reflection images. Confidence in the technique can be further improved by comparing fracture orientations from seismic-curvature analysis with data from image logs or core data (Chopra and Marfurt, 2007).

3.2.5 Prediction of Faults and Fractures

Fault systems typically comprise many faults with maximum vertical displacements ranging from millimetres to 100s of metres or kilometres and lengths from centimetres to 10s of kilometres. Fault populations from seismic-reflection datasets typically apply to a limited size range defined at the lower bound by the effective limit of seismic resolution and at the upper bound by the largest fault in the sample area (e.g., Yielding et al., 1992). Cumulative frequency vs fault size (e.g., fault length and maximum displacement) curves typically comprise a central straight-line segment over at least one order of magnitude and define a power-law distribution with slopes of 2-3 for two-dimensional samples (e.g., Heffer and Bevan 1990, Yielding et al. 1992 & 1996, Manzocchi et al., 2009). In addition to describing the scaling properties of the fault system and providing a basis for generating synthetic fault systems (e.g., Manzocchi et al., 2009), such curves also permit prediction of the numbers of sub-seismic faults greater than a given size within an area or volume (Figure 3.7). When using cumulative frequency curves to estimate the numbers of sub-seismic faults, care must be taken to ensure that, as far as possible, sampling biases (e.g., length censoring and fault size bias; see Manzocchi et al., 2009) are accounted for. Fracture data from wells may be combined with one-dimensional data sampled from seismic-reflection lines to test the validity of predictions (e.g., Figure 3.7). In the case of Figure 3.7, for example, it can be inferred that the fault/fracture population remains approximately power-law down to the scale of well observations.

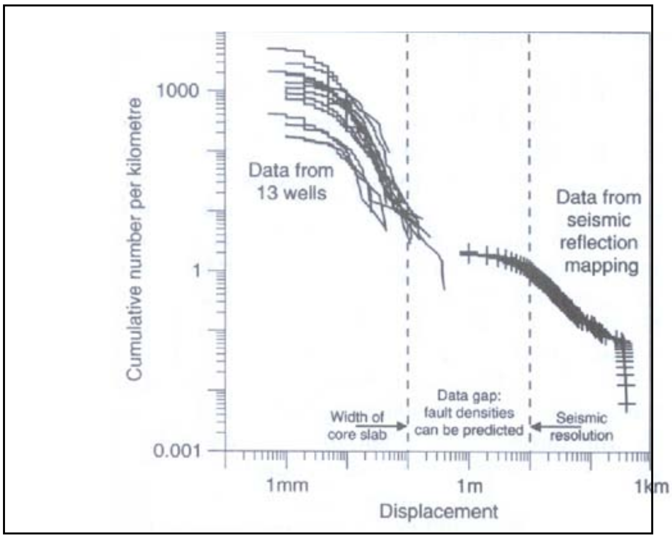

Figure 3.7 **Comparison of fault vertical displacements from a 3D seismic reservoir scale multiple line sample and 13 wells in a hydrocarbon field, offshore United Kingdom (Needham et al., 1996). The slope of the curve for seismic data can be projected across the data gap (faults with vertical displacements of 10 cm to 10 m) into the field of well data. The seismic-scale faults and well-core fractures appear to generally form part of the same**

power-law population, although the spread in well observations suggest that locally there may be departures from the broad scaling properties of the system.

While it is possible to estimate the number of sub-seismic faults (above a given size) using population analysis, their precise locations remain unknown. One approach to this uncertainty in the locations of sub-seismic faults is to randomly position the centres of faults in the reservoir area. Using this strategy multiple fault system models can be constructed to examine the range of possible fault configurations and its impact on fluid flow. Randomly positioned faults are, however, unlikely to routinely account for the clustering (Gillespie et al., 1993) or anticlustering (Ackermann et al., 2001) of smaller faults near larger faults which are sometimes observed in nature. Horizon curvature analysis offers an alternative method for estimating fracture densities across CO_2 storage sites. The principle behind this technique is that rock strains, and associated fracture densities, are highest where horizon curvature is greatest (Lisle, 1994). Curvature measured using a number of methods (e.g., Gaussian, strike, and dip) correlates with fractures observed in outcrop, supporting the utility of the method (Lisle, 1994).

3.2.6 Faults and Fractures in Fluid Flow Models

Modelling of fault and fracture systems is important for characterising fluid flow in the petroleum and groundwater industries (e.g., Odling et al., 1999; Barr, 2007; Manzocchi et al., 2008, 2010; Walsh et al., 2009). Well constructed flow models offer a means of predicting how faulted and fractured CO_2 reservoirs and caprocks will respond to injection. The manner in which faults and fractures influence fluid flow is highly variable and can be dependent on many factors, including, orientations, lithology of the faulted sequence, timing of faulting, type of faulting and stress conditions. To successfully model flow, simulators should incorporate fault and fracture attributes including their locations, dimensions, intersecting relations, permeabilities, relative permeabilities and fault-rock capillary threshold pressure (Manzocchi et al., 2008, 2010).

An important starting point for constructing these models is the generation of a robust three-dimensional reservoir-seal static model which incorporates as much detail as is supported by the available data. Data that might be used to construct such a model are detailed in previous sections and are widely documented in the literature (see Jolley et al., 2007 and references therein). Fault and fracture models generated by the petroleum industry typically incorporate seismically resolvable faults but rarely explicitly include individual sub-seismic faults and fractures. The exclusion of sub-seismic faults and dilational fractures in part arises due to computational limitations of the software, which define the minimum size of grid blocks, limitations in the time available to setup and run the models, and also to our limited knowledge of where to position these structures and what flow properties to assign to their surfaces. Sub-seismic structure is, however, incorporated into static fluid flow models by modifying the flow properties of the grid blocks. In CO_2 storage systems more work is required to ensure that the up-scaling of fault/fracture flow properties to those of grid blocks produces geologically reasonable results.

Assigning realistic flow properties to fault surfaces is a crucial step for correctly modelling the flow of CO_2 across and along faults (e.g., Manzocchi, 1999; Sperrevik et al., 2002; Manzocchi et al., 2008, 2010; Walsh et al., 2009). In many sandstone hydrocarbon reservoirs, fault rocks have lower porosity and permeability than the enclosing host rock. In such circumstances the decrease in permeability is thought to arise mainly due to smearing of mudstone beds along the faults, which represent barriers or baffles to lateral flow. A number of techniques have been developed to infer the sealing potential of fault rocks in mixed sand-shale sequences including, calculation of Shale Smear Factors (Lindsay et al., 1993), Shale Gouge Ratios (Yielding et al., 1997) and Clay Smear Potential (Bouvier et al., 1989) together with construction of stratigraphic juxtaposition across fault surfaces. Shale Gouge Ratio (SGR), which is the percentage of clay beds that have passed a given point of a fault surface, is widely used to infer fault rock permeability, with values of 0.2 or above typically corresponding to faults sealing to lateral flow in sandstone-dominated strata (Yielding et al., 1997). SGR values provide a proxy for fault-clay content which can be correlated with capillary threshold pressure and provides a basis for predicting the potential for fault membrane seal (Manzocchi et al, 2010 and references therein). Faults within caprocks that do not completely displace these units are likely to have lateral flow properties comparable to these mudstones. In such cases SGR values will be high (e.g., >0.5) and indicate that fault rocks are likely to be sealing to lateral flow. Similarly, analysis of stratigraphic juxtaposition across faults that do not completely offset caprocks will indicate that these faults are sealing where they displace caprocks. The issue with SGR and juxtaposition analysis is that neither provides information about the up-dip flow properties of fault zones in caprocks; this information is crucial for understanding when and where CO_2 could migrate through the seal.

Because across fault flow is critical to the petroleum industry, algorithms are available for calculating across fault transmissibility in fluid flow models. These transmissibilities are dependent on a number of variables including fault displacement, fault permeability, fault-zone thickness, lithology and heterogeneity of the host rock and the model grid-block size (e.g., Manzocchi et al., 1999). These algorithms permit across fault transmissibilities to be calculated for single-phase flow along all grid blocks in contact with a fault and vary from 0 (fully sealing) to 1 (fully open), sometimes over an individual fault surface. Temporal changes in fault transmissibilities, perhaps associated with fracture dilation facilitated by rising pore pressures, is a desirable component of flow simulations at CO_2 storage sites. At the present time, however, such functionality is not routinely included in flow simulators and may not be a realistic expectation in the near future.

Vertical or up-fault permeability in the reservoir and caprocks is extremely important for CO_2 containment and, although considered in some studies (e.g., Moretti, 1998; Wilkins and Naruk, 2007), are not as well understood as across fault flow. Up-fault permeability will most likely be controlled by the densities, connectivity, clay content and apertures of fractures within fault zones. Because fractures and shear fabrics within fault zones are typically sub-parallel to the principal fault surface, up-fault permeability can be up to three orders of magnitude higher than across-fault permeability (Faulkner and Rutter, 1998). Fault vertical permeability is most likely to exceed host rock permeability when the host rock is fine grained (e.g., in caprocks). Although it is widely recognised that up-fault permeabilities may be crucial for the migration of CO_2 through caprocks, strategies for explicitly incorporating these permeabilities into fluid flow models are not widely identified in the literature. One approach would be to increase transmissibilities along the upper and lower boundaries of grid cells immediately adjacent to faults in flow simulation models. A significant question remains however as to what up-fault permeabilities can be expected for faults and how these estimates should be up-scaled to derive transmissibilities for the grid-cell sizes employed in flow models.

3.2.7 Discussion

Generally, the mere existence of faults should not automatically prohibit geological storage of carbon dioxide. On the contrary, faults commonly trap hydrocarbons and compartmentalize oil and gas reservoirs For example sealing faults compartmentalize gas reservoirs in the Rotliegendes gas fields in the North Sea (Leveille et al, 1997). Sealing faults that successfully trap hydrocarbons could also form suitable confining barriers at CO_2 storage sites. Thus, faults and fractures have the potential to both retard the lateral flow of CO_2 or enhance its vertical migration. In circumstances where these structures predate CO_2 injection they are most often of tectonic origin. The locations, dimensions, geometries and connectedness of open fractures may have particular importance for the flow of CO_2 through caprocks. These fractures form due to a number of processes including, fault displacement, folding and regional stresses. High fracture densities are frequently observed in fault zones where they form in high strain zones at bends or steps in the fault surface, fault intersections and fault tips. Detecting faults and fractures is routinely achieved using 2D and 3D seismic-reflection surveys together with image logs and core analysis. New seismic techniques (e.g., shear-wave splitting and curvature analysis) are also proving useful for detecting faults and fractures, some of which are below the resolution limit of conventional seismic-reflection interpretation techniques. The numbers and densities of sub-seismic faults and fractures can also be predicted using fault-population and fold-curvature analyses. Collectively these data provide a basis for generating 3D fault networks in fluid flow models. These models are important for understanding how faults and fractures may impact on the migration CO_2 from the storage container and through caprocks. While the lateral permeabilities of faults in these models is well constrained by research conducted for the petroleum industry, the up-dip permeabilities is poorly understood. Inclusion of realistic up-dip fault and fracture permeabilities is crucial for producing robust flow models of CO_2 storage sites. For this reason, future studies should focus on characterising these permeabilities, both to understand how they vary with rock type and what factors influence their variability over an individual fault or fracture surface.

Faults and fractures are most frequently observed lithified sandstone or limestone units, perhaps because these rock types are often well exposed (as they are typically more indurated and less easily eroded than mudstones), and because they form hydrocarbon reservoirs which are of particular interest to the petroleum industry. The lack of studies documenting faults and fractures in mudstone-dominated rocks represents a knowledge gap which is likely to limit our understanding of when these structures will negatively impact caprock integrity. Given the rheological differences between sandstones (reservoir) and mudstones (caprocks), the permeabilities and geometries of fault and fracture networks may change from one rock type to another. It is widely observed, for example, that fault and fracture sets are confined to sandstone units and/or are less abundant in mudstone beds or formations (e.g., Ramsay and Huber, 1987; Nicol et al., 1996; Bai and Pollard, 2000). It is also sometimes the case that faults are restricted to mudstone beds (e.g., Gross et al., 1997; Wilkins and Gross, 2002). The available data suggests that stronger rock types most often deform via brittle processes, while weaker rocks are more prone to ductile or plastic deformation. Brittleness index (Zhu and Tang, 2004) provides a means of identifying when caprocks are most likely to fault and fracture (rather than deform in a ductile or plastic manner), and when caprock integrity at CO_2 storage sites could be compromised. For example,, caprocks comprising relatively high carbonate or silica content or that have experienced secondary mineralisation are most likely have a higher brittleness indices and to contain extensive fracture networks. More detailed information is however required on the role of rheology in the occurrence and geometries of faulting and fracturing of mudstone lithologies; this includes establishing the relationship between brittleness index and occurrence (e.g., densities, geometries and displacements) of natural faults and fractures in caprocks. Thus, in order to produce robust flow models for CO_2 reservoir and caprock systems, the architecture and permeabilities of faults/fractures in mudstones should be the target of future study.

3.3 Geomechanical Modelling of Faults

3.3.1 Fault Slip and Dilation Tendency

Variations in effective stress conditions along faults may locally modify their permeability and fluid flow properties. A number of geomechanical parameters, including slip tendency, dilation tendency and fault reactivation potential have been developed for predicting what faults and what parts of faults are most likely to experience perturbations and associated up-dip migration of hydrocarbons.

Morris et al. (1998) defined the tendency of fault surface to slip in a given stress field, as a function of the frictional characteristics of the fault (primarily controlled by rock type) and the ratio of shear to normal stress acting on the surface. The ratio of the shear stress over the normal stress is defined as slip tendency (determined by orientation of the surface within the stress field).

When the resolved shear stress, τ, equals or exceeds the frictional resistance to sliding, *F*, which is proportional to the normal stress, σ_n, and acting across that surface, slip is likely to occur (Jaeger et al., 1979). The cohesive strength of the surface and the coefficient of static friction (μ) will condition whether a fault surface will actually slip. Thus, for a cohesionless fault, at the instant of sliding:

$$F \leq \tau = \mu\sigma_n \qquad \text{(Equation 3.3)}$$

and

$$\mu = \frac{\tau}{\sigma_n} \quad \text{(Equation 3.4)}$$

The slip tendency (T_s) of a surface is then defined as the ratio of shear stress to normal stress on that surface:

$$T_s = \frac{\tau}{\sigma_n} \quad \text{(Equation 3.5)}$$

Thus, the slip tendency depends on the stress field, orientation of the fault surface, pore pressure and strength of the fault (ie, low T_s). As discussed above, increases in pore fluid pressure associated with CO_2 injection will reduce the effective stress and increase the slip tendency. Dilation tendency (Morris and Ferrill, 2009) is the ability of a fracture to dilate, and thus to serve as a potential path for fluid flow. Its ability to transmit fluid is directly related to its aperture, which is in turn related to the effective normal stress acting on the fracture. The effective normal stress imposed on a fracture depends on the magnitude and direction of the principal stresses relative to the fracture plane.

The dilation tendency (T_d) for a surface is defined as (Ferrill and Morris, 2002):

$$T_d = \frac{(\sigma_1 - \sigma_n)}{(\sigma_1 - \sigma_3)} \quad \text{(Equation 3.6)}$$

with σ_1 being the maximum principal compressive stress, and σ_3 being the minimum principal compressive stress.

Therefore, faults oriented perpendicular to the minimum principal stress are most likely to dilate and behave in a transmissive manner with respect to CO_2.The direct implication of CO_2 injection is to modify the pore pressure at depth. Considering that neither the fault orientation nor the regional stress field will be modified during the injection process and for a timescale beyond human life considerations, this variation in pore pressure triggered by the injection of CO_2 at the storage site is one of the defining factors for fault reactivation risk in such settings.

3.3.2 Fault Reactivation Potential

Fault reactivation potential is often estimated using the fault analysis seal technology (FAST), which evaluates the increase in pore pressure (P) required to reduce the effective stress to the point that fault reactivation will theoretically occur (Mildren et al., 2002; Mildren et al., 2005). This method allows integrating of the in-situ stress field, strength of the fault and structural geometry in order to generate maps of the fault reactivation potential at different points on the fault surface.

In the FAST method, failure of the fault is investigated through the potential development of elements of structural permeability (tensile fractures, shear fractures and mixed-mode fractures)(Table 3.2), which provide a flow path for the fluids initially trapped. The risk of reactivation is analysed using the Mohr circle methodology presented earlier and usually assesses the fluid pressure to reactivate a fault in shear mode (eg. Lyon et al., 2005; Reynolds et al., 2005; Vidal-Gilbert et al., 2010). Tensile failure of a fault will only occur if the differential stress is very low, with the fault possessing some degree of cohesion (and therefore tensile strength) As discussed previously, injection of CO_2 and the concomitant increase in fluid pressure shifts the effective stress state of the reservoir and seal closer to the failure envelope which defines the point at which fault reactivation will theoretically occur. The pore fluid pressure which can be sustained before such failure occurs depends on the magnitudes of the principal stresses, the orientation of the different parts of the fault, the friction on the fault and finally the fault cohesion. An example of the FAST technique applied to the CO2CRC's Otway Project is shown in Figure 3.8. In this example from Vidal-Gilbert et al. (2010), an assumption was made that friction was 0.6 and the cohesion of the fault zone was 0 MPa. Fault friction and cohesion are in fact the largest uncertainties when conducting FAST modelling, as fault friction has been shown to be dependent on lithology (Moore et al., 1997; Olsen et al., 1998) and cohesion is likely to change depending on the degree of cementation within the fault zone (Tenthorey and Cox, 2006). As a result of these significant uncertainties, the FAST methodology is probably best used to gain a first pass approximation of fault stability and also to determine locations on the fault that are most prone to reactivation.

Table 3.2 **Failure criteria expressed as a function of pore pressure (Pp). σ_n : Normal stress; τ: Shear stress; $\sigma_1, \sigma_2, \sigma_3$: maximum, intermediate and minimum principal stresses. The necessary stress conditions for the different failure mode, assuming a Griffith-Coulomb criterion, are indicated. (Modified from Mildren, 2003)**

Failure Mode	Criterion	Condition
Tensile (Hydraulic)	$P_p = \sigma_3 + T$	$(\sigma_1 - \sigma_3) < 4T$
Tensile/Shear	$P_p = \sigma_n + \frac{(4T^2 - \tau^2)}{\mu}$	$4T < (\sigma_1 - \sigma_3) < 6T$
Shear	$P_p = \sigma_n + \frac{(C - \tau)}{\mu}$	$(\sigma_1 - \sigma_3) < 6T$

Studies on fault reactivation are based on a set of common assumptions. Such fault-slip analysis assumes that the state of normal and shear stress for a fault or fracture of any orientation can be calculated within a stress tensor (e.g., Ramsay, 1967). Characterizing fault-slip risking also assumes that the resolved shear and normal stresses on a surface are first order constraints on both the likelihood and direction of slip on that surface (Wallace, 1951; Bott, 1959; Lisle and Srivastava, 2004). Therefore, fault slip analysis provides the best results when the reservoir/caprock is critically stressed, and thus is already segmented by numerous faults and fractures (e.g., Stock et al., 1985). Fault reactivation analysis often deal with large uncertainties (Jones and Hillis, 2003). In the case of fault reactivation risk, the key uncertainties are the orientation and magnitude of the in-situ principal stresses, pore pressure, fault architecture, and the geomechanical properties of the fault. Finally, in the various methods introduced above, the intermediate principal stress was ignored (Morris and Ferrill, 2009) and the understanding of the role of the small structures forming a potential permeable network in the fault zone, such as foliation, cleavage, or fractures is still limited.

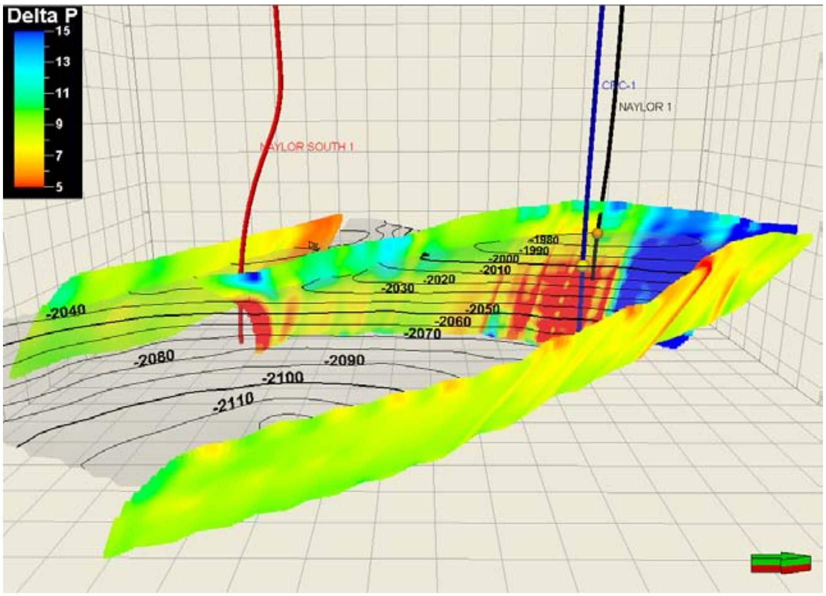

Figure 3.8: **3D illustration of the CO2CRC's Otway Project at the Naylor Field in Victoria, Australia. The contoured surface is the top of the Waarre C Formation, into which CO_2 rich gas was injected. Also shown are the three bounding faults, color coded according to the modeled pressure increase required to potentially reactivate the faults. Delta P units are in MPa. This illustration assumes a strike-slip faulting regime, with 0 MPa cohesion and a friction coefficient of 0.6.**

3.4 Geomechanical Response of Caprocks During Injection

Elevated pore fluid pressures associated with CO_2 injection are generally highest near the well bore, and become reduced with increasing distance from the wellbore. It is important to understand the evolution and magnitude of any such pore pressure increases, as they can result in damage to the reservoir and/or cap rock, thereby increasing the risk for containment loss of CO_2. The magnitude of the pressure pulse that is felt by the reservoir is dependent on a number of factors, the most obvious being the permeability of the reservoir and the CO_2 injection rate, although pressure and temperature also have an impact. Even after cessation of CO_2 injection into a given formation, pressures will remain higher than the original pressure state due to the buoyancy force of injected CO_2. For CO_2 injection into a saline aquifer, the maximum radial extent of the CO_2 plume can be expressed by the following equation (Nordbotten et al., 2005):

$$r_{\max}(t) = \sqrt{\frac{\lambda_C Q\ t}{\phi\ \pi\ \lambda_W B}} \qquad \text{(Equation 3.7)}$$

where Q is the volumetric injection rate, λ_C and λ_W are functions of CO_2 and water relative permeability and viscosity, respectively, ϕ is porosity and B is the thickness of the aquifer. It is therefore critical that any features, such as faults or fracture systems, or other geomechanical considerations are well understood within the radius of influence. It should be noted that modelling indicates that the radius of influence extends to distances that are significantly greater than those for which the actual injected CO_2 extends (Gupta et al., 2000).

Anomalously high pore fluid pressures which vary laterally and vertically within the reservoir may have deleterious effects on the overlying caprock system(s) (Hawkes et al., 2005). In the most simple of cases, elevated pore pressure results in a reduction of effective stress, which brings the system closer to tensile and shear failure as described in the previous section and may lead to induced seismicity (Lucier et al., 2006). If localized failure does occur under the high fluid pressures near the wellbore, then the fracture might propagate unstably into the overlying caprock, which would then provide a possible avenue for CO_2 leakage. The effects of elevated pore fluid pressures can also be far more complex, requiring finite element modelling techniques to fully understand the repercussions (Berard et al., 2008; Rutqvist et al., 2008). For example, elevated reservoir pressures can result in expansion of the reservoir, thereby deforming the overlying cap rock (Rutqvist et al., 2010) and possibly changing the local vertical stresses due to arching effects. Furthermore, data from a number of hydrocarbon reservoirs confirm that changes in fluid pressures can actually result in changes to the *in situ* stress field locally due to poroelastic feedbacks (Hillis 2001, Teufel et al. 1991). This phenomenon is referred to as the reservoir stress path and is a critical process to understand when undertaking a CO_2 injection project. In this section, the complex interactions between injection pressures, stress and deformation will be discussed as they relate to cap rocks and potential risk for leakage. A discussion will also be presented which outlines the current state of knowledge regarding coupled geomechanical modelling and the information that is required to generate useful geomechanical models.

3.4.1 Stress Arching Processes

Stress arching is one type of geomechanical phenomenon that has been well studied in depleting hydrocarbon fields (Hettema et al., 2002, Dusseault et al., 2007). It generally refers to the transfer of stress in the reservoir's overburden due to reservoir compaction driven by reductions in pore fluid pressure. As the reservoir compacts, it may no longer bear the full vertical stress, thereby transferring some of the vertical stress to the overburden at the edge of the reservoir. This phenomenon will only occur if the overburden is stiff and the depleted zone is of limited extent, so that the overburden acts as a stiff beam across the reservoir. For the case of CO_2 injection, the opposite effect would be expected if the rock mechanical properties and pressurized zone has these optimal characteristics. So stress arching in an injection scenario would lead to an increase in the vertical stress above the reservoir and a reduction in the vertical stress at the edges (Figure 3.9). This would have important implications for cap rock integrity, especially in a normal faulting regime, where the largest stress was the vertical stress. Increasing the vertical stress in such an environment would facilitate the reactivation of high angle normal faults or lead to shear failure, with possible fractures forming at low angles to the vertical stress. Such a scenario would result in the formation weak zones which could then be used as channels for fluid flow and potential CO_2 leakage.

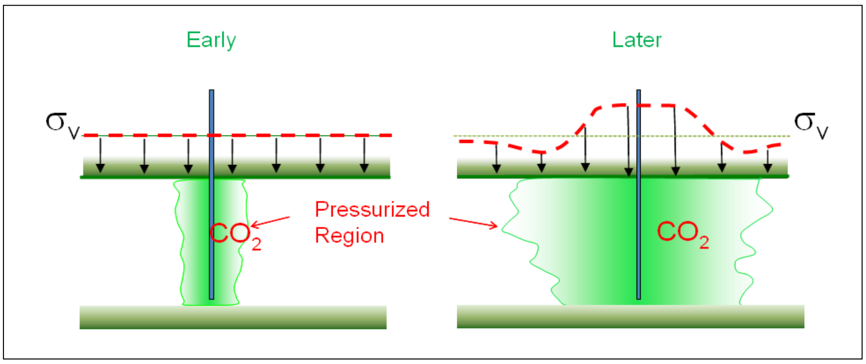

Figure 3.9 **Schematic cross-section of a reservoir-cap rock system, showing how CO_2 injection can lead to stress arching effects, wherein the vertical stress becomes heterogeneous across the reservoir. In the case that the cap rock possesses sufficient stiffness, reservoir dilatancy during injection can lead to an increase in vertical stress above the reservoir, which is accompanied by reduced vertical stress at the edges of the injection zone. In a normal faulting regime, increases in vertical stress within the reservoir and cap rock will increase the reactivation propensity of near-vertically oriented (high angle) faults (modified from M. Dusseault, unpublished).**

In the case that the overburden is relatively compliant and/or the reservoir possesses a large width to height ratio, then stress arching processes will be very limited due to the inability of the overburden to support such a laterally extensive region. If such is the case, volume changes within the reservoir due to depletion or injection, may potentially be transmitted to the surface to be manifested as ground deformation (Geertsma, 1973; Dusseault and Rothenburg, 2002; Hettema, 2002). Such deformation has been observed for depleting hydrocarbon fields (Segall et al., 1994; Chan and Zoback, 2007), EOR injection projects (Bruno and Bilak, 1994; Qobi et al. 2010; Tamburini et al., 2010), and most recently during CO_2 injection at the In Salah project (Tamburini et al., 2010; Rutqvist et al., 2010).

3.4.2 Reservoir Stress Path

The reservoir stress path (sometimes referred to as pore pressure stress coupling) is another important geomechanical phenomenon that can greatly impact on the mechanical integrity of caprock formations. The reservoir stress path describes the degree to which the minimum horizontal stress changes in response to perturbations of pore fluid pressure, either in an injection or withdrawal scenario. The coupling between pore pressure state and the magnitude of the minimum horizontal stress has been observed during depletion of hydrocarbon fields (Whitehead et al., 1987; Teufel et al., 1991; Goulty, 2003) and in wells possessing variable overpressure (Salz, 1977; Breckels and van Eekelen, 1982; Bell, 1990; Addis 1997; Hillis and Reynolds, 2000;). In most of the above case studies, the minimum horizontal stress increases or decreases at about 50-80% of the concomitant pore fluid pressure change.

The reservoir stress path can be understood in terms of poroelastic theory, which describes how a lithified, porous rock behaves as it is filled with fluid and pressurized to different levels. According to theory, a change in pore fluid pressure will result in a volume change of the rock according to (Engelder and Fischer, 1994):

$$\frac{\Delta V}{V} = \alpha\beta \bullet \Delta P_p \quad \text{(Equation 3.8)}$$

where ΔV is the volume change, V is the initial volume, α is the Biot coefficient, β is the compressibility of the rock and ΔP_p is the change in pore pressure. Assuming that the compressibility β is (1/V)($\Delta V/\Delta P_p$) yields:

$$\Delta P_c = \alpha \bullet \Delta P_p \quad \text{(Equation 3.9)}$$

An expression for the reservoir stress path can then be derived assuming uniaxial strain conditions:

$$\frac{\Delta S_h}{\Delta P_p} = \alpha \frac{1-2\nu}{1-\nu} \quad \text{(Equation 3.10)}$$

where v is the drained Poisson ratio. From Equation 3.4 it is clear that reservoir lithologies with smaller Poisson ratios will lead to stronger reservoir stress paths. Likewise, poorly cemented rocks with reduced bulk moduli will cause α to be close to one, thereby favouring strong pore pressure coupling.

The reservoir stress path and its effect on the reservoir and caprock may be understood conceptually as follows. As a liquid or gas is injected into a reservoir, pore fluid pressure builds up and the reservoir tries to expand in all directions (Figure 3.10). As the vertical direction is bound by a free surface (the Earth's surface), there is no change to the vertical stress. However, as the reservoir tries to expand laterally, there is a counteracting force that is imparted into the reservoir which causes the minimum horizontal stress to increase. In a normal faulting or strike slip faulting environment, an increase in the minimum horizontal stress does not favour reactivation of faults, but rather "stabilizes" existing faults by reducing the shear stress/normal stress ratio on the fault surface. However, the expected stress change in the overlying caprock is expected to be significantly different. This is due to the fact that the whole system must stay in equilibrium with the far-field stresses, and that elevated σ_h at reservoir level will be counterbalanced by reduced σ_h in the caprock above the reservoir and also in the formation below the reservoir. This is an example of stress transfer within a reservoir-caprock system. The implication of such a scenario is an increased propensity for tensile fracturing and reactivation of steeply dipping normal faults within the caprock (Figure 3.10). Development of such damage zones within the caprock would greatly enhance the possibility of CO_2 leakage and therefore would not be a favourable result in any CO_2 injection project.

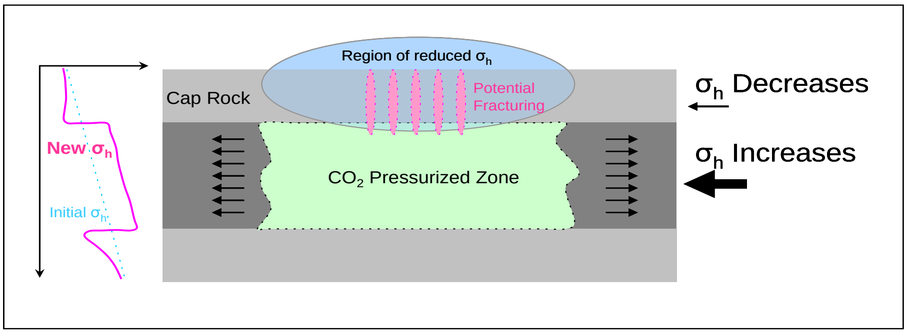

Figure 3.10 **Schematic illustration to explain conceptually how the reservoir stress path operates. As a reservoir is pressurized with CO_2 or any other fluid, the reservoir tries to expand laterally due to poroelastic deformation. However, because the reservoir is confined laterally, the minimum horizontal stress increases together with the increase in pore pressure, albeit at a reduced rate. The increase in the minimum horizontal stress at reservoir level leads to a corresponding decrease in horizontal stress in the cap rock due to stress transfer processes. This reduced stress in the cap rock may lead to potential fracturing due to a lowering of the fracture gradient (modified from Marsden, 2007).**

3.4.3 Thermo-Mechanical Effects of CO_2 Injection

Injection of CO_2 into a reservoir will likely perturb the thermal profile within the injection horizon and possibly in the overlying caprock. In most cases the CO_2 at the surface will have a lower temperature than the reservoir and will therefore depress reservoir temperatures. This can result in elastic stressing of the reservoir rock, which will decrease the magnitude of the horizontal stresses locally and lead to a reduction of the fracture gradient (Perkins and Gonzalez, 1985). If the fracture gradient is reduced sufficiently, then the elevated fluid pressures associated with CO_2 injection may be sufficient to cause fracturing or reactivate older fractures. Additionally, adiabatic (Joule-Thompson) cooling may occur near the wellbore as the CO_2 drops in pressure during transit from the wellbore, through the perforations and into the reservoir (Oldenburg, 2007). Currently, there is limited information relating to the importance of these thermal effects on reservoir and caprock integrity.

The temperature of the CO_2 injected into a reservoir will depend on factors such as the CO_2 source, the thermal properties of the construction and completion materials and the injection rate (Luo and Bryant, 2010). CO_2 which has been transported via pipeline is likely to be cool, while CO_2 emanating directly from a combustion source will be warmer, while materials with a high heat transfer coefficient will warm the CO_2 during injection and reduce the thermal disturbance to the reservoir. Simple modelling presented by Luo and Bryant (2010) shows how the temperature difference between the CO_2 and the reservoir at depth is a competition between CO_2 temperature at the surface and the injection rate of injection. They suggest that one solution to minimize the thermal perturbation is to heat the CO_2 at the surface before injecting. Preisig and Prevost (2011) conducted fully coupled, two-phase flow modelling of CO_2 injection at the In Salah project, Algeria. Their modelling results show that for certain CO_2 injection temperatures, cooling of both the reservoir and caprock may occur, thereby leading to the creation or re-opening of fractures perpendicular to the well.

Joule-Thompson cooling of CO_2 gas may also result in a temperature drop of the reservoir near the wellbore. Such cooling occurs as the CO_2 transits from the wellbore into the reservoir, and is caused by iso-caloric decompression of the gas. In most situations, the magnitude of the cooling is expected to be very small and is not expected to significantly change the fracture gradient (Oldenburg, 2007; Luo and Bryant, 2010; Preisig and Prevost, 2011). A detailed study on Joule-Thomson cooling due to CO_2 injection (Oldenburg,2007), indicates that for most realistic injection scenarios in the Sacramento Valley, California, temperature drops are likely to be < 4° C. However, Oldenburg notes that in the extreme case of a high-pressure injection scenario, the temperature drop could be as great as 20 °C. In such a case, gas hydrate formation might occur near the wellbore, leading to a detrimental reduction in reservoir permeability.

3.4.4 Geomechanical Modelling Involving Poroelastic Processes

Although Figure 3.10 is effective in describing the reservoir stress path concept, most natural systems are significantly more complex, with reservoirs and caprocks possessing highly variable lithologic units. This leads to complex stress transfer patterns that can be difficult to characterize. Furthermore, understanding stress transfer associated with the reservoir stress path and combining this with other geomechanical phenomena such as stress arching, requires complex analytical or finite element modelling. To date there is a lack of publicly available work on such modelling in situations involving CO_2 injection. Due to computing power needed to conduct 4D geomechanical modelling, much of the published work is either analytical (Soltanzadeh and Hawkes, 2008; Vidal-Gilbert et al, 2010) or of a 2D nature (Rouania et al., 2006; Orlic, 2009; Vilarrasa et al., 2010). Rutqvist et al. (2008) present 2D modelling results exploring the potential for tensile failure and shear fracture in a multilayered system, which would approximate the reservoir-baffle system of the Sleipner injection project. This study underscores the importance of understanding *in-situ* stress variations (driven by stress transfer) around the main reservoir, as they may play key roles in determining the location of failure zones. A number of other notable studies have conducted 3D finite element modelling which incorporate complex poroelastic phenomena during CO_2 injection (Minkoff et al., 2003; Lucier et al. 2006; Lucier and Zoback, 2008; Shi and Durucan, 2009; Vidal-Gilbert et al. 2009; Rutqvist et al., 2010). The benefit of such 3D finite element models is that complex lithological and structural systems can be modelled. As a result, such models are very useful for characterizing the geomechanical response of specific reservoir or fields to CO_2 injection. Furthermore, most of the models provide for geomechanical coupling to fluid flow, meaning that any changes to porosity and permeability driven by depletion or pressurization will be fed back into the model as the dynamic simulation proceeds. Although a number of different methodologies have been used to perform such 3D geomechanical models, the outputs appear to be broadly consistent with each other (Dean et al., 2006).

One uncertainty related to the complex poroelastic responses of reservoir and caprock relates to the “elasticity” of the system. In other words, although the reservoir stress path is adequately understood during depletion, it is uncertain whether the reservoir stress follows a reversible path upon repressurization. This question has been explored by Santarelli et al. (1998), who looked at results from mini-frac, fall off tests and step rate tests at different stages of the depletion and pressurization cycle. They found that upon repressurization, the fracture pressures were lower than expected when the depletion stress path was used. This suggests that the reservoir stress path was weaker during repressurization of the reservoir, possibly due to elasto-plastic behaviour of the reservoir during depletion. This non-elastic behaviour can be visualized using a Mohr diagram, which as described earlier, plots the shear stress/normal stress ratio of all planes within a rock mass (Figure 3.11). If the observations of Santarelli et al. (1998) are applicable more broadly to depleted reservoirs, then added caution should be taken when pressurizing a reservoir with CO_2, as a reduced stress path increases the likelihood of shear failure within the reservoir.

The development of highly detailed 3D geomechanical models, which describe the geomechanical state of a three dimensional system through time, have only become more commonplace in recent years. This is partly due to the increased computing power available, but also because operators are increasingly becoming aware of the negative impact and great expense that can be associated with a poor geomechanical understanding of reservoir-carprock systems. Successful development of such models not only requires a detailed geomechanical characterization of the reservoir interval, but also of the rock volume enclosing it (Vidal-Gilbert et al., 2009; Rutqvist et al., 2010). A number of different methods must be used to assign poromechanical properties to the reservoir and surrounding formations. The best and most direct manner of assigning rock mechanical properties is through rock mechanical testing of the different rock types. In such a case, the static moduli of interest (Poisson's ratio and Young's modulus), can be used directly in the model. However, in many cases rock mechanical measurements will not be available and sonic logs must be used to assign poro-mechanical properties to the reservoir and cap rock. These sonic logs can be used to calculate the undrained dynamic moduli , which can then be converted to drained dynamic moduli using the Biot-Gassmann (Gassmann, 1951) equation or similar. Finally drained dynamic moduli are converted to static moduli either by calibration to rock mechanical testing or using empirical relationships (Wang, 2000). It is also critical to have a quantitative understanding of the brittle failure parameters such as unconfined compressive strength and friction angle, as these properties will control whether the reservoir and cap rock will be able to support the changes in pore fluid pressure, or whether new fault and fracture networks form.

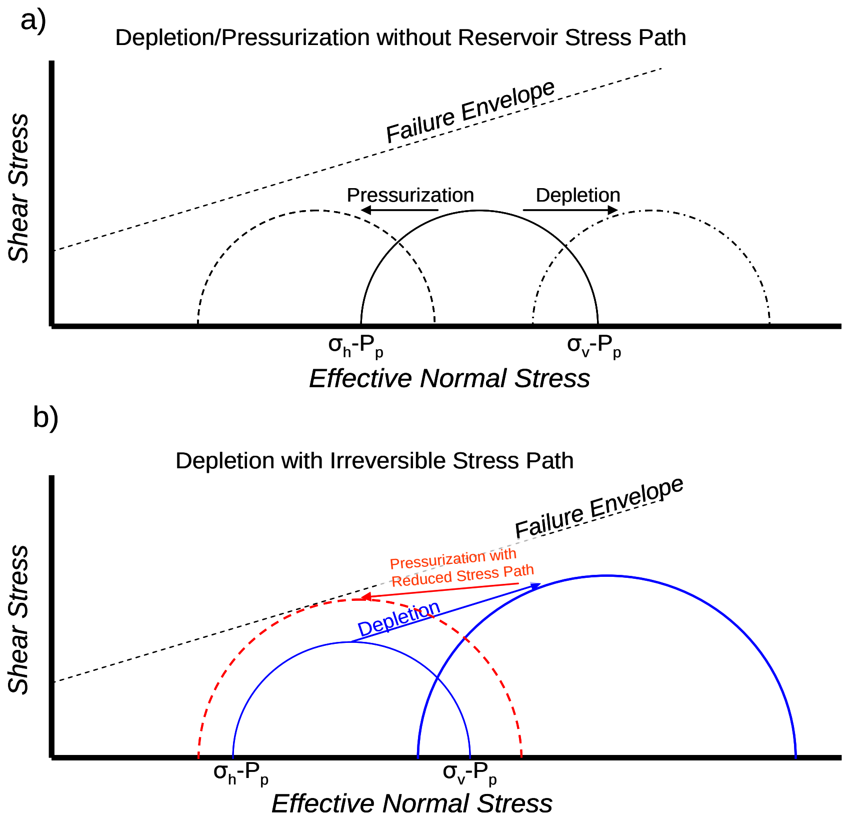

Figure 3.11 **Mohr diagrams showing the evolution of shear and normal stresses within reservoir domains. In a) there is no reservoir stress path associated with depletion or pressurization. As a result, the difference between the effective minimum horizontal stress and the vertical stress stays the same. Figure b) shows the implications of having a strong reservoir stress path during depletion, which is not followed by the same behaviour during re-pressurization. During depletion, the effective horizontal stress does not increase at the same rate as the vertical stress due to a strong reservoir stress path which leads to a reduction in the in situ minimum horizontal stress. This leads to an increase in the differential stress on the reservoir. Based on limited data, Santarelli et al. (1998) found that upon repressurization of the reservoir, the stress path is weaker, causing the effective stresses to migrate toward the failure envelope in a manner similar to a).**

Although the gridding of the geomechanical model may be coarser than the geological model, it must be compatible with the dynamic simulation mesh as the two will eventually be coupled to each other. The level of detail within the geomechanical model depends on the purpose of the model, the data detail available and the computing power available to the modeller. However, it is generally desirable to have greater geomechanical detail within the reservoir interval as this is where fluid pressures will vary most both spatially and temporally. For the purposes of modelling CO_2 storage systems and understanding containment risk it may be necessary to extend this detail into the caprock. From the practical point of view, a number of different finite element packages are available to conduct such modelling. These include (but are not restricted to) ABAQUS (Dassault Systemes), FLAC3D (Itasca), Visage (Schlumberger) and JAS3D (Sandia National Labs). The facility with which these different packages interface with the different dynamic flow simulators varies significantly and should be investigated before modelling is embarked upon. Following the construction of the detailed geomechanical model, coupling must be made to the reservoir simulator so that the effect of variable CO_2-driven fluid pressures can be explored. Outputs from the geomechanical modelling will include information on changes to the local in situ stress field caused by injection pressures, induced failure, fault reactivation and strain within the reservoir and surrounding formations, including and induced ground movement.

Development of a solid geomechanical model is key to ensuring the safe and effective operation of a CCS project. CO_2 injection into a depleted hydrocarbon field or a deep saline aquifer may give rise to a variety of coupled processes which can alter the *in situ* stress field in the immediate vicinity of the project. Such changes may result in the reactivation of previously stable faults or tensile failure of the reservoir or cap rock; both of which may contribute to leakage of CO_2 from the reservoir. Before embarking on any detailed modelling study related to the geomechanical evolution of a potential project, it is first essential to compile all the geomechanical data. In addition to careful characterization of the in situ stress field, detailed geological modelling of the reservoir and cap rock must also be conducted, with careful attention to existing fault and fracture systems. Only once these steps have been taken can the three dimensional geomechanical model be constructed and run to determine effects of complex processes such as the reservoir stress path and stress arching.

4. Hydrodynamics

The impact of hydrodynamics on the sealing capacity of caprocks and faults has been discussed in the literature primarily with respect to hydrocarbon migration. However, those findings are directly applicable to CO_2 geological storage as CO_2 in its supercritical state is a buoyant fluid and the same principle of capillary threshold pressure applies. As is often the case in petroleum systems, hydrodynamic impacts on the sealing capacity for CO_2 storage are probably of secondary importance compared to other seal properties (i.e. permeability) and stress regime. Still, the significance of hydrodynamics increases the more subsurface pressure regimes diverge from hydrostatic conditions. Therefore, fluid pressures on both sides of the seal of a potential storage reservoir need to be considered when assessing the sealing capacity. The term 'membrane seals' (seals that rely on capillary processes) has already been introduced in this paper (Section 2.1). This section deals with hydrodynamic or 'hydraulic resistance seals' (seals that rely on low leakage rates). Top or fault seals may fail mechanically if the formation pressure below the seal exceeds the mechanical strength of the seal rock leading to fracturing or fault reactivation. It has been suggested that faults may represent membrane seals either through juxtaposition of reservoir against a seal or by the low permeability of the fault zone itself (Watts, 1987). This section will focus on understanding the impact of hydrodynamics on the seal capacity of membrane seals for both top seal (caprock) and fault seal geometries.

4.1 Basics of Hydrodynamics

A major concern of all CO_2 storage options is the ability of low-permeable caprocks overlying potential storage reservoirs to retain commercial quantities of CO_2. Hydrodynamically, such low-permeable sequences can be divided into two classes: aquicludes, which are rocks such as halite that are essentially impermeable if not fractured; and aquitards, rocks such as shales and mudstones that have significant porosity but, owing to their very small pore throat size, very low permeability and thus act as seals (Holloway, 2007).

The effect of hydrodynamics as a driving force on the movement of hydrocarbons within carrier beds or reservoirs was described by Hubbert (1953) and has since been documented with field examples throughout the world. Schowalter (1979) discussed how hydrodynamic conditions might affect secondary migration of hydrocarbon and impact on top or fault seal capacity. Seals have been classified into various types depending on the sealing mechanism (e.g., Watts, 1987; Heum, 1996; Bretan et al., 2003; Brown, 2003).

As discussed earlier, for a membrane seal, capillary pressure is simply the difference between the pressure in the wetting phase (normally formation water) and that in the non-wetting phase (hydrocarbons or CO_2). At a sealing interface where there is a change of permeability from reservoir rock to seal rock, the non-wetting phase is trapped until the capillary entry pressure is exceeded. If a trap is filled to its seal capacity, the threshold pressure of the seal is balanced by the upwards buoyancy pressure of the hydrocarbon or CO_2, leading to:

$$T_P = \Delta\rho \, gH \qquad \text{(Equation 4.1)}$$

where $\Delta\rho$ is the density contrast between the formation water and the hydrocarbon or CO_2, g is the gravitational constant and H is the height of the hydrocarbon or CO_2 column above the free water level (FWL) at the point the seal is breached. The equation above assumes that the formation water pressure relevant to understanding column height (H) is the pressure at the FWL. However, there is currently debate in the literature as to which formation water pressure value should be used, and if modification of the equation is required (Bjorkum et al., 1998; Clayton, 1999; Rodgers, 1999; Brown, 2003; Teige et al., 2005).

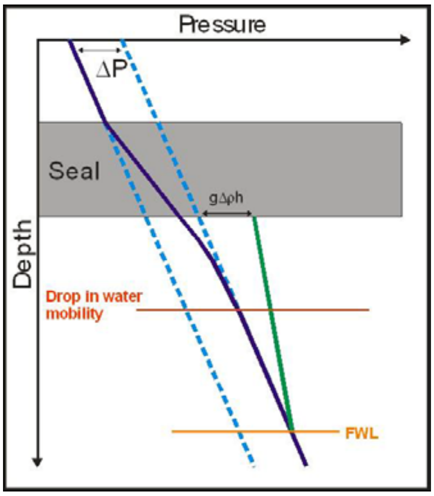

Figure 4.1 **Excess pressure within a hydrocarbon or CO_2 column (after Rodgers, 1999). The drop in water mobility occurs at the top of the transition zone where the reservoir approaches irreducible water saturation. The FWL is located at the intersection of the formation water pressure gradient (thick solid line) and the hydrocarbon (or CO_2) pressure gradient (thin solid line). The buoyancy pressure ($D_q gH$) at the top of the hydrocarbon column is calculated using the formation water pressure gradient extrapolated upwards from the FWL. The assumed excess pressure (DP) is the pressure difference between the hydrostatic formation water pressure gradients above and below the seal. The thick solid line is the actual formation water pressure gradient including that portion through the hydrocarbon column and seal.**

4.2 Impact of Hydrodynamics on Caprock and Fault Seals

Underschultz (2007) further investigates the impacts of hydrodynamics on membrane seal capacity by looking at a series of differential excess pressure across both top and fault seals. He demonstrates that pressure differences of formation water between the two sides of a seal have an impact on the total membrane (capillary) seal capacity for the seal. In fact, the high-pressure side of the seal, independent from the location of the hydrocarbon or CO_2 accumulation, determines the height of the hydrocarbon column that can be supported by the top or fault seal. In other words, the side with the lower pressure can hold more hydrocarbons or CO_2 because, in addition to the capillary entry pressure of the sealing rock, migrating hydrocarbons or CO_2 also have to overcome the increasing pore pressure gradient through the seal. On the other hand, in the static case, the seal capacity depends only on the capillary entry pressure. When considering hydrodynamic effects, the ability of sustaining a pressure gradient across the seal depends on seal thickness and permeability.

The work of Bjorkum et al. (1998), supported by the experiment of Teige et al. (2005), imply that the hydrodynamic regime will not impact capillary leakage as the excess pressure term is not required. However, these papers only deal with the boundary between the uppermost pore of the reservoir and the lowermost pore of the seal. In a risking sense, a seal has failed only if CO_2 has breached its entire thickness (assuming that the volume of CO_2 charge is not a limiting factor). In order to better predict the behaviour of CO_2 caprock systems, it is worthwhile using the principles for hydrocarbon systems established by Bjorkum et al. (1998) and Teige et al. (2005) to re-examine the relation between hydrodynamics and membrane seals for the entire seal thickness. To do this, consider a simple geometry of two aquifers separated by a seal (Figure 4.2). Various seal excess pressure conditions need to be considered along with their effect on seal capacity. Assume that the seal is of uniform permeability and that it has a particular seal capacity expressed as a CO_2 buoyancy pressure equal to the capillary threshold pressure. In reality, both top and fault seals are heterogeneous and this adds further complications to seal capacity calibrations (e.g. Bretan &Yielding, 2005).

Figure 4.2A shows the case to of excess pressure (higher hydraulic head) in the upper aquifer. As a CO_2 column accumulates below the seal, the CO_2 buoyancy pressure increases until it equals the capillary threshold pressure. At this point, CO_2 enters the lowermost pores of the seal. The next pores vertically within the seal will have slightly higher excess pressure than the lowermost pores as the formation water pressure through the seal is following the respective pressure profile. This suggests that the uppermost pores at the top of the seal form the critical part of the seal; hence defining its total membrane seal capacity. In this case, where excess pressure occurs above the seal, a larger CO_2 column (below the base of the seal) can be held prior to complete seal breach than that expected from the threshold pressure at the base of the seal. At the point of maximum CO_2 column prior to seal breach, the capillary pressure in the lower part of the seal will be well above the threshold pressure for the lowermost pores of the seal. This suggests that the CO_2 saturation in the lower part of the seal will be higher and consequently more of the pores will be invaded by the non-wetting fluid during the percolation process. Figure 4.2A shows schematically how the lower part of the seal may have a high hydrocarbon saturation which then decreases upwards. The case of excess pressure in the aquifer above the seal highlights a situation where standard seals analysis would attribute the observed CO_2 column to a buoyancy pressure calculated with the water pressure gradient from the FWL 2. This would result in the calibration of an erroneously high seal capacity to the measured threshold pressure from MICP data. To be done correctly, the buoyancy pressure in this case should be calculated with the water pressure gradient in the aquifer above the seal.

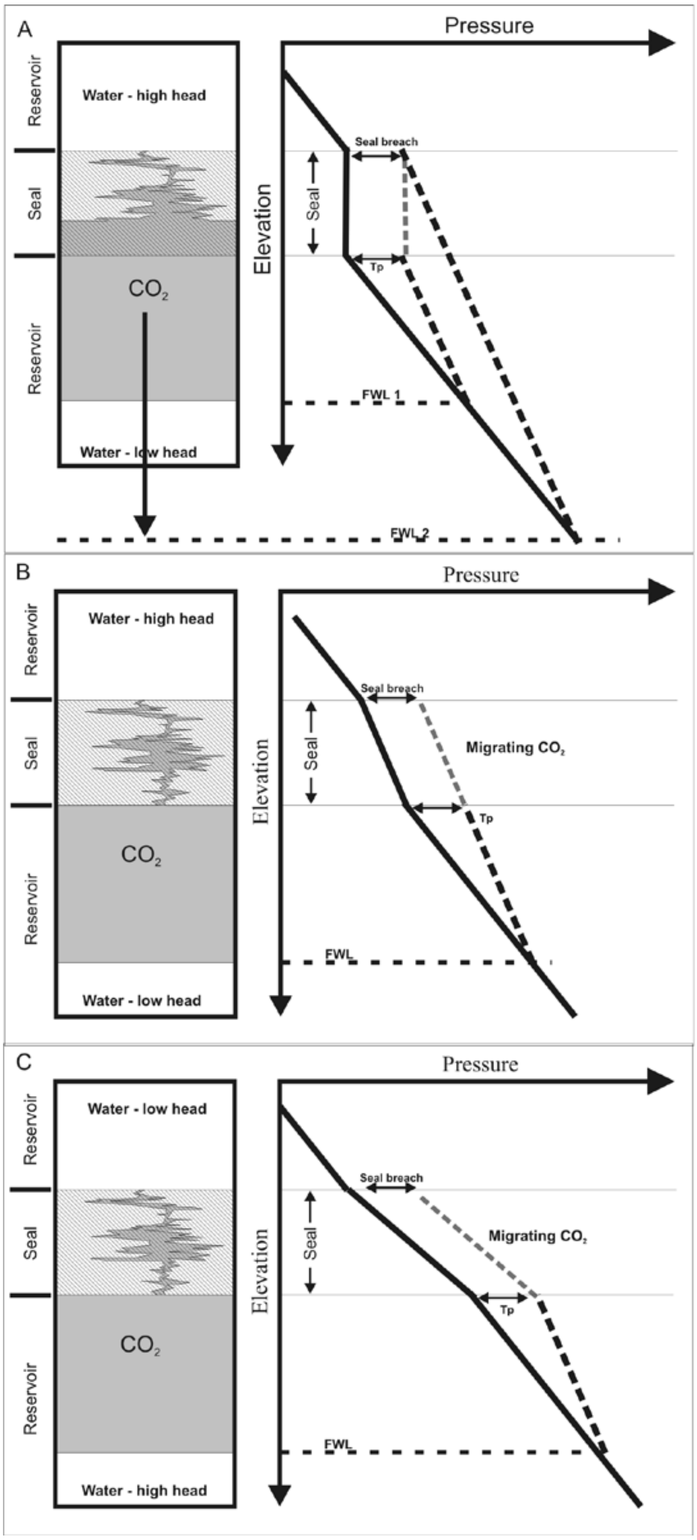

A. Excess pressure above the seal. The threshold pressure of the lowermost pores of the seal (T_P) underestimates the total seal capacity due to the water pressure profile through the seal (thick solid line). The total seal capacity is determined by the uppermost pores of the seal which is balanced by the buoyancy pressure of the CO_2 column defined by FWL 2.

B. Excess pressure above the seal matching the critical head contrast Δh. Here the water pressure gradient through the seal (thick solid line) exactly matches the CO_2 hydrostatic pressure gradient (dashed line).

C. Excess pressure below the seal. The threshold pressure of the lowermost pores of the seal defines the total seal capacity and is balanced by the buoyancy pressure of the CO_2 column.

Figure 4.2 **Conceptual models of a CO_2 accumulation below a seal at the threshold pressure and corresponding pressure elevation profiles for different pressure gradients across the seal.**

There is a situation where the amount of excess pressure in the aquifer above the seal exactly balances the buoyancy pressure of the hydrocarbon column. The geometry required for this condition is shown in Figure 4.2B, where the hydraulic head in the upper aquifer is higher than in the lower aquifer, thus defining downwards vertical flux across the seal. The head difference across the seal is the particular condition that defines a vertical water pressure gradient within the seal exactly equal to the hydrostatic gradient of the trapped CO_2. As a CO_2 column accumulates below the seal, the CO_2 buoyancy pressure increases until it equals the capillary threshold pressure. At this point, CO_2 enters the lowermost pores of the seal. The next pores vertically in the seal will again have slightly higher excess pressure than the lowermost pore but this time the increase will be equal to the CO_2 hydrostatic pressure gradient. This suggests that the entire seal thickness requires the same threshold pressure at the base of the seal for it to be breached. If we assume that any additional CO_2 charge is at a similar rate as leakage, the implication is that the seal will have low CO_2 saturation even after breach, as the CO_2 buoyancy pressure at the base of the seal will never much exceed the capillary threshold pressure. This case marks the point at which any additional excess pressure in the aquifer above the seal will increase the seal capacity. Further, the critical hydraulic head contrast across the seal (Δh) required to match this condition can be calculated according to:

$$\Delta h = \frac{\Delta \rho D}{\rho_w} \qquad \text{(Equation 4.2)}$$

where $\Delta\rho$ is the density contrast between the formation water and the hydrocarbon or CO_2, D is the seal thickness and ρ_w is the formation water density. Knowing this condition has application for CO_2 storage capacity estimates as excess pressure conditions exceeding this equation will enhance seal capacity. The Δh value is also important for top seal capacity calibrations as situations with seal excess pressure less than Δh have seal capacity controlled by aquifer pressure at the FWL, while situations with seal excess pressure greater than Δh have seal capacity controlled by aquifer pressure on the high pressure side of the seal. Note that the seals most affected by the head gradient effects will be the thinnest seals, where the analysis of top seal risk is most critical.

Figure 4.2C shows a water pressure profile through a homogeneous seal with hydraulic head in the upper aquifer less than that in the lower aquifer (i.e. the case of excess pressure below the seal). As a CO_2 column accumulates below the seal, the CO_2 buoyancy pressure increases until it equals the capillary threshold. At this point CO_2 enters the lowermost pores of the seal. The next vertical increment in the seal will have infinitesimally less excess pressure than the lowermost pores as the formation water pressure vertically through the seal is following the respective pressure profile shown in Figure 4.2C. This suggests that the first pores at the base of the seal are the critical part of the seals capacity and once overcome; a filament of the CO_2 will percolate freely and migrate across the seal. Put simply, seal thickness has no effect on seal capacity in this case. The cap rock, previously a membrane seal, becomes a hydraulic resistance seal as soon as CO_2 invasion commences. If we assume that any additional CO_2 charge is at a similar rate as leakage, the implication is that the seal will have low CO_2 saturation even after breach, as the CO_2 buoyancy pressure will never much exceed the capillary threshold pressure.

In cases of a vertical or fault seals, hydrodynamic impacts are very similar to the case of lateral seals. Figure 4.3 shows the impact of formation water flow on a CO_2 accumulation sealed updip by a fault seal. It is assumed that the fault zone has low uniform isotropic permeability, there is no up-fault leakage, and the seal capacity of the fault zone is less than the top seal. The formation water flow in Figure 4.3A is parallel to bedding. As the beds are shown to be dipping, it follows that there is a slight vertical component to flow recorded by a vertical well. This results in the pressure gradients defined by vertical wells having a slope slightly different from hydrostatic (shallower than hydrostatic for up-dip flow and steeper than hydrostatic for down-dip flow). To understand seal capacity, the pressure profile is required along each edge of the fault zone. In this simple example, the hydraulic head between the top and the base of the aquifer along the surface of the fault would be the same as this surface is perpendicular to the flow direction. Thus, the entire flux moves parallel to bedding and across the fault zone. The thin pressure gradient lines representing the formation water pressure on either side of the fault are parallel to the hydrostatic gradient, and at a slight angle to the pressure gradients recorded by the vertical wells. Also, the two thin pressure gradients intersect the pressure gradient from Well 2 where it crosses either side of the fault zone. As a CO_2 column accumulates to the left of the fault, the CO_2 buoyancy pressure increases until it equals the capillary threshold of the fault rock. As the top of the reservoir has an offset across the fault, the critical leak point occurs at the highest elevation of aquifer–aquifer juxtaposition. Given that the permeability of the aquifer is much higher than the permeability of the fault zone, most of the potential energy change will occur within the fault zone. The thin solid line is the correct water pressure gradient to use for understanding breach of the first pore of the fault seal. The thin dashed line is the correct water pressure gradient to use for understanding breach of the last pore of the fault seal. Once hydrocarbon enters the leftmost pore of the fault seal at the elevation of the critical leak point (where buoyancy pressure equals T_P relative to the thin solid line in the pressure-elevation plot), the next pore through the fault seal will have infinitesimally less excess pressure than the leftmost pore as the formation water pressure through the seal is following the pressure profile shown by the thick dashed line for that portion of the well where it crosses the fault seal. This suggests that the first pore at the left of the fault seal at the critical leak point controls the fault seal capacity and once overcome, a filament of the hydrocarbon is free to migrate across the seal, and the fault zone, previously a membrane seal, becomes a hydraulic resistance seal. Also, note that the position of the FWL defined by the water pressure at the edge of the fault zone (thin solid line) is different from that at Well 1 due to a variation in hydraulic head in the aquifer at the base of the pool (i.e. a tilted FWL).

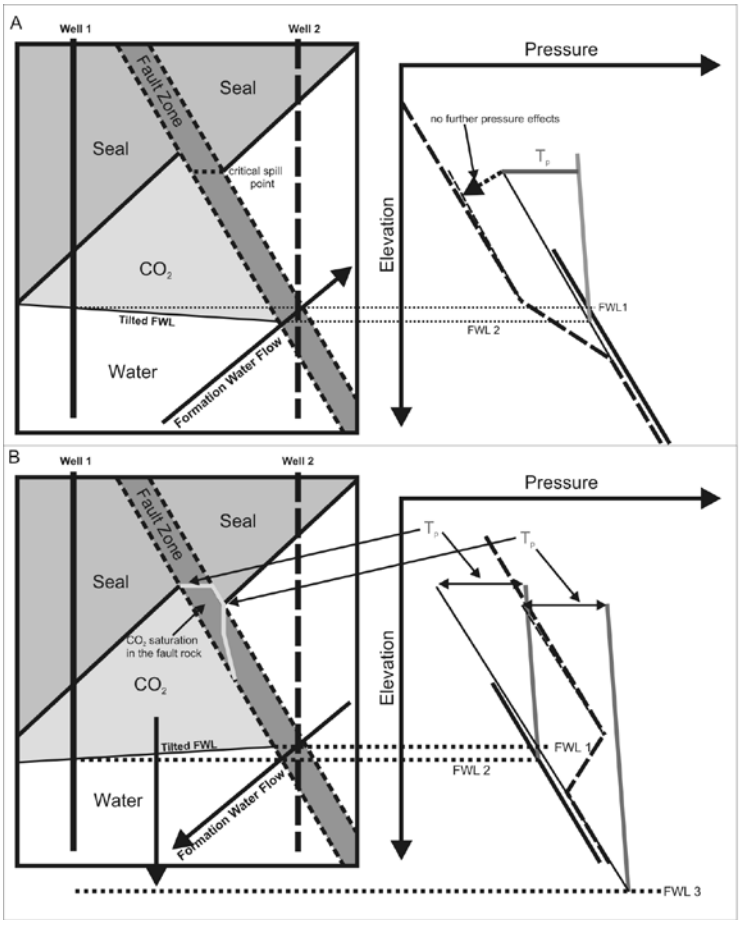

A. The water pressure within the fault is described by the lower part of the thick dashed line over the elevation interval where Well 2 intersects the fault. The thin dashed line represents the formation water pressure perpendicular to bedding on the right side of the fault and the thin solid line represents the formation water pressure perpendicular to bedding on the left side of the fault. The threshold pressure of the leftmost pores of the seal (T_P) defines the total seal capacity and is balanced by the buoyancy pressure of the CO_2 column.

B. The threshold pressure of the leftmost pores of the seal (T_P) underestimates the total seal capacity due to the water pressure profile through the seal (thick dashed line). The total seal capacity is determined by the rightmost pores of the seal which is balanced by the buoyancy pressure of the CO_2 column defined by FWL 3.

Figure 4.3 Schematic fault seal geometry with two wells, downdip CO_2 accumulation and corresponding pressure elevation profiles for the wells: A. up-dip flow across the fault; B. down-dip flow across the fault.

Figure 4.3B shows the opposite flow to Figure 4.3A, with higher aquifer pressures on the aquifer side of the fault than in the compartment containing the CO_2 column. With flow in the opposite direction, the relative slope between the thin and thick dashed lines is opposite to that in Figure 4.3A and the direction of tilt to the FWL is correspondingly in the opposite direction. As a CO_2 column accumulates against the fault and top seal, the CO_2 buoyancy pressure increases until it equals the capillary threshold pressure of the fault seal at the top of the structure (shown by FWL 1). At this point, CO_2 enters the leftmost pore of the fault seal. The next pore through the fault seal will have slightly larger excess pressure than the leftmost pore as the formation water pressure through the seal follows a pressure profile like the thick dashed line (for that part of Well 2 where it crosses the fault zone). This suggests that the last pore at the right of the fault seal at the critical leak point elevation determines the total seal capacity. The CO_2 column required to generate sufficiently high buoyancy pressure to balance this total seal capacity is defined by FWL 3. The two cases in Figure 4.3 demonstrate that there is a significant change in the total seal capacity as the result of a difference in the excess pressure distribution across the seal. Interestingly, for Figure 4.3B the fault zone itself would become partially saturated with CO_2 during the percolation process as shown by the saturated area outlined by the white line. As with the cases described in Figure 4.3A, standard seals analysis would overestimate the seal capacity attributed to the measured rock properties (SGR), in this case. Similar to the case for the top seal demonstrated in Figure 4.3B, there is one condition of excess pressure in the aquifer across the fault from the CO_2 where the increase in pressure across the fault zone exactly balances the CO_2 buoyancy pressure. It is only after this excess pressure condition is exceeded, that the seal capacity increases. In theory, the critical hydraulic head contrast (Δh) across the fault required to balance the buoyancy pressure can be calculated according to Equation 4.3.

$$\Delta h = \frac{\Delta\rho D}{\rho_w} \qquad \text{(Equation 4.3)}$$

In practice, the fault zone thickness (seal thickness D) will be small and thus the head contrast required to reach Δh will be negligible. Because of this, the aquifer pressure gradient on the high pressure side of the seal should always be used to calculate buoyancy pressure for seal capacity calibration.

4.3 Modelling Case Study

A case study incorporating two-phase numerical flow modelling of carbon dioxide migration under hydrodynamic conditions, using the Tough2 code is described by Michael & Underschultz, 2009). The intent of these simulations was to focus on the relationship between the height of the CO_2 column that can be sustained by a fault seal and the hydraulic gradient across the fault zone. Lateral migration (viscous coupling forces) and temperature effects are not investigated. The model domain has the dimensions 10 m x 10 m x 200 m (Figure 4.4), with fixed pressure and concentrations at its lower boundary and no-flow boundaries along the remaining borders. Consequently, mainly vertical migration of CO_2 results in fast accumulation times below the top seal and against the fault, reducing simulation times compared to a gently dipping reservoir layer. A large thickness was chosen to allow the accumulation of a sufficiently high CO_2 column to breach fault and top seals that may have a varying range of permeabilities. The fault zone is 2 m thick, but only the outer 25 cm on either side represent slip surfaces. This was based on outcrop characterization of actual fault seals. The vertical length of the fault seals is 5 m on the left and 20 m on the right, below which a 0.001 mD barrier restricts fluid flow across the fault zone. Three cases were modelled for this permeability configuration: a) no initial formation water flow, b) across-fault hydraulic gradient with higher pressure on the right side of the fault, and c) across-fault hydraulic gradient with lower pressure on the right side of the fault (Figure 4.5). The respective hydraulic gradients are induced by injecting or producing water from a well at 100 m depth on the right side of the fault. The carbon dioxide is introduced through a 100 m long source with fixed CO_2 saturation (0.6) along the left boundary of the model for 300 days, after which it is turned off. The pressure is fixed at 16,000 kPa along the lower model boundary, which is approximately equivalent to pressure conditions at 1650 m depth. The temperature is assumed to be at constant 50 ^{o}C, which results in a range of CO_2 density between 680 and 700 kg/m^3 in the upper 100 m of the model.

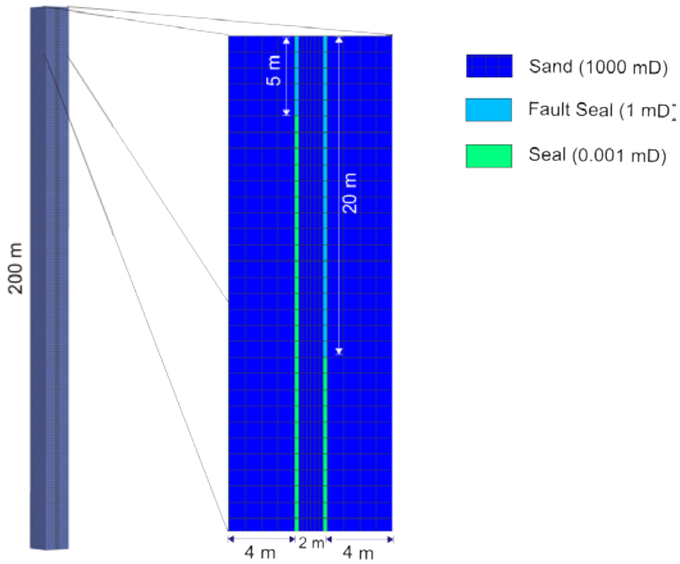

Figure 4.4 **Modeled domain and permeability distribution.**

A. No pumping

Initially, CO_2 migrates to the top of the model, where it accumulates and after approximately 300 days breaches the fault seal on the left. As a result of the CO_2 migration, formation water is displaced downwards where it leaves the model domain through the fixed pressure boundary at the bottom. After 300 days no more CO_2 is added into the model column. Carbon dioxide continues to build against the top seal in the compartment between the two fault seals, until the CO_2 column reaches sufficient height (~20 m) and capillary pressure to breach the fault seal on the right at approximately 350 days. The CO_2 fills the right side of the reservoir until the column on the left side of the fault cannot provide sufficient buoyancy drive to overcome the fault seal entry pressure after approximately 700 days. During this period, formation water re-imbibes the left side of the reservoir through the fixed head boundary below and only residual saturation of CO_2 remains. At this point in time, all reservoir rock that has been contacted by the CO_2 plume contains formation water fully saturated with CO_2. On the right side, the dissolution of CO_2 results in a downward moving finger of dense formation water at the bottom of the CO_2 column.

B. Injection

The same initial conditions are used in this case and CO_2 is allowed to accumulate for 300 days. Subsequently, injecting water at a rate of 0.1 kg/s in the lower part of the column on the right hand side of the fault results in an upward and, more importantly across-fault hydraulic gradient with approximately 10 m difference in hydraulic head. Breach of the right fault seal occurs slightly later as in Case A and the respective threshold pressure is larger (Figure 4.5). The maximum CO_2 column in the middle reservoir unit reaches 25 m as indicated by the residual saturation (light blue), 5 m more than in the "non-pumping" case. There are two reasons why this maximum column cannot be sustained. Firstly, although the threshold pressure is overcome and the fault is breached, additional CO_2 can accumulate as long as the migration rate into the middle reservoir is larger than the leakage rate across the fault. Secondly, and maybe more importantly, the increased circulation of formation water due to the pumping enhances dissolution of CO_2 at the base of the CO_2 column and subsequent downward migration of the denser, CO_2 saturated water (Figure 4.5B, third diagram).

C. Production

The same initial conditions are used in this case and CO_2 is allowed to accumulate for 300 days. Subsequently, continuous production of water at a rate of 0.1 kg/s in the lower part of the column on the right hand side of the fault results in a downward and, across-fault hydraulic gradient with approximately 10 m decrease in hydraulic head from right to left. In this case, breach of the right fault seal occurs slightly earlier than in the previous cases and the respective threshold pressure is lower. The maximum CO_2 column after 1000 day in-between the two faults reached approximately 17 m, which is 5 m less than in the “non-pumping” case. Similar to Case B, the increased circulation of formation water enhances dissolution of CO_2, however, in this case on the right side of the fault. The denser, CO_2 saturated water migrates downwards, ahead of the separate-phase CO_2 plume (Figure 4.5C, third diagram).

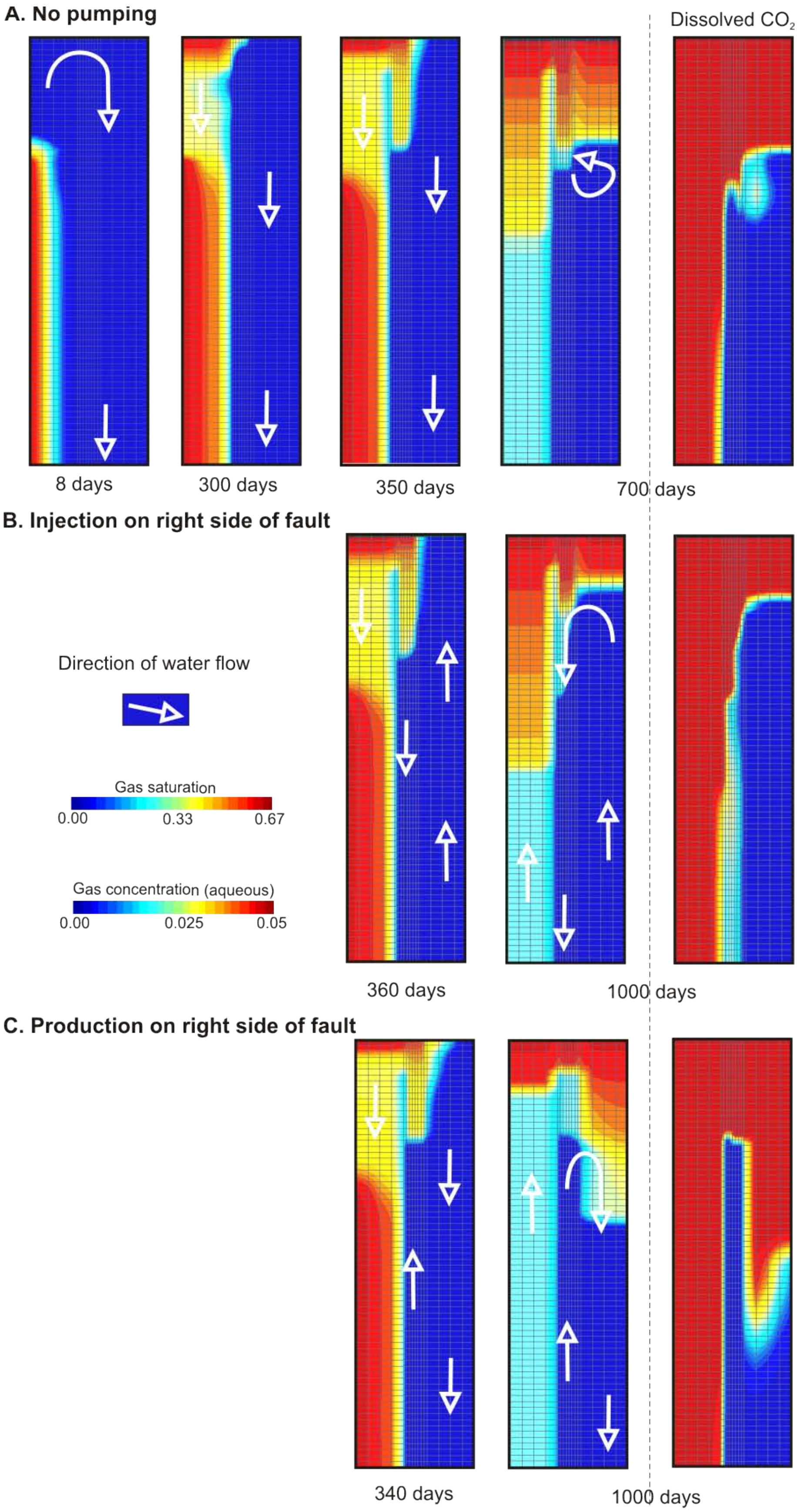

Figure 4.5 **Modelling results showing CO_2 saturation and dissolved CO_2 concentration for cases of A) no pumping, B) injection, and C) pumping.**

4.4 Discussion

The ability for the assessment of actual water flow through undisturbed low-permeability environments is very limited as has been discussed in a landmark review paper by Neuzil (1986):

- Pressure dissipation and flow occur over a long time scale and changes are relatively small, which makes it impossible to monitor;
- Geologic processes that influence stress, temperature chemical and other effects and, in turn, impact on hydraulic gradients and seal properties may occur on similar time scales as pressure dissipation change over time; but these changes are difficult to predict.
- While flow processes in low-permeability formations can be numerically modeled and rock hydraulic properties can be tested in the laboratory, validation of the respective results for natural systems is problematic due to up-scaling issues with respect to time and space.

However, even if there is no significant water flow component through the confining unit, the hydraulic gradient across a seal may affect the threshold pressure and migration of a non-aqueous fluid (hydrocarbons, CO_2). Initial modelling results confirm the theoretical findings that across-fault hydrodynamic gradients enhance or reduce fault seal capacity depending on the direction of flow. However, the enhancement of fault seal capacity can only increase up to that point where the hydrodynamic drive becomes sufficiently high to sweep the hydrocarbons or carbon dioxide out of the trap. Obviously, the across-fault flux of water declines with decreasing fault zone permeability for a given hydraulic gradient. At the same time, lower fault zone permeability results in a higher threshold pressure and higher sustainable hydrocarbon column. As a result, fault seal enhancement (without sweeping) due to across-fault hydraulic difference (Δh) is limited to a range of permeabilities, fluid densities and hydraulic gradients according to:

$$\frac{(\rho_w - \rho_b)}{\rho_w} \cdot D \le \Delta h \le \frac{k_r}{k_f} \cdot \frac{(\rho_w - \rho_b)}{\rho_w} \cdot D \cdot \nabla E \qquad \text{(Equation 4.4)}$$

for $\Delta h = h_{nr} - h_r > 0$

where ρ_w = water density (kg/m^3), ρ_b = density of buoyant fluid (kg/m^3), D = fault thickness (m), k_r = aquifer permeability (m^2), k_f = fault permeability (m^2), ∇ E = aquifer slope, h_r = hydraulic head on reservoir side of the fault (m), h_{nr} = hydraulic head on non-reservoir side of the fault (m).

Cases of vertical hydraulic gradients across seals or aquitards are very common in sedimentary basins. However, the actual importance of hydrodynamic impacts on membrane seal capacity is difficult to assess due to the lack of properly analysed field examples. In the case of leaking hydrocarbon reservoirs, the nature of the membrane seal failure is generally not scrutinized, particularly not in the scientific literature. Cases in which hydrodynamics had demonstrated effects on seal failure are related to production-induced hydraulic gradients (e.g. Jev et al., 1993; Davies et al., 2003). These can still be valid analogies for what might be expected under natural gradient over geological time scales. Numerical simulations by Manzocchi et al. (2010) confirm that capillary seal failure due to an across-seal hydraulic gradient is feasible, but they question the prevalence of this phenomenon in the case of fault seals as it is backed up only by “unpublished anecdotes”. In any case, injecting CO_2 in either underpressured formations or on the low flow potential (low hydraulic head) side of a top or fault seal should improve the storage security with respect to breach of the membrane seal.

4.5 Impact of Pressure

Pressure build-up due to injection in both saline aquifers and depleted hydrocarbon reservoirs has been identified as being one of the most limiting factor for large-scale geological storage Commonly, existing analytical models and numerical simulations model CO_2 storage reservoirs as either open or closed systems, thereby largely ignoring the hydraulic properties of the sealing units. Capacity and injectivity estimates using an open- or closed system approach can vary significantly, which has led to the publication of contradicting results (IEAGHG 2010 a, b and references therein). Open- and closed systems obviously represent only the two end members for most geological environments and there will always be a certain amount of leakage through the surrounding seals, even if this might be considered negligibly small. Only recently, Chadwick et al. (2009) investigated the impact of flow barriers on aquifer pressurisation and storage capacity. Their modelling studies using TOUGH2 indicate that even in aquifers with lateral and vertical flow boundaries, there probably will be some single-phase water flow through the sealing unit and seal permeability will have an impact on reservoir pressures. A recent study by the Permedia Research Group for the IEAGHG investigates in more detail the sensitivity of the impact of seal thickness and permeability on the pressure response in CO_2 storage reservoirs (IEAGHG, 2010b; Cavanagh and Wildgust, 2011). This report concludes that “all but the smallest deep saline formations will experience significant natural pressure dissipation as a result of brine displacement into the surrounding strata via shale-mediated flow. For regional formations, the zeroflow boundary approximation is only valid for small pressure compartments and shales with permeabilities in the nanodarcy range. The surface area of the pressure compartment within a regional formation, the boundary layer thickness, and the average shale permeability are the critical constraints on luminal conditions.” The authors also acknowledge that actual data from active storage sites are needed to confirm and calibrate numerical model results.

4.6 Applications of Percolation Theory

Conventional reservoir simulation is based on Darcy's law for flow of a viscous fluid. Darcy's law is applicable when permeability and viscosity determine fluid migration. It allows the calculation of pressure changes, such as pressure buildup in the vicinity of an injection well. However, when viscous forces are negligible, very slow two-phase flows are dominated by capillary and gravity forces. There is evidence that these slow flows are best modelled by pore-scale network models, with the simplest of these models being based on percolation theory (Larson et al., 1981). Percolation models have two main variants: ordinary percolation and invasion percolation. Gravity was first introduced into the invasion percolation algorithm through the application of a simple linear weighting on the invasion thresholds in the direction of buoyancy (Wilkinson & Willemsen, 1983; Wilkinson, 1984).

An important application of invasion percolation with buoyancy has been to the secondary migration of oil. Secondary migration is the slow process occurring over geological timescales where oil migrates from the source rocks where it is formed into structural or stratigraphic traps. In a series of papers, researchers at the University of Oslo have explored invasion percolation as a model for secondary migration (Meakin et al., 1995; Wagner et al., 1997; Vedvik et al., 1998; Meakin et al., 2000;). For further references see Thomas and Clouse (1995), Ringrose et al. (1996) and Boettcher et al. (2002).

Over the last decade Permedia Research Group has developed a code, MPath, based on invasion percolation for secondary migration (Carruthers, 2003). This code has recently been applied to CO_2 migration at Sleipner (Cavanagh & Haszeldine, 2009) and In Salah (Cavanagh & Ringrose, 2009).

In a separate application, Zhang et al. (2010) have applied percolation theory to calculate the connectivity of stochastic fracture networks for estimating the probability of CO_2 leakage through the caprock into shallow aquifers. However, this work applies percolation theory to the solid rather than the fluids meaning that if the fracture density is below the percolation threshold, the fractures are disconnected and do not create a migration path.

5. Geochemical Interactions

5.1 Introduction

During the last decade, fundamental research has focused increasingly on the short and long term effects of the injection of carbon dioxide into various geological environments, such as depleted oil and gas reservoirs (Li et al., 2006), saline aquifers (e.g. Xu et al., 2005), coal beds (e.g. Bromhal et al., 2005) and (ultra) basic rocks (e.g. Daval et al., 2009) in order to assess the feasibility of storing large amounts of CO_2 in the subsurface. These studies suggest that immediately after injection into a reservoir, CO_2 will be stored as a free phase within the host rock. Over time it will dissolve in the local formation water. This chemical interaction causes a dramatic increase in total aqueous carbon concentration and a substantial decrease in pH which may initiate a variety of geochemical reactions.

If included into these studies, caprocks such as shale or mudstone were observed to participate actively in the coupled dissolution/precipitation process. For example, Xu et al. (2005) considered the effects of injecting carbon dioxide into a common sedimentary basin sequence, a shale bounded sandstone. The total quantity of CO_2 trapped in carbonate minerals depends greatly on the rock composition, but they find that a significant amount of CO_2 can be trapped over 100,000 years, mainly in the sandstone. Much of this CO_2 trapping is a consequence of the presence of an adjacent shale unit, which provides many of the cations that form the CO_2 trapping carbonates. The relative high Mg concentration in clay-rich shales e.g. can lead to the following simplified dissolution/precipitation reaction (Johnson et al., 2005):

$$\underset{\text{K-feldspar}}{KAlSi_3O_8} + 2.5\ \underset{\text{Mg-chlorite}}{Mg_5Al_2Si_3O_{10}(OH)_8} + 12.5\ CO_2(aq) \Leftrightarrow$$

$$\underset{\text{muscovite}}{KAl_3Si_3O_{10}(OH)_2} + 1.5\ \underset{\text{kaolinite}}{Al_2Si_2O_5(OH)_4} + 12.5\ \underset{\text{magnesite}}{MgCO_3} + 4.5\ \underset{\text{quartz}}{SiO_2} + 6\ H_2O$$

Understanding the rock fluid interaction potential between the CO_2 and contacted minerals is important. The interaction of acidic –rich fluids with the caprock, can be either advantageous or disadvantageous for its containment. Though typical caprocks can provide the metals essential to trapping CO_2 in carbonate minerals, the leaching of these metals may increase the shale's permeability leading to the escape of CO_2 from the storage reservoir. Gaus et al. (2005) performed reactive transport models of the interaction between CO_2-rich solutions and the caprock of the Sleipner storage site in Norway. They find that the porosity and permeability of the caprock can be either increased or decreased depending on the exact composition of the rock. An increase in permeability could facilitate CO_2 movement through the caprock. In contrast, a decrease in permeability could further seal off the caprock and contribute to an improved sealing capacity. In most instances, because of their low permeability and capillary properties, CO_2 is unlikely to enter seals. Therefore, any potential reactions are likely to be limited to the base of the caprock. In addition, because the pH buffering capabilities of the seal lithology are generally greater than the dissolution capabilities of carbonic acid, reactions are likely to be mineral precipitation rather than dissolution, thus leading to seal capacity enhancement instead of degradation (Watson et al., 2004). Coupled mineral dissolution/precipitation reactions within shale typically involve Fe-Mg-rich clays and lead to the precipitation of carbonates. Modelling results for Sleipner-like settings imply that such precipitation is virtually limited to the basal caprock layer (< 5m) during the active injection phase. During the post-injection phase the immiscible CO_2 trapped below the caprock will continue to promote carbonate cementation within the basal layer, significantly reducing porosity and initial permeability and therefore improving caprock integrity (Johnson et al., 2004). A natural analogue to these processes has been documented in the Belfast Mudstone, Otway Basin, where CO_2 influx has converted feldspars, clays and Fe-rich volcanic fragments to siderite ($FeCO_3$), kaolinite (Watson et al., 2004).

5.2 Effects of Impurities on CO_2 Storage

An important aspect of subsurface CO_2 storage is the purity of the CO_2. Streams originating from gas processing plants may contain H_2S, while streams origination from power plants will contain NO_x, SO_x and CO (Bachu, 2008). These may or may not have an effect on the long-term caprock seal integrity. For example the dissolution of SO_2 in formation water creates a far stronger acid than the dissolution of CO_2; which might also affect the long-term caprock stability in CO_2 storage (Benson and Cook, 2005).

CO is highly reductive and will be oxidized to CO_2 by oxygen or mineral oxides (Wang et al., 2011. There have been several studies on co-injection of H_2S and/or SO_2 with CO_2 (e.g. Knauss et al., 2005; Xu et al., 2007). The general view is that H_2S is not an issue, and it has been co-injected with CO_2 for 20 years in Canada in acid gas disposal (e.g. Emberley et al. 2005). However, Knauss et al. (2005) suggest that SO_x injection with CO_2 produces substantially different chemical, mobilization and mineral reactions. SO_2 can greatly lower the pH of the formation water and hence enhance the dissolution of rock minerals. In CO_2 streams from oxyfuel combustion and post-combustion capture plants O_2 and NO_x will also be present. NO_x is known to catalyze SO_2 oxidation and hence the formation of sulfuric acid (Wang et al., 2011).

Because there has not been a systematic and comprehensive assessment yet, of how these additional constituents would affect caprock integrity during CO_2 storage, it is difficult to quantify their effects. However, the soon to be released IEAGHG report on the “Effects of Impurities on Geological Storage of Carbon Dioxide” will, amongst others, evaluate this issue.

5.3 Case Studies

One major concern of all CO_2 storage options is the investigation of the sealing efficiency of low-permeable sequences overlying potential storage reservoirs – the caprocks. Caprocks need small pore sizes, so the vast majority of caprocks are fine-grained siliciclastics (clays and shales), evaporates (e.g. halite) and organic rich rocks. Other lithologies such as limestone are also known as seals (Allen and Allen, 2005). The case studies/papers presented below provide an overview of current research work, aiming to provide insights into the long-term geochemical effects of CO_2 on caprocks.

5.3.1 Case Study 1 – Shale: Silurian Maplewood Shale, Monroe County, New York, USA

Much research effort has been focused on the mineral trapping of CO_2, which occurs via carbonate precipitation. A study on the availability of metal cations, originating from non-carbonate minerals, which can combine with the dissolved CO_2 is presented by Kaszuba et al. (2005). The authors attempt to simulate the reactions of a typical storage site by reacting a mixture of quartz, feldspar, biotite and shale under physical chemical conditions relevant to geologic storage (CO_2-rich, 5.5 molal NaCl-brine at 200 ºC and 200 bar).

Examination of the shale sample, using optical and scanning electron microscopy and X-ray diffraction, identified clay minerals (illite and mica comprising 65 vol.% of the shale), quartz (27%), feldspar (5%), chlorite (2%, may include some kaolinite), and trace quantities of framboidal pyrite. Mineral grains range in size from approximately 2 to 15 Am.

The supercritical carbon dioxide-brine-rock experiment was performed in a gold reaction cell (108 cm^3) loaded with 3.1 g of arkose (1:1:1:0.3 quartz/ plagioclase/microcline/biotite), 2.7 g of Maplewood Shale chips, and 90 g of brine. Following the extraction of 33.3 g of brine as samples during the initial 771 hours of reaction time, approximately 6 g of carbon dioxide was injected into the reaction cell. Thus, the initial brine to rock mass ratio was 15.5:1 and the initial brine to carbon dioxide mass ratio was approximately 9.5:1.

A number of significant observations were made over the course of the experiment. Changes in elemental abundances in the brine following the addition of CO_2 include pH decrease and depletion of sodium due to accelerated growth of zeolithe minerals. Magnesite and siderite ($FeCO_3$) were observed to precipitate, validating the potential for mineral trapping, while the nucleation and growth of siderite on the shale suggests the aquitard is a reactive component in the system. Precipitation of the mixed hydroxyl carbonate mineral dawsonite, predicted in many 76haracte studies as a stable carbonate phase during carbon storage, was not observed in this study. Substantial aqueous Si was observed to be released to the solution, which could serve as a source of quartz cement or Si 76haracterize76n in veins.

This experimental study thus demonstrates that CO_2-mixed fluid-rock reactions and related processes have the potential for geochemical reactions that have not been sufficiently understood. A loss of caprock integrity, due to acid-dominated reactions within the caprock, and the leakage of carbon dioxide may occur just as readily as a self-healing of fractures, due to the return of silica supersaturated brine to a rock dominated system buffered to neutral pH conditions.

5.3.2 Case Study 2 – Limestone: Upper Mioscene limestone, Campos Basin, Mallorca, Balearic Islands, Spain

A study that experimentally investigated geochemical processes which arise from the interactions between CO_2 and carbonates is provided by Noiriel et al. (2009). It explores the dynamics of porosity and reactive surface area changes during porous limestone dissolution by CO_2-rich water. The Sr and Ca concentrations in both the rock and the outlet solution are used to evaluate the reactive surface area changes of the two rock-forming calcites, micrite grains and sparite crystals.

The mineralogical composition of the sample rock was determined by X-ray diffraction (XRD). Only calcite was detected. The proportions of micrite and sparite were estimated on a thin section to be around 60% and 40%, respectively. Triple-weight porosity measurements give the rock a total porosity of 15.8%, a connected porosity of 8.9%, and a non-connected porosity of 6.9%.The flow-through experiment was carried out at room temperature (about 20 °C) and CO_2 partial pressures representative for storage sites of 1 ± 0.1 bar. The inlet fluid used in the experiment was a 0.010 ± 0.001 mol l^{-1} NaCl solution prepared from reagent-grade NaCl diluted in deionised water. The fluid, initially degassed, was maintained at equilibrium with CO_2 during the experiment.

At the end of the experimental run X-ray microtomography reveals a slight decrease in geometric surface area whereas the reactive surface area increases continuously with increasing porosity from 20.3 to 30.2%. Surprisingly, changes in reactive surface areas are very different between the two calcites. The reactive surface area changes in the micrite are parabolic while the reactive surface area of sparite increases greatly, suggesting that the variations in reactive surface area of minerals can significantly influence reactive transport properties within a rock.

5.3.3 Case Study 3 – Carbonate-rich shale: Numerical modelling of CO_2-induced caprock alteration

Experimental studies as above provide input data for comprehensive geochemical models aimed at predicting the behaviour and consequences of CO_2 injection in a number of different subsurface systems. Many examples of such studies can be found in recent literature. For example Gherardi et al. (2007) performed reactive transport models of the interaction between CO_2 rich solutions and a seal made of potentially highly reactive, carbonate-rich shale (made up of 33% by volume of calcite+dolomite and 47% by volume of silicate clay minerals. Non-clay silicates include quartz, which amounts to 20% by volume.

Simulations were carried out for isothermal conditions of 45 °C and 105 bar total pressure using the TOUGHREACT code. Permeability, porosity and grain density have been set to average values with a caprock initial porosity between 0.05 and 0.15 and permeability 0.001×10^{-15} to 0.1×10^{-15} m^2.

The most important process, controlling the chemical evolution of the investigated caprock system was the dissolution/precipitation of calcite. Calcite tends to dissolve within the lower part of the caprock, which is driven by acid pH conditions induced by high P_{CO2} values. Calcite dissolution makes Ca and C available which then diffuse into the upper part of the caprock column, where lower concentrations of these species are available. This diffusive flux leads to calcite precipitation and sealing of void spaces in the upper part of the caprock column were near neutral (pH ~ 7.0) conditions still persist. The leakage of carbon dioxide thus becomes self-limiting and pores become clogged after a very short time.

The dominant role played by calcite overwhelms the effects of other mineralogical changes involving precipitation/dissolution of Al-silicate minerals. Other effects include the formation of new minerals such as dawsonite, siderite and ankerite. These finding is in agreement with other recent findings and demonstrates that ferric iron in sediments may act as a trap for CO_2, as other divalent metals such as Ca and Mg are likely to be present in the shale caprock matrix (Gherardi et al., 2007).

5.3.4 Case Study 4 – Halite: Natural analogue studies for CO_2 storage

One way to test the quality of geochemical modelling efforts is through their comparison with natural analogues which have experienced the effects of high CO_2 pressure over substantial time frames. One excellent example is presented by Wilkinson et al. (2009) who investigated the evolution and consequences of high CO_2 pressures in a southern North Sea (United Kingdom) gas accumulation with high natural CO_2 content (c. 50%), the so called Fizzy accumulation. As a control, a geologically similar Orwell Field was studied as well, which lies some 7 km to the NW of the Fizzy accumulation but in which the gas charge has only a low CO_2 content (< 2%).

The reservoir in the Fizzy and Orwell accumulations is part of the Early Permian Rotliegend Group. Here sediments are predominantly sandstones that are overlain by hundreds of meters of Late Permian Zechstein halite evaporites. The entire available conventional core from the Fizzy accumulation and the Orwell field was examined and logged. Thin sections were made for conventional petrographic examination; all were stained for feldspars and carbonates. Rock chips and polished thin sections were studied using Scanning Electron Microscopy with x-ray microanalysis, back-scatter and cathodoluminescence. Mineral identification was aided by XRD analyses.

Some mineral trapping of CO_2 was observed through the precipitation of dawsonite, but it was calculated that only 2.4 % of the CO_2 present within the structure is currently locked up as dawsonite, and a similar quantity in solution in the pore waters. Comparison of stable O and C isotopes with a neighbouring field with low CO_2 content gas suggests that up to 0.7 % solid volume dolomite cement is associated with the CO_2 charge, equivalent to 0-25% of the total CO_2. The remaining 70-95% of the CO_2 is present as a free phase, after ten of millions of years. Consequently, geological storage of anthropogenic CO_2 in reservoirs similar to the Rotliegend Group must rely on physical containment and not mineral trapping.

5.4 Summary

Caprocks and intraformational seals made up of shale or mudstone could interact geochemically with injected CO_2 and other gases, predominantly in the coupled dissolution/precipitation process. Depending on the particular impurity, impurities may or may not have an effect on the long-term caprock seal integrity. The case studies presented conclude that the nature and scale of, CO_2 interactions with caprocks depending on site specific circumstances, and may have significant consequences. Some of the reactions could be beneficial, helping to chemically contain or ‘trap’ the CO_2; others may be deleterious, and actually aid the migration of CO_2. Carbon dioxide - water - (cap) rock interactions, therefore, are highly variable, and require very precise characterisation of minerals and fluids from the host formation. Investigations into potential reactions also benefit from the combined outputs of laboratory studies, numerical modelling, field monitoring and comparisons with natural analogues.

6. Risk Assessment

6.1 Introduction

Understanding how CO_2 will migrate once injected is critical for assessing its potential to contaminate valuable resources above caprocks (e.g., water, coal, gas and oil) and/or to leak into the atmosphere. These outcomes could present health and safety, economic, social and technical risks which impact on the ability of some CCS projects to be successfully completed (e.g., Wildenborg et al., 2003; Bowden & Rigg, 2004; Benson, 2005). The ability of caprocks to contain CO_2 migration will be controlled by a number of factors, including their bulk permeability and lateral continuity above the reservoir. The bulk permeability may be influenced by faults and fractures, and pre-existing wells. Therefore, in addition to measuring the local flow properties of caprocks (e.g., from core) specific consideration should be given to documenting the stratigraphic architecture of caprocks, to determining the up-dip permeabilities of faults and fractures and to locating pre-existing wells. Which of these factors is of greatest importance for caprock integrity and risk to containment will likely vary between sites. At the Weyburn Field in Canada, for example, there are about ~4000 wells in the region of the container and leakage up wells may present an important risk to containment (Stenhouse et al., 2005), whereas at the Otway Basin site in Australia the pre-existing well was utilised during operations and does not pose a significant risk to containment (Bowden and Rigg, 2004).

Assessment of the risks to containment arising from a CO_2 breach of the caprock is generally undertaken using 3D fluid-flow models. These models are populated with geometric and flow properties of caprock (and reservoir) and incorporate pressure and temperature conditions in, and surrounding, the container. They include the dynamic effects of CO_2 injection and enable the movement of the CO_2 plume and any potential leakage through caprocks to be predicted over a specified period of time. An important aspect of determining the risks posed by migration of injected CO_2 through caprocks is establishing how long the CO_2 should remain in the sub-surface and what rates of migration from the primary container are acceptable. In circumstances where the pre-defined targets are unlikely to be met risks to the project are elevated. Acceptable levels of leakage from a geological container (e.g., into the atmosphere or aquifers) will vary between sites depending on the resulting levels of exposure of people, ecosystems and resources to CO_2. Leakage rates of$\leq$0.01% per ye ar of the total injected volume are required for long-term climate benefit (Herzog, 2001; Enting et al., 2008), while CO_2 concentrations in the atmosphere of 7-10% are often fatal to humans (Vendrig et al., 2003). Although these leakage rates are significantly higher than what would be expected for caprocks not penetrated by pre-existing wells or open fractures, measurement and modelling of CO_2 flow rates through caprocks will be an essential part of the risk assessment process.

6.2 Leakage Time Frames and Volumes

Leakage of stored CO_2 from its intended containment in terms of timeframes (flux rates) and volumes is intrinsically related to the specifics of the geology and in-situ conditions of each storage site. The range of possibilities conceptually spans everything from catastrophic to virtually no leakage. However, one can characterise what might be expected by examining some case studies of typical cap or fault rock, reservoir rock and fluid properties and calculating the resulting fluxes assuming a mobile phase of CO_2 is available to migrate. It should further be noted that loss of containment from the intended storage reservoir does not necessarily equate to leakage to the atmosphere where the leaked CO_2 will impact climate.

The review of natural and industrial analogues (Streit and Watson, 2004; Lewicki et al., 2007) resulted in a wide range of observed CO_2 leakage rates, ranging between 0 to 14 t/day (Table 6.1). In these cases, leakage occurs largely along distinct flow pathways like faults or abandoned wells. For the Rangely EOR field leakage amounts to 0.005% of injected CO_2 (Klusman, 2003a,b), compared to a maximum of 5.6% leakage modeled for the Atzbach-Schwanenstadt gas field (CO2EGR) (Polak and Grimstad, 2009).

Table 6.1 **Calculated leakage rates from natural CO_2 accumulations in Australia, North America and Europe.**

Site	Leakage pathway	Method	Flux/(Flow rate)	Reference
Otway (Penola)	Fault conduit	soil flux data	5.7 E-03 t/yr/m^2	Streit and Watson (2004)
Otway (Pine Lodge)	Fault conduit	soil flux data	1.5 E-02 t/yr/m^2	Streit and Watson (2004)
Otway (Pine Lodge)	Permeable zone	soil flux data	3.7 E-03 to 3.7 E-03 t/yr/m^2	Streit and Watson (2004)
Vorderrhon, Germany	Fault conduit	soil flux data	0 t/yr/m^2	Pearce et al. (2002)
Matraderecske, Hungary	Fault conduit	soil flux data	< 6.4 t/yr/m^2	Pearce et al. (2002)
Matraderecske, HungaryLatera, Tuscany	Permeable zone	soil flux data	0.1 to 0.2 t/yr/m^2	Pearce et al. (2002)
Latera, Tuscany	Permeable zone	soil flux data	39.4 t/yr/m^2	Pearce et al. (2002)
Mesozoic carbonate	Permeable zone	soil flux data	1.76 E-05 to 3.96 E-04 t/yr/m^2	Chiodini et al. (1999)
Mammoth Mountain, CA USA	Faults & fractures	atmospheric CO_2 concentrations and fluxes	0.2 t/yr/m2 (250 t/day)	Lewicki et al. (2007)
Solfatara, Italy	Faults & fractures	soil flux data	1.1 t/yr/m2 (1500 t/day)	Lewicki et al. (2007)
Albani Hills, Italy	Faults & fractures	soil flux data	0.44 t/yr/m^2 (74 t/day)	Lewicki et al. (2007)
Laacher See (Germany)		lake surface CO_2 concentrations and fluxes	(14 t/day)	Lewicki et al. (2007)
Paradox Basin, UT, USA	Faults & fractures	atmospheric CO_2 concentrations	(33 t/day)	Lewicki et al. (2007)
Rangely EOR field		soil flux data	(0.5 t/day)	Klusman (2003a)
Atzbach-Schwanenstadt	Abandoned wells	modelled	(1.5 t/day)	Polak and Grimstad (2009)

Due to the low migration rates of CO_2 through intact shales, dispersed leakage processes are not considered to be important when considering long term CO_2 storage, even at geological time scales (Busch et al., 2008). Rates of movement through fine grained muddy cap seal rocks are in the order of 700's of years per metre (Lindeberg and Bergmo 2002) to 33,000+ years per metre for water (Dewhurst et al. 1999) for the low volumes that could migrate through these sub-micron pore throats. Dewhurst et al. (1999) notes a hydraulic conductivity data band from 10^{-16} to 10^{-10}m/s, which represents fluid migration rates from 3µm to 30mm/1000 years. In studies of the Sleipner gas field (Norwegian North Sea), Lindeberg and Bergmo (2002) suggest that CO_2 will take more than 500 000 years to reach the sea floor at Sleipner via diffusion with resulting ppm rates of leakage. They also reiterate that CO_2 entry and pathway establishment through the seal is a function of the surface tension between the fluids (IFT) and the pore throat size distribution, so that ideally pore throat diameters are <100 nm (nanometers).

Recently, using experimental results, Teige et al. (2011) claimed that capillary sealing for hydrocarbons is effective only for a limited time period. With time oil-wet flow paths are established through a shale seal, which would allow for membrane leakage. According to Teige et al. (2011), the creation of oil-wet seals is due to changes in wettability, based on the interaction between shale mineralogy and oil chemistry. However, the applicability of this migration mechanism to CO_2 leakage has not been investigated to date.

Long residence time can lead to either a deterioration or enhancement of seal properties due to various diagenetic processes taking place during the CO_2 storage period (Hildenbrand et al., 2004). Yet, Wollenweber et al. (2010) could not detect any short-term mineral reactions in laboratory CO_2 flow tests through a clay-rich marlstone and a calcite-rich limestone. However, repetitive CO_2 gas breakthrough experiments on the same sample revealed a continuous lowering of the threshold pressures and a slight increase in permeability coefficients (Wollenweber et al., 2010). Still, it is important to consider each potential site for possible local diagenetic reactions, particular with respect to long time frames.

Buoyancy-driven flow of CO_2 through a percolating network of permeable sand bodies or faults in a sealing caprock has been modeled by Grimstad et al. (2009) and Zhang et al. (2009), respectively. Applying percolation theory to the slow migration of CO_2 in low-permeability environments is a promising methodology because it provides relatively faster solutions than computationally extensive two-phase flow models.

Primary migration of hydrocarbons within and out of low-permeability source rocks has been discussed widely in the petroleum literature. It is commonly accepted, that the capillary threshold of intact shale is too large for significant gas or oil migration to occur. However, overpressures due to hydrocarbon generation (Osborne and Swarbrick, 1997 and references therein) are believed to induce discrete flow pathways in the form of microfissures, along which hydrocarbons preferentially migrate through the source rock (i.e. Hedberg, 1974; Duppenbecker et al., 1991; Hunt, 1996; Harrington and Horseman, 1999). Expulsion of hydrocarbons from the source rock results in pressure dissipation, and microfissures will close after there is no more sufficient kerogen for hydrocarbon generation or if the temperature decrease to below that necessary for the conversion of kerogen to hydrocarbons. With application to the CO_2 leakage through caprocks, laboratory studies confirmed that the migration of CO_2 would occur primarily along pressure-induced pathways, after applying increasing excess pressure to water-saturated shale samples (Angeli et al., 2009; Harrington et al., 2009; Skurtveit et al., 2010). Limiting CO_2 injection pressures to below the fracture pressures of the reservoir rock and seal should prevent the creation of pressure-induced pathways.

6.2.1 Flow Rates Along Faults and Fractures

The rates at which CO_2 migrate through mudstone-rich caprocks is dependent on a number of factors including, the permeability of the caprock, the geometry and dimensions of fractures contained within the caprock and the pressure gradient across the caprock interval. In the absence of fractures caprocks typically have permeabilities in the range of 10^{-1} to 10^{-4} mD, with lower values for rocks with higher percentage clay fraction and lower porosity (e.g., Dewhurst et al., 1999). These low permeabilities are accompanied by similarly low flow rates or hydraulic conductivity through caprocks, which are of the order of 10^{-9} m/yr (e.g., Eichhubl and Boles, 2000). In circumstances where bulk flow rates through a rock mass are higher than would be predicted from core plug analysis, conductive faults and fractures are often inferred to locally elevate permeabilities (see Dewhurst et al., 1999 and references therein). While the permeabilities of fault rock (i.e. 10^{-2} to 10^{-6} mD) may be similar to the enclosing caprock, the presence of open fractures within fault zones has the potential to significantly increase rock permeability and flow rates along faults. Modelling of temperature anomalies at faults is, for example, consistent with flow rates of the order of 10^{1} to 10^{3} m/yr within fault zones (Matthai and Roberts, 1996; Roberts et al., 1996; Losh et al., 1999). Still higher flow rates of 10^{4} to 10^{8} m/yr have been inferred from mineralisation in fault zones (Eichhubl and Boles, 2000). These high rates of flow (i.e. 10^{1} to 10^{8} m/yr) are generally considered to be transient and may be focused or channelised along parts of fault or fracture surfaces. Increases in pore pressure and/or permeability during fault-slip events (e.g., earthquakes) may be an important mechanism for generating pulsed fluid flow (e.g., Sibson, 1990; Losh et al., 1999; Eichhubl and Boles, 2000). The seismic pumping or fault valving hypothesis is consistent with the view that fault reactivation arising from CO_2 injection could temporally elevate flow rates and should, as far as possible, be avoided. In the absence of significant fault reactivation flow rates within CO_2 reservoirs and overlying caprocks may be significantly lower than the rates presented here. Further, it should also be noted that the present sample of inferred flow rates along faults is small, that these rates are most likely to record values towards the upper limit of what is possible (i.e., because high flow rates would be most easily identified and measured), and that these flow rates would be expected to vary between sites dependent on local stress, strain and fluid conditions. Therefore, caution should be exercised when interpreting the available flow rates for fault zones and fracture systems. Further research is required to quantify better flow rates of CO_2 migrating through faulted or fractured caprocks and to establish under what circumstances they will be sufficiently high to pose a risk to containment.

6.3 Monitoring of Caprock Integrity

Seismic imagery, fluid, atmospheric and soil gas measurements are necessary to confirm *containment* of injected CO_2 in the reservoir, and to provide *assurance* that groundwater, soil and air are unaffected In addition, these techniques are useful to validate dynamic and geochemical models at storage sites. The assurance measurements compare pre- and post-injection properties, and thus need to begin well before CO_2 injection commences, continue throughout the injection period, and continue for some years post-injection. Seismic measurements investigate an overlying aquifer, while groundwater, soil gas and atmospheric monitoring provide assurance at increasing distances from the reservoir. These assurance measurements will only show changes if leakage out of the reservoir (presumably through the caprock) occurs.

6.3.1 Geophysical Monitoring

Different remote sensing techniques are available to monitor the effects of gas injection or depletion in geological reservoirs. Amongst these, the most widespread in the oil and gas industry are 4D seismic and micro-seismic monitoring techniques. Microseismic events, related to either induced displacements on preexisting faults or fractures, or the creation of new fractures, capture deformations as the rock mass reacts to stresses and strains associated with pressure changes in the reservoir (Maxwell and Urbancic, 2001). Micro-seismic monitoring is performed real-time, by determining accurately the location of detected microseismic events. The quality of the location is a function of the velocity model, receiver orientation, quality, and reliability of the arrival-time picks. These micro-seismic events can be used to localize fracturing indicative of variation in the geomechanical conditions of the reservoir or the caprock and, thus, evaluating potential leakage risks. Passive seismic experiment to monitor CO2 storage sites have been carried out at Weyburn in the USA (Verdon et al., 2010), Aneth oil field (Utah, USA; Zhou et al., 2010) amongst other.

4D or time-lapse seismic methods are based on comparing different vintage of 3D seismic volumes recorded over the same field (e.g, Lumley, 2010). The data are processed to visualize changes in attributes related to expressions of fluid content. These techniques are routinely used to monitor producing oil and gas fields (Staples et al., 2005). 4D seismic data has been mostly used to track the displacement of a single hydrocarbon phase by water (e.g. Kloosterman et al., 2003), sometimes used to monitor pressure changes (e.g. Landro et al., 2001)), and occasionally used to measure compaction (e.g. Barkved et al., 2003). A successful experiment of monitoring CO_2 injection in depleted reservoir has been carried out for the Otway site in Australia (e.g, Urosevic et al., 2010), for the Sleipner Gas field in Norway (e.g., Chadwick et al., 2005; Chadwick et al., 2010) and Weyburn in Canada (e.g. Li, 2003).

6.3.2 Geochemical and Atmospheric monitoring

Direct measurements of subsurface reservoir fluids are the primary confirmation of containment. Monitoring wells are useful for achieving this objective but these must be adequately instrumented with what are commonly complex bottom-hole assemblies such as the U-tube fluid sampling apparatus (Freifeld et al., 2005) that was used to recover pressurized reservoir fluids at regular intervals in the Australian CO2CRC Otway Project (Kirste et al., 2010) as well as at the East Texas Frio Brine Project (Freifeld et al., 2005; Freifeld and Trautz, 2006). Similarly, there has been some direct monitoring of downhole fluids in existing wells in the zone above the caprock at Denbury's Cranfield, Mississippi, USA, EOR project (Hovorka et al., 2011).

Another effective method of monitoring is the inclusion of tracers to ensure unambiguous detection of injected CO_2. The Otway Project, for instance, labeled its injected gas with tracers (SF_6, Kr and CD_4), to allow verification of the presence of the injected CO_2 at various monitoring sites (Stalker et al., 2009). Integrity of containment can be tested directly through a comparison of predicted gas or formation fluid composition with measured molecular, isotopic, and tracer compositions.

Groundwater is an over-riding community concern. It is vital to confirm that potable aquifers are unaffected by CO_2. Once the baseline hydrogeology of the region is defined, the composition and chemistry of water in deep and shallow water wells should be measured on a regular basis (Hortle et al., 2009). Vadose zone soil gas composition could also be measured regularly to ensure that injected CO_2 has not escaped (Schacht et al., 2011).

Atmospheric monitoring, to record changes in concentrations and fluxes of CO_2, can be utilized at storage sites. These relatively inexpensive measuring arrays can monitor concentrations, isotopic composition ($\delta^{13}C\ CO_2$) and tracer concentrations and compared these to the base-line background atmospheric composition measured near the storage site (Leuning, et al., 2008).

7. Conclusions and Knowledge Gaps

7.1 Conclusions

The geological storage of CO_2 requires a porous reservoir rock (such as a sandstone or limestone) overlain by an impermeable caprock or seal. The importance of the caprock is that it provides containment of buoyant CO_2, displaced brine and other mobilised substances ensuring that these do not leak into overlying strata and towards sensitive environmental receptors. Any lithology can theoretically act as a caprock; however, shales, evaporates (halite and anhydrite) are the most common seals and are responsible for the majority of all trapping of oil and gas in hydrocarbon reservoirs as well as other gasses such as CO_2, N_2 and He. Factors such as lithology, thickness, ductility and fracture density influence the seal properties, and are determined by microscopic and macroscopic analyses of the caprock. Determining which seals have the potential to trap economically viable hydrocarbon accumulations, versus those that hold sub-economic volumes, has become an important aspect of evaluating both basin-wide hydrocarbon systems and field scale prospects in the petroleum industry. Similarly, determining the viability of caprocks for the retention of economic volumes of CO_2 is a critical element in the selection of sites for safe CO_2 injection and secure storage.

The storage security, especially in the early stages after the start of CO_2 injection, is largely influenced by the caprock seal potential, defined as seal capacity, geometry and integrity. Seal capacity refers to the CO_2 column thickness that can be held back by the seal through capillary forces. Seal geometry refers to the structural position, thickness, and areal extent of the caprock relative to the reservoir and/or structure. Where the caprock's areal extent is equal to or greater than the areal extent of the reservoir or structure, (ie the caprock overlies the entire reservoir / structure), the membrane properties of the caprock seal are in effect throughout. Similarly, as caprock thickness increases, the likelihood of sub-seismic through-going faults or fractures decreases. Generally, if the thickness of the caprock is greater than the fault throw, the integrity of the caprock is enhanced. Caprocks can be in the form of laterally extensive, thick, single seal layers that extend over the entire storage formation, or part of a multilayered system, where permeable layers are interbedded with thin low permeability layers (intraformational seals). Each type presents different analytical challenges based on its unique set of stratigraphic, geophysical, geomechanical, and hydrodynamic characteristics. Increased volumes of CO_2 can potentially be stored in multilayered sand/shale caprock systems compared to a single caprock/reservoir couplet (Gibson-Poole et al., 2006). However, multilayered systems are more risky because small faults and fractures, which are below seismic detection, can create a connected leakage pathway through fractures and fault-offset inter-connected permeable intervals.

The seal integrity of the caprock refers to its geomechanical properties. These are controlled by the interplay between the regional stress regime, pre-existing faults, fractures and microfractures, and can be enhanced by pressure changes from the injection of CO_2. The magnitude of the pressure on the caprock depends on the permeability, the location of the injection well and whether the system is open or closed Understanding the geomechanical properties of the caprock, the change in stress state with CO_2 injection, and identification and understanding of changes in material properties as a result of interaction with CO_2 rich fluids are essential for the overall evaluation of its sealing integrity.

Mechanical deformation or damage of the seal can be related to the effect of induced pressure from the injection of CO_2. This pressure may theoretically induce fracturing of the seal or reactivate existing fractures and faults. Fault reactivation represents a major risk to caprock integrity and CO_2 retention. A combination of rock physics, fault zone architecture, and an understanding of fault kinematics allows for predictive risking of fault reactivation when the effective stress of a reservoir is changed through CO_2 injection. The role of CO_2 influx-triggered pressure perturbation on microfracture evolution is also important. Microfractures rapidly open up during the initial plume ascent associated with CO_2 accumulation during the active injection phase, They then asymptotically close and continue to do so during the post-injection phase. However, unless counterbalanced by geochemical effects, this geomechanical widening could facilitate CO_2 migration into the caprock.

Depending on regional hydrodynamic and pressure regimes, hydrodynamics may play a significant role on the sealing capacity of caprocks and faults. The findings from hydrocarbon-focused studies are directly applicable to CO_2 geological storage as CO_2 in its supercritical state is a buoyant fluid and the same principle of capillary movement applies. Pressure differences of formation water between the two sides of a seal have an impact on the total membrane (capillary) seal capacity for the seal. In fact, the high-pressure side of the seal, independent from the location of the hydrocarbon or CO_2 accumulation, determines the height of the hydrocarbon column that can be supported by the top or fault seal. In other words, the side with the lower pressure can hold more hydrocarbons or CO_2 because, in addition to the capillary entry pressure of the sealing rock, migrating hydrocarbons or CO_2 also have to overcome the increasing pore pressure gradient through the seal. On the other hand, in the static case, where hydrodynamic forces are minimal, the seal capacity depends mainly on the capillary entry pressure. As is often the case in petroleum systems, hydrodynamic impacts on the sealing capacity for CO_2 storage are probably of secondary importance compared to other seal properties (i.e. permeability) and stress regime. Still, the significance of hydrodynamics increases the more subsurface pressure regimes diverge from hydrostatic conditions. Therefore, fluid pressures on both sides of the seal of a potential storage reservoir need to be considered when assessing the sealing capacity.

After injection of CO_2 into a reservoir, the lower boundary of the caprock will be in contact with CO_2 saturated pore water or pore fluid consisting of pure CO_2. Geochemical interaction between the pore fluid and the caprock may change the mineralogical and petrophysical properties of the caprock as well. Therefore knowledge of the composition of the seal rock as well as the formation fluids is important to predict the geochemical reactions and the minerals formed after CO_2 injection. There may be coupling between CO_2 and geochemical reactions that could be self-enhancing (with permeability increases due to dissolution) or self-limiting (with permeability decreases due to precipitation of new minerals).

For typical shale caprocks, CO_2 influx-triggered geochemical and geomechanical processes may act in opposition or in conjunction. For example the pressure increase on the caprock can cause an existing microfracture to widen, which then causes more fluid to flow through, which can cause mineral precipitation, thereby lowering the permeability. Which process has the greater effect will determine whether the permeability and integrity of the seal is increased or decreased. The effect of $CO_{2,}$ across a range of pressures, on caprocks is clearly important for risk assessment on leakage and determination of possible leakage pathways.

For stacked seal systems, the cumulative impact of multiple caprocks interspersed with reservoirs that each has storage capacity should result in a cumulative mitigation of risk for leakage to sensitive environmental receptors. Also, the relative pressure regimes between the multiple layers are a determinant of the interplay between buoyant forces and hydrodynamic flow gradients.

Several mechanisms can lead to potential migration of the stored CO_2 from its intended containment after injection. Timeframes (flux rates) and volumes of such movement of CO_2 is related to the specifics of the geology and in-situ conditions of each storage site and ranges from catastrophic to virtually no movement. Migration of the CO_2 may also take place through diffusion and capillary forcing due to changes in wettability and/or interfacial tension caused by CO_2-caprock interaction. Such changes in the caprock mineralogy due to geochemical interactions may lead to either the dissolution of some minerals and thus to an increase in permeability or to the precipitation of minerals, leading to decreased permeability. Such geochemical reactions would impact both the membrane seal capacity and the geomechanical seal integrity. The uncertainty surrounding the coupling between these geomechanical and geochemical processes has been identified as a major containment risk for natural gas/CO_2 geological storage projects.

Although one of the most significant risks for containment identified is the risk of leakage through wellbores (Celia et al., 2004), only leakage through natural systems (caprock, faults and fractures) are addressed in this report.

7.2 Identified Gaps in Caprock Understanding

Site-specific data will always need to be collected before either multiple reservoir/caprock or single reservoir/caprock systems can be utilized for CO_2 storage. A compendium (database) of caprock properties from existing sites (mainly EOR and demonstration sites) is lacking and would be useful for future projects. Such a database should include caprock properties (including seal capacity, mineralogy, well-log, geochemical and petrophysical characteristics) of regional, local and intraformational seals. This type of data could be used as analogs when assessing containment potential for a specific area where data are lacking. The types of data that can be captured are detailed in Appendix A2.

Mercury injection capillary pressure (MICP) analysis has been used extensively in the petroleum industry to determine the effectiveness of the top seal in relation to hydrocarbon column height retention. To date, however, this technique has had limited application to prediction of containment in geological storage of CO_2. In addition, up-scaling MICP measurements remains a key challenge. The role of IFT and wettability in the CO_2-water-rock systems is not well understood and it is unclear how supercritical CO_2 ($scCO_2$) affects these two properties, particularly as the water front becomes saturated with $scCO_2$ at high pressure reservoir conditions. Important considerations are the phase properties of CO_2 and formation water, once the water acidifies from CO_2 dissolution, and any impurities (e.g. the acid gases H_2S, SO_x and NO_x). These tend to alter the wettability up to and into the supercritical P/T range. However, limited research showing experimental evidence on a) the state of the CO_2 saturated water and b) its effect on seal rock mineralogy with respect to capillary pressure has been conducted. These are pertinent to the associated controls in determining CO_2 column height of the sealing lithology.

Calculation of CO_2-water interfacial tension is a function of pressure, temperature and CO_2 density. There is an increasing amount of experimental work being carried out in this area, which has been summarised by recent significant experimental work by Bachu and Bennion (2008), where an IFT relationship has been developed using pressure, temperature and salinity data. An important ongoing step would be to verify these contact angle and interfacial tension data in a field pilot study, so that contact angles and IFT's can be quantified at ambient CO_2 injection conditions.

The impact of hydrodynamics on the sealing capacity of top seals and faults has been discussed in the literature only with respect to hydrocarbon migration. The change in capillary sealing capacity due to hydraulic gradients has been demonstrated theoretically and numerically, however the magnitude and significance of this process needs to be confirmed by studies utilizing empirical field examples. With respect to CO_2 geological storage, little research has been published on this issue, though the IEAGHG report on *Pressurization and Brine Displacement Issues for Deep Saline Formation CO_2 Storage* has begun to address this gap. The most critical knowledge gap on this topic is the absence of data to calibrate analytical and numerical models and to quantify the impact of seal properties on reservoir pressure and capacity calculations.

Current research on understanding what conditions allow faults to seal and leak occur principally in the domain of hydrocarbon exploration, where significant effort has been devoted to identifying and predicting up fault leakage in the deep subsurface. Various hydrocarbon leakage indicators have been identified, where such indicators can be used as proof of valid hydrocarbon systems in a basin and used as exploration leads. These studies rely on a multidisciplinary approach involving rock mechanics, hydrodynamics, structural geology, fluid inclusion technology and complex seismic interpretation and rock physics. While these same methodologies and techniques can be used to predict the containment security of faults, including the reactivation potential, for CO_2 storage in the deep subsurface, studies in this regard have not been done. Also, few studies have been reported on faults and fractures in mudstone-rich caprocks. Furthermore, no clear methods for assigning up-fault permeability have been described. In a broader sense, further research is required to establish which caprock types are most likely to be faulted and fractured.

Sealing faults that successfully trap hydrocarbons could also form suitable confining barriers at CO_2 storage sites. However, it is almost a given, by proponents, regulatory agencies and the public that suitable sites for the geological storage of carbon dioxide, be devoid of faults. However no studies demonstrating the positive, containment-enhancing role of faults for CO_2 containment have been provided to the CCS community to date.

Hydrodynamic, geochemical and geomechanical properties of both the reservoir and caprock are important to determine whether multiple reservoir/caprock and/or single reservoir/caprock systems can be utilised for safe, long-term storage. Very little work has been done towards understanding the interplay between the combined effects of these properties on caprocks.

Chemical interaction between CO_2 and caprock minerals may affect the mechanical strength and transport properties of the sealing formation, possibly inducing slip along currently sealing faults, or creating pathways, allowing carbon dioxide migration. However, very few studies attempt to couple chemical and mechanical processes occurring within the caprock as a result of CO_2 injection. Modelling of the hydraulic integrity of the reservoirs to quantify connectivity between the systems and continuity of intraformational seals and barriers is lacking. Collected data can then be integrated in predictive models of caprock integrity.

Apart from the leakage risk, the integrity and geometry of caprocks has a large impact on the pressurisation of CO_2 storage reservoirs. Therefore, incorporating findings from the recent Permedia study on Pressurisation and Brine Displacement may be an important aspect of the understanding containment issues in caprocks. Monitoring of the caprock directly is rarely considered. However, opportunities for doing such measurements may be available in EOR projects. Such projects (e.g. Weyburn, Cranfield) with adequate well control may allow the use of wells for monitoring downhole pressure and temperature in the caprock and not just in the reservoir.

8. References

A

Abrams, M.A., 1996. Distribution of subsurface hydrocarbon seepage in near-surface marine sediments. AAPG Memoir, 66: 1-14.

Ackermann, R.V., Schlische, R.W. and Withjack, M.O., 2001. The geometric and statistical evolution of normal fault systems: An experimental study of the effects of mechanical layer thickness on scaling laws. Journal of Structural Geology, 23(11): 1803-1819.

Addis, M.A., 1997. Reservoir depletion and its effect on wellbore stability evaluation. International Journal of Rock Mechanics and Mining Sciences, 34: 3-4.

Al-Dossary, S. and Marfurt, K.J., 2006. 3D volumetric multispectral estimates of reflector curvature and rotation. Geophysics, 71(5): P41-P51.

Allen, P. and Allen, J., 2005. Basin Analysis - Principles and Applications. Blackwell Publishing Ltd, 549 pp.

Al-Siyabi, Z., Danesh, A., Tohidi, B. and Todd, A.C., 1999. Variation of gas-oil-solid contact angle with interfacial tension. Petroleum Geoscience, 5(1): 37-40.

Ambrose, W.A., Ferrer, E.R., Dutton, S.P., Wang, F.P., Padron-Carrasquel, W.A., Yeh, J.S., and Tyler, N., 1995. Production optimisation of tide-dominated deltaic reservoirs of the Lower Misoa Formation (Lower Eocene), LL—652 Area, Lagunillas Field, Lake Maracaibo, Venezuela, The University of Texas at Austin, Bureau of Economic Geology.

Ambrose, W.A., Lakshminarasimhan, S., Holtz, M.H., Nunez-Lopez, V., Hovorka, S.D., and Duncan I., 2008. Geologic factors controlling CO_2 storage capacity and permanence: Case studies based on experience with heterogeneity in oil and gas reservoirs applied to CO_2 storage. Environmental Geology, 54(8): 1619-1633.

Aminzadeh, F., Connolly, D.L. and Ligtenberg, J.H., 2004. Hydrocarbon phase detection and other applications of chimney technology, AAPG International Conference & Exhibition, Cancun, Mexico.

Anderson, E.M., 1951. The Dynamics of Faulting and Dyke Formation with Application to Britain. Oliver and Boyd, Edinburgh.

Anderson, W., 1986. Wettability literature survey: Part 2. Wettability measurement. Journal of Petroleum Technology, 38: 1242-1262.

Aydin, A., 2000. Fractures, faults, and hydrocarbon entrapment, migration and flow. Marine and Petroleum Geology, 17(7): 797-814.

B

Bachu, S., 2008. CO_2 storage in geological media: Role, means, status and barriers to deployment. Progress in Energy and Combustion Science, 34(2): 254-273.

Bachu, S. and Bennion, B., 2008. Effects of in-situ conditions on relative permeability characteristics of CO_2-brine systems. Environmental Geology, 54(8): 1707-1722.

Bachu, S. and Bennion, D.B., 2009. Interfacial tension between CO_2, freshwater, and brine in the range of pressure from 2 to 27 MPa, temperature from 20 to 125 °C, and water salinity from 0 to334 000 mg/L. Journal of Chemical and Engineering Data, 54(3): 765-775.

Bai, T. and Pollard, D.D., 2000. Closely spaced fractures in layered rocks: Initiation mechanism and propagation kinematics. Journal of Structural Geology, 22(10): 1409-1425.

Baines, S.J. and Worden, R.H., 2000. Geological disposal: Understanding the long term fate of CO_2 in naturally occurring accumulations. In: D. Williams, R. Durie, P. McMullan, C. Paulson and A. Smith (Editors), Proceedings of the 5th International Conference on Greenhouse Gas Control Technologies (GHGT-5), Cairns, Australia: 311-316.

Barkved, O., Buer, K., Halleland, K.B., Kjelstadli, R., Kleppan, T., and Kristiansen, T., 2003. 4D seismic response of primary production and waste injection at the Valhall field, 65th EAGE Conference, Stavanger, Norway: A22.

Barr, D., Savory, K.E., Fowler, S.R., Arman, K. and Mcgarrity, J.P., 2007. Pre-development fracture modelling in the Claire field, west of Shetland. Geological Society Special Publication, 270: 205-225.

Bath, P.G.H., 1989. Status report on miscible/immiscible gas flooding. Journal of Petroleum Science and Engineering, 2(2-3): 103-117.

Bell, J.S., 1990. The stress regime of the Scotian Shelf offshore eastern Canada to 6 kilometers depth and implications for rock mechanics and hydrocarbon migration. In: V. Maury and D. Fourmaintraux (Editors), Rock at Great Depth. Balkema, Rotterdam: 1243-1265.

Bennion, B. and Bachu, S., 2006a. The impact of interfacial tension and pore-size distribution/capillary pressure character on CO_2 relative permeability at reservoir conditions in CO_2-brine systems, Proceedings - SPE Symposium on Improved Oil Recovery: 142-151.

Bennion, D.B. and Bachu, S., 2006b. Dependence on temperature, pressure, and salinity of the IFT and relative permeability displacement characteristics of CO_2 injected in deep saline aquifers, Proceedings - SPE Annual Technical Conference and Exhibition: 1049-1057.

Bennion, D.B. and Bachu, S., 2008. A correlation of the interfacial tension between supercritical phase CO_2 and equilibrium brines as a function of salinity, temperature and pressure, Proceedings - SPE Annual Technical Conference and Exhibition: 224-237.

Benson, S.M., 2005. Lessons Learned From Industrial and Natural Analogs for Health, Safety and Environmental Risk Assessment for Geologic Storage of Carbon Dioxide. In: D.C. Thomas and S.M. Benson (Editors), Carbon Dioxide for Storage in Deep Geologic Formations. Elsevier: 1133-1141.

Benson, S.M. and Cook, P., 2005. Underground geological storage. In: B. Metz, O. Davidson, H. de Coninck, M. Loos and L. Meyer (Editors), IPCC special report on carbon dioxide capture and storage. Cambridge University Press, Cambridge: 195-276.

Berard, T., Jammes, L., Lecampion, B., Vivalda, C. and Desroches, J., 2007. CO_2 storage geomechanics for performance and risk management, Offshore Europe Conference – Proceedings: 189-196.

Berg, R.R., 1975. Capillary pressures in stratigraphic traps. AAPG Bulletin, 59(6): 939-956.

Bi, Z., Zhang, Z., Xu, F., Qian, Y. and Yu, J., 1999. Wettability, oil recovery, and interfacial tension with an SDBS- dodecane-kaolin system. Journal of Colloid and Interface Science, 214(2): 368-372.

Bjorkum, P.A., Walderhaug, O. and Nadeau, P.H., 1998. Physical constraints on hydrocarbon leakage and trapping revisited. Petroleum Geoscience, 4(3): 237-239.

Bolas, H.M.N. and Hermanrud, C., 2003. Hydrocarbon leakage processes and trap retention capacities offshore Norway. Petroleum Geoscience, 9(4): 321-332.

Bott, M.H.P., 1959. The mechanics of oblique slip faulting. Geological Magazine, 96: 109-117.

Bouvier, J.D., Kaars-Sijpesteijn, C.H., Kluesner, D.F., Onyejekwe, C.C. and Van Der Pal, R.C., 1989. Three-dimensional seismic interpretation and fault sealing investigations, Nun River Field, Nigeria. AAPG Bulletin, 73(11): 1397-1414.

Bowden, A.R. and Rigg, A., 2004. Assessing Risk in CO_2 Storage Projects. APPEA Journal Australia, 44: 677-702.

Breckels, I.M. and van Eekelen, H.A.M., 1982. Relationship between horizontal stress and depth in sedimentary basins. Journal of Petroleum Technology, 34: 2191- 2198.

Bretan, P. and Yielding, G., 2005. Using buoyancy pressure profiles to assess uncertainty in fault seal calibration. In: P. Boult and J. Kaldi (Editors), Evaluating fault and cap rock seals. AAPG Hedberg Series, Tulsa, OK: 151-162.

Bretan, P., Yielding, G. and Jones, H., 2003. Using calibrated shale gouge ratio to estimate hydrocarbon column heights. AAPG Bulletin, 87(3): 397-413.

Bromhal, G.S., Neal Sams, W., Jikich, S., Ertekin, T. and Smith, D.H., 2005. Simulation of CO_2 sequestration in coal beds: The effects of sorption isotherms. Chemical Geology, 217(3-4 Special Issue): 201-211.

Brown, A., 2000. Evaluation of possible gas micro-seepage mechanisms. AAPG Bulletin, 84(11): 1775-1789.

Brown, A., 2003. Capillary effects on fault-fill sealing. AAPG Bulletin, 87(3): 381-395.

Brudy, M., Zoback, M.D., Fuchs, K., Rummel, F. and Baumgartner, J., 1997. Estimation of the complete stress tensor to 8 km depth in the KTB scientific drill holes: Implications for crustal strength. Journal of Geophysical Research B: Solid Earth, 102(B8): 18453-18475.

Bruno, M.S. and Bilak, R.A., 1994. Cost-effective monitoring of injected steam migration using surface deformation analysis, Proceedings - SPE Annual Western Regional Meeting: 397-412.

Busch, A., Alles, S., Gensterblum, Y., Prinz, D., Dewhurst, D.N., Raven, M.D., Stanjek, H., and Krooss, B.M., 2008. Carbon dioxide storage potential of shales. International Journal of Greenhouse Gas Control, 2(3): 297-308.

Byerlee, J., 1978. Friction of rocks. Pure and Applied Geophysics PAGEOPH, 116(4-5): 615-626.

C

Caine, J.S., Evans, J.P. and Forster, C.B., 1996. Fault zone architecture and permeability structure. Geology, 24(11): 1025-1028.

Caine, J.S. and Forster, C.B., 1999. Fault zone architecture and fluid flow: Insights from field data and numerical modeling. In: W.C. Haneberg (Editor), Faults and subsurface fluid flow in the shallow crust. American Geophysical Union Geophysical Monograph: 101-127.

Cappa, F., Rutqvist, J. and Yamamoto, K., 2009. Modeling crustal deformation and rupture processes related to upwelling of deep CO_2-rich fluids during the 1965-1967 Matsushiro earthquake swarm in Japan. Journal of Geophysical Research B: Solid Earth, 114(10).

Carruthers, D. and Ringrose, P., 1998. Secondary oil migration: oil-rock contact volumes, flow behaviour and rates. Geological Society Special Publication, London: 205-220.

Carruthers, D.J., 2003. Modeling of secondary petroleum migration using invasion percolation techniques. In: S. Duppenbecker and R. Marzi (Editors), Multidimensional basin modeling. Datapages Discovery Series. AAPG: 21-37.

Cartwright, J., Huuse, M. and Aplin, A., 2007. Seal bypass systems. AAPG Bulletin, 91(8): 1141-1166.

Cavanagh, A. and Wildgust, N., 2011. Pressurization and brine displacement issues for deep saline formation CO_2 storage. Energy Procedia, 4: 4814-4821.

Cavanagh, A.J. and Haszeldine, R.S., 2009. A calibrated model for the first decade of the Sleipner CO_2 plume development, AAPG/SEG/SPE Hedberg Conference - Geological carbon sequestration: prediction and verification, Vancouver, Canada.

Cavanagh, A.J. and Ringrose, P., 2009. Simulation of CO_2 distribution at the In Salah storage site using high-resolution field scale models, AAPG/SEG/SPE Hedberg Conference - Geological carbon sequestration: prediction and verification, Vancouver, Canada.

Celia, M.A. and Bachu, S., 2002. Geological sequestration of carbon dioxide: Is leakage unavoidable and acceptable?, Proceedings of the 6th International Conference on Greenhouse Gas Control Technologies (GHGT-6), Kyoto, Japan: 477-482.

Celia, M.A., Bachu, S., Nordbotten, J.M., Gasda, S.E. and Dahle, H.K., 2004. Quantitative estimation of CO_2 leakage from geological storage: Analytical models, numerical models, and data needs, Proceedings of the 7th International Conference on Greenhouse Gas Control Technologies (GHGT-7), Vancouver, Canada: 663-671.

Chadwick, A., Williams, G., Delepine, N., Clochard, V., Labat, K., Sturton, S., Buddensiek, M.-L., Dillen, M., Nickel, M., Lima, A. L., Arts, R., Neele, F., and Rossi, G., 2010. Quantitative analysis of time-lapse seismic monitoring data at the Sleipner CO_2 storage operation. Leading Edge (Tulsa, OK), 29: 170-177.

Chadwick, R.A., Arts, R. and Eiken, O., 2005. 4D seismic quantification of a growing CO_2 plume at Sleipner, North Sea, Petroleum Geology: North West Europe and Global Perspectives - Proceedings of the 6th Petroleum Geology Conference, London, UK: 1385-1399.

Chadwick, R.A., Noy, D., Arts, R. and Eiken, O., 2009a. Latest time-lapse seismic data from Sleipner yield new insights into CO_2 plume development. Energy Procedia, 1: 2103-2110.

Chadwick, R.A., Noy, D.J. and Holloway, S., 2009b. Flow processes and pressure evolution in aquifers during the injection of supercritical CO_2 as a greenhouse gas mitigation measure. Petroleum Geoscience, 15(1): 59-73.

Chalbaud, C., Robin, M. and Egermann, P., 2006. Interfacial tension data and correlations of brine/CO_2 systems under reservoir conditions, Proceedings - SPE Annual Technical Conference and Exhibition: 3401-3411.

Chan, A.W. and Zoback, M.D., 2007. The role of hydrocarbon production on land subsidence and fault reactivation in the Louisiana coastal zone. Journal of Coastal Research, 23(3): 771-786.

Chiaramonte, L., Zoback, M.D., Friedmann, J. and Stamp, V., 2008. Seal integrity and feasibility of CO_2 sequestration in the Teapot Dome EOR pilot: Geomechanical site characterization. Environmental Geology, 54(8): 1667-1675.

Childs, C., Manzocchi, T., Walsh, J.J., Bonson, C.G., Nicol, A., and Schopfer, M.P.J., 2009. A geometric model of fault zone and fault rock thickness variations. Journal of Structural Geology, 31(2): 117-127.

Childs, C., Nicol, A., Walsh, J.J. and Watterson, J., 1996. Growth of vertically segmented normal faults. Journal of Structural Geology, 18(12): 1389-1397.

Childs, C., Watterson, J. and Walsh, J.J., 1995. Fault overlap zones within developing normal fault systems. Geological Society Special Publication, London: 535-549.

Chiodini, G., Frondini, F., Kerrick, D.M., Rogie, J., Parello, F., Peruzzi, L., and Zanzari, A. R., 1999. Quantification of deep CO_2 fluxes from Central Italy. Examples of carbon balance for regional aquifers and of soil diffuse degassing. Chemical Geology, 159(1-4): 205-222.

Chiquet, P., Broseta, D. and Thibeau, S., 2005. Capillary alteration of shaly caprocks by carbon dioxide, 67th European Association of Geoscientists and Engineers, EAGE Conference and Exhibition, incorporating SPE EUROPE2005 - Extended Abstracts: 17-26.

Chiquet, P., Broseta, D. and Thibeau, S., 2007a. Wettability alteration of caprock minerals by carbon dioxide. Geofluids, 7(2): 112-122.

Chiquet, P., Daridon, J.-L., Broseta, D. and Thibeau, S., 2007b. CO_2/water interfacial tensions under pressure and temperature conditions of CO_2 geological storage. Energy Conversion and Management, 48(3): 736-744.

Chopra, S. and Marfurt, K., 2007. Curvature attribute applications to 3D surface seismic data. Leading Edge (Tulsa, OK), 26(4): 404-414.

Chueng, P.S., 1999. Microresistivity and ultra sonic imagers: Toll operations and processing principles with reference to commonly encountered image artefacts. In: M.A. Lovell, G. Williamson and P.K. Harvey (Editors), Borehole Imaging: Applications and Case Histories. Geological Society Special Publication, London: 45-57.

Chun, B.-S. and Wilkinson, G.T., 1995. Interfacial tension in high-pressure carbon dioxide mixtures. Industrial and Engineering Chemistry Research, 34(12): 4371-4377.

Clayton, W.S., 1999. A new displacement experiment technique to measure unsteady state two-phase relative permeability-saturation-capillary head relationships. Water Resources Research, 35(10): 3199-3203.

Cowie, P.A., 1998. A healing-reloading feedback control on the growth rate of seismogenic faults. Journal of Structural Geology, 20(8): 1075-1087.

Crossey, L.J., Karlstrom, K.E., Springer, A.E., Newell, D., Hilton, D.R., and Fischer, T., 2009. Degassing of mantle-derived CO_2 and He from springs in the southern Colorado Plateau region - Neotectonic connections and implications for groundwater systems. Bulletin of the Geological Society of America, 121(7-8): 1034-1053.

Cuiec, L., 1987. Effect of drilling fluids on rock surface properties, Society of Petroleum Engineers of AIME: 149-158.

D

Damen, K., Faaij, A. and Turkenburg, W., 2006. Health, safety and environmental risks of underground CO_2 storage - Overview of mechanisms and current knowledge. Climatic Change, 74(1-3): 289-318.

Daniel, R.F., 2005. Boggy Creek carbon dioxide seal capacity study, Otway Basin, Victoria, Australia. CO2CRC Report, RPT05-0045: 47.

Daniel, R.F. and Kaldi, J.G., 2008. Evaluating seal capacity of caprocks and intraformational barriers for the geosequestration of CO_2, Eastern Australasian Basins Symposium, Sydney, NSW.

Daniel, R.F. and Kaldi, J.G., 2009. Evaluating seal capacity of cap rocks and intraformational barriers for CO_2 containment. In: M. Grobe, J.C. Pashin and R.I. Dodge (Editors), Carbon dioxide sequestration in geological media - State of the Science. AAPG Studies in Geology: 335-345.

Daniel, R.F. and Kaldi, J.G., in press. Atlas of Australian and New Zealand hydrocarbon seals: Analogues for worldwide seals. AAPG Special Publication, 60.

Daval, D., Martinez, I., Corvisier, J., Findling, N., Goffe, B., and Guyot, F., 2009. Carbonation of Ca-bearing silicates, the case of wollastonite: Experimental investigations and kinetic modeling. Chemical Geology, 265(1-2): 63-78.

Davies, R.K., An, L., Jones, P., Mathis, A. and Cornette, C., 2003. Fault-seal analysis South Marsh Island 36 field, Gulf of Mexico. AAPG Bulletin, 87(3): 479-491.

Dean, C., Jones, G. and Nugali, S., 2006. Fluidized catalytic cracking (FCC) kinetic model to support operation optimization and catalyst development for fuels and petrochemical products, World Petroleum Congress Proceedings.

Dewhurst, D.N., Jones, R.M. and Raven, M.D., 2002. Microstructural and petrophysical characterization of Muderong Shale: Application to top seal risking. Petroleum Geoscience, 8(4): 371-383.

Dewhurst, D.N., Siggins, A.F., Kuila, U., Clennell, M.B., Raven, M.D., and Nordgard-Bolas, H.M., 2008. Elastic, geomechanical and petrophysical properties of shales, 42nd U.S. Rock Mechanics - 2nd U.S.-Canada Rock Mechanics Symposium.

Dewhurst, D.N., Yang, Y. and Aplin, A.C., 1999. Permeability and fluid flow in natural mudstones. Geological Society Special Publication, London: 23-43.

Dockrill, B. and Shipton, Z.K., in press. Structural controls on leakage from a natural CO_2 geologic storage site: Central Utah, U.S.A. Journal of Structural Geology.

Donaldson, E.E., Thomas, R.D. and Lorenz, P.B., 1969. Wettability determination and its effect on recovery efficiency. SPE Journal: 13-20.

Downey, M.W., 1984. Evaluating seals for hydrocarbon accumulations. AAPG Bulletin, 68(11): 1752-1763.

Dragomirescu, D., Kaldi, J., Lemon, N. and Alexander, E., 2001. Triassic Seals in the Cooper Basin, Eastern Australasian Basins Symposium: 311-320.

Duppenbecker, S.J., Dohmen, L. and Welte, D.H., 1991. Numerical modelling of petroleum expulsion in two areas of the Lower Saxony Basin, northern Germany. In: W.A. England and A.J. Fleet (Editors), Petroleum Migration. Geological Society Special Publication: 47-64.

Dusseault, M.B. and Rothenburg, L., 2002. Analysis of deformation measurements for reservoir management. Oil and Gas Science and Technology, 57(5): 539-554.

Dusseault, M.B., Yin, S., Rothenburg, L. and Han, H., 2007. Seismic monitoring and geomechanics simulation. Leading Edge (Tulsa, OK), 26(5): 610-620.

E

Egermann, P., Chalbaud, C., Duquerroix, J.-P. and Le Gallo, Y., 2006. An integrated approach to parameterize reservoir models for CO_2 injection in aquifers, Proceedings - SPE Annual Technical Conference and Exhibition: 1620-1628.

Eichhubl, P. and Boles, J.R., 2000. Focused fluid flow along faults in the Monterey Formation, coastal California. GSA Bulletin, 112(11): 1667-1679.

Eichhubl, P., Davatzes, N.C. and Becker, S.P., 2009. Structural and diagenetic control of fluid migration and cementation along the Moab fault, Utah. AAPG Bulletin, 93(5): 653-681.

Emberley, S., Hutcheon, I., Shevalier, M., Durocher, K., Mayer, B., Gunter, W.D., and Perkins, E.H., 2005. Monitoring of fluid-rock interaction and CO_2 storage through produced fluid sampling at the Weyburn CO_2-injection enhanced oil recovery site, Saskatchewan, Canada. Applied Geochemistry, 20(6): 1131-1157.

Engelder, T., 1992. Stress regimes in the lithosphere. Princeton University Press, Princeton, 492 pp.

Engelder, T. and Fischer, M.P., 1994. Influence of poroelastic behaviour on the magnitude of minimum horizontal stress, Sh, in overpressured parts of sedimentary basins. Geology, 22(10): 949-952.

Engelder, T. and Geiser, P., 1980. On the use of regional joint sets as trajectories of paleostress fields during the development of the Appalachian plateau, New York. Journal of Geophysical Research, 85(B11): 6319-6341.

Ennis-King, J. and Paterson, L., 2000. Reservoir engineering issues in the geological disposal of carbon dioxide. In: D. Williams, R. Durie, P. McMullan, C. Paulson and A. Smith (Editors), Proceedings of the 5th International Conference on Greenhouse Gas Control Technologies (GHGT-5), Cairns, Australia: 290-295.

Ennis-King, J. and Paterson, L., 2002. Engineering aspects of geological sequestration of carbon dioxide, SPE - Asia Pacific Oil and Gas Conference: 134-146.

Ennis-King, J. and Paterson, L., 2003. Role of convective mixing in the long-term storage of carbon dioxide in deep saline formations, Proceedings - SPE Annual Technical Conference and Exhibition: 2521-2532.

Enting, I.G., Etheridge, D.M. and Fielding, M.J., 2008. A perturbation analysis of the climate benefit from geosequestration of carbon dioxide. International Journal of Greenhouse Gas Control, 2(3): 289-296.

Evans, J.P., Forster, C.B. and Goddard, J.V., 1997. Permeability of fault-related rocks, and implications for hydraulic structure of fault zones. Journal of Structural Geology, 19(11): 1393-1404.

F

Faulkner, D.R. and Rutter, E.H., 1998. The gas permeability of clay-bearing fault gorge at 20°C. Geological Society Special Publication, London: 147-156.

Ferer, M., Bromhal, G.S. and Smith, D.H., 2002. Pore-level modelling of carbon dioxide sequestration in brine fields. Journal of Energy and Environmental Research, 2: 120-132.

Ferrill, D.A. and Morris, A.P., 2002. Dilational normal faults. Journal of Structural Geology, 25(2): 183-196.

Fetter, C.W., 2000. Applied Hydrogeology. Prentice Hall, 598 pp.

Flett, M.A., Gurton, R.M. and Taggart, I.J., 2004. Heterogeneous saline formations: Long term benefits for geosequestration of greenhouse gases. In: E.S. Rubin, D.W. Keith and Gilboy (Editors), Proceedings of the 7th International Conference on Greenhouse Gas Control Technologies (GHGT-7), Vancouver, Canada: 501-509.

Folk, R.L., 1968. Petrology of Sedimentary Rocks. The University of Texas, Hemphill Publications, Austin, Texas, 170 pp.

Fox, R., 1974. The Rise and Fall of Laplacian Physics. In: R. McCormmach (Editor), Historical Studies in the Physical Sciences. Princeton University Press: 89-136.

Freifeld, B.M. and Trautz, R.C., 2006. Real-time quadrupole mass spectrometer analysis of gas in borehole fluid samples acquired using the U-tube sampling methodology. Geofluids, 6(3): 217-224.

Freifeld, B.M., Trautz, R.C., Kharaka, Y.K., Phelps, T.J., Myer, L.R., Hovorka, S.D., and Collins, D.J., 2005. The U-tube: A novel system for acquiring borehole fluid samples from a deep geologic CO_2 sequestration experiment. Journal of Geophysical Research B: Solid Earth, 110(10): 1-10.

G

Galloway, W.E. and Cheng, E.S., 1985. Reservoir facies architecture in a micro tidal system: Frio Formation, Texas Gulf Coast. The University of Texas at Austin, Bureau of Economic Geology Investigation Report, 144: 36.

Gartrell, A., Bailey, W.R. and Brincat, M., 2005. Strain localisation and trap geometry as key controls on hydrocarbon preservation in the Laminaria High area. The APPEA Journal, 45: 477-492.

Gartrell, A., Bailey, W.R. and Brincat, M., 2006. A new model for assessing trap integrity and oil preservation risks associated with postrift fault reactivation in the Timor Sea. AAPG Bulletin, 90(12): 1921-1944.

Gartrell, A., Zhang, Y., Lisk, M. and Dewhurst, D., 2004. Fault intersections as critical hydrocarbon leakage zones: Integrated field study and numerical modelling of an example from the Timor Sea, Australia. Marine and Petroleum Geology, 21(9): 1165-1179.

Gassmann, F., 1951. Ueber die Elastizitaet poroser Medien. Vierteljahrschrift der Naturforschenden Gesellschaft in Zurich, 96: 1-23.

Gaus, I., Azaroual, M. and Czernichowski-Lauriol, I., 2005. Reactive transport modelling of the impact of CO_2 injection on the clayey cap rock at Sleipner (North Sea). Chemical Geology, 217(3-4 SPEC. ISS.): 319-337.

Geertsma, J., 1973. Land subsidence above compacting oil and gas reservoirs. Journal of Petroleum Technology, 25: 734-744.

Gherardi, F., Xu, T. and Pruess, K., 2007. Numerical modeling of self-limiting and self-enhancing caprock alteration induced by CO_2 storage in a depleted gas reservoir. Chemical Geology, 244(1-2): 103-129.

Gibson, R.G., 1998. Physical character and fluid-flow properties of sandstone-derived fault zones. Geological Society Special Publication, London: 83-97.

Gibson-Poole, C.M., Edwards, S., Langford, R.P. and Vakarelov, B., 2007. Review of geological storage opportunities for carbon capture and storage (CCS) in Victoria - Summary report. CO2CRC Report, ICTPL-RPT07-0526: 9.

Gibson-Poole, C.M., Root, R.S., Lang, S.C., Streit, J.E., Hennig, A.L., Otto, C.J., and Underschultz, J., 2004. Conducting comprehensive analyses of potential sites for geological CO_2 storage. In: E.S. Rubin, D.W. Keith and Gilboy (Editors), Proceedings of the 7th International Conference on Greenhouse Gas Control Technologies (GHGT-7), Vancouver, Canada: 673-682.

Gibson-Poole, C.M., Svendsen, L., Ennis-King, J., Watson, M.N., Daniel, R.F., and Rigg, A.J., 2006a. Using stratigraphic heterogeneity to improve containment and capacity in the geological storage of CO_2, Proceedings of the 8th International Conference on Greenhouse Gas Control Technologies (GHGT-8), Trondeim, Norway.

Gibson-Poole, C.M., Svendsen, L., Ennis-King, J., Watson, M.N., Daniel, R.F., and Rigg, A.J., 2009. Understanding stratigraphic heterogeneity: A methodology to maximise the efficiency of the geological storage of CO_2. In: M. Grobe, J.C. Pashin and R.I. Dodge (Editors), Carbon dioxide sequestration in geological media - State of the science. AAPG Studies in Geology: 347-364.

Gibson-Poole, C.M., Svendsen, L., Underschultz, J., Watson, M.N., Ennis-King, J., Van Ruth, P.J., Nelson, E.J., Daniel, R.F., and Cinar, Y., 2006b. Gippsland Basin geosequestration: Potential solution for the Latrobe Valley brown coal CO_2 emissions. The APPEA Journal, 46: 413-433.

Gillespie, P.A., Howard, C.B., Walsh, J.J. and Watterson, J., 1993. Measurement and characterisation of spatial distributions of fractures. Tectonophysics, 226(1-4): 113-141.

Goulty, N.R., 2003. Reservoir stress path during depletion of Norwegian chalk oilfields. Petroleum Geoscience, 9(3): 233-241.

Grimstad, A.-A., Georgescu, S., Lindeberg, E. and Vuillaume, J.-F., 2009. Modelling and simulation of mechanisms for leakage of CO_2 from geological storage. Energy Procedia, 1: 2511-2518.

Gross, M.R., Gutie'rrez-Alonso, G., Bai, T., Wacker, M.A., Collinsworth, K.B., and Behl, R.J., 1997. Influence of mechanical stratigraphy and kinematics on fault scaling relations. Journal of Structural Geology, 19(2): 171-183.

Gunter, W.D., Perkins, E.H. and McCann, T.J., 1993. Aquifer disposal of CO_2-rich gases: Reaction design for added capacity. Energy Conversion and Management, 34(9-11): 941-948.

Gupta, N., Wang, P., Sass, B., Bergman, P. and Byrer, C., 2000. Regional and site-specific hydrogeologic constraints on CO_2 sequestration in the midwestern United States saline formations. In: R. Durie, D. Williams, A. Smith, P. McMullan and C. Paulson (Editors), Proceedings of the 5th International Conference on Greenhouse Gas Control Technologies (GHGT-5), Cairns, Australia: 385- 390.

H

Halliday, E.J., Barrie, J.V., Chapman, N.R. and Rohr, K.M.M., 2008. Structurally controlled hydrocarbon seeps on a glaciated continental margin, Hecate Strait, offshore British Columbia. Marine Geology, 252(3-4): 193-206.

Hancock, P.L., 1985. Brittle microtectonics: principles and practice. Journal of Structural Geology, 7(3-4): 437-457.

Haney, M.M., Snieder, R., Sheiman, J. and Losh, S., 2005. Geophysics: A moving fluid pulse in a fault zone. Nature, 437(7055): 46.

Hardy, R. and Tucker, M., 1988. X-ray powder diffraction of sediments. In: M. Tucker (Editor), Techniques in Sedimentology. Blackwell Scientific Publications, Oxford: 191-228.

Harrington, J.F. and Horseman, S.T., 1999. Gas transport properties of clays and mudrocks. In: A. Aplin, A.J. Fleet and J.H.S. Macquaker (Editors), Muds and Mudstones: Physical and Fluid Flow Properties. Geological Society Special Publication: 107-124.

Hawkes, C.D., Mclellan, P.J. and Bachu, S., 2005. Geomechanical factors affecting geological storage of CO_2 in depleted oil and gas reservoirs. Journal of Canadian Petroleum Technology, 44(10): 52-61.

Hebach, A., Oberhof, A., Dahmen, N., Kogel, A., Ederer, H., and Dinjus, E., 2002. Interfacial tension at elevated pressures-measurements and correlations in the water + carbon dioxide system. Journal of Chemical and Engineering Data, 47(6): 1540-1546.

Hedberg, H.D., 1974. Relation of methane generation to undercompacted shales, shale diapirs and mud volcanoes. AAPG Bulletin, 58: 661-673.

Heffer, K.J. and Bevan, T.G., 1990. Scaling relationships in natural fractures. Data, theory, and application, European Petroleum Conference: 367-376.

Heggland, R., 1997. Detection of gas migration from a deep source by the use of exploration 3D seismic data. Marine Geology, 137(1-2): 41-47.

Heggland, R., 2002. Seismic evidence of vertical fluid migration through faults, applications of chimney and fault detection, AAPG Hedberg Conference, Vancouver, Canada.

Heggland, R., 2004. Definition of geohazards in exploration 3-D seismic data using attributes and neural-network analysis. AAPG Bulletin, 88(6): 857-868.

Heggland, R., 2005. Using gas chimneys in seal integrity analysis: a discussion based on case histories. In: P. Boult and J. Kaldi (Editors), Evaluating fault and cap rock seals. AAPG Hedberg Series, Tulsa, OK: 237-245.

Herzog, H., 2001. What future for carbon capture and sequestration? Environmental Science and Technology, 35(7): 148A-153A.

Hettema, M., Papamichos, E. and Schutjens, P., 2002a. Subsidence delay: Field observations and analysis. Oil and Gas Science and Technology, 57(5): 443-458.

Hettema, M.H.H., Hanssen, T.H. and Jones, B.L., 2002b. Minimizing coring-induced damage in consolidated rock, Proceedings of the SPE/ISRM Rock Mechanics in Petroleum Engineering Conference: 62-73.

Heum, O.R., 1996. A fluid dynamic classification of hydrocarbon entrapment. Petroleum Geoscience, 2(2): 145-158.

Hildenbrand, A., Schlomer, S. and Krooss, B.M., 2002. Gas breakthrough experiments on fine-grained sedimentary rocks. Geofluids, 2(1): 3-23.

Hildenbrand, A., Schlomer, S., Krooss, B.M. and Littke, R., 2004. Gas breakthrough experiments on pelitic rocks: Comparative study with N_2, CO_2 and CH_4. Geofluids, 4(1): 61-80.

Hillis, R.R., 2001. Coupled changes in pore pressure and stress in oil fields and sedimentary basins. Petroleum Geoscience, 7(4): 419-425.

Hillis, R.R. and Reynolds, S.D., 2000. The Australian Stress Map. Journal of the Geological Society, 157(5): 915-921.

Hirsch, I.M. and Thompson, A.H., 1995. Saturations and buoyancy in secondary migration. AAPG Bulletin, 79: 696-710.

Holloway, S., 1997a. An overview of the underground disposal of carbon dioxide. Energy Conversion and Management, 38(SUPPL. 1): S193-S198.

Holloway, S., 1997b. Safety of the underground disposal of carbon dioxide. Energy Conversion and Management, 38(SUPPL. 1): S241-S245.

Holloway, S., 2007. Carbon dioxide capture and geological storage. Philosophical Transactions of the Royal Society A: Mathematical, Physical and Engineering Sciences, 365(1853): 1095-1107.

Hortle, A., Xu, J. and Dance, T., 2009. Hydrodynamic interpretation of the Waarre Fm Aquifer in the onshore Otway Basin: Implications for the CO2CRC Otway Project, Energy Procedia: 2895-2902.

Hovorka, S.D., Doughty, C., Benson, S.M., Pruess, K. and Knox, P.R., 2004. The impact of geological heterogeneity on CO_2 storage in brine formations: A case study from the Texas Gulf Coast. Geological Society Special Publication, London: 147-163.

Hovorka, S.D., Meckel, T.A., Trevino, R.H., Lu, J., Nicot, J.-P., Choi, J.-W., Freeman, D., Cook, P., Daley, T.M., Ajo-Franklin, J.B., Freifeld, B.M., Doughty, C., Carrigan, C.R., La Brecque, D., Kharaka, Y.K., Thordsen, J.J., Phelps, T.J., Yang, C., Romanak, K.D., Zhang, T., Holt, R.M., Lindler, J.S., and Butsch, R.J., 2011. Monitoring a large volume CO_2 injection: Year two results from SECARB project at Denbury's Cranfield, Mississippi, USA. Energy Procedia, 4: 3478-3485.

Hubbert, M.K., 1953. Entrapment of petroleum under hydrodynamic conditions. AAPG Bulletin, 37: 1954-2026.

Hull, J., 1988. Thickness-displacement relationships for deformation zones. Journal of Structural Geology, 10(4): 431-435.

Hunt, J.M., 1996. Petroleum Geochemistry and Geology. W.H. Freeman and Company, New York., 743 pp.

I

IEAGHG, 2010a. Injection strategies for CO_2 storage sites, Cooperative Research Centre for Greenhouse Gas Technologies, Australia.

IEAGHG, 2010b. Pressurisation and brine displacement issues for deep saline formation CO_2 storage, The Permedia Research Group Inc.

Illing, V.C., 1942. Geology applied to petroleum. Proceedings of the Geologists' Association, 53(3-4): 156-187.

Ingram, G.M. and Urai, J.L., 1999. Top-seal leakage through faults and fractures: the role of mudrock properties. Geological Society Special Publication, London: 125-135.

J

Jaeger, J.C., Cook, W. and Zimmerman, R., 2007. Fundamentals of Rock Mechanics. Wiley-Blackwell, 488 pp.

Jev, B.I., Kaars-Sijpesteijn, C.H., Peters, M.P.A.M., Watts, N.L. and Wilkie, J.T., 1993. Akaso field, Nigeria: use of integrated 3-D seismic, fault slicing, clay smearing, and RFT pressure data on fault trapping and dynamic leakage. AAPG Bulletin, 77(8): 1389-1404.

Jimenez, J.A. and Chalaturnyk, R.J., 2002. Are disused hydrocarbon reservoirs safe for geological storage of CO_2?, Proceedings of the 6th International Conference on Greenhouse Gas Control Technologies (GHGT-6), Kyoto, Japan: 471-476.

Johnson, J., Nitao, J.J. and Morris, J.P., 2005. Reactive transport modelling of cap-rock integrity during natural and engineered CO_2 storage. In: D.C. Thomas and S.M. Benson (Editors), Carbon Dioxide Capture for Storage in Deep Geologic Formations: 787-813.

Johnson, J.W., Nitao, J.J. and Morris, J.P., 2004. Modelling the long term isolation performance of natural and engineered geologic CO_2 storage sites. In: E.S. Rubin, D.W. Keith and Gilboy (Editors), Proceedings of the 7th International Conference on Greenhouse Gas Control Technologies (GHGT-7), Vancouver, Canada.

Jolley, S.J., Barr, D., Walsh, J.J. and Knipe, R.J., 2007. Structurally complex reservoirs: an introduction. In: S.J. Jolly, D. Barr, J.J. Walsh and R.J. Knipe (Editors), Structurally complex reservoirs. Geological Society Special Publication, London: 1-24.

Jolly, R.J.H., Wei, L. and Pine, R.J., 2000. Stress-Sensitive Fracture-Flow Modelling in Fractured Reservoirs, Proceedings of the SPE International Petroleum Conference and Exhibition of Mexico: 473-482.

Jones, R.M. and Hillis, R.R., 2003. An integrated, quantitative approach to assessing fault-seal risk. AAPG Bulletin, 87(3): 507-524.

K

Kaldi, J.G., 2000. Assessing reservoir quality and seal potential, AAPG/IPA Workshop Notes. unpublished, Bali, Indonesia.

Kaldi, J.G. and Atkinson, C.D., 1997. Evaluating seal potential: Example from the Talang Akar Formation, offshore Northwest Java, Indonesia. AAPG Memoir, 67: 85-101.

Kaluza, M.J. and Doyle, E.H., 1996. Detecting fluid migration in shallow sediments: continental slope environment, Gulf of Mexico. AAPG Memoir, 66: 15-26.

Kaszuba, J.P., Janecky, D.R. and Snow, M.G., 2005. Experimental evaluation of mixed fluid reactions between supercritical carbon dioxide and NaCl brine: Relevance to the integrity of a geologic carbon repository. Chemical Geology, 217(3-4 SPEC. ISS.): 277-293.

Kim, Y.-S., Peacock, D.C.P. and Sanderson, D.J., 2004. Fault damage zones. Journal of Structural Geology, 26(3): 503-517.

Kim, Y.-S. and Sanderson, D.J., 2010. Inferred fluid flow through fault damage zones based on the observation of stalactites in carbonate caves. Journal of Structural Geology, 32(9): 1305-1316.

Kirste, D., Perkins, E., Boreham, C., Stalker, L., Schacht, U., and Underschultz, J., 2010. Geochemical monitoring and geochemical modeling of the CO2CRC Otway Project CO_2 storage pilot, Victoria, Australia. Geochimica et Cosmochimica Acta, 74(12): A521.

Kivior, T., Kaldi, J.G. and Lang, S.C., 2002. Seal potential in Cretaceous and late Jurassic rocks of the Vulcan Sub-basin, Northwest Shelf, Australia. The APPEA Journal, 42: 203-224.

Kloosterman, H.J., Kelly, R.S., Stammeijer, J., Hartung, M., vanWard, J., and Chajecki, C., 2003. Successful application of time lapse seismic in Shell Expro's Gannet Fields, central North Sea UKCS. Petroleum Geoscience, 9: 25-34.

Klusman, R.W., 2003a. A geochemical perspective and assessment of leakage potential for a mature carbon dioxide-enhanced oil recovery project and as a prototype for carbon dioxide sequestration; Rangely field, Colorado. AAPG Bulletin, 87(9): 1485-1507.

Klusman, R.W., 2003b. Rate measurements and detection of gas microseepage to the atmosphere from an enhanced oil recovery/sequestration project, Rangely, Colorado, USA. Applied Geochemistry, 18(12): 1825-1838.

Knauss, K.G., Johnson, J.W. and Steefel, C.I., 2005. Evaluation of the impact of CO_2, co-contaminant gas, aqueous fluid and reservoir rock interactions on the geologic sequestration of CO_2. Chemical Geology, 217(3-4 SPEC. ISS.): 339-350.

Kvamme, B. and Liu, S., 2009. Reactive transport of CO_2 in saline aquifers with implicit geomechanical analysis. Energy Procedia, 1: 3267-3274.

L

Landro, M., 2001. Discrimination between pressure and fluid saturation changes from time-lapse seismic data. Geophysics, 66(3): 836-844.

Larson, R.G., Scriven, L.E. and Davis, H.T., 1981. Percolation theory of two phase flow in porous media. Chemical Engineering Science, 36(1): 57-73.

Leckenby, R.J., Sanderson, D.J. and Lonergan, L., 2005. Estimating flow heterogeneity in natural fracture systems. Journal of Volcanology and Geothermal Research, 148(1-2): 116-129.

Leuning, R., Etheridge, D., Luhar, A. and Dunse, B., 2008. Atmospheric monitoring and verification technologies for CO_2 geosequestration. International Journal of Greenhouse Gas Control, 2(3): 401-414.

Leveille, G.P., Knipe, R., More, C., Ellis, D., Dudley, G., Jones, G., Fisher, Q.J., and Allinson, G., 1997. Compartmentalization of Rotliegendes gas reservoirs by sealing faults, Jupiter Fields area, southern North Sea, Geological Society Special Publication 123: 87-104.

Lewicki, J.L., Birkholzer, J. and Tsang, C.-F., 2007. Natural and industrial analogues for leakage of CO_2 from storage reservoirs: Identification of features, events, and processes and lessons learned. Environmental Geology, 52(3): 457-467.

Li, G., 2003. 4D seismic monitoring of CO_2 flood in a thin fractured carbonate reservoir. Leading Edge (Tulsa, OK), 22: 690-695.

Li, Y. and Wardlaw, N.C., 1986. The influence of wettability and critical pore-throat size ratio on snap-off. Journal of Colloid And Interface Science, 109(2): 461-472.

Li, Z., Dong, M., Li, S. and Huang, S., 2006. CO_2 sequestration in depleted oil and gas reservoirs-caprock characterization and storage capacity. Energy Conversion and Management, 47(11-12): 1372-1382.

Ligtenberg, J.H., 2005. Detection of fluid migration pathways in seismic data: Implications for fault seal analysis. Basin Research, 17(1): 141-153.

Ligtenberg, J.H. and Thomsen, R.O., 2003. Fluid migration path detection and its application to basin modelling, EAGE 65th Conference and Meeting.

Lindeberg, E., 1997. Escape of CO_2 from aquifers. Energy Conversion and Management, 38(SUPPL. 1): S235-S240.

Lindeberg, E. and Bergmo, P., 2002. The long term fate of CO_2 injected into an aquifer, Proceedings of the 6th Conference on Greenhouse Gas Control Technologies (GHGT-6), Kyoto, Japan: 489-495.

Lindsay, N.G., Murphy, F.C., Walsh, J.J. and Watterson, J., 1993. Outcrop studies of shale smears on fault surfaces. The geological modelling of hydrocarbon reservoirs and outcrop analogues: 113-123.

Lisle, R.J., 1994. Detection of zones of abnormal strains in structures using Gaussian curvature analysis. AAPG Bulletin, 78(12): 1811-1819.

Lisle, R.J. and Srivastava, D.C., 2004. Test of the frictional reactivation theory for faults and validity of fault-slip analysis. Geology, 32(7): 569-572.

Longuemare, P., Mainguy, M., Lemonnier, P., Onaisi, A., Gerard, C., and Koutsabeloulis, N., 2002. Geomechanics in reservoir simulation: Overview of coupling methods and field case study. Oil and Gas Science and Technology, 57(5): 471-483.

Losh, S., Eglinton, L., Schoell, M. and Wood, J., 1999. Vertical and lateral fluid flow related to a large growth fault, South Eugene Island Block 330 field, offshore Louisiana. AAPG Bulletin, 83(2): 244-276.

Losh, S. and Haney, M., 2006. Episodic fluid flow in an aseismic overpressured growth fault, northern Gulf of Mexico. In: R. Abercrombie, A. McGarr, G. Di Toro and H. Kanamori (Editors), Earthquakes: Radiated Energy and the Physics of Faulting. American Geophysical Union Geophysical Monograph Series: 199-206.

Lucier, A. and Zoback, M., 2008. Assessing the economic feasibility of regional deep saline aquifer CO_2 injection and storage: A geomechanics-based workflow applied to the Rose Run sandstone in Eastern Ohio, USA. International Journal of Greenhouse Gas Control, 2(2): 230-247.

Lucier, A., Zoback, M., Gupta, N. and Ramakrishnan, T.S., 2006. Geomechanical aspects of CO_2 sequestration in a deep saline reservoir in the Ohio River Valley region. Environmental Geosciences, 13(2): 85-103.

Lumley, D., 2010. 4D seismic monitoring of CO_2 sequestration. Leading Edge (Tulsa, OK), 29(2): 150-155.

Luo, Z. and Bryant, S.L., 2010. Influence of thermo-elastic stress on CO_2 injection induced fractures during storage. SPE Journal: 139719.

Lyon, P.J., Boult, P., Hillis, R.R. and Mildren, S.D., 2005. Sealing by Shale Gouge and subsequent seal breach by reactivation: A case study of the Zema Prospect, Otway Basin. In: P. Boult and J. Kaldi (Editors), Evaluating fault and cap rock seals. AAPG Hedberg Series, Tulsa, OK: 179-197.

M

Makel, G.H., 2007. The modelling of fractured reservoirs: Constraints and potential for fracture network geometry and hydraulics analysis. Geological Society Special Publication, London: 375-403.

Manzocchi, T., Childs, C. and Walsh, J.J., 2010. Faults and fault properties in hydrocarbon flow models. Geofluids, 10(1-2): 94-113.

Manzocchi, T., Heath, A.E., Palananthakumar, B., Childs, C. and Walsh, J.J., 2008. Faults in conventional flow simulation models: A consideration of representational assumptions and geological uncertainties. Petroleum Geoscience, 14(1): 91-110.

Manzocchi, T., Walsh, J.J. and Bailey, W.R., 2009. Population scaling biases in map samples of power-law fault systems. Journal of Structural Geology, 31(12): 1612-1626.

Manzocchi, T., Walsh, J.J., Nell, P. and Yielding, G., 1999. Fault transmissibility multipliers for flow simulation models. Petroleum Geoscience, 5(1): 53-63.

Marsden, R., 2007. Geomechanics for reservoir management, Algeria Well Evaluation Conference: 398.

Matthai, S.K. and Roberts, S.G., 1996. The influence of fault permeability on single-phase fluid flow near fault-sand intersections: Results from steady-state high-resolution models of pressure-driven fluid flow. AAPG Bulletin, 80(11): 1763-1779.

Maultzsch, S., Chapman, M., Liu, E. and Li, X.-Y., 2003. The potential of measuring fracture sizes with frequency-dependent shear-wave splitting. First Break, 21(7): 45-51.

Maxwell, S.C. and Urbancic, T.I., 2001. The role of passive microseismic monitoring in the instrumented oil field. Leading Edge (Tulsa, OK), 20(6): 636-639.

Mazumder, S., Plug, W.-J. and Bruining, H., 2003. Capillary pressure and wettability behavior of coal - water - carbon dioxide system, Proceedings - SPE Annual Technical Conference and Exhibition: 2467-2476.

Meakin, P., Wagner, G., Frette, V., Feder, J. and Jossang, T., 1995. Fractals and secondary migration. Fractals: 799-806.

Meakin, P., Wagner, G., Vedvik, A., Amundsen, H., Feder, J., and Jossang, T., 2000. Invasion percolation and secondary migration: Experiments and simulations. Marine and Petroleum Geology, 17(7): 777-795.

Meckel, T., 2010. Capillary seals for trapping carbon dioxide (CO_2) in underground reservoirs. In: M.M. Maroto-Valer (Editor), Developments and innovation in carbon dioxide (CO_2) capture and storage technology, Volume 2: Carbon dioxide (CO_2) storage and utilisation. Woodhead Publishing Series in Energy.

Meyer, V., Nicol, A., Childs, C., Walsh, J.J. and Watterson, J., 2002. Progressive localisation of strain during the evolution of a normal fault population. Journal of Structural Geology, 24(8): 1215-1231.

Michael, K. and Underschultz, J., 2009. The impact of hydrodynamics on CO_2 migration and sealing capacity of faults, AAPG/SEG/SPE Hedberg Conference - Geological carbon sequestration: prediction and verification, Vancouver, Canada: 4.

Mildren, S.D., 1997. The contemporary stress field of Australia's Northwest Shelf and collision related tectonics. PhD Thesis, The University of Adelaide, Adelaide, 208 pp.

Mildren, S.D., Hillis, R.R., Dewhurst, D.N., Lyon, P.J., Meyer, J.J., and Boult, P.J., 2005. FAST: A new technique for geomechanical assessment of the risk of reactivation-related breach of fault seals. In: P. Boult and J. Kaldi (Editors), Evaluating fault and cap rock seals. AAPG Hedberg Series, Tulsa, OK: 73-85.

Mildren, S.D., Hillis, R.R. and Kaldi, J., 2002. Calibrating prediction of fault seal reactivation in the Timor Sea. APPEA Journal, 42: 187-202.

Minkoff, S.E., Stone, C.M., Bryant, S., Peszynska, M. and Wheeler, M.F., 2003. Coupled fluid flow and geomechanical deformation modeling. Journal of Petroleum Science and Engineering, 38(1-2): 37-56.

Moore, J., Adams, M., Allis, R., Lutz, S. and Rauzi, S., 2005. Mineralogical and geochemical consequences of the long-term presence of CO_2 in natural reservoirs: An example from the Springerville-St. Johns Field, Arizona, and New Mexico, U.S.A. Chemical Geology, 217(3-4 SPEC. ISS.): 365-385.

Moretti, I., 1998. The role of faults in hydrocarbon migration. Petroleum Geoscience, 4(1): 81-94.

Morley, C.K., 2010. Stress re-orientation along zones of weak fabrics in rifts: An explanation for pure extension in 'oblique' rift segments? Earth and Planetary Science Letters, 297(3-4): 667-673.

Morris, A., Ferrill, D.A. and Henderson, D.B., 1996. Slip-tendency analysis and fault reactivation. Geology, 24(3): 275-278.

Morris, A.P. and Ferrill, D.A., 2009. The importance of the effective intermediate principal stress (o'2) to fault slip patterns. Journal of Structural Geology, 31(9): 950-959.

Morrow, N.R., 1990. Wettability and its effect on oil recovery. Journal of Petroleum Technology, 42: 1476-1484.

Morrow, N.R., Cram, P.J. and McCaffery, F.G., 1973. Displacement studies in dolomite with wettability control by octanoic acid. SPE Journal, 13(4): 221-232.

Murris, R.J., 1980. Middle East: stratigraphic evolution and oil habitat. AAPG Bulletin, 64(5): 597-618.

N

Nakanishi, T. and Lang, S.C., 2001. The search for stratigraphic traps goes on - visualisation of fluvial-lacustrine successions in the Moorari 3D Survey, Cooper-Eromanga basin. The APPEA Journal, 41: 115-137.

Nakanishi, T. and Lang, S.C., 2002. Towards an efficient exploration frontier: constructing a portfolio of stratigraphic traps in fluvio-lacustrine successions, Cooper-Eromanga Basin. The APPEA Journal, 42: 203-223.

Needham, T., Yielding, G. and Fox, R., 1996. Fault population description and prediction using examples from the offshore U.K. Journal of Structural Geology, 18(2-3): 155-167.

Neglia, S., 1979. Migration of fluids (water and hydrocarbons) in sedimentary basins. AAPG Bulletin, 63(4): 573-597.

Neuzil, C.E., 1986. Groundwater flow in low-permeability environments. Water Resources Research, 22(8): 1163-1195.

Nicol, A., Watterson, J., Walsh, J.J. and Childs, C., 1996. The shapes, major axis orientations and displacement patterns of fault surfaces. Journal of Structural Geology, 18(2-3): 235-248.

Noiriel, C., Luquot, L., Made, B., Raimbault, L., Gouze, P., and van der Lee, J., 2009. Changes in reactive surface area during limestone dissolution: An experimental and modelling study. Chemical Geology, 265(1-2): 160-170.

Nordbotten, J.M., Celia, M.A. and Bachu, S., 2005. Injection and storage of CO_2 in deep saline aquifers: Analytical solution for CO_2 plume evolution during injection. Transport in Porous Media, 58: 339-360.

O

O'Brien, G.W. and Woods, E.P., 1995. Hydrocarbon related diagenetic zones (HRDZs) in the Vulcan Sub-basin, Timor Sea: Recognition and exploration implications. Tectonophysics, 35: 220-252.

Odling, N.E., Gillespie, P., Bourgine, B., Castaing, C., Chiles, J.-P., Christensen, N.P., Fillion, E., Genter, A., Olsen, C., Thrane, L., Trice, R., Aarseth, E., Walsh, J.J., and Watterson, J., 1999. Variations in fracture system geometry and their implications for fluid flow in fractured hydrocarbon reservoirs. Petroleum Geoscience, 5(4): 373-384.

Oldenburg, C.M., 2007. Joule-Thomson cooling due to CO_2 injection into natural gas reservoirs. Energy Conversion and Management, 48(6): 1808-1815.

Olsen, K.B., Madariaga, R. and Archuleta, R.J., 1997. Three-dimensional dynamic simulation of the 1992 Landers earthquake. Science, 278(5339): 834-838.

Orlic, B., 2009. Some geomechanical aspects of geological CO_2 sequestration. KSCE Journal of Civil Engineering, 13(4): 225-232.

Osborne, M.J. and Swarbrick, R.E., 1997. Mechanisms for generating overpressure in sedimentary basins: A reevaluation. AAPG Bulletin, 81(6): 1023-1041.

P

Pearce, J., Baker, J., Beaubien, S., Brune, S., Czemichowski-Lauriol, I., Faber, E., Hatziyannis, G., Hildenbrand, A., Krooss, B. M., Lombardi, S., Nador, A., Pauwels, H., and Schroot, B., 2002. Natural CO_2 accumulations in Europe: understanding long-term geological processes in CO_2 sequestration, Proceedings of the 6th International Conference on Greenhouse Gas Control Technologies (GHGT-6), Kyoto, Japan: 105 – 111.

Perkins, T.K. and Gonzalez, J.A., 1985. The effect of thermoelastic stresses on injection well fracturing. SPE Journal: 11332.

Picknell, J.J., Swanson, B.F. and Hickman, W.B., 1966. Application of air-mercury capillary pressure data in the study of pore structure and fluid distribution. SPE Journal, 6: 55-61.

Polak, S. and Grimstad, A.-A., 2009. Reservoir simulation study of CO_2 storage and CO_2 -EGR in the Atzbach-Schwanenstadt gas field in Austria. Energy Procedia, 1: 2961-2968.

Preisig, M. and Prevost, J.H., in press. Coupled multi-phase thermo-poromechanical effects. Case study: CO_2 injection at In Salah, Algeria. International Journal of Greenhouse Gas Control.

Price, N., 1966. Fault and Joint Development in Brittle and Semi-brittle Rock. Pergamon Press, Oxford, 176 pp.

Price, N.J. and Cosgrove, J.W., 1990. Analysis of geological structures. Cambridge University Press, Cambridge, 502 pp.

Purcell, W.R., 1949. Capillary pressures - their measurement using mercury and the calculation of permeability therefrom. Petroleum Transactions - American Institute of Mining, Metallurgical and Petroleum Engineers, 186: 39-48.

Q

Qobi, L., Alexander, D., Strauss, J., Mukmin and Kindy, F., 2010. EOR geomechanical screening-identification of risks to mitigate and opportunities to pursue, SPE EOR Conference at Oil and Gas West Asia 2010, OGWA - EOR Challenges, Experiences and Opportunities in the Middle East: 152-164.

R

Ramsay, J.G., 1967. Folding and Fracturing of Rocks. McGraw Hill, New York, 568 pp.

Ramsay, J.G. and Huber, M.I., 1987. Folds and Fractures. The Techniques of Modern Structural Geology, 2. Academic Press, London, 391 pp.

Ren, Q.-Y., Chen, G.-J., Yan, W. and Guo, T.-M., 2000. Interfacial tension of (CO_2 + CH_4) + water from 298 K to 373 K and pressures up to 30 MPa. Journal of Chemical and Engineering Data, 45(4): 610-612.

Reynolds, S.D., Paraschivoiu, E., Hillis, R.R. and O'Brien, G.W., 2005. A regional analysis of fault reactivation and seal integrity based on geomechanical modeling: An example from the Bight Basin, Australia. In: P. Boult and J. Kaldi (Editors), Evaluating fault and cap rock seals. AAPG Hedberg Series, Tulsa, OK: 57-71.

Ringrose, P., Larter, S.R., Corbett, P.W.M., Carruthers, D.L., Thomas, M.M., and Clouse, J.A., 1996. Scaled physical model of secondary oil migration; discussion and reply. AAPG Bulletin, 80: 292-294.

Roberts, H.H., Hardage, B.A., Shedd, W.W., Hunt, J. and Herron, D., 2006. Seafloor reflectivity; an important seismic property for interpreting fluid/gas expulsion geology and the presence of gas hydrate. The Leading Edge, 25(5): 620-628.

Robin, M., 2001. Interfacial phenomena: Reservoir wettability in oil recovery. Oil and Gas Science and Technology, 56(1): 55-62.

Rochelle, C.A., Czernichowski-Lauriol, I. and Milodowski, A.E., 2004. The impact of chemical reactions on CO_2 storage in geological formations: A brief review. Geological Society Special Publication, London: 87-106.

Rodgers, S., 1999. Discussion: 'Physical constraints on hydrocarbon leakage and trapping revisited' by Bjorkum et al. - further aspects. Petroleum Geoscience, 5: 421-423.

Root, R., Gibson-Poole, C., Lang, S., Striet, J., Underschultz, J., and Ennis-King, J., 2004. Opportunities for geological storage of carbon dioxide in the offshore Gippsland Basin, SE Australia: An example from the upper Latrobe Group. In: P. Boult, D. John and S.C. Lang (Editors), Eastern Australasian Basins Symposium, Adelaide, SA: 367-388.

Root, R.S., 2007. Geological evaluation of the Eocene Latrobe Group in the offshore Gippsland Basin for CO_2 geosequestration. PhD Thesis, The University of Adelaide, Adelaide, 284 pp.

Rose, R., 2001. Risk analysis and management of petroleum exploration ventures. Methods in Exploration Series, 12. AAPG, 178 pp.

Rouainia, M., Lewis, H., Pearce, C., Bicanic, N., Couples, G.D., and Reynolds, M.A., 2006. Hydro-geomechanical modelling of seal behaviour in overpressured basins using discontinuous deformation analysis. Engineering Geology, 82(4): 222-233.

Rowe Jr., A.M. and Chou, J.C.S., 1970. Pressure-volume-temperature-concentration relation of aqueous NaCl solutions. Journal of Chemical and Engineering Data, 15(1): 61-66.

Rutqvist, J., Birkholzer, J., Cappa, F. and Tsang, C.-F., 2007. Estimating maximum sustainable injection pressure during geological sequestration of CO_2 using coupled fluid flow and geomechanical fault-slip analysis. Energy Conversion and Management, 48(6): 1798-1807.

Rutqvist, J., Birkholzer, J.T. and Tsang, C.-F., 2008. Coupled reservoir-geomechanical analysis of the potential for tensile and shear failure associated with CO_2 injection in multilayered reservoir-caprock systems. International Journal of Rock Mechanics and Mining Sciences, 45(2): 132-143.

Rutqvist, J. and Tsang, C.-F., 2002. A study of caprock hydromechanical changes associated with CO_2-injection into a brine formation. Environmental Geology, 42(2-3): 296-305.

Rutqvist, J. and Tsang, C.-F., 2005. Coupled hydromechanical effects of CO_2 injection, Developments in Water Science: 649-679.

Rutqvist, J., Vasco, D.W. and Myer, L., 2010. Coupled reservoir-geomechanical analysis of CO_2 injection and ground deformations at In Salah, Algeria. International Journal of Greenhouse Gas Control, 4(2): 225-230.

S

Salz, L.B., 1977. Relationship between fracture propagation pressure and pore pressure, SPE 52nd Annual Conference, Denver, USA: SPE Paper 6870.

Santarelli, F.J., Tronvoll, J.T., Svennekjaer, M., Skeie, H., Henriksen, R., and Bratli, R. K., 1998. Reservoir stress path: the depletion and the rebound, Proceedings of the SPE/ISRM Rock Mechanics in Petroleum Engineering Conference: 203-209.

Sayers, C.M., 2010. Geomechanical Applications of Seismic and Borehole Acoustic Waves, SEG 2010 Distinguished Instructor Short Course, 152 pp.

Sayers, J., Marsh, C., Scott, A., Cinar, Y., Bradshaw, J., Hennig, A., Barclay, S., and Daniel, R., 2006. Assessment of a potential storage site for carbon dioxide: A case study, southeast Queensland, Australia. Environmental Geosciences, 13(2): 123-142.

Schacht, U., 2008. CO_2-related diagenesis in Tuna Field, Gippsland Basin: A natural analogue study for geosequestration, Eastern Australasian Basins Symposium, Sydney, NSW: 485-488.

Schacht, U., Regan, M., Boreham, C. and Sharma, S., 2011. CO2CRC Otway Project – Soil gas baseline and assurance monitoring 2007–2010. Energy Procedia, 4: 3346-3353.

Schlumberger, 2010. Oilfield Glossary. http://www.glossary.oilfield.slb.com/.

Schowalter, T.T., 1979. Mechanics of secondary hydrocarbon migration and entrapment. AAPG Bulletin, 63: 723-760.

Segall, P. and Fitzgerald, S.D., 1998. A note on induced stress changes in hydrocarbon and geothermal reservoirs. Tectonophysics, 289(1-3): 117-128.

Segall, P., Grasso, J.-R. and Mossop, A., 1994. Poroelastic stressing and induced seismicity near the Lacq gas field, southwestern France. Journal of Geophysical Research, 99(B8): 15,423-15,438.

Shah, V., Broseta, D. and Mouronval, G., 2008a. Capillary alteration of caprocks by acid gases, Proceedings - SPE Symposium on Improved Oil Recovery: 567-577.

Shah, V., Broseta, D., Mouronval, G. and Montel, F., 2008b. Water/acid gas interfacial tensions and their impact on acid gas geological storage. International Journal of Greenhouse Gas Control, 2(4): 594-604.

Shapiro, S.A. and Dinske, C., 2009. Scaling of seismicity induced by nonlinear fluid-rock interaction. Journal of Geophysical Research B: Solid Earth, 114: B09307.

Shi, J.-Q. and Durucan, S., 2009. A coupled reservoir-geomechanical simulation study of CO_2 storage in a nearly depleted natural gas reservoir. Energy Procedia, 1: 3039-3046.

Sibson, R.H., 1990. Rupture nucleation on unfavourably oriented faults. Seismological Society of America Bulletin, 80(6A): 1580-1604.

Sibson, R.H., 1995. Selective fault reactivation during basin inversion: potential for fluid redistribution through fault-valve action. Basin Inversion: 3-19.

Sibson, R.H., 1996. Structural permeability of fluid-driven fault-fracture meshes. Journal of Structural Geology, 18(8): 1031-1042.

Sibson, R.H., 2000. Fluid involvement in normal faulting. Journal of Geodynamics, 29(3-5): 469-499.

Sibson, R.H., 2003. Brittle-failure controls on maximum sustainable overpressure in different tectonic regimes. AAPG Bulletin, 87(6): 901-908.

Siemons, N., Bruining, H., Castelijns, H. and Wolf, K.-H., 2006. Pressure dependence of the contact angle in a CO_2-H_2O-coal system. Journal of Colloid and Interface Science, 297(2): 755-761.

Skurtveit, E., Aker, E., Soldal, M., Angeli, M. and Hallber, E., 2010. Influence of micro fractures and fluid pressure on sealing efficiency of caprock: a laboratory study on shale, 10th International Conference on Greenhouse Gas Control Technologies (GHGT-10), Amsterdam, The Netherlands.

Sluijk, D. and Nederlof, M.H., 1984. Worldwide geologic experience as a systematic basis for prospect appraisal. AAPG Memoir, 35: 15-26.

Sluijk, D. and Parker, J.R., 1986. Comparison of predrilling predictions with postdrilling outcomes, using Shell's Propsect Appraisal System. In: D.D. Rice and W.R. James (Editors), Oil and gas assesement methods and applications. AAPG Studies in Geology: 55-58.

Smith, D.A., 1966. Theoretical considerations of sealing and non-sealing faults. AAPG Bulletin, 50: 363-374.

Sneider, R.M., 1987. Practical petrophysics for exploration and development. AAPG Education Department Short Course Notes.

Soltanzadeh, H. and Hawkes, C.D., 2008. Semi-analytical models for stress change and fault reactivation induced by reservoir production and injection. Journal of Petroleum Science and Engineering, 60(2): 71-85.

Soltanzadeh, H. and Hawkes, C.D., 2009. Assessing fault reactivation tendency within and surrounding porous reservoirs during fluid production or injection. International Journal of Rock Mechanics and Mining Sciences, 46(1): 1-7.

Span, R. and Wagner, W., 1996. A new equation of state for carbon dioxide covering the fluid region from the triple-point temperature to 1100 K at pressures up to 800 MPa. Journal of Physical and Chemical Reference Data, 25(6): 1509-1596.

Sperrevik, S., Gillespie, P.A., Fisher, Q.J., Halvorsen, T. and Knipe, R.J., 2002. Empirical estimation of fault rock properties. Norwegian Petroleum Society Special Publications, 11: 109-125.

Stalker, L., Boreham, C., Underschultz, J., Freifeld, B., Perkins, E., Schacht, U., and Sharma, S., 2009. Geochemical monitoring at the CO2CRC Otway Project: Tracer injection and reservoir fluid acquisition, Energy Procedia, 1: 2119-2125.

Stearns, D.W. and Friedman, M., 1972. Reservoirs in fractured rocks. AAPG Memoir, 10: 82-106.

Stenhouse, M., Zhou, W., Savage, D. and Benbow, S., 2005. Framework Methodology for Long-Term Assessment of the Fate of CO_2 in the Weyburn Field. In: D.C. Thomas and S.M. Benson (Editors), Carbon Dioxide for Storage in Deep Geologic Formations. Elsevier: 1251-1262.

Stock, J.M., Healy, J.H., Hickman, S.H. and Zoback, M.D., 1985. Hydraulic fracturing stress measurements at Yucca Mountain, Nevada, and relationship to the regional stress field (USA). Journal of Geophysical Research, 90(B10): 8691-8706.

Streit, J.E. and Watson, M.N., 2004. Estimating rates of potential CO_2 loss from geological storage sites for risk and uncertainty analysis. In: E.S. Rubin, D.W. Keith and Gilboy (Editors), Proceedings of the 7th International Conference on Greenhouse Gas Control Technologies GHGT-7, Vancouver, Canada: 1309-1314.

T

Tamburini, A., Bianchi, M., Giannico, C. and Novali, F., 2010. Retrieving surface deformation by PSInSAR (TM) technology: A powerful tool in reservoir monitoring. International Journal of Greenhouse Gas Control, 4(6): 928-937.

Teige, G.M.G., Hermanrud, C. and Rueslatten, H.G., 2011. Membrane seal leakage in non-fractured caprocks by the formation of oil-wet flow paths. Journal of Petroleum Geology, 34(1): 45-52.

Teige, G.M.G., Hermanrud, C., Thomas, W.H., Wilson, O.B. and Nordgard Bolas, H.M., 2005. Capillary resistance and trapping of hydrocarbons: A laboratory experiment. Petroleum Geoscience, 11(2): 125-129.

Tenthorey, E. and Cox, S.F., 2006. Cohesive strengthening of fault zones during the interseismic period: An experimental study. Journal of Geophysical Research B: Solid Earth, 111: B09202.

Terzaghi, K., 1943. Theoretical soil mechanics. John Wiley and Sons, New York, 528 pp.

Teufel, L.W., Rhett, D.W. and Farrell, H.E., 1991. Effect of reservoir depletion and pore pressure drawdown on in situ stress and deformation in the Ekofisk Field, North Sea. In: J.C. Roegrers (Editor), Rock Mechanics as a Multidisciplinary Science. Balkema, Rotterdam: 63-72.

Thomas, M.M. and Clouse, J.A., 1995. Scaled physical model of secondary oil migration. AAPG Bulletin, 79(1): 19-29.

Tonnet, N., Shah, V., Chiquet, P., Diaz, M.G. and Broseta, D., 2008. Wettability alteration of caprock minerals by acid gas, 10th International Symposium of Reservoir Wettability, Abu Dhabi.

Tyler, N. and Ambrose, W.A., 1985. Facies architecture and production characteristics of strand plain reservoirs in the Frio Formation, Texas. The University of Texas at Austin, Bureau of Economic Geology Report, 146: 42.

U

Underschultz, J., 2007. Hydrodynamics and membrane seal capacity. Geofluids, 7(2): 148-158.

Underschultz, J.R., Otto, C.J. and Cruse, T., 2003. Hydrodynamics to assess hydrocarbon migration in faulted strata - Methodology and a case study from the North West Shelf of Australia. Journal of Geochemical Exploration, 78-79: 469-474.

Underschultz, J.R., Otto, C.J. and Bartlett, R., 2005. Formation fluids in faulted aquifers: Examples from the foothills of Western Canada and the North West Shelf of Australia. In: P. Boult and J. Kaldi (Editors), Evaluating fault and cap rock seals. AAPG Hedberg Series, Tulsa, OK: 247-260.

Urosevic, M., Pevzner, R., Kepic, A., Wisman, P., Shulakova, V., and Sharma, S., 2010. Time-lapse seismic monitoring of CO_2 injection into a depleted gas reservoir - Naylor Field, Australia. Leading Edge (Tulsa, OK), 29(2): 164-169.

V

Van der Meer, L.G.H., Arts, R.J. and Paterson, L., 2000. Prediction of migration of CO_2 after injection into a saline aquifer: reservoir history matching of a 4D seismic image with a compositional gas/water model. In: D. Williams, R. Durie, P. McMullan, C. Paulson and A. Smith (Editors), Proceedings of the 5th International Conference on Greenhouse Gas Control Technologies (GHGT-5), Cairns, Australia: 378-384.

Varma, S., Underschultz, J., Dance, T., Langford, R., Esterle, J., Dodds, K., and van Gent, D., 2009. Regional study on potential CO_2 geosequestration in the Collie Basin and the Southern Perth Basin of Western Australia. Marine and Petroleum Geology, 26(7): 1255-1273.

Vavra, C.L., Kaldi, J.G. and Sneider, R.M., 1992a. Capillary Pressure. In: D. Morton-Thompson and A.M. Woods (Editors), Development Geology Reference Manual. AAPG Methods in Exploration Series, Tulsa, OK: 221-225.

Vavra, C.L., Kaldi, J.G. and Sneider, R.M., 1992b. Geological applications of capillary pressure: a review. AAPG Bulletin, 76(6): 840-850.

Vedvik, A., Wagner, G., Oxaal, U., Feder, J., Meakin, P., and Jossang, T., 1998. Fragmentation transition for invasion percolation in hydraulic gradients. Physical Review Letters, 80(14): 3065-3068.

Vendrig, M., Spouge, J., Bird, A., Daycock, J. and Johnsen, O., 2003. Risk Analysis of the geological sequestration of carbon dioxide.

Vidal-Gilbert, S., Tenthorey, E., Dewhurst, D., Ennis-King, J., Van Ruth, P., and Hillis, R., 2010. Geomechanical analysis of the Naylor Field, Otway Basin, Australia: Implications for CO_2 injection and storage. International Journal of Greenhouse Gas Control, 4(5): 827-839.

Vilarrasa, V., Bolster, D., Olivella, S. and Carrera, J., 2010. Coupled hydromechanical modeling of CO_2 sequestration in deep saline aquifers. International Journal of Greenhouse Gas Control, 4(6): 910-919.

W

Wade, A., 1913. The natural history of petroleum. Proceedings of the Geologists' Association, 24(1): 1-13.

Wagner, G., Meakin, P., Feder, J. and Jossang, T., 1997. Buoyancy-driven invasion percolation with migration and fragmentation. Physica A: Statistical Mechanics and its Applications, 245(3-4): 217-230.

Wallace, R.E., 1951. Geometry of shearing stress and relationship to faulting. Journal of Geology, 59: 111-130.

Walraven, D., Connolly, D.L. and Aminzadeh, F., 2005. Determining migration pathway in Marco Polo field using chimney technology, 67th European Association of Geoscientists and Engineers, EAGE Conference and Exhibition, incorporating SPE EUROPE2005 - Extended Abstracts: 1153-1156.

Walsh, J.J., Childs, C. and Manzocchi, T., 2009. The structure, content and growth of fault zones within sedimentary sequences. Bulletin for Applied Geology, 13: 59-62.

Walsh, J.J., Childs, C., Meyer, V., Manzocchi, T., Imber, J., Nicol, A., Tuckwell, G., Bailey, W.R., Bonson, C.G., Watterson, J., Nell, P.A., and Strand, J., 2001. Geometric controls on the evolution of normal fault systems. Geological Society Special Publication, London: 157-170.

Wang, J., Ryan, D., Anthony, E.J., Wildgust, N. and Aiken, T., 2011. Effects of impurities in CO_2 transport, injection and storage. Energy Procedia, 4: 3071-3078.

Wang, Z. and Nur, A.M., 2000. Seismic and Acoustic Velocities in Reservoir Rocks: Recent Developments. Geophysics Reprint Series, 19. Society of Exploration Geophysicists, 633 pp.

Wardlaw, N.C. and Taylor, R.P., 1976. Mercury capillary pressure curves and the interpretation of pore structure and capillary behaviour in reservoir rocks. Bulletin of Canadian Petroleum Geology, 24(2): 225-262.

Washburn, E.W., 1921. A note on the method of determining the distribution of pore sizes in a porous material. Proceedings of the National Academy, 7: 155-116.

Watson, M.N., Daniel, R.F., Tingate, P.R. and Gibson-Poole, C.M., 2004. CO_2-related seal capacity enhancement in mudstones: Evidence from the Pine Lodge natural CO_2 accumulation, Otway Basin, Australia. In: E.S. Rubin, D.W. Keith and Gilboy (Editors), Proceedings of the 7th International Conference on Greenhouse Gas Control Technologies (GHGT-7), Vancouver, Canada.

Watts, N.L., 1987. Theoretical aspects of cap-rock and fault seals for single- and two-phase hydrocarbon columns. Marine and Petroleum Geology, 4(4): 274-307.

Webb, P.A., 2001. An introduction to the physical characterisation of material by mercury intrusion porosimetry with emphasis on reduction and presentation of experimental data. Micromeritics Instrument Corporation, USA: http://www.micromeritics.com/library/Technical-Articles-Research-Applications.aspx.

Weir, G.J., White, S.P. and Kissling, W.M., 1995. Reservoir storage and containment of greenhouse gases. Energy Conversion and Management, 36(6-9): 531-534.

Whibley, M. and Jacobson, T., 1990. Exploration in the northern Bonaparte Basin, Timor Sea-WA-199-P. The APPEA Journal, 30: 7-25.

Whitehead, W.S., Hunt, E.R. and Holditch, S.A., 1987. Effects of lithology and reservoir pressure on the in-situ stresses in the Waskom (Travis Peak) Field, Society of Petroleum Engineers of AIME, (Paper) SPE: 139-152.

Wibberley, C.A.J., Kurtz, W., Imber, J., Holdsworth, R.E. and Collettini, C., 2008a. The Internal Structure of Fault Zones: Implications for Mechanical and Fluid-Flow Properties, 299. Geological Society Special Publication, London, 376 pp.

Wibberley, C.A.J., Yielding, G. and Di Toro, G., 2008b. Recent advances in the understanding of fault zone internal structure: A review. Geological Society Special Publication, London: 5-33.

Wildenborg, A.F.B., Leijsne, A.L., Kreft, E., Nepveu, M.N., Obdam, A.N.M., Wipfler, E.L., van der Grift, B., Hofstee, C., van Kesteren, W., Gaus, I., Czernichowski-Lauriol, I., Torfs, P., Wojcik, R., and Orlic, B., 2003. Safety assessment methodology for CO_2 Storage (SAMCARDS). CCP Report, 2.1.1, 149 pp.

Wilkins, S.J. and Gross, M.R., 2002. Normal fault growth in layered rocks at Split Mountain, Utah: Influence of mechanical stratigraphy on dip linkage, fault restriction and fault scaling. Journal of Structural Geology, 24(9): 1413-1429.

Wilkins, S.J. and Naruk, S.J., 2007. Quantitative analysis of slip-induced dilation with application to fault seal. AAPG Bulletin, 91(1): 97-113.

Wilkinson, D., 1984. Percolation model of immiscible displacement in the presence of buoyancy forces. Physical Review A, 30(1): 520-531.

Wilkinson, D. and Willemsen, J.F., 1983. Invasion percolation: A new form of percolation theory. Journal of Physics A: General Physics, 16(14): 3365-3376.

Wilkinson, M., Haszeldine, R.S., Fallick, A.E., Odling, N., Stoker, S.J., and Gatliff, R.W., 2009. CO_2-mineral reaction in a natural analogue for CO_2 storage - Implications for modeling. Journal of Sedimentary Research, 79(7-8): 486-494.

Wollenweber, J., Alles, S., Busch, A., Krooss, B.M., Stanjek, H., and Littke, R., 2010. Experimental investigation of the CO_2 sealing efficiency of caprocks. International Journal of Greenhouse Gas Control, 4(2): 231-241.

X

Xu, T., Apps, J.A. and Pruess, K., 2005. Mineral sequestration of carbon dioxide in a sandstone-shale system. Chemical Geology, 217(3-4 SPEC. ISS.): 295-318.

Xu, T., Apps, J.A., Pruess, K. and Yamamoto, H., 2007. Numerical modeling of injection and mineral trapping of CO_2 with H_2S and SO_2 in a sandstone formation. Chemical Geology, 242: 319-346.

Y

Yang, D. and Gu, Y., 2004. Interfacial interactions of crude oil-brine-CO_2 systems under reservoir conditions, Proceedings - SPE Annual Technical Conference and Exhibition: 1767-1778.

Yang, D., Gu, Y. and Tontiwachwuthikul, P., 2008. Wettability determination of the reservoir brine - Reservoir rock system with dissolution of CO_2 at high pressures and elevated temperatures. Energy and Fuels, 22(1): 504-509.

Yang, D., Tontiwachwuthikul, P. and Gu, Y., 2005. Interfacial interactions between reservoir brine and CO_2 at high pressures and elevated temperatures. Energy and Fuels, 19(1): 216-223.

Yielding, G., Freeman, B. and Needham, D.T., 1997. Quantitative fault seal prediction. AAPG Bulletin, 81: 897-917.

Yielding, G., Needham, T. and Jones, H., 1996. Sampling of fault populations using sub-surface data: A review. Journal of Structural Geology, 18(2-3): 135-146.

Yielding, G., Walsh, J. and Watterson, J., 1992. The predictions of small-scale faulting in reservoirs. First Break, 10(12): 449-460.

Z

Zhang, L., Ren, L. and Hartland, S., 1997. Detailed analysis of determination of contact angle using sphere tensiometry. Journal of Colloid and Interface Science, 192(2): 306-318.

Zhang, Y., Oldenburg, C.M. and Finsterle, S., 2009. Percolation-theory and fuzzy rule-based probability estimation of fault leakage at geologic carbon sequestration sites. Environmental Earth Sciences, 59(7): 1447-1459.

Zhou, R., Huang, L. and Rutledge, J., 2010. Microseismic event location for monitoring CO_2 injection using double-difference tomography. Leading Edge (Tulsa, OK), 29(2): 208-214.

Zoback, M., 2007. Reservoir Geomechanics. Cambridge University Press, Cambridge, 449 pp.

Zoback, M.L., 1992. First-and second-order patterns of stress in the lithosphere: the World Stress Map Project. Journal of Geophysical Research, 97(B8): 11,703-11,728.

Zoback, M.L. and Zoback, M., 1980a. State of stress in the conterminuous United States. Journal of Geophysical Research, 85(B11): 6113-6156.

Zoback, M.L. and Zoback, M., 1980b. Tectonic stress field of the conterminous United States. Geological Society of America Memoirs, 172: 523-539.

Zweigel, P., Linderberg, E., Moen, A. and Wessel-Berg, D., 2004. Towards a methodology for top seal efficacy assessment for underground CO_2 storage. In: E.S. Rubin, D.W. Keith and Gilboy (Editors), Proceedings of the 7th International Conference on Greenhouse Gas Control Technologies (GHGT-7), Vancouver, Canada: 1323-1328.

Appendix A Data Collection and Sample Preparation

A.1 Protocol for Sampling Seals

Sampling for seal capacity analysis is summarised in Figure A.1.

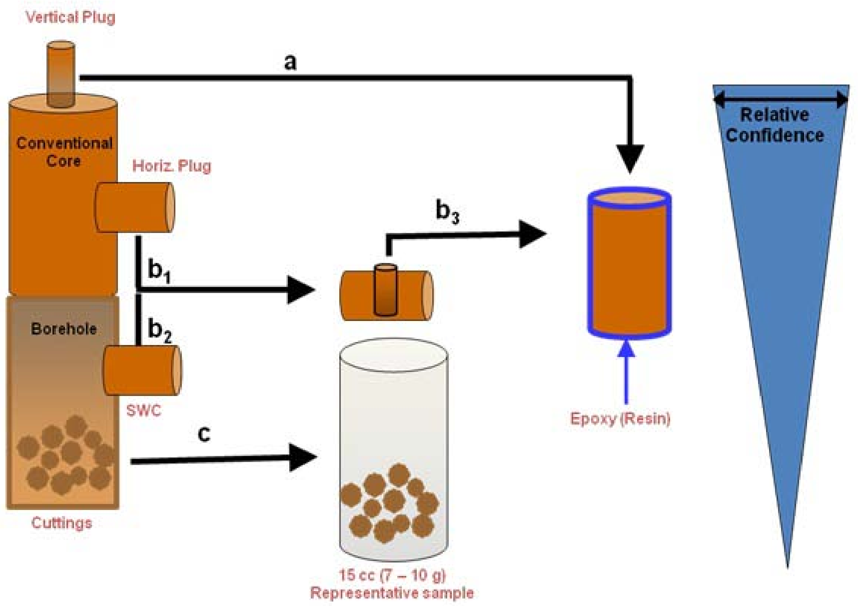

Figure A.1 Summary of sampling methods for determining seal capacity, highlighting relative confidences in sampling procedures.

The ideal methodology to sample for seal capacity using MICP technology is done by first obtaining a conventional core through the seal interval of interest. Next, a vertical plug is taken from the core and the plug is coated with an epoxy resin on all sides, leaving only the upper and lower faces exposed (a). This forces the mercury (non-wetting phase) to mimic the behaviour of CO_2 in the reservoir by moving only in a cross-lamellar direction. If only horizontal plugs (b1) or sidewall cores (SWC) are available (b2), the procedure is to take a vertical sub-cut off the main plug,(b3) and coat the outside of the sub-cut sample with epoxy, again leaving the lower and upper faces exposed. If no conventional core is available, cuttings may be used. The procedure with cuttings is complicated by the fact that the samples must be hand-picked to exclude non-representative material (cavings that may have fallen in from shallower formations, lost circulation material, etc.). When evaluating the MICP capillary threshold pressures from cuttings, it is important to correct for the conformance (the volume of mercury that enters the spaces between the cuttings) which is not representative of the actual rock pore system. The degree of confidence in analyses is greatest where vertical plugs are taken and least where cuttings are analysed. This is indicated by the relative confidence wedge. Once samples are selected, a se4ries of analytical procedures take place. The procedures include MICP analysis, SEM/ EDX analysis, XRD analysis (detailed in Figures A.2 to A.6 below). A well log indicating petrophysical characteristics of the sampled interval (Figure A.7) should always be included as well.

A.1.1 Mercury Porosimeter for MICP analysis

MICP analyses for caprocks are usually performed using a mercury injection porosimeter (Figure A.2). The instrument comprises two separate systems, one for low pressures and the second for the high pressures.

The low pressure run must always be done first, followed quickly by the high pressure run, to preclude the possibility of extra mercury intrusion into the sample by capillary action while the sample is held at atmospheric pressure at the conclusion of the low pressure run.

The system operates using the equilibration by time method - after the required pressure for a reading is attained it is held for twenty five seconds to allow the amount of mercury entering the pores to stabilise. This is done because the process of mercury filling the pores is not an instantaneous one. Mercury begins entering the pores as soon as the pressure exceeds the value required for the pore throats' diameter, but the time required to fill the pores depends on the volume and shape of the pores. The equilibration by time process allows the pores to fill. If equilibration is not allowed, then the filling may not be complete when the reading is taken, which leads to estimation of lower pore volumes and smaller pore sizes than is actually the case. Readings of mercury intrusion are taken by measuring the electrical capacitance of the penetrometer. This varies as the mercury is intruded from the precision bore stem into the pore space of the sample by the increasing pressure of during the analysis).

Each sample is usually dried at 55°C for at least twenty four hours, weighed and placed into a penetrometer (a glass chamber attached to a precision bore glass tube, which has been nickel-plated) and the entire assembly is weighed. This is placed in the low pressure port and evacuated to 0.05 torr. This vacuum is held for thirty minutes to ensure that no vapour remains in the sample. After this time the penetrometer is filled with mercury and the low pressure run is carried out. The pressure is increased incrementally from 13.8 kPa (2 psia) to 199.5 kPa (28.94 psia), with a reading taken after 25 seconds of equilibration at each pressure. At the end of the low pressure run the penetrometer returns to atmospheric pressure. It is removed from the instrument and weighed to obtain its weight plus that of the mercury.

The penetrometer is then placed in the high pressure chamber, which uses hydraulic oil to take the pressure incrementally from 199.5 kPa (28.94 psia) to 413.7 MPa (60,000 psia). Again readings are taken after a 25 second equilibration period. The pressure is then decreased incrementally from 413.7 MPa (60,000 psia) to 139kPa (20 psia), with readings taken after the equilibration period. The sample is removed from the penetrometer and weighed. The specific gravity and porosity of the sample can be calculated when it is removed from the penetrometer and weighed.

Figure A.2 High-pressure Mercury Porosimeter (image courtesy Micromeritics Pty Ltd). Data are acquired by injecting mercury into cleaned and evacuated core plug or cuttings; Mercury injection pressure is increased in a stepwise manner until equilibrium is reached at each pressure. Mercury injection pressure is then plotted against mercury saturation. Such MICP units can reach up to 60,000 psi pressure, sufficient to force mercury into even sub-micron scale pores.

A.2 Methodology for a Caprock Database

Having a readily accessible database of caprock properties such as seal capacity, mineralogy, well-log, geochemical and petrophysical characteristics of regional, local and intraformational seals would be extremely useful when assessing containment potential for a specific area. Even if data from that area is not available, the samples in the database could be utilised as analogs for the area of potential interest. The types of data that can be captured include mercury injection capillary pressure analysis (MICP), Scanning Electron Microscopy (SEM) with an Energy Dispersive X-ray Analyser (EDS), X-Ray Diffraction (XRD) and "V" Shale log (Vsh). Techniques used to a lesser extent are; thin-section petrography, grain / pore size distribution, coupled with lithofacies identification (see Table A.1 and Figures A.2 to A.6 on the following pages).

A.2.1 XRD Analysis

Some clay minerals are not easily detectable in a randomly packed loose powder preparation. An oriented preparation is required because it gives enhanced basal reflections and more accurate intensity and spacing measurements. For example, the detection limit of smectite in an oriented preparation is probably 0.1% but in a randomly packed loose powder preparation would be 20-50%.

A portion of the sample is taken and dispersed in demineralized water with the aid of deflocculants and allowed to settle. A -2µm size fraction is extracted by pipetting from a particular depth (determined by time elapsed, density of the particle and temperature of the water).

The resulting dispersion is then used to prepare oriented clay preparations on porous ceramic plates. This is done by placing the slurry on the plate while applying suction. As the water is drawn through the plate the clay "flakes" settle on their flat face (i.e. become oriented so that their basal plane is parallel to the plate surface). After a thick enough layer is placed on the plate it is saturated with Mg^{++} ions by addition magnesium chloride solution. The purpose of this to flush out exchangeable cations from smectite in particular, because the basal d-spacing of smectite varies according to which cations are loosely held between the basal planes. When these are replaced by Mg^{++} ions the d-spacing is predictable. The plate may also be treated with glycerol, because the glycerol molecule penetrates spacing between the basal planes of smectite and pushes them apart by a predictable distance. There may be other treatments e.g. adding other chemicals or heating to varying temperatures, depending on the types of clay suspected of being present. These include adding formaldehyde to determine the presence of halloysite, adding KCl to determine the presence of vermiculite, and heating at 550º to collapse smectite, vermiculite and interstratified smectite – illite to 10 Å.

When air-dry, the oriented preparation is examined in the X-ray diffractometer. The XRD trace is recorded from an angle of 2^o to 25^o. The low angle of 2^o is due to some clay peaks having d-spacings as large as 50 Å. The X-ray source is a tube with a cobalt target and the XRD trace is recorded on a chart of digital display.

Table A.1 Typical work flow spreadsheet for determining seal capacity/ column height is shown below, in this case for supercritical CO_2. Subsurface pressure, temperature and salinity are required to determine phase densities and interfacial tension.

Depth of sample (m TVDSS)	Pressure at sample depth (MPa)	Temp. at sample depth (°C)	Salinity at sample depth	CO_2 density (g/cm^3)	Brine density (g/cm3)	Interfacial tension (mN/m or dynes/cm)	Contact Angle (°)	Seak threshold pressure (air-Hg system) (psia)	Reservoir threshold pressure (air-Hg system) (psia)	Seal threshold pressure (brine-CO_2 system) (psia)	Reservoir threshold pressure (brine-CO_2 system) (psia)	Height of CO_2 column (m)
1901.5	18.97697	77	25000	0.5878	1.0086	26.88	40	6972	10	390	0.6	652

The relative amounts of the clay minerals in the -2μm size fraction are estimated from the XRD trace. The peak areas of the first order basal diffraction peaks of kaolinite, illite and glyceroled smectite were measured and summed to 100%. Peak areas are measured by multiplying the peak height by the width of the peak at half height. Because XRD peaks of clay minerals tend to be broad, peak areas are measured rather than peak heights (Figure A.6)

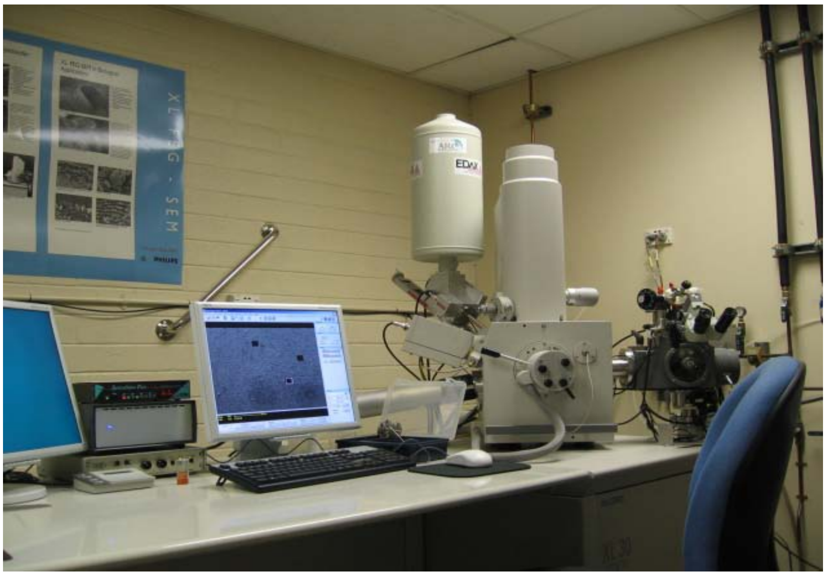

Figure A.3 **Scanning Electron Microscopy and Energy Dispersive X-ray Analyser.**

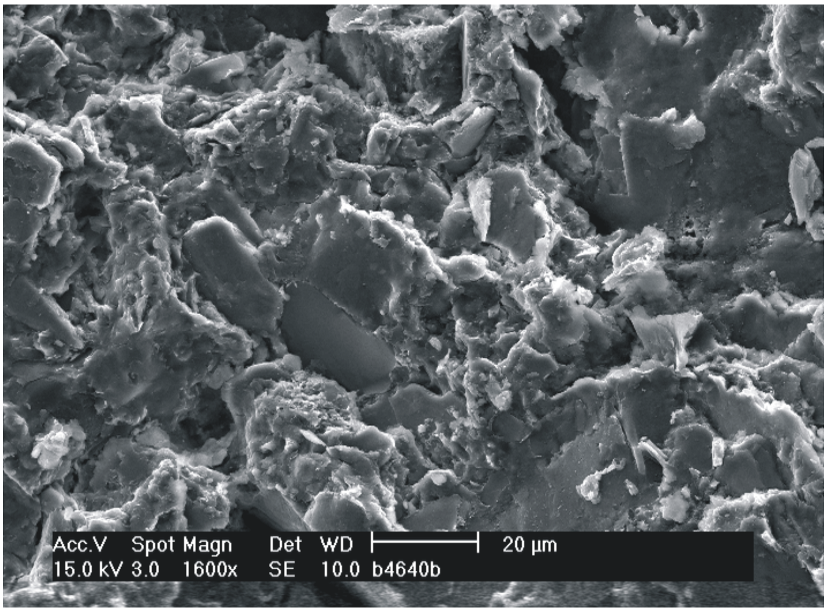

Figure A.4 **SEM example of a seal rock with clay platelets surrounding silt-sized quartz grains; perpendicular to bedding**

The instrument used is a Philips XL30 FEGSEM with Oxford CT1500HF Cryo stage and EDAX DX4 integrated Energy Dispersive X-ray Analyser (Figure A.3).

Micro-structural and elemental constituents are imaged and analysed with magnifications up to 50,000; i.e. image clarity at <200 nm (nanometres) scale (Figure A.4). Imaging at this scale can be important when describing seals with calculated pore throat sizes to 3 nm, sizes that cannot be imaged with the instruments commonly available at present.

Energy dispersive X-ray spectroscopy (EDS, EDX or EDXRF) is an analytical technique used for the elemental analysis of a sample. Its characterisation capabilities are due in large part to the fundamental principle that each element has a unique atomic structure allowing x-rays that are characteristic of an element's atomic structure to be identified uniquely from each other (Figure A.5).

Identification of the principal elements; C, O, Na, Mg, Al, Si, S, Cl, K, Ca, Ti, Mn, Fe, have been carried out on most samples using the EDS technique.

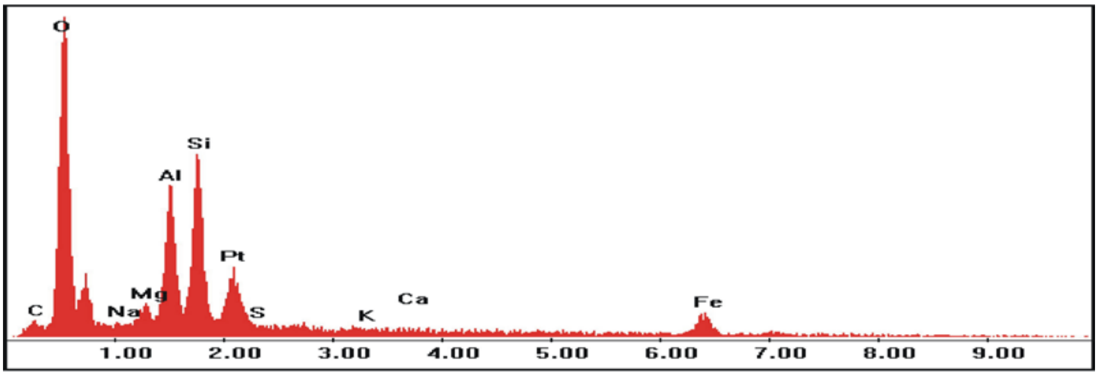

Figure A.5 **EDS Spectrum indicates silica and kaolinite with minor calcite and muscovite; trace pyrite. Platinum coating.**

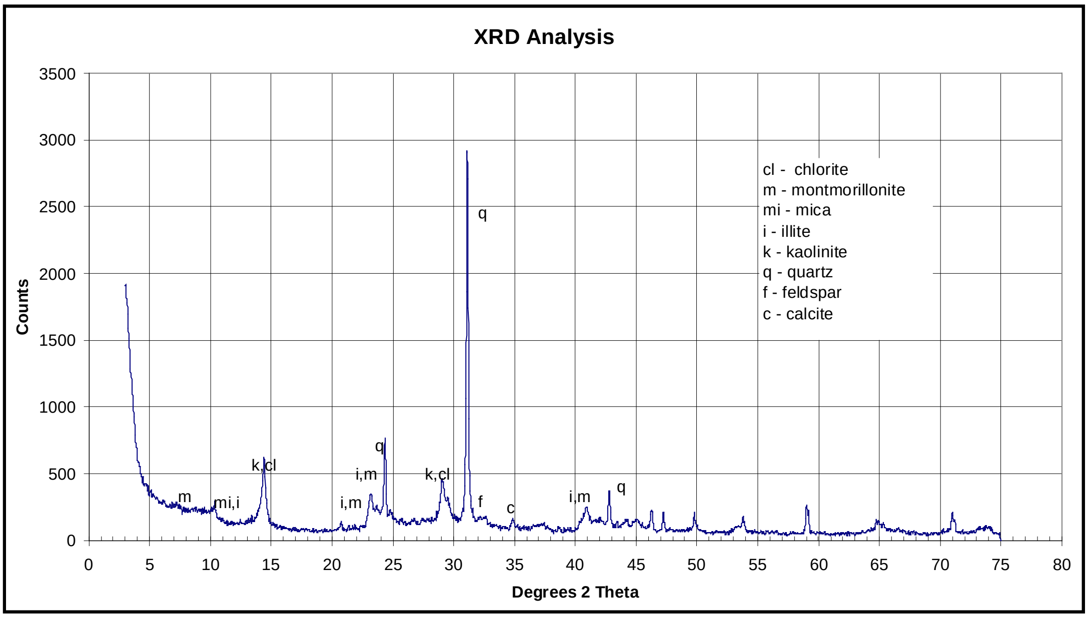

Figure A.6 **X-ray Diffraction plot of a (powder) spectrum indicating the crystallographic peaks of minerals present i.e. kaolinite and quartz with illite, smectite and trace calcite and feldspar.**

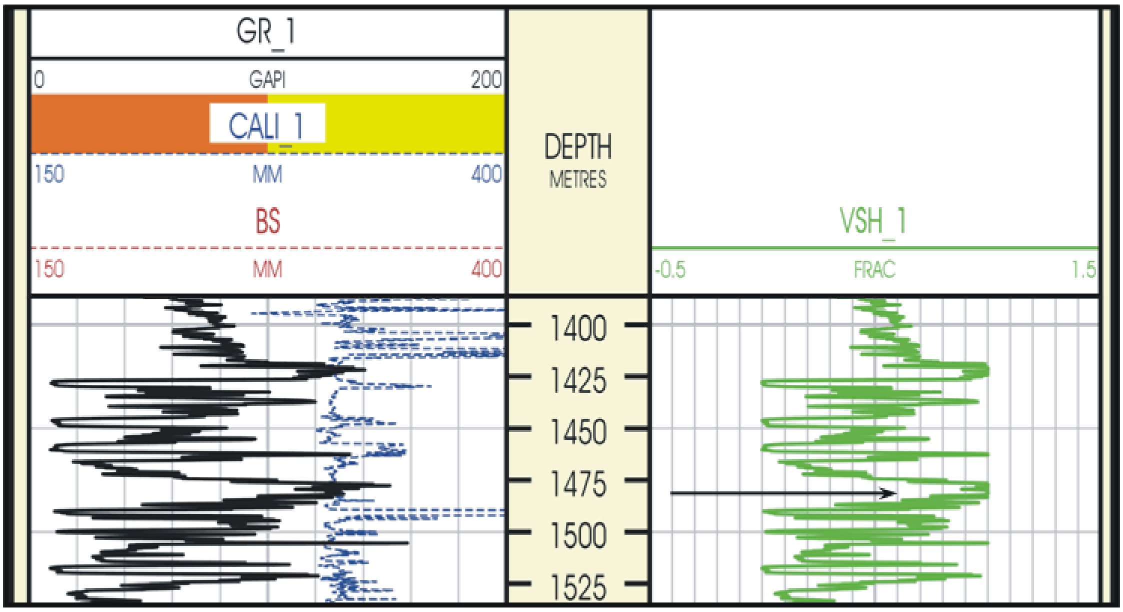

Figure A.7 400m section of 'V' Shale log (Vsh), centrally located either side of the sample depth, highlighting mud-rich intervals. The curve is derived from the V shale algorithm in the Geolog 6 desktop package. Gamma and calliper curves are shown on the left.

Appendix B Glossary

This glossary defines a selection of terms used in this report or provides background which has been collated from:

1 IPCC special report on carbon dioxide capture and storage, 2005. Cambridge University Press, Cambridge, 431 pp.

2 Schlumberger, 2010. Oilfield Glossary. http://www.glossary.oilfield.slb.com/.

3 Gibson-Poole, C.M., Edwards, S., Langford, R.P. and Vakarelov, B., 2007. Review of geological storage opportunities for carbon capture and storage (CCS) in Victoria - Summary report. CO2CRC Report, ICTPL-RPT07-0526: 9.

4 Fetter, C.W., 2000. Applied Hydrogeology. Prentice Hall, 598 pp.

Absorption[1]: Chemical or physical take-up of molecules into the bulk of a solid or liquid, forming either a solution or compound.

Acoustic impedance[2]: The product of density and seismic velocity, which varies among different rock layers, commonly symbolized by Z. The difference in acoustic impedance between rock layers affects the reflection coefficient.

Adsorption[1]: The uptake of molecules on the surface of a solid or a liquid.

Alluvial[2]: Pertaining to the subaerial (as opposed to submarine) environment, action and products of a stream or river on its floodplain, usually consisting of clastic sediments, and distinct from subaqueous deposition such as in lakes or oceans and lower energy fluvial deposition.

Amplitude[2]: The difference between the maximum displacement of a wave and the point of no displacement, or the null point. The common symbol for amplitude is α.

Anthropogenic source[1]: Source which is man-made as opposed to natural.

Aquifer[1]: Geological structure containing water and with significant permeability to allow flow; may be bound by seals.

Anticline[1]: Folded geological strata that is convex upwards.

Baseline[1]: The datum against which change is measured.

Basin[1]: A geological region with strata dipping towards a common axis or centre.

Bed[2]: A layer of sediment or sedimentary rock, or stratum. A bed is the smallest stratigraphic unit, generally a centimetre or more in thickness. To be labelled a bed, the stratum must be distinguishable from adjacent beds.

Bicarbonate ion[1]: The anion formed by dissolving carbon dioxide in water, HCO_{3-}.

Brine[2]: Water containing more dissolved inorganic salt than typical seawater.

Buoyancy[1]: Tendency of a fluid or solid to rise through a fluid of higher density.

Cap rock[1]: Rock of very low permeability that acts as an upper seal to prevent fluid flow out of a reservoir.

Capillary entry pressure[1]: Additional pressure needed for a liquid or gas to enter a pore and overcome surface tension.

Capillary forces[1]: The forces acting on soil moisture in the unsaturated zone, attributable to molecular attraction between soil particles and water.

Carbonate[1]: Natural minerals composed of various anions bonded to a CO_3^{2-} cation (e.g. calcite, dolomite, siderite, limestone).

CBM[3]: Coal Bed Methane is the process whereby methane is extracted from coal seams for energy generation.

CCS[1]: Carbon dioxide Capture and Storage.

Cementation[2:] The process of precipitation of cement between mineral or rock grains and forming solid clastic sedimentary rock, one phase of lithification.

Clastic sediment[2]: Sediment consisting of broken fragments derived from pre-existing rocks and transported elsewhere and re-deposited before forming another rock.

Clay[2]: Fine-grained sediments less than 0.0039 mm in size.

Closure[2]: The vertical distance from the apex of a structure to the lowest structural contour that contains the structure. Measurements of both the areal closure and the distance from the apex to the lowest closing contour are typically incorporated in calculations of estimated hydrocarbon content of a trap.

CO_2 avoided[1]: The difference between CO_2 captured, transmitted and/or stored, and the amount of CO_2 generated by a system without capture, net of the emissions not captured by a system with CO_2 capture.

CO_2 equivalent[1]: A measure used to compare emissions of different greenhouse gases based on their global warming potential.

Coal[2]: A carbon-rich sedimentary rock that forms from the remains of plants deposited as peat in swampy environments. Burial and increase in temperature bring about physical and chemical changes called coalification.

Coal bed storage[3]: Coals are known to adsorb CO_2 more strongly than methane (which commonly occurs in coals) and to have a substantially greater capacity to store CO_2 than methane (about twice as much). The storage capacity for coal seams can't be calculated using pore volumes and gas compressibility as for conventional porous reservoirs, as the gas in coals is stored in the coal matrix on the surface of micropores, in a free state in the coal cleats or is dissolved in water. To calculate CO_2 storage capacity in coals requires knowledge of the gas content and type, adsorption isotherms, permeability, coal seam rank and seam architecture, moisture and ash content, which vary for each coal type. There are concerns that storage of CO_2 in coals may not actually produce any net greenhouse gas mitigation when it is associated with production of methane (ECBM - Enhanced Coal Bed Methane). The range of permeability typical of coal beds is at the lower end of the range of permeability possible in siliciclastic and carbonate rocks. Storage of CO_2 in coals is an emerging science, and more research is required to fully understand the processes and interactions involved, such as the effect of swelling of coals during injection of CO_2. The trapping mechanism operates immediately.

Coal measures[3]: A succession of sedimentary rocks ranging in thickness and consisting of coal seams with interstratified beds of claystones, shales, siltstones, sandstones and carbonate.

Conformity[2]: A bedding surface separating younger from older strata, along which there is no evidence of subaerial or submarine erosion or of non-deposition, and along which there is no evidence of a significant hiatus.

Containment[1]: Restriction of movement of a fluid to a designated volume (e.g. reservoir).

Continental shelf[1]: The extension of the continental mass beneath the ocean.

Contour[2]: A line that includes points of equal value and separates points of higher value from points of lower value. Contours are commonly drawn on maps to portray the structural configuration of the Earth's surface or formations in the subsurface.

Core plug[2]: A plug, or sample, taken from a conventional core for analysis. Core plugs are typically 1” to 1 ½” (2.5 to 3.8 cm) in diameter and 1” to 2” (5 cm) long.

Crust[3]: The thin, outermost shell of the earth that is typically 5 to 75 km thick. Generally divided into continental crust and oceanic crust; crustal- adjective.

D, Darcy[1]: A non-SI unit of permeability, abbreviated D, and approximately = 1μm^2.

Datum[2]: An agreed and known value, such as the elevation of a benchmark or sea level, to which other measurements are corrected.

Deep saline aquifer[1]: A deep underground rock formation composed of permeable materials and containing highly saline fluids.

Deep sea[1]: The sea below 1000m depth.

Delta[3]: A low, nearly flat accumulation of sediment deposited at the mouth of a river or stream generally into a marine or lake environment, commonly triangular or fan-shaped; deltaic - adjective.

Density[2]: Mass per unit of volume. Density is typically reported in g/cm^3 (for example, rocks) or pounds per barrel (drilling mud) in the oilfield.

Depleted[1]: Of a reservoir: one where production is significantly reduced.

Deposit[2]: Sediments that have accumulated, usually after being moved by wind, water or ice.

Depositional energy[2]: The relative kinetic energy of the environment. A high-energy environment might consist of a rapidly flowing stream that is capable of carrying coarse-grained sediments, such as gravel and sand.

Depositional environment[2]: The area in which and physical conditions under which sediments are deposited, including sediment source; depositional processes such as deposition by wind, water or ice; and location and climate, such as desert, swamp or river.

Depositional system[2]: The three-dimensional array of sediments or lithofacies that fills a basin. Depositional systems vary according to the types of sediments available for deposition as well as the depositional processes and environments in which they are deposited.

Depth map[2]: A two-dimensional representation of subsurface structure with contours in depth that have been converted from seismic travel times.

Dip[1]: In geology, the angle below the horizontal taken by rock strata.

ECBM[1]: Enhanced coal bead methane recovery; the use of CO_2 to enhance the recovery of methane present in unmineable coal beds through the preferential adsorption of CO_2 on coal.

Effective permeability[2]: The ability to preferentially flow or transmit a particular fluid when other immiscible fluids are present in the reservoir (e.g., effective permeability of gas in a gas-water reservoir).

Effective porosity[2]: The interconnected pore volume or void space in a rock that contributes to fluid flow or permeability in a reservoir. Effective porosity excludes isolated pores and pore volume occupied by water adsorbed on clay minerals or other grains.

EGR[1]: Enhanced gas recovery: the recovery of gas additional to that produced naturally by fluid injection or other means.

EOR[1]: Enhanced oil recovery: the recovery of oil additional to that produced naturally by fluid injection or other means.

Erosion[2]: The process of denudation of rocks, including physical, chemical and biological breakdown and transportation.

ESSCI[3]: Environmental Sustainable Site for Carbon dioxide Injection. Used in GEODISC™.

Facies[2]: The characteristics of a rock unit that reflect its origin and permit its differentiation from other rock units around it. Facies usually are characterised using all the geological characteristics known for that rock unit.

Fault[1]: In geology, a surface at which strata are no longer continuous, but displaced.

Fault reactivation[1]: The tendency for a fault to become active, i.e. for movement to occur.

Fault slip[1]: The extent to which a fault has slipped in past times.

Fault trap[2]: A type of structural hydrocarbon trap in which closure is controlled by the presence of at least one fault surface.

Feldspar[1]: A group of alumina-silicate minerals that makes up much of the Earth's crust.

Field[2]: An accumulation, pool, or group of pools of hydrocarbons or other mineral resources in the subsurface. A hydrocarbon field consists of a reservoir in a shape that will trap hydrocarbons and that is covered by an impermeable, sealing rock.

Flood[1]: The injection of a fluid into an underground reservoir.

Flooding surface[2]: A surface exhibiting evidence of an abrupt increase in water depth, separating younger from older strata. The surface may also display evidence of minor submarine erosion.

Flue gas[1]: Gases produced by combustion of a fuel that are normally emitted to the atmosphere.

Fluvial[2]: Pertaining to an environment of deposition by a river or running water. Fluvial deposits tend to be well sorted, especially in comparison with alluvial deposits, because of the relatively steady transport provided by rivers.

Folding[1]: In geology, the bending of rock strata from the plane in which they were formed.

Formation[1]: A body of rock of considerable extent with distinctive characteristics that allow geologists to map, describe, and name it.

Four-dimensional seismic data[2]: Three-dimensional (3D) seismic data acquired at different times over the same area to assess changes in a producing hydrocarbon reservoir with time. Changes may be observed in fluid location and saturation, pressure and temperature. 4D seismic data is one of several forms of time-lapse seismic data. Such data can be acquired on the surface or in a borehole.

Fracture[1]: Any break in rock along which no significant movement has occurred.

FWL – Free Water level

Gasification[1]: Process by which a carbon-containing solid fuel is transformed into a carbon- and hydrogen-containing gaseous fuel by reaction with air or oxygen and steam.

Geochemical trapping[1]: The retention of injected CO_2 by geochemical reactions.

Geological setting[1]: The geological environment of various locations.

Geological time[1]: The time over which geological processes have taken place.

Geomechanics[1]: The science of the movement of the Earth's crust.

Geophone[2]: A device used in surface seismic acquisition, both onshore and on the seabed offshore, that detects ground velocity produced by seismic waves and transforms the motion into electrical impulses.

Geosphere[1]: The earth, its rocks and minerals, and its waters.

Geothermal[1]: Concerning heat flowing from deep in the earth.

Geothermal gradient[3]: Rocks lying deeper in the earth are at high temperatures than the rocks above. The rate of temperature change is called the geothermal gradient. This gradient varies from place to place and is dependent on the crustal thickness and thermal conductivity of the rocks in area. Reservoirs that are at higher temperatures will store CO_2 at a lower density and will be somewhat less efficient as storage sites.

GHG[1]: Greenhouse gases: carbon dioxide (CO_2), methane (CH_4), nitrous oxide (N_2O), hydroflurocarbons (HFCs), perfluorocarbons (PFCs), and sulphur hexafluoride (SF_6).

Groundwater[2]: Water in the subsurface below the water table. Groundwater is held in the pores of rocks, and can be connate, from meteoric sources, or associated with igneous intrusions.

H - Height

Hetrogeneous[4]: Pertaining to a substance having different characteristics in different locations.

Homogeneity[2]: The quality of uniformity of a material. If irregularities are distributed evenly in a mixture of material, the material is homogeneous.

Host rock[1]: In geology, the rock formation that contains a foreign material.

Hydrocarbon[2]: A naturally occurring organic compound comprising hydrogen and carbon. Hydrocarbons can be as simple as methane (CH_4), but many are highly complex molecules, and can occur as gases, liquids or solids.

Hydrocarbon pore space[3]: Pore space in the subsurface that contains (or has contained) hydrocarbons, i.e. pore space within a hydrocarbon field or a depleted hydrocarbon field.

Hydrostatic[1]: Pertaining to the properties of a stationary body of water.

IFT – Interfacial tension

IFP – Institut Français du Pétrole

Impermeable[2]: Pertaining to a rock that is incapable of transmitting fluids because of low permeability. Shale has a high porosity, but its pores are small and disconnected, so it is relatively impermeable. Impermeable rocks are desirable sealing rocks or cap rocks for reservoirs because hydrocarbons cannot pass through them readily

Injection[1]: The process of using pressure to force fluids down wells.

Injection well[1]: A well in which fluids are injected rather than produced.

Injectivity[1]: A measure of the rate at which a quantity of fluid can be injected into a well.

Isochore[2]: A contour connecting points of equal true vertical thickness of strata, formations, reservoirs or other rock units.

Lacustrine[2]: Pertaining to an environment of deposition in lakes, or an area having lakes.

Leakage[1]: In respect of carbon storage, the escape of injected fluid from storage.

Lignite/sub-bituminous coal[1]: Relatively young coal of low rank with a relatively high hydrogen and oxygen content.

Limestone[1]: A sedimentary rock made mostly of the mineral calcite (calcium carbonate), usually formed from shells of dead organisms.

LNG[1]: Liquefied natural gas.

Lithology[1]: Science of the nature and composition of rocks.

Lithostatic pressure[2]: The pressure of the weight of overburden, or overlying rock, on a formation; also called geostatic pressure.

Log[1]: Records taken during or after the drilling of a well.

Ma[2]: Mega annum. The abbreviation for million years that is most commonly used in the geologic literature.

Maturation[1]: The geological process of changing with time. For example, the alteration of peat into lignite, then into sub-bituminous and bituminous coal, and then into anthracite.

MICP Mercury Injection Capillary Pressure

Microseismicity[1]: Small-scale seismic tremors.

Migration[1]: The movement of fluids in reservoir rocks.

Mitigation[1]: The process of reducing the impact of any failure.

Monitoring[1]: The process of measuring the quantity of carbon dioxide stored and its location.

Mudstone[1]: A very fine-grained sedimentary rock formed from mud.

Natural analogue[1]: A natural occurrence that mirrors in most essential elements an intended or actual human activity.

Natural gas[2]: A naturally occurring mixture of hydrocarbon gases that is highly compressible and expansible. Methane (CH_4) is the chief constituent of most natural gas (constituting as much as 85% of some natural gases), with lesser amounts of ethane (C_2H_6), propane (C_3H_8), butane (C_4H_{10}) and pentane (C_5H_{12}). Impurities can also be present in large proportions, including carbon dioxide, helium, nitrogen and hydrogen sulphide.

Observation well[1]: A well installed to permit the observation of subsurface conditions.

Oil field[2]: An accumulation, pool or group of pools of oil in the subsurface. An oil field consists of a reservoir in a shape that will trap hydrocarbons and that is covered by an impermeable or sealing rock. Typically, industry professionals use the term with an implied assumption of economic size.

Orogeny[2]: A major episode of plate tectonic activity in which lithospheric plates collide and produce mountain belts, in some cases including the formation of subduction zones and igneous activity. Thrust faults and folds are typical geological structures seen in areas of orogeny.

Outcrop[1]: The point at which a particular stratum reaches the earth's surface.

Overburden[1]: Rocks and sediments above any particular stratum.

Overpressure[1]: Pressure created in a reservoir that exceeds the pressure inherent at the reservoir's depth.

Permeability[3]: Ability to flow or transmit fluids through a porous solid such as rock, typically measured in the petroleum industry in darcies or millidarcies (one thousandths of a darcy). Rocks that transmit fluids readily, such as sandstones, are described as permeable and tend to have many large, well-connected pores. Impermeable formations, such as shales and siltstones, tend to be finer grained or of a mixed grain size, with smaller, fewer, or less interconnected pores.

Petroleum system[2]: Geologic components and processes necessary to generate and store hydrocarbons, including a mature source rock, migration pathway, reservoir rock, trap and seal.

pH[2]: Hydrogen ion potential, which is the $\log_{10}$ of the reciprocal of hydrogen ion, H^+, concentration. Mathematically, $pH = \log_{10}(1/[H^+])$, where [ ] represents mole/L. pH is derived from the ion-product constant of water, which at room temperature is $1 \times 10^{-14} = [H^+] \times [OH^-]$. Pure water (at neutral pH) has equal concentrations of its two ions: $[H^+] = [OH^-] = 10^{-7}$ mole/L. $\mathrm{Log}_{10}\ 1/[H^+]$ is 7, which is the pH of a neutral solution. The pH scale ranges from 0 to 14, and values below 7 are acidic and above 7 are basic.

Pore[2]: A discrete void within a rock that can contain air, water, hydrocarbons or other fluids. In a body of rock, the percentage of pore space is the porosity.

Porosity[1]: Measure for the amount of pore space in a rock.

Post-combustion capture[1]: The capture of carbon dioxide after combustion.

Pre-combustion capture[1]: The capture of carbon dioxide following the processing of the fuel before combustion.

Prospectivity[3]: A term used in the exploration for any geological resource, in this case pore volume for CO_2 storage. Prospectivity is a perception in the mind of a geoscientist/explorer of the likelihood that a resource is present in a given area based on the available information. This perception is developed through; examining data (if possible), examining existing knowledge, application of established conceptual models and ideally the generation of new conceptual models or applying an analogue from a neighbouring basin or some other geologically similar setting.

Often prospectivity assessment involves an element of professional judgement (experience) and is influenced considerably by the level of uncertainty associated with absence and/or presence of conflicting or confirming data for a concept. When the level of uncertainty is very high (as in this report) the prospectivity of an area can and will change with new knowledge and changes in economic and technological factors.

In the case of this study, some specific aspects that enter into consideration include; distance to sources of CO_2, rate of CO_2 emission of near-by sources, presence of reservoir-seal pairs, extent of reservoir-seal pairs, heterogeneity/homogeneity, porosity and permeability, coal presence, coal rank, availability of depleted hydrocarbon fields, basin structure, basin age, basin history, pore water salinity, geothermal gradients and pressures. The list is not exhaustive. Availability of information on these factors in the literature for any given basin will vary markedly. Detailed investigation of these matters is not possible in a "desk top" study such as this report.

Recovery[2]: The fraction of hydrocarbons that can or has been produced from a well, reservoir or field; also, the fluid that has been produced.

Regional scale[1]: A geological feature that crosses an entire basin.

Relative permeability[2]: A dimensionless term devised to adapt the Darcy equation to multiphase flow conditions. Relative permeability is the ratio of effective permeability of a particular fluid at a particular saturation to absolute permeability of that fluid at total saturation. If a single fluid is present in a rock, its relative permeability is 1.

Remote sensing[2]: The process of measuring, observing or analysing features of the Earth from a distance. Satellite photography and radar are techniques commonly used for remote sensing.

Renewables[1]: Energy sources that are inherently renewable such as solar energy, hydropower, wind, and biomass.

Reserve[1]: A resource from which it is generally economic to produce valuable minerals or hydrocarbons.

Reservoir[1]: A subsurface body of rock with sufficient porosity and permeability to store and transmit fluids.

Seal : Caprock

Reservoir-seal pair[3]: To prevent the upward migration of CO_2 due to buoyancy, any porous rock (saline reservoir) used to store CO_2 requires the existence of an overlying impermeable seal or caprock. A reservoir formation and seal formation stratigraphically related in this way is called a reservoir-seal pair. Use of this term does not necessarily imply the presence of a structure or trap.

Resource[1]: A body of a potentially valuable mineral or hydrocarbon.

Saline formation[1]: Sediment or rock body containing brackish water or brine.

Salt dome[2]: A mushroom-shaped or plug-shaped diapir made of salt, commonly having an overlying cap rock. Salt domes form as a consequence of the relative buoyancy of salt when buried beneath other types of sediment.

Sandstone[1]: Sand that has turned into a rock due to geological processes.

$scCO_2$ – supercritical Carbon Dioxide

Seal[1]: An impermeable rock that forms a barrier above and around a reservoir rock such that fluids are held in the reservoir.

Secondary recovery[1]: Recovery of oil by artificial means, after natural production mechanisms like overpressure have ceased.

Sedimentary basin[1]: Natural large-scale depression in the earth's surface that is filled with sediments.

Seismic profile[1]: A two-dimensional seismic image of the subsurface.

Seismic section[2]: A display of seismic data along a line, such a 2D seismic profile or a profile extracted from a volume of 3D seismic data. A seismic section consists of numerous traces with location given along the x-axis and two-way travel time or depth along the y-axis.

Seismic technique[1]: Measurement of the properties of rocks by the speed of sound waves generated artificially or naturally.

Seismicity[1]: The episodic occurrence of natural or man-induced earthquakes.

Sequence[2]: A group of relatively conformable strata that represents a cycle of deposition and is bounded by unconformities or correlative conformities. Sequences are the fundamental unit of interpretation in sequence stratigraphy. Sequences comprise systems tracts.

Shale[1]: Clay that has changed into a rock due to geological processes.

Siliciclastic[2]: Silica-based non-carbonaceous sediments that are broken from pre-existing rocks, transported elsewhere, and re-deposited before forming another rock. Examples of common siliciclastic sedimentary rocks include conglomerate, sandstone, siltstone and shale. Carbonate rocks can also be broken and reworked to form other types of clastic rocks.

Sink[1]: The natural uptake of CO_2 from the atmosphere, typically in soils, forests or the oceans.

Solubility trapping[1]: A process in which fluids are retained by dissolution in liquids naturally present.

Source[1]: Any process, activity or mechanism that releases a greenhouse gas, an aerosol, or a precursor thereof into the atmosphere.

Source rock[2]: A rock rich in organic matter which, if heated sufficiently, will generate oil or gas. Typical source rocks, usually shales or limestones, contain about 1% organic matter and at least 0.5% total organic carbon (TOC), although a rich source rock might have as much as 10% organic matter.

Storage[1]: A process for retaining captured CO_2 so that it does not reach the atmosphere.

Stratigraphic[1]: The order and relative position of strata.

Stratigraphic column[1]: A column showing the sequence of different strata.

Stratigraphic trap[1]: A sealed geological container capable of retaining fluids, formed by changes in rock type, structure or facies.

Stimulation[1]: The enhancement of the ability to inject fluids into, or recover fluids from, a well.

Structural trap[1]: Geological structure capable of retaining hydrocarbons, sealed structurally by a fault or fold.

Structure[1]: Geological feature produced by the deformation of the Earth's crust, such as a fold or a fault; a feature within a rock such as a fracture; or, more generally, the spatial arrangement of rocks.

Structure contour map[1]: Map showing the contours of geological structures.

Sub-bituminous coal[1]: Coal of a rank between lignite and bituminous coal.

Subduction[2]: A plate tectonic process in which one lithospheric plate descends beneath another into the asthenosphere during a collision at a convergent plate margin.

Subsidence[2]: The relative sinking of the Earth's surface. Plate tectonic activity (particularly extension of the crust, which promotes thinning and sinking), sediment loading and removal of fluid from reservoirs are processes by which the crust can be depressed.

Sustainable[1]: Of development, that which is sustainable in ecological, social and economic areas.

Supercritical[1]: At a temperature and pressure above the critical temperature and pressure of the substance concerned. The critical point represents the highest temperature and pressure at which the substance can exist as a vapour and liquid in equilibrium

Syncline[2]: Basin- or trough-shaped fold in rock in which rock layers are downwardly convex. The youngest rock layers form the core of the fold and outward from the core progressively older rocks occur.

Tectonic environment[2]: Location relative to the boundary of a tectonic plate, particularly a boundary along which plate tectonic activity is occurring or has occurred.

Temperature gradient[2]: The rate of increase in temperature per unit depth in the Earth.

Tracer[1]: A chemical compound or isotope added in small quantities to trace flow patterns.

Transgression[2]: The migration of shoreline out of a basin and onto land during retrogradation. A transgression can result in sediments characteristic of shallow water being overlain by deeper water sediments.

Trap[1]: A geological structure that physically retains fluids that are lighter than the background fluids, e.g. an inverted cup.

Two-dimensional seismic data[2]: A group of 2D seismic lines acquired individually, as opposed to the multiple closely spaced lines acquired together that constitute 3D seismic data.

Two-way travel time (TWT)[2]: The elapsed time for a seismic wave to travel from its source to a given reflector and return to a receiver at the Earth's surface. Minimum two-way travel time is that of a normal-incidence wave with zero offset.

Three-dimensional seismic data[2]: A set of numerous closely-spaced seismic lines that provide a high spatially sampled measure of subsurface reflectivity.

Unconformity[1]: A geological surface separating older from younger rocks and representing a gap in the geological record.

Updip[1]: Inclining upwards following a structural contour of strata.

Velocity anomaly[2]: A feature in seismic data that results from changes in velocity, both laterally and vertically. Pull-up and push-down are examples of velocity anomalies.

Viscosity[2]: A property of fluids and slurries that indicates their resistance to flow, defined as the ratio of shear stress to shear rate.

Water saturation[2]: The fraction of water in a given pore space. It is expressed in volume/volume, percent or saturation units. Unless otherwise stated, water saturation is the fraction of formation water in the undisturbed zone.

Well[1]: Manmade hole drilled into the earth to produce liquids or gases, or to allow the injection of fluids.

Zone[2:] An interval or unit of rock differentiated from surrounding rocks on the basis of its fossil content or other features, such as faults or fractures. For example, a fracture zone contains numerous fractures.

Appendix C Abbreviations, Acronyms, Units and Conversion Factors

Term	Definition
2D	Two-dimensional
3D	Three-dimensional
Bcf	Billion cubic feet (10^9)
B_g	Formation volume factor
°C	Degrees Celsius
CBM	Coal bed methane
CCS	Carbon Capture and Storage
CH_4	Methane (natural gas)
CO_2	Carbon dioxide
CO2CRC	Cooperative Research Centre for Greenhouse Gas Technologies
CO2TECH	CO2CRC Technologies Pty Ltd. (The commercial arm of CO2CRC)
D	Darcy (1 D = 1000 mD)
DPI	Victorian Department of Primary Industries
ECBMR	Enhanced coal bed methane recovery
EGR	Enhanced gas recovery
EOR	Enhanced oil recovery
ESSCI	Environmentally Sustainable Site for CO_2 Injection (as used by GeoDisc)
°F	Degrees Fahrenheit
ft	Feet (1 ft = 0.3048 m)
ft^3	Cubic foot (1 ft^3 = 0.02832 m^3)
GEODISC™	Research program of the former Australian Petroleum Cooperative Research Centre
Gt	Giga tonnes (10^9 tonnes)
IEAGHG	International Energy Agency Greenhouse Gas R&D Programme
IPCC	Intergovernmental Panel on Climate Change
kg	Kilogram
km	Kilometre
km^2	Square kilometre (1 km^2 = 1,000,000 m^2)
kv/kh	Ratio of vertical permeability to horizontal permeability
LVCSA	Latrobe Valley CO_2 Storage Assessment (conducted by CO2CRC in 2005)
m	Metre (1 m = 3.2808 ft)
m^3	Cubic metre (1 m^3 = 35.3147 ft^3)
Ma	Million years
mD	Millidarcy (1 mD = 0.001 D)
mGL	Depth in metres measured relative to ground elevation
mKB	Depth in metres measured relative to well elevation
MPa	Mega Pascal (1MPa = 145.0377 psi)
mSS	Depth in metres measured relative to sea level

Term	Definition
Mt	Mega tonnes (10^6 tonnes)
ppm	Parts per million
psia	Pounds per square inch absolute (1 psi = 0.006894757 MPa)
R_o	Vitrinite reflectance
scf	Standard cubic feet
t	Metric tonnes
Tcf	Trillion cubic feet (10^{12}) (1 Tcf CO_2 = 53.0657705140448 Mt CO_2 at standard surface temperatures and pressures of 60°F and 14.65 psia respectively)

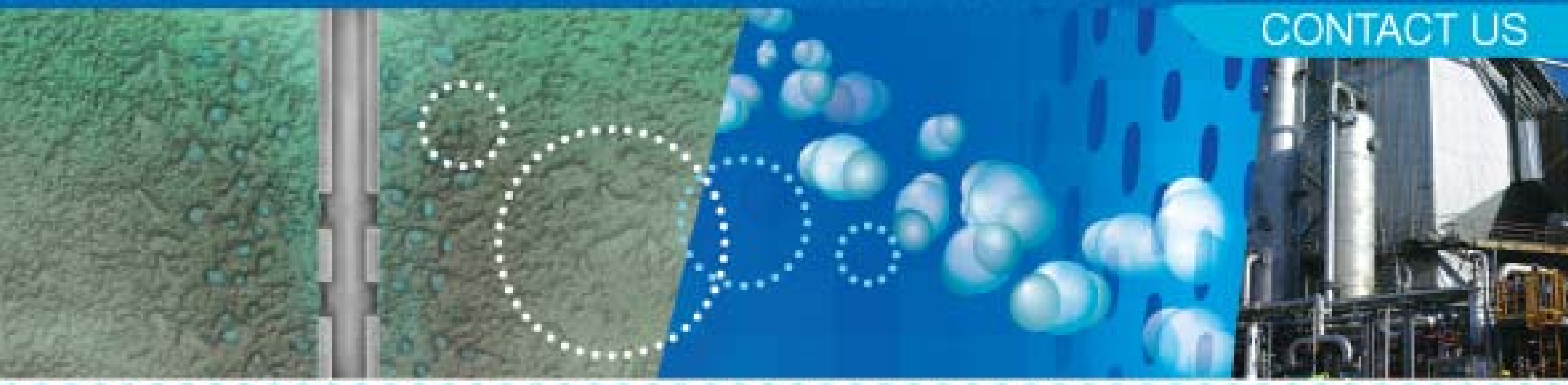

Canberra

Dr Peter Cook
Chief Executive
GPO Box 463, Canberra, ACT 2601
Ph: + 61 2 6120 1600
Fax: + 61 2 6273 7181
Email: pjcook@co2crc.com.au

Ms Carole Peacock
Business Manager
GPO Box 463, Canberra, ACT 2601
Ph: + 61 2 6120 1605
Fax: + 61 2 6273 7181
Email: cpeacock@co2crc.com.au

Melbourne

Mr Barry Hooper
Chief Technologist
Room 232/Level 2
School of Electrical & Electronic
Engineering, The University
of Melbourne, VIC 3010
Ph: + 61 3 8344 6622
Fax: + 61 3 9347 7438
Email: bhooper@co2crc.com.au

Mr Rajindar Singh
Otway Project Manager
Room 449
School of Earth Science
The University of Melbourne
VIC 3010
Ph: + 61 3 8344 9007
Fax: + 61 3 8344 7761
Email: rssingh@co2crc.com.au

Sydney

Prof Dianne Wiley
Program Manager for CO_2 Capture
The University of New South Wales
UNSW Sydney, 2052
Ph: + 61 2 9385 4755
Email: dwiley@co2crc.com.au

Adelaide

Prof John Kaldi
Chief Scientist
Australian Schtool of Petroleum
The University of Adelaide, SA 5005
Ph: + 61 8 8303 4291
Fax: + 61 8 8303 4345
Email: jkaldi@co2crc.com.au

Perth

Mr David Hilditch
Commercial Manager (CO2TECH)
PO Box 1130, Bentley
Western Australia 6102
Ph: + 61 8 6436 8655
Fax: + 61 8 6436 8555
Email: dhilditch@co2crc.com.au

researching carbon capture and storage